CHEMICAL AND ELECTROCHEMICAL REACTIONS IN ZINC CHLORIDE BASED MELTS

by

Nicholas Andrew Carthey B.Sc. M.Phil. G.R.S.C.

A thesis submitted for the degree of Doctor of Philosophy of the University of London

August 1988

Department of Materials

Royal School of Mines

Imperial College of Science and Technology

ABSTRACT

The thermodynamics of pure molten $ZnCl_2$ and mixtures with NaCl and KCl were studied by means of a formation cell involving zinc and chlorine electrodes. Activity values so-derived are compared with those of other workers obtained using various methods, and reasons suggested for discrepancies between alternative techniques.

Cyclic voltammetric studies of these melts, both purified and unpurified, with various working electrodes, indicated that residual water could be largely removed by a standard purification technique.

The redox behaviour of chromium(II) was examined by cyclic voltammetry as the melt composition was varied. In relatively "acidic" melts, an electrode deposit of pure chromium(III) chloride was obtained. The peak potential of the reversible chromium(II) oxidation wave was found to correlate with the melt acidity (activity of $ZnCl_2$).

The behaviour of gallium(III) was similarly examined by cyclic voltammetry. In relatively acidic melts, Ga(III) could be reduced only to the unusual Ga(I) oxidation state, which was stable, but as the melt was made basic, Ga(I) appeared to disproportionate, and ultimately metallic gallium could be co-deposited with zinc.

Finally, the electrochemistry of titanium(III) produced by reaction of titanium metal with the melts was examined, and compared with the behaviour of solutions produced by reaction of $TiCl_3$. Such solutions could be oxidised to Ti(IV), which was then lost as $TiCl_4$ from the electrode vicinity, the reaction being particularly influenced by temperature and Ti(III) concentration.

CONTENTS

	page
TITLEPAGE	1
ABSTRACT	2
CONTENTS	3
LIST OF FIGURES	8
LIST OF TABLES	20
CHAPTER ONE: INTRODUCTION	28
1.1 General	28
1.2 Thermodynamics of molten salt mixtures	29
1.3 Solution models for molten salts	31
1.4 Chloroaluminate melts	35
1.5 Applications of zinc chloride-based melts	41
1.6 Proposed research	43
CHAPTER TWO: LITERATURE SURVEY	44
2.1 General	44
2.2 Melt preparation and reactivity with water	44
2.3 Structural studies	46
2.4 Transport and physico-chemical properties:-	48
2.4.1 General	48
2.4.2 Electrical conductance	49
2.4.3 Density	49

2.4.4 Viscosity 51

2.4.5 Phase diagrams 51

2.4.6 Vapour pressure 54

2.5 Electrochemical studies:- 54

2.5.1 Formation and concentration cells 54

2.5.2 Voltammetric studies 61

2.5.3 Chronopotentiometric studies 63

2.6 Solute behaviour 64

2.7 Overall summary 64

CHAPTER THREE: EXPERIMENTAL 66

3.1 Melt preparation:- 66

3.1.1 Zinc chloride 66

3.1.2 Sodium chloride and potassium chloride 68

3.1.3 Lithium chloride-potassium chloride eutectic 68

3.2 Vacuum and gas supply 68

3.3 Furnace and temperature control 68

3.4 Electrochemical cell 69

3.5 Electrodes 71

3.6 Pulse-generating equipment 77

3.7 Cyclic voltammetry 79

3.8 AC impedance 79

3.9 X-ray diffraction 80

3.10 Optical microscopy 80

3.11 Electron microscopy 80

3.12 Electron spectroscopy for chemical analysis (ESCA) 80

3.13 Atomic absorption 81

3.14 Materials 81

CHAPTER FOUR: THERMODYNAMICS OF ZINC CHLORIDE-ALKALI CHLORIDE MIXTURES 84

4.1 Generation of formation cells by a current pulse method 84

4.2 Results and discussion:- 85

4.2.1 Stability of zinc electrode potential 85

4.2.2 Behaviour of planar vitreous carbon electrode 85

4.2.3 Behaviour of indented vitreous carbon electrode 88

4.2.4 Conclusions 92

4.3 Conventional formation cells-General 93

4.4 Results and discussion:- 96

4.4.1 Pure zinc chloride 96

4.4.2 Sodium chloride-zinc chloride 99

4.4.3 Potassium chloride-zinc chloride 107

4.5 Concentration cell-General 109

4.6 Results and discussion 112

4.7 Calculated solute activities in zinc chloride melts 114

CHAPTER FIVE: CYCLIC VOLTAMMETRY OF ZINC CHLORIDE-BASED MELTS WITHOUT ADDED SOLUTE SPECIES

5.1 General 118

5.2 Principles of cyclic voltammetry 118

5.3 Results and discussion:- 123

5.3.1 Counter and reference electrodes 123

5.3.2 Working electrodes 124

5.4 Conclusions 134

CHAPTER SIX: CYCLIC VOLTAMMETRY OF CHROMIUM COMPOUNDS IN ZINC CHLORIDE-ALKALI CHLORIDE MIXTURES

6.1 Procedure and general observations 137

6.2 Cyclic voltammetry of chromium(II) solutions- Results and discussion:- 138

6.2.1 Potassium chloride-zinc chloride melts 138

6.2.2 Sodium-chloride-zinc chloride melts 182

6.2.3 Summary of voltammetric results 193

6.2.4 Effect of melt acidity on peak potential 197

6.3 Characterisation of anodic oxidation product:- 198

6.3.1 Isolation of the product 198

6.3.2 Morphology of the electrode product 201

6.3.3 Analysis of the deposit 204

6.4 AC impedance measurements 212

6.5 Overall conclusions and further work 216

CHAPTER SEVEN: CYCLIC VOLTAMMETRY OF GALLIUM COMPOUNDS IN ZINC CHLORIDE-ALKALI CHLORIDE MIXTURES

7.1 Procedure and general observations 218

7.2 Cyclic voltammetry of gallium(III) solutions- Results and discussion:- 218

7.2.1 Potassium chloride-zinc chloride melts 218

7.2.1 Sodium chloride-zinc chloride melts 228

7.2.3 Lithium chloride-potassium chloride eutectic 242

7.3 Conclusions and further work 245

CHAPTER EIGHT: CYCLIC VOLTAMMETRY OF TITANIUM COMPOUNDS IN ZINC CHLORIDE-ALKALI CHLORIDE MIXTURES

8.1 Procedure and general observations 247

8.2 Cyclic voltammetry of titanium(III) solutions- Results and discussion:- 250

8.2.1 Titanium metal in potassium chloride-zinc chloride melt 250

8.2.2 Titanium(III) chloride in potassium chloride-zinc chloride melts 271

8.3 Characterisation of anodic oxidation product 275

8.4 Conclusions and further work 277

REFERENCES 279

ACKNOWLEDGEMENTS 289

LIST OF FIGURES

Figure 1.1. Calculated and experimental activities for cadmium bromide in KBr-$CdBr_2$ melts at 600°C, assuming the formation of $CdBr_4^{2-}$ ions. . . . . page 34

Figure 1.2. Activities of aluminium chloride and sodium chloride in NaCl-$AlCl_3$ melts at 175°C. . . . . page 38

Figure 1.3. Activity coefficients of an idealised solute s in NaCl-$AlCl_3$ melt at 175°C, as calculated from the coordination cluster theory. . . . . page 38

Figure 2.1. Typical conductivity isotherms obtained for the KCl-$ZnCl_2$ melt. . . . . page 50

Figure 2.2. Typical conductivity isotherms obtained for the KCl-$AlCl_3$ melt. . . . . page 50

Figure 2.3. Phase diagrams for MCl-$ZnCl_2$ systems. . . . . page 52

Figure 2.4. Comparison of E° values for $ZnCl_2$. . . . . page 56

Figure 2.5. Activity of zinc chloride in the MCl-$ZnCl_2$ systems. . . . . page 58

Figure 2.6. Activities of sodium chloride and zinc chloride as a function of melt composition in the sodium chloride-zinc chloride system at 700K. . . . . page 59

Figure 3.1. Melt purification apparatus. . . . . page 67

Figure 3.2. Electrochemical cell and miscellaneous electrodes. . . . . page 70

Figure 3.3. Electrodes. . . . . page 72

Figure 3.4. Electrodes. . . . . page 74

Figure 3.5. Electrodes for formation cell. . . . page 76

Figure 3.6. Apparatus for current pulse emf measurements. . . . . page 78

Figure 4.1. Variation in potential perturbation with current density on vitreous carbon in pure zinc chloride at 400°C. . . . . page 87

Figure 4.2. Typical emf/time decay curves on vitreous carbon at 400°C. . . . . page 89

Figure 4.3. Emf decay curves on vitreous carbon at 400°C. . . . . page 91

Figure 4.4. E° values for pure zinc chloride. page 97

Figure 4.5. The variation of emf with temperature for the formation cell $Zn/ZnCl_2+NaCl/Cl_2$. . . . . page 102

Figure 4.6. Activities of zinc chloride in $NaCl-ZnCl_2$ mixtures. . . . . page 104

Figure 4.7. Alkali chloride activities in mixtures with zinc chloride. . . . . page 106

Figure 4.8. The variation of emf with temperature for the formation cell $Zn/ZnCl_2+KCl/Cl_2$. . . . . page 108

Figure 4.9. Activities of zinc chloride in $KCl-ZnCl_2$ mixtures. . . . . page 110

Figure 4.10. Variation of emf with composition for the concentration cell $Zn/KCl+ZnCl_2(ref)/KCl+ZnCl_2/Zn$ at 408°C. . . . . page 113

Figure 4.11. Typical Coordination cluster calculations for a solute in the system $AlkCl-ZnCl_2$ as a function of melt composition (Alk = K or Na). . . . . page 116

Figure 5.1. Cyclic voltammogram for a reversible reduction process with both reactant and product soluble. . . . . page 120

Figure 5.2. Cyclic voltammogram of purified 15 mole per cent NaCl-$ZnCl_2$ melt at 391°C under argon (W electrode). . . . . page 125

Figure 5.3. Cyclic voltammogram of purified 15 mole per cent NaCl-$ZnCl_2$ melt at 391°C under argon. . page 126

Figure 5.4. Cyclic voltammogram of purified 15 mole per cent NaCl-$ZnCl_2$ melt at 391°C after a 3-day exposure to air . . . . . page 128

Figure 5.5. Cyclic voltammogram of unpurified 15 mole per cent NaCl-$ZnCl_2$ melt at 391°C . . . . . page 129

Figure 5.6. Cyclic voltammogram of unpurified 15 mole per cent NaCl-$ZnCl_2$ melt at 391°C after 3 days under argon . . . . . page 130

Figure 5.7. Typical cyclic voltammogram using vitreous carbon working electrode: purified, unpurified or air-exposed 15 mole per cent NaCl-$ZnCl_2$ melt at 391°C . . . . . page 132

Figure 5.8. Cyclic voltammogram of purified 15 mole per cent NaCl-$ZnCl_2$ melt at 391°C (Pt electrode). page 133

Figure 5.9. Cyclic voltammogram of purified 15 mole per cent NaCl-$ZnCl_2$ melt at 391°C (Au electrode). page 135

Figure 6.1. Typical cyclic voltammogram for the oxidation of chromium(II) (0.065M) in 0.6 mole fraction $KCl-ZnCl_2$ at 388°C . . . . . page 140

Figure 6.2. Plot of peak current against square root of scan rate for the oxidation of chromium(II) (0.065M) in 0.60 mole fraction $KCl-ZnCl_2$ at 388°C . . . . page 144

Figure 6.3. Plots of peak current against square root of scan rate for the oxidation of chromium(II) (0.16M) in 0.50 mole fraction $KCl-ZnCl_2$ at various temperatures . . . . . page 145

Figure 6.4. Arrhenius plots for the variation of diffusion coefficient of chromium(II) with temperature in various $KCl-ZnCl_2$ melts . . . . . page 147

Figure 6.5. Plot of peak current against square root of scan rate for the oxidation of chromium(II) (0.35M) in 0.40 mole fraction $KCl-ZnCl_2$ at 400°C . . . . page 152

Figure 6.6. Typical cyclic voltammograms for the oxidation of chromium(II) (0.35M) in 0.40 mole fraction $KCl-ZnCl_2$ at 282°C . . . . . page 154

Figure 6.7. Typical cyclic voltammogram for the oxidation of chromium(II) (0.52M) in 0.39 mole fraction $KCl-ZnCl_2$ at 400°C . . . . . page 155

Figure 6.8. Plot of peak current against square root of scan rate for the oxidation of chromium(II) (0.52M) in 0.39 mole fraction KCl-$ZnCl_2$ at 400°C . . . . page 157

Figure 6.9. Typical cyclic voltammograms for the oxidation of chromium(II) (0.26M) in 0.30 mole fraction KCl-$ZnCl_2$ at 414°C . . . . . page 161

Figure 6.10. Plot of peak current against square root of scan rate for the oxidation of chromium(II) (0.26M) in 0.30 mole fraction KCl-$ZnCl_2$ at 414°C . . . . page 163

Figure 6.11. Typical cyclic voltammograms for the oxidation of chromium(II) (0.26M) in 0.30 mole fraction KCl-$ZnCl_2$ at 328°C . . . . . page 165

Figure 6.12. Plot of peak current against square root of scan rate for the oxidation of chromium(II) (0.26M) in 0.30 mole fraction KCl-$ZnCl_2$ at 328°C . . . . page 166

Figure 6.13. Typical cyclic voltammograms for the oxidation of chromium(II) (0.58M) in 0.30 mole fraction KCl-$ZnCl_2$ at 400°C . . . . . page 167

Figure 6.14. Cyclic voltammogram for the oxidation of chromium(II) (0.58M) in 0.30 mole fraction KCl-$ZnCl_2$ at 400°C: Comparison with reversible case . . . . page 170

Figure 6.15. Typical cyclic voltammogram for the oxidation of chromium(II) (0.023M) in 0.21 mole fraction KCl-$ZnCl_2$ at 400°C . . . . . page 174

Figure 6.16. Typical cyclic voltammograms for the oxidation of chromium(II) (0.081M) in 0.21 mole fraction KCl-$ZnCl_2$ at 412°C . . . . . page 175

Figure 6.17. Typical cyclic voltammograms for the oxidation of chromium(II) (0.57M) in 0.21 mole fraction KCl-$ZnCl_2$ at 414°C . . . . . page 176

Figure 6.18. Typical cyclic voltammograms for the oxidation of chromium(II) (0.74M) in pure zinc chloride at 400°C . . . . . page 179

Figure 6.19. Cyclic voltammogram for the oxidation of chromium(II) (0.32M) in "pure" zinc chloride at 400°C (after HCl bubbling): Comparison with reversible case . . . . . page 181

Figure 6.20. Plot of peak current against square root of scan rate for the oxidation of chromium(II) (0.26M) in 0.54 mole fraction NaCl-$ZnCl_2$ at 328°C . . . page 184

Figure 6.21. Typical cyclic voltammograms for the oxidation of chromium(II) (0.33M) in 0.40 mole fraction NaCl-$ZnCl_2$ at 400°C . . . . . page 185

Figure 6.22. Typical cyclic voltammograms for the oxidation of chromium(II) (0.11M) in 0.40 mole fraction $NaCl-ZnCl_2$ at 400°C . . . . . page 188

Figure 6.23. Typical cyclic voltammograms for the oxidation of chromium(II) (0.10M) in 0.30 mole fraction $NaCl-ZnCl_2$ at 405°C . . . . . page 190

Figure 6.24. Typical cyclic voltammograms for the oxidation of chromium(II) (0.27M) in 0.30 mole fraction $NaCl-ZnCl_2$ at 400°C . . . . . page 192

Figure 6.25. Typical cyclic voltammograms for the oxidation of chromium(II) (0.41M) in 0.15 mole fraction $NaCl-ZnCl_2$ at 400°C . . . . . page 194

Figure 6.26. Variation of the reversible voltammetric peak potential for chromium(II) oxidation with melt acidity in alkali chloride-zinc chloride systems . . . . . page 199

Figure 6.27. Morphology of chromium(III) chloride electrode deposit . . . . . page 202

Figure 6.28. Layer structure of chromium(III) chloride . . . . . page 205

Figure 6.29. X-ray photoelectron spectrum of chromium(III) chloride samples (wide scan) . . . page 209

Figure 6.30. X-ray photoelectron spectrum of chromium(III) chloride sample deposited from KCl-$ZnCl_2$ melt:- Cr 2p 3/2 region . . . . . page 211

Figure 6.31 Complex plane impedance plots for chromium(III) deposited on vitreous carbon from 0.5M chromium(II) in a 0.25M fraction KCl-$ZnCl_2$ melt at 400°C . . . . . page 213

Figure 6.32. Plot of real impedance component at 20kHz versus number of coulombs passed during deposition of chromium(III) chloride from a 0.5M chromium(II) solution in 0.25 mole fraction KCl-$ZnCl_2$ melt at 400° . . . . . page 215

Figure 7.1. Typical cyclic voltammograms for the reduction of gallium(III) (0.09M) in pure zinc chloride at 400°C . . . . . page 219

Figure 7.2. Plot of peak current against square root of scan rate for the oxidation of gallium(II) (0.09M) in pure zinc chloride at 400°C . . . . . page 222

Figure 7.3. Typical cyclic voltammograms for the reduction of gallium(III) (0.07M) in 0.13 mole fraction KCl-$ZnCl_2$ at 400°C . . . . . page 224

Figure 7.4. Typical cyclic voltammograms for the reduction of gallium(III) (0.06M) in 0.40 mole fraction KCl-$ZnCl_2$ at 400°C . . . . . page 227

Figure 7.5. Typical cyclic voltammogram for the reduction of gallium(III) (0.06M) in 0.50 mole fraction KCl-$ZnCl_2$ at 400°C . . . . . page 229

Figure 7.6. Typical cyclic voltammogram for the reduction of gallium(III) (0.06M) in 0.60 mole fraction KCl-$ZnCl_2$ at 400°C . . . . . page 230

Figure 7.7. Typical cyclic voltammograms for the reduction of gallium(III) (0.13M) in 0.40 mole fraction NaCl-$ZnCl_2$ at 400°C . . . . . page 232

Figure 7.8. Typical cyclic voltammograms for the reduction of gallium(III) (0.11M) in 0.50 mole fraction NaCl-$ZnCl_2$ at 400°C . . . . . page 234

Figure 7.9. Typical cyclic voltammogram for the reduction of gallium(III) (0.06M) in 0.60 mole fraction NaCl-$ZnCl_2$ at 400°C . . . . . page 236

Figure 7.10. Cyclic voltammogram for the reduction of gallium(III) (0.06M) in 0.60 mole fraction NaCl-$ZnCl_2$ at 400°C . . . . . page 237

Figure 7.11. Cyclic voltammogram for the reduction of gallium(III) (0.06M) in 0.60 mole fraction NaCl-$ZnCl_2$ at 400°C . . . . . page 238

Figure 7.12. Typical cyclic voltammogram for the reduction of gallium(III) (0.12M) in 0.60 mole fraction NaCl-$ZnCl_2$ at 400°C . . . . . page 240

Figure 7.13. Typical cyclic voltammogram for the reduction of gallium(III) (0.07M) in lithium chloride-potassium chloride eutectic at 400°C . page 243

Figure 8.1. Typical cyclic voltammograms for the oxidation of titanium(III) (0.60M) in pure zinc chloride at 350°C (reaction product of titanium metal) . page 251

Figure 8.2. Typical cyclic voltammograms for the oxidation of titanium(III) (0.60M) in pure zinc chloride at 400°C (reaction product of titanium metal) . page 256

Figure 8.3. Typical cyclic voltammograms for the oxidation of titanium(III) (1.00M) in 0.10 mole fraction KCl-$ZnCl_2$ at 412°C (reaction product of titanium metal) . . . . . page 257

Figure 8.4. Typical cyclic voltammograms for the oxidation of titanium(III) (0.36M) in 0.30 mole fraction KCl-$ZnCl_2$ at 400°C (reaction product of titanium metal) . . . . . page 260

Figure 8.5. Typical cyclic voltammograms for the oxidation of titanium(III) (0.06M) in 0.50 mole fraction KCl-$ZnCl_2$ at 405°C (reaction product of titanium metal) . . . . . page 262

Figure 8.6. Typical cyclic voltammograms for the oxidation of titanium(III) (0.70M) in 0.60 mole fraction KCl-$ZnCl_2$ at 416°C (reaction product of titanium metal) . . . . . page 266

Figure 8.7. Typical cyclic voltammogram for the oxidation of titanium(III) (0.70M) in 0.60 mole fraction KCl-$ZnCl_2$ at 272°C (reaction product of titanium metal) . . . . . page 270

Figure 8.8. Typical cyclic voltammograms for the oxidation of titanium(III) (0.34M) in 0.25 mole fraction KCl-$ZnCl_2$ at 400°C (reaction product of titanium(III) chloride) . . . . . page 273

LIST OF TABLES

Table 2.1. Raman spectra assignments for the KCl-$ZnCl_2$ system . . . . . page 47

Table 2.2. Structural details for solid and molten zinc chloride . . . . . page 47

Table 3.1. Reagents and electrode materials . . page 82

Table 4.1. E° values for pure zinc chloride at 450°C . . . . . page 98

Table 4.2. Least squares analyses of emf/temperature formation cell data for alkali chloride-zinc chloride systems . . . . . page 100

Table 4.3. Selected thermodynamic properties of zinc chloride calculated for the alkali chloride- zinc chloride systems . . . . . page 101

Table 6.1. Voltammetric Parameters for 0.065M chromium(II) in 60/40 mole p.c. KCl/$ZnCl_2$ at 388°C . . . . . page 141

Table 6.2. Voltammetric Parameters for 0.15M chromium(II) in 50/50 mole p.c. KCl/$ZnCl_2$ at 412°C, 333°C, 293°C, 260°C . . . . . page 141

Table 6.3. Stokes radii for chromium(II) in KCl-$ZnCl_2$ and LiCl-KCl melts. . . . . page 148

Table 6.4. Voltammetric Parameters for 0.35M chromium(II) in 40/60 mole p.c. KCl/$ZnCl_2$ at 400°C . . . . . page 151

Table 6.5. Voltammetric Parameters for 0.35M chromium(II) in 40/60 mole p.c. KCl/$ZnCl_2$ at 312°C . . . . . page 151

Table 6.6. Voltammetric Parameters for 0.52M chromium(II) in 39/61 mole p.c. KCl/$ZnCl_2$ at 400°C . . . . . page 156

Table 6.7. Voltammetric Parameters for 0.26M chromium(II) in 40/60 mole p.c. KCl/$ZnCl_2$ at 319°C . . . . . page 156

Table 6.8. Diffusion coefficients and Stokes radii for chromium(II) in 0.4 mole fraction KCl-$ZnCl_2$ melt . . . . . page 160

Table 6.9. Voltammetric Parameters for 0.26M chromium(II) in 30/70 mole p.c. KCl/$ZnCl_2$ at 414°C . . . . . page 164

Table 6.10. Voltammetric Parameters for 0.26M chromium(II) in 30/70 mole p.c. KCl/$ZnCl_2$ at 328°C . . . . . page 164

Table 6.11. Voltammetric Parameters for 0.58M chromium(II) in 27/73 mole p.c. KCl/$ZnCl_2$ at 400°C . . . . . page 168

Table 6.12. Diffusion coefficients and Stokes radii for chromium(II) in 0.3 mole fraction KCl-$ZnCl_2$ melt . . . . . page 171

Table 6.13. Voltammetric Parameters for 0.023M chromium(II) in 21/79 mole p.c. KCl/$ZnCl_2$ at 400°C . . . . . page 173

Table 6.14. Voltammetric Parameters for 0.081M chromium(II) in 21/79 mole p.c. KCl/$ZnCl_2$ at 414°C . . . . . page 173

Table 6.15. Voltammetric Parameters for 0.57M chromium(II) in 20/80 mole p.c. KCl/$ZnCl_2$ at 400°C . . . . . page 177

Table 6.16. Voltammetric Parameters for 0.74M chromium(II) in pure zinc chloride at 400°C . . . . . page 177

Table 6.17. Voltammetric Parameters for 0.72M chromium(II) in .06/94 mole p.c. KCl/$ZnCl_2$ at 400°C . . . . . page 180

Table 6.18. Voltammetric Parameters for 0.26M chromium(II) in 54/46 mole p.c. NaCl/$ZnCl_2$ at 400°C . . . . . page 183

Table 6.19. Voltammetric Parameters for 0.33M chromium(II) in 40/60 mole p.c. NaCl/$ZnCl_2$ at 400°C . . . . . page 183

Table 6.20. Voltammetric Parameters for 0.11M chromium(II) in 40/60 mole p.c. NaCl/$ZnCl_2$ at 398°C . . . . . page 187

Table 6.21. Voltammetric Parameters for 0.075M chromium(II) in 40/60 mole p.c. NaCl/$ZnCl_2$ at 388°C . . . . . page 187

Table 6.22. Voltammetric Parameters for 0.10M chromium(II) in 30/70 mole p.c. NaCl/$ZnCl_2$ at 405°C . . . . . page 191

Table 6.23. Voltammetric Parameters for 0.27M chromium(II) in 30/70 mole p.c. NaCl/$ZnCl_2$ at 400°C . . . . . page 191

Table 6.24. Voltammetric Parameters for 0.41M chromium(II) in 15/85 mole p.c. $NaCl/ZnCl_2$ at 400°C . . . . . page 195

Table 6.25. X-ray powder diffraction data for chromium(III) chloride electrode deposit . . . . page 207

Table 7.1. Voltammetric Parameters for 0.09M gallium(III) in pure zinc chloride at 400°C . . page 220

Table 7.2. Voltammetric Parameters for 0.07M gallium(III) in 13/87 mole p.c. $KCl/ZnCl_2$ at 400°C . . . . . page 220

Table 7.3. Voltammetric Parameters for 0.032M gallium(III) in 35/65 mole p.c. $KCl/ZnCl_2$ at 400°C . . . . . page 225

Table 7.4. Voltammetric Parameters for 0.060M gallium(III) in 40/60 mole p.c. $KCl/ZnCl_2$ at 400°C . . . . . page 225

Table 7.5. Voltammetric Parameters for 0.13M gallium(III) in 40/60 mole p.c. $NaCl/ZnCl_2$ at 400°C . . . . . page 233

Table 7.6. Voltammetric Parameters for 0.11M gallium(III) in 50/50 mole p.c. $NaCl/ZnCl_2$ at 405°C . . . . . page 233

Table 7.7. Voltammetric Parameters for 0.07M gallium(III) in LiCl/KCl eutectic at 400°C . . page 244

Table 8.1. Voltammetric Parameters for 0.60M titanium(III) in pure zinc chloride at 350°C. . page 252

Table 8.2. Voltammetric Parameters for 0.60M titanium(III) in pure zinc chloride at 400°C. . page 252

Table 8.3. Voltammetric Parameters for 0.60M titanium(III) in pure zinc chloride at 440°C. . page 253

Table 8.4. Voltammetric Parameters for 0.10M titanium(III) in pure zinc chloride at 438°C. . page 253

Table 8.5. Voltammetric Parameters for 1.00M titanium(III) in 10/90 mole p.c $KCl/ZnCl_2$ at 412°C . . . . . page 258

Table 8.6. Voltammetric Parameters for 0.36M titanium(III) in 30/70 mole p.c. $KCl/ZnCl_2$ at 412°C . . . . . page 258

Table 8.7. Voltammetric Parameters for 0.36M titanium(III) in 50/50 mole p.c. $KCl/ZnCl_2$ at 400°C . . . . . page 261

Table 8.8. Voltammetric Parameters for 0.06M titanium(III) in 50/50 mole p.c. $KCl/ZnCl_2$ at 405°C . . . . . page 261

Table 8.9. Voltammetric Parameters for 0.06M titanium(III) in 50/50 mole p.c. $KCl/ZnCl_2$ at 380°C . . . . . page 263

Table 8.10. Voltammetric Parameters for 0.06M titanium(III) in 50/50 mole p.c. $KCl/ZnCl_2$ at 338°C . . . . . page 263

Table 8.11. Voltammetric Parameters for 0.02M titanium(III) in 50/50 mole p.c. $KCl/ZnCl_2$ at 400°C . . . . . page 265

Table 8.12. Calculated rate constants for 0.06M titanium(III) in 50/50 mole p.c. $KCl/ZnCl_2$ at 380°C assuming E_rC_i mechanism . . . . . page 265

Table 8.13. Voltammetric Parameters for 0.70M titanium(III) in 60/40 mole p.c. $KCl/ZnCl_2$ at 416°C . . . . . page 267

Table 8.14. Voltammetric Parameters for 0.70M titanium(III) in 60/40 mole p.c. $KCl/ZnCl_2$ at 346°C . . . . . page 267

Table 8.15. Voltammetric Parameters for 0.70M titanium(III) in 60/40 mole p.c. KCl/$ZnCl_2$ at 310°C . . . . . page 268

Table 8.16. Voltammetric Parameters for 0.70M titanium(III) in 60/40 mole p.c. KCl/$ZnCl_2$ at 290°C . . . . . page 268

Table 8.17. Voltammetric Parameters for 0.70M titanium(III) in 60/40 mole p.c. KCl/$ZnCl_2$ at 272°C . . . . . page 268

Table 8.18. Voltammetric Parameters for 0.34M titanium(III) in 25/75 mole p.c. KCl/$ZnCl_2$ at 398°C . . . . . page 272

Table 8.19. Voltammetric Parameters for 0.012M titanium(III) in 44/56 mole p.c. KCl/$ZnCl_2$ at 382°C . . . . . page 276

Table 8.20. Voltammetric Parameters for 0.012M titanium(III) in 44/56 mole p.c. KCl/$ZnCl_2$ at 236°C . . . . . page 276

CHAPTER ONE

INTRODUCTION

1.1 General

This thesis is concerned with electrochemical reactions in molten zinc chloride and its mixtures with alkali metal chlorides, and with the thermodynamics of the mixtures. Interest in the properties of such melts arises from both practical and theoretical considerations.

In the molten state pure zinc chloride is considered to be an associated liquid, as is indicated by the relatively high viscosity and low electrical conductivity. However, the addition of an alkali chloride will break up the network structure of the melt, forming entities such as "$ZnCl_4^{2-}$". This latter interaction may be interpreted as a Lewis acid-base reaction of the base (alkali chloride) with acidic zinc chloride, forming a mixture of lower Lewis acidity, as compared with the pure zinc chloride melt.

By analogy with melts based on the Lewis acid aluminium chloride, which is also an associated liquid in the pure state, the Lewis acidity of zinc-chloride-alkali chloride melts is expected to change relatively abruptly at certain critical melt compositions. This change is a consequence of changes in the activities of the melt components; such variations can have marked effects on the behaviour of solute species (e.g. metallic compounds) in these melts. For example, a soluble species may become insoluble, so that precipitation could be induced by a change in melt composition. Furthermore, miscibility gaps are known to

occur in aluminium chloride-based melts, leading to two-phase systems. Phenomena such as the above have obvious potential for the development of metal extraction and refinement processes (1). These aspects will be considered further below.

1.2 Thermodynamics of Molten Salt mixtures

Basic aspects of thermodynamics relating to molten mixtures have been considered by Bloom (2). The following discussion is partly taken from this work. More involved treatments can be found in other reviews of fused salt chemistry (3,4,6).

In theory, the activity of a component in a solution may be determined by measuring the emf of a formation cell. A generalised cell for a molten chloride system ACl_2 + MCl (A= divalent metal,M= alkali metal) would be:

$$A \;/\; ACl_2 + MCl \;/\; Cl_2\,(g),C$$

The metal electrode A can be either liquid or solid. Both electrodes must be reversible, that is, the potential determining reactions must occur sufficiently rapidly so that equilibrium potentials are established at both electrodes.

In the formation cell shown above, the overall reaction corresponds to:

$$A + Cl_2 \text{ ---> } ACl_2 \qquad (1.1)$$

The emf of the cell is related to the free energy change of reaction (1.1) by the well-known relation:

$$\Delta G = -nFE \qquad (1.2)$$

Also, from the Nernst equation, the following relation is

obtained:

$$E = E^\circ - (RT/2F)\ln (ACl_2) \qquad (1.3)$$

assuming that both chlorine gas and the metal A are at unit activity. E° is the cell potential when the pure divalent metal chloride is the cell electrolyte; i.e unit activity of ACl_2. Calculated values of E° have been tabulated for a large selection of metal chlorides (5).

Thus the thermodynamic properties of the ACl_2-MCl mixture may be derived from the formation cell emf. For the pure ACl_2, the thermodynamic quantities for reaction (1.1) may be expressed as follows:

$$\Delta G^\circ = -2FE^\circ \qquad (1.4)$$

$$\Delta S^\circ = 2F(\partial E^\circ/\partial T)_p \qquad (1.5)$$

$$\Delta H^\circ = 2FT(\partial E^\circ/\partial T)_p - 2FE^\circ \qquad (1.6)$$

Analogous relations may be written for ACl_2 in the mixture with MCl, in terms of the cell emf E.

Partial molar thermodynamic quantities may be defined for the mixture:

$$\Delta\overline{G} = \Delta G - \Delta G^\circ \qquad (1.7)$$

$$= -2F(E-E^\circ) \qquad (1.8)$$

$$= RT\ln (ACl_2) \qquad (1.9)$$

Equation (1.9) defines the activity of ACl_2. Similar expressions may be written for the enthalpy and entropy of mixing, for example:

$$\Delta\overline{S} = 2F[(\partial E/\partial T)_p - (\partial E^\circ/\partial T)_p] \qquad (1.10)$$

If the components of MCl_2-ACl form an ideal solution, then:

$$\Delta\overline{G}_{ideal} = RT\ln x \qquad (1.11)$$

where x is the mole fraction of the divalent chloride.

Also:

$$\Delta\bar{H}_{ideal} = 0 \qquad (1.12)$$

$$\Delta\bar{S}_{ideal} = -R\ln x \qquad (1.13)$$

To express deviations from ideal behaviour, excess partial thermodynamic functions may be defined, for example:

$$\Delta\bar{G}^{E} = \Delta\bar{G} - \Delta\bar{G}_{ideal} \qquad (1.14)$$

$$= RT\ln (ACl_2) - RT\ln x \qquad (1.15)$$

$$= RT\ln \gamma \qquad (1.16)$$

(γ = activity coefficient).

In order to calculate the thermodynamic properties for the second component of a binary mixture (mole fraction x_2, say), the Gibbs-Duhem relationship may be employed:

$$d\Delta\bar{G}_2 = -(x_1/x_2)\, d\Delta\bar{G}_1 \qquad (1.17)$$

Equation (1.17) may be re-written in terms of activities or activity coefficients for mathematical convenience, and integration between limits $x_2=1$ ($\gamma_2=1$) and x_2 yields

$$\ln \gamma_2 = -\int_1^{X_2} (x_1/x_2)\, d\ln \gamma_1 \qquad (1.18)$$

Thus a plot of x_1/x_2 versus $\ln \gamma_1$ enables $\ln \gamma_2$ to be evaluated by graphical integration.

1.3 Solution models for molten salts

"Ideal" salt melts may be considered as being made up of anions and cations, with positive ions surrounded by negative and vice-versa. The assumption of random mixing of cations with cations and anions with anions gives the ideal entropy of mixing as:

$$\Delta S = -R \sum n_r \ln x_r \qquad (1.19)$$

where the summation is taken over the cations and anions r of the mixture AX+BY, n denoting the number of moles and x the ion mole fraction ($=n_A/(n_A+n_B)$ for the cation mole fraction of A, for example.). The Temkin rule for activities may be derived from (1.19):

$$(AX) = x_A.x_X \qquad (1.20)$$

$$(BY) = x_B.x_Y \qquad (1.21)$$

Hence, for a mixture AX+BX, $x_X=1$, and thus the activity of say, AX, is equal to its mole fraction.

If a divalent cation is mixed with a monovalent cation, vacancies will be created in the cation "lattice". These holes however apparently do not affect the configurational entropy of mixing and hence the activity may be calculated from the Temkin model.Again, this leads to the relation that the activity of say, AX_2, is equal to the mole fraction.

However, in most molten salt systems, significant interaction occurs between the various ions on mixing, leading to a change in enthalpy and possibly in configurational entropy. If the entropy of mixing is thus ideal (a "regular" solution), then for example, the activities in the mixture $AX+BX_2$ (6) are given by :

$$RT\ln (BX_2) = RT\ln x_2 + 2bx_1^2/(1+x_2)^2 \qquad (1.22)$$

$$RT\ln (AX) = RT\ln x_1 + 4bx_2^2/(1+x_2)^2 \qquad (1.23)$$

(x_1, x_2, respective mole fractions of AX, BX_2).

Here b is a constant which takes into account the various cation interactions in the system.

If the components of a system interact so strongly that complex ion formation may be supposed, then it is likely

that the above equations will not be closely obeyed. Such mixtures include $KCl-MgCl_2$, $NaCl-AlCl_3$, and melts based on $ZnCl_2$. The properties of such systems may sometimes be approximated by assuming a mixture of ions, e.g. K^+, Cl^-, and $CdCl_4^{2-}$ in the case of the melt $CdCl_2-KCl$, and that these ions form an ideal mixture (2). The Temkin model may then be applied, giving:

$$(KBr) = x_{K^+} . x_{Br^-} = (x_1-2x_2)/(x_1-x_2) \qquad (1.24)$$

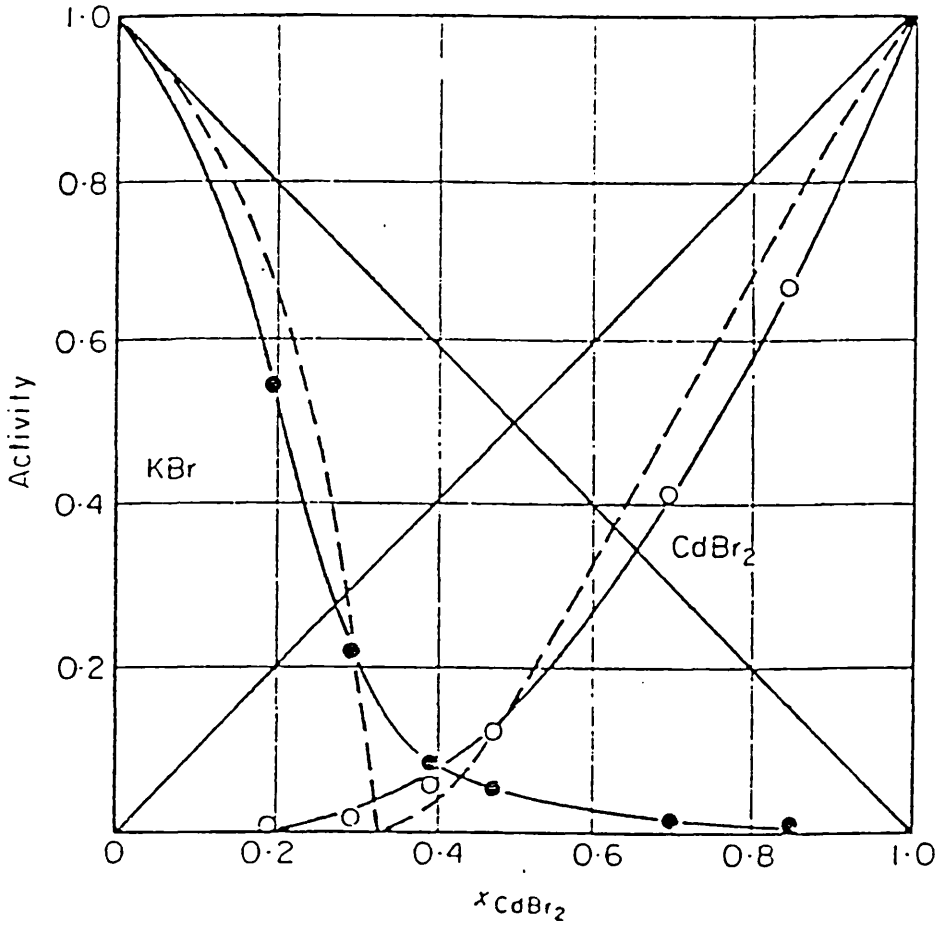
$$(CdBr_2) = x_{Cd^{2+}} . x^2_{Br^-} = (x_2-.5x_1)/(x_2+.5x_1) . \{(2x_2-x_1)/(2x_2-.5x_1)\}^2 \qquad (1.25)$$

where x_1 and x_2 represent the mole fraction of KBr and $CdBr_2$ respectively.

These latter equations give a reasonable fit to the measured activities when these are greater than about 0.2 (fig. 1.1), but are otherwise too small. This is probably due to the dissociation of the cadmium complex ion at compositions around o.67 mole fraction KBr. In these instances probably a range of complex ion equilibria should be considered, as has been done for chloroaluminates (see below).

The tendency to form "complex ions", i.e. the strength of interaction between the basic and acidic melt components in alkali halide mixtures increases markedly with increasing size of alkali ion, due to enhanced halide ion donor ability. This is shown, for example, in mixtures with $MgCl_2$ (6), where the heats of mixing increase significantly on passing from Li to Cs. Thus a whole range of ion interactions may be encountered in melts, culminating in the stable complex ion.

Figure 1.1. Calculated (- - -) and experimental (———) activities for potassium bromide and cadmium bromide in $KBr-CdBr_2$ melts at 600°C, assuming the formation of $CdBr_4^{2-}$ ions.



(From M.A.Bredig, J. Chem. Phys. 37, 451, (1962))

The models outlined above may be refined by taking into account non-random association of ions (3,6), and also may be applied to multi-component systems. In the case of a sufficiently dilute solute in a generalised binary system A + B, Blander et al (8) have derived a general equation relating the activity coefficient γ_o of the solute C, as a function of composition, to the solute activity coefficients ($\gamma_{o(A)}, \gamma_{o(B)}$) in the the pure components. This is:

$$1/\gamma_o = \sum_{i=0}^{Z} Z!/\{(Z-i)!/i!\}.\{(x_A\gamma_A^t)/(\gamma_{o(A)}^{1/z})\}^{z-i}$$
$$.\{(x_B\gamma_B^t)/(\gamma_{o(B)}^{1/z})\}^{i}.\exp(-g^E_i/RT) \qquad (1.26)$$

where Z is the coordination number of C, t=1/Z for a binary system with a common anion, x_A, x_B are mole fractions, γ_A, γ_B are activity coefficients, and the g^E_i term represents an excess free energy of mixing of A and B in the coordination shell of C.

This approach, the "Coordination cluster theory" has been successfully applied to binary alloys, and qualitatively to solutes in chloroaluminate melts (see below), where g^E_i is set to zero (equivalent to assuming that all B-C interactions are equal).

1.4 Chloroaluminate Melts

These might be considered the "model" systems from which to deduce the properties of chlorozincate melts. Theoretical interest in these $AlCl_3$-based systems arises from the fact that enormous changes in basicity can be achieved by relatively small composition changes, and this can cause dramatic variations in solute behavior (e.g.

solubility, oxidation state stability). A further advantage of these systems is that relatively low melting temperatures (<200°C) are found over a wide composition range. Indeed, mixtures of aluminium chloride with the chloride salts of large organic cations (e.g. n-butylpyridinium) result in the so-called "room-temperature" molten salts.

To understand the reasons for such behaviour, it is necessary to consider the properties of pure aluminium chloride. This compound is electron deficient (electron-pair acceptor or Lewis acid) and on melting forms chloride-bridged polymers. It is thus a low-melting molecular liquid, and of low specific conductivity.

However the addition of alkali chloride results in the formation of complex ions such as $AlCl_4^-$ and, for example, the predominant equilibrium near the equimolar point in NaCl-$AlCl_3$ melts is:

$$2AlCl_4^- \rightleftharpoons Al_2Cl_7^- + Cl^- \qquad (1.27)$$

with a mole fraction equilibrium constant at 175°C of $1.1*10^{-7}$ (9). Thus $AlCl_4^-$ is the major anionic species in the equimolar melt, with the heptachloroaluminate anion becoming more abundant in $AlCl_3$-rich (acidic) melts, and conversely, the presence of the simple chloride ion becomes significant in NaCl-rich (basic) melts.

In order to quantify the acid-base properties of chloroaluminate melts it has become customary to refer to a quantity $-\ln a_{Cl^-} = pCl^-$, deduced from the emf variation of concentration cells such as:

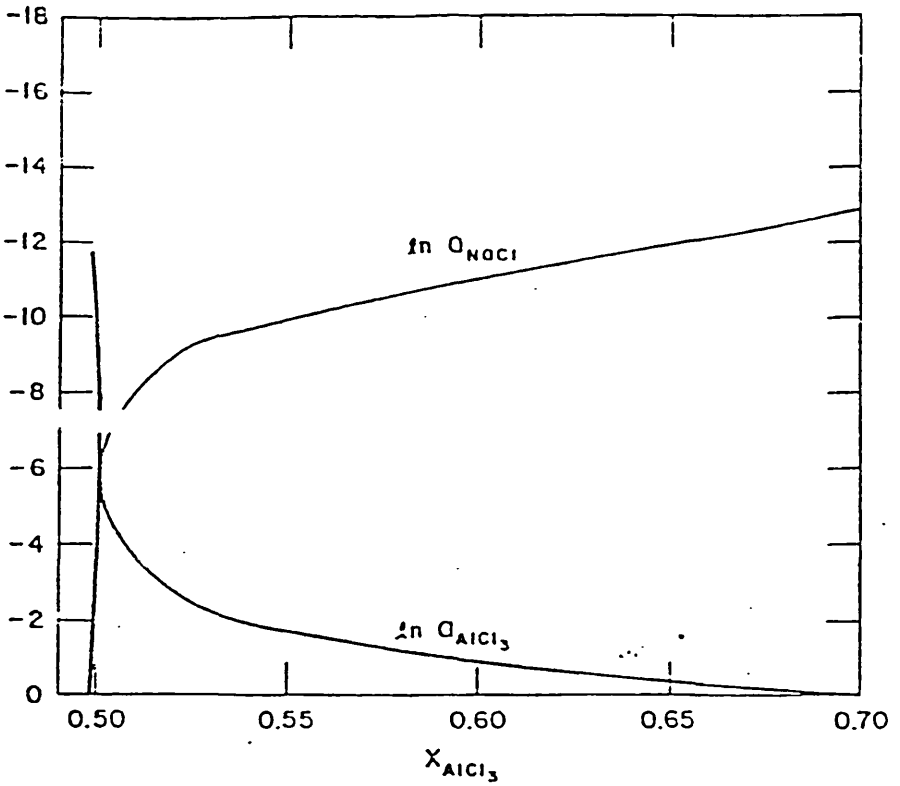
$Al/NaCl(solid)-AlCl_3//NaCl-AlCl_3/Al$

However Saboungi and Blander (10) have argued that this concept can only provide a relative basicity scale for a given melt and that a more satisfactory quantity is the activity of NaCl, or better, of $AlCl_3$, since this salt is common to all chloroaluminates. It was shown by the latter authors that it is possible to relate pCl^- to $-\ln a_{NaCl}$ (10) but that these quantities may differ greatly according to melt composition and temperature.

One striking feature of the concentration cell formulated above is that the emf changes abruptly by over 300mv as the $AlCl_3$ content changes from .500 to .504 mole fraction (10). This is analogous to a strong acid-base titration in aqueous solution where large changes in pH are observed. In thermodynamic terms the activities of $AlCl_3$ and NaCl vary by ten orders of magnitude around the .5 mole fraction composition (fig. 1.2). The effect of such variations on solute species in these melts can be pronounced; for example substances such as $NiCl_2$ or UCl_3 though soluble in relatively basic or relatively acidic melts, become virtually insoluble at the .5 mole fraction composition (11). This behaviour is predicted by the coordination cluster theory of Blander et al (8). If an idealised solute is considered, that is, one having similar activity coefficients in pure $AlCl_3$ or in pure NaCl, then the calculated activity coefficient exhibits a pronounced maximum at the .5 mole fraction composition, thus indicating insolubility (fig. 1.3).

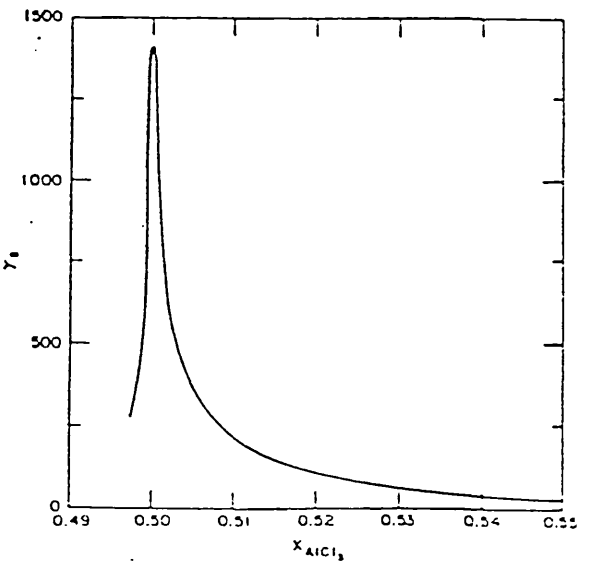
One further consequence of these positive deviations

Figure 1.2. Activities of aluminium chloride and sodium chloride in $NaCl-AlCl_3$ melts at 175°C.



(adapted from ref. 10)

Figure 1.3. Activity coefficients of an idealised solute s in $NaCl-AlCl_3$ melt at 175°C, as calculated from the coordination cluster theory.



(from ref. 10).

from ideality is the existance of miscibility gaps, for example, in the LiCl-KCl-$AlCl_3$ system (12). Such two phase systems may be employed in solvent extraction processes (1).

To continue this discussion on chloroaluminate melts, some specific examples of solute chemistry will be considered. As indicated above, these melts provide acidic or basic media according to composition. In fact the acidic melts show certain analogies with so-called "superacid" systems, eg HSO_3F-SbF_5 (13). In these very acidic media unusually low oxidation states of elements may be stabilised, for example in $AlCl_3$-NaCl the cations Bi_x^{y+} may be formed (14), where x= 1,5,8 and y= 1,3, 2 respectively. These species are in equilibrium with Bi^{3+}, eg:

$$6Bi^{+} \text{ ----> } Bi_5^{3+} + Bi^{3+} \qquad (1.28)$$

For this equation, the equilibrium constant favours the right-hand side in $ZnCl_2$-KCl melt, but in the more acidic $AlCl_3$-NaCl solvent a marked shift to the left is found. Generally, an increase in acidity favours Bi^{+} at the expense of Bi^{3+}, which illustrates the principle that the higher acidic oxidation states of metals are stabilised in basic melts, and conversely, that acidic melts favour the lower oxidation states.

In certain instances the lower oxidation state can be isolated as solid salts eg; $Cd_2^{2+}(AlCl_4^-)_2$ (16); gallium (I) tetrachloroaluminate (15); and salts of the bismuth cations described above (14).

Moving on to the non-metals, it is similarly found that

low positive oxidation states can be produced in acidic chloroaluminates for such elements as iodine (17), sulphur (18) and selenium (19). Again, solid compounds can be isolated, e.g. I_3AlCl_4 (17). The negative oxidation states may show basic behaviour by releasing chloride ions i.e.

$$S^{2-} + AlCl_4^- = AlSCl + 3Cl^- \qquad (1.29)$$

This equilibrium is shifted to the left in basic melts (21).

The acid-base properties of chloroaluminates may also influence the electronic spectra of species in the melts by giving rise to coordination changes. For example, nickel(II) and cobalt(II) both show a tendency towards octahedral configurations over tetrahedral with increasing melt acidity (20,22). This effect is explained by the polarisation of the chloride ions by the Al^{3+} cation, reducing the electron pair donation, so that the solute cations require a higher coordination number for effective charge neutralisation.

One further consequence of these acidity variations of potential application to metal refinement processes may be mentioned: the fact that the distribution coefficient of a solute between metal-melt phases can be maximised by adjustment of the melt composition. An example is the partition of actinide elements between molten aluminium-$AlCl_3$-KCl phases as studied by Moore (1). A sharp maximum in the distribution coefficient (metal phase preference) was found at the 1:1 mole ratio, and separate equilibria were proposed for acidic and basic melts.

Finally, a comparatively recent topic of study is the effect of acidity changes on organic reactions in chloroaluminates (23). Organic bases such as amines (e.g. dimethylaniline) appear to form adducts with acid moieties in the melts and thus give rise to a pCl^--dependent chemistry.

1.5 Applications of Zinc chloride-based melts

Several processes exploiting the acid-base properties of zinc chloride are currently being developed. Of direct relevance to this research is the "Pyroredox" process for the, refinement of low-grade plutonium scrap (24). The first step is the oxidation of plutonium metal:

$$2Pu(impure) + 3ZnCl_2 \text{ ---> } 3Zn + 2PuCl_3 \qquad (1.30)$$

This is carried out at 750°C in $ZnCl_2$-KCl melt. The second step involves reduction by calcium metal at 850°C:

$$2PuCl_3 + 3Ca \text{ ---> } 2Pu + 3CaCl_2 \qquad (1.31)$$

The principal use of this procedure has so far been for the upgrading of spent anodes employed in electrorefining, whereby plutonium is oxidised into a chloride melt and redeposited. The major impurity is gallium, added to ensure a critically safe anode. This metal is not oxidised into the salt phase in step(1) but concentrates in the heavier zinc metal phase. Other more reactive impurities e.g. americium, aluminium and rare earths transfer with plutonium into the salt phase. These latter elements together with excess zinc chloride are reduced to metal in step(2). However the plutonium metal is now of sufficient purity (95%) to be effectively electrorefined.

Obviously the efficiency of the pyroredox process depends upon the selective oxidation of plutonium in step(1) and the solubility of plutonium(III) and impurities in the resulting salt phase, factors which might be influenced by controlling the acidity of the mixture.

Another application of current interest is the use of zinc chloride as a hydrocracking catalyst. For example, polynuclear aromatics may be cracked to benzene and alkanes. Work by Salim and Bell (25) has indicated that zinc chloride is a more selective catalyst than aluminium chloride; though the latter compound is more active, it also promotes the formation of tarry materials. In the case of zinc chloride, the catalytic species may in fact be a protonic acid formed thus:

$$ZnCl_2 + H_2O \longrightarrow H^+[ZnCl_2OH]^- \qquad (1.32)$$

Other species may also be invoked (26). Water, of course, is a common impurity in zinc chloride, and in any case may be formed during the cracking of oxygen-containing compounds. Its presence has indeed been shown to enhance the catalytic activity of zinc chloride (25).

Mixtures of zinc chloride and other transition metal chlorides have also been investigated as catalysts, examples being $CrCl_3$, CuCl, and $MoCl_5$ (28). These chlorides are individually weaker catalysts than zinc chloride, but act to enhance the activity of the latter substance. Still greater enhancement is achieved by the use of ternary or quarternary melts with alkali metal chlorides (28,29). However the interactions occurring in

such melts are still largely unknown.

1.6 Proposed research

These two processes describe above indicate that a study of the reactions of metal halides in zinc chloride-based melts would be fruitful in facilitating the further development of such applications. It was also of interest to re-determine the activities of the melt components in the sodium chloride and potassium chloride-containing systems and use these as a basis for interpreting the behaviour of solute species. For the activity determinations, conventional formation cells were most likely to deliver unambiguous data; however these can present considerable experimental difficulties. Thus, the in-situ generation of formation cells by a novel current pulse technique was explored, as well as the "conventional" formation cells, and a concentration cell.

The solute species investigated were chromium, gallium, and titanium, chosen because:

a) their chemistry had previously been studied in other chloride melts.

b) they have multiple oxidation states, whose behaviour could be studied as a function of melt acidity.

c) their study was relevant to the pyroredox process.

The main technique employed in the solute studies was cyclic voltammetry, a method which is particularly suited to the elucidation of new systems, yielding data on oxidation states, redox potentials, kinetic behaviour, etc, from short time scale experiments. The technique is reviewed in chapter five.

CHAPTER TWO

LITERATURE SURVEY

2.1 General

Relatively few studies have been carried out on certain aspects of zinc chloride melts of relevance to this thesis. However, useful comparisons can often be made with the more extensively studied aluminium chloride-based melts, since the latter compound, like zinc chloride, is a (stronger) Lewis acid, and an associated liquid in the pure state.

Analogies may also be made with melt systems of form ACl_2-MCl, for instance, the cadmium chloride -potassium-chloride mixture. Differences in Lewis acidity and the structural units present in such melts will of course cause variations in solvent properties.

2.2 Melt preparation and reactivity with water

The presence of water has long been recognised as an undesirable impurity in molten chlorides, and a number of studies have presented evidence for the hydrolysis reaction (see e.g. 27,30):

$$H_2O + 2Cl^- \longrightarrow O^{2-} + 2HCl \qquad (2.1)$$

For example, in $NaCl-ZnCl_2$ melt at 360°C, the equilibrium constant for reaction (2.1) has been determined by means of of an oxide-responsive electrode as $1.9X10^{-7}$ (31),a surprisingly low value considering the hygroscopic nature of zinc chloride at room temperature. However, the anhydrous substance at 90°C is apparently not deliquescent if the water vapour pressure is less than 10mm Hg (32). Also, molten zinc chloride in

a hydrocracker at 400°c is not readily hydrolysed, though reactions with ammonia and hydrogen sulphide go to completion (33). Neutron diffraction studies of pure zinc chloride melts indicate that water molecules only enter the first coordination sphere of zinc at relatively high H_2O-Cl^- ratios (2:1) (34). The mixtures with alkali halides are considerably less hygroscopic at ambient (and higher) temperatures and less readily hydrolysed (35).

However, commercial zinc chloride contains considerable amounts of moisture. To purify the compound, the procedures reviewed by White (36) may be invoked. Non-chemically bound water can be removed by warming under vacuum, while oxide, hydroxide etc, may be converted to chloride by treatment of the melt with hydrogen chloride gas or chlorine . The latter substances may subsequently be purged from the melt by flowing argon. The treatment is completed by controlled-potential electrolysis to remove metallic impurities, followed by filtration. The authors reviewed in this survey have generally employed some or all of these stages; particularly the treatment with hydrogen chloride or chlorine. Estimations of melt purity are rarely reported, though for KCl-$ZnCl_2$ melts, treatment with HCl for 2-3 hours can achieve an oxygen content of < 500ppm (analysis by neutron activation) (37). The alternative approach to preparing dry zinc chloride, i.e. from the anhydrous elements, has rarely been used.

Finally, it may be noted that it is uncertain to what extent soluble oxychlorides may be formed in zinc

chloride-based melts or even in chloroaluminate melts, though insoluble oxides are known to be formed by hydrolysis (38).

2.3 Structural studies

Early raman spectral studies of pure zinc chloride indicated that, at almost 200°C above the melting point, the majority of Zn-Cl bonds are bridging rather than terminal (39) suggesting a polymeric structure is retained even at this temperature. Progressive additions of an alkali chloride e.g. potassium chloride causes a reduction in intensity of the bands due to bridging Zn-Cl bonds, while the intensity of the terminal bonds is initially increased, but then decreases. At the $2ZnCl_2.3KCl$ composition, the bands attributed to $ZnCl_4^{2-}$ dominate the spectrum. A recent raman study (40) supports this model of progressive depolymerisation on addition of potassium chloride to the melt. Table 2.1, taken from this reference, shows the various species assigned to the observed raman bands in $ZnCl_2$-KCl mixtures: $(ZnCl_2)_n$, $ZnCl_2$, $ZnCl^+$, $ZnCl_3^-$, and $ZnCl_4^{2-}$ are all postulated.

Thus the raman data can be interpreted to provide a picture of largely covalent polymeric melts dissociated to various degrees into ionic species. A rather different view was taken by Biggin and Enderby (41). On the basis of neutron diffraction studies, the authors concluded that pure molten zinc chloride has a structure explainable by a largely ionic Zn-Cl bond. The anomalous transport properties attributed to "association", i.e. high

Table 2.1 Raman Spectra assignments for the KCl - $ZnCl_2$ system.

compn	Raman shift $\Delta\nu$, cm^{-1} [a]							
$ZnCl_2$		233	233			292		
$2ZnCl_2 \cdot 1KCl$			233			292		
$1ZnCl_2 \cdot 1KCl$	85					292		
$1ZnCl_2 \cdot 2KCl$	92				280			
$1ZnCl_2 \cdot 4KCl$	92				280			
assignt			poly		$ZnCl_4^{2-}$	$ZnCl_3^-$		
$ZnCl_2$	75 w		226 s, p	250 w			305 w	306 w
$4ZnCl_2 \cdot 1KCl$	80 w		226 s, p			288 w, p		349 w
$2ZnCl_2 \cdot 1KCl$	75 w		226 s, p			290 w, p		344 w, p
$1ZnCl_2 \cdot 1KCl$	80 w	125 w	218 vw			292 m, p		
$2ZnCl_2 \cdot 3KCl$	70 w	120 w				294 s, p		
$1ZnCl_2 \cdot 2KCl$	75 w	124 w				283 s, p		
assignt	poly, b, def		poly, b	poly, b		poly, t	poly, t	poly, t
$ZnCl_2$			230	266			305	
assignt			poly	$ZnCl_n^{2-n}$			$ZnCl_2$	
$ZnCl_2$	80 w, d	90, w, d	227, s, p	270 w, p			310 w, p	350 vw
$9ZnCl_2 \cdot 1KCl$	82 w, d	106 2, p	230 s, p	262 w, p			300 w, p	340 w, p
$7ZnCl_2 \cdot 1KCl$		95 w, d	232 s, p	260 w			304 w, p	350 w, p
$4ZnCl_2 \cdot 1KCl$	80 w, d	106 w, d	230 m, p	260 vw			30 ..	w
$3ZnCl_2 \cdot 1KCl$	80 w, d	106 w, d	230 m, p				304 m, p	350 w
$2ZnCl_2 \cdot 1KCl$		95 w, d	235 w, d			290 s, p	304 w	
$1ZnCl_2 \cdot 1KCl$	80 w, d	95 w, d	230 vw			290 s, p	310 vw	350 vw
$1ZnCl_2 \cdot 3KCl$			230 vvw		270 s, p			360 vvw
assignt			poly	Zn–Cl–Zn [b]	$ZnCl_4^{2-}$	$ZnCl_3^-$	$ZnCl_2$	$ZnCl^+$
$1ZnCl_2 \cdot 1KCl$	75 d		230 p			295 s, p		
$5ZnCl_2 \cdot 6KCl$	75 d		230 p			291 s, p		
$3ZnCl_2 \cdot 4KCl$	75 d					290 s, p		
$2ZnCl_2 \cdot 3KCl$	75 d					286 s, p		
$1ZnCl_2 \cdot 2KCl$		110 d			280 s, p			
assignt					$ZnCl_4^{2-}$	poly [c]		

a, Abbreviations: s, strong; w, weak; vw, very weak; vvw, very very weak; p, polarised; d, depolarised; b, bridge Zn–Cl stretch; def, deformation; t, terminal Zn–Cl stretch; poly, $(ZnCl_2)_n$ polymer. b, The band is assumed to be associated with an unstable species containing at least one Zn–Cl–Zn stretch. c, These bands are assigned to a smaller $(ZnCl_2)_n$ polymer.

(from ref. 40)

Table 2.2 Structural details for solid and molten $ZnCl_2$

Form of $ZnCl_2$	Zn–Zn Distance (Å)	Zn–Zn Coordination number	Cl–Cl Distance (Å)	Cl–Cl Coordination number	Zn–Cl Distance (Å)	Zn–Cl Coordination number
α solid	3.82	4	3.82	8	2.34	4
β solid	3.77	4	3.78	12	2.31	4
γ solid	3.70	4	3.70	8	2.27	4
δ solid	—	4	3.71	12	2.27	4
Glassy state at 120 K (EXAFS)	—	—	—	—	2.34	5.22
Liquid state at 603 K (EXAFS)	—	—	—	—	2.35	5.07
Liquid at 596 K (x-ray)	3.66†	4†	3.85†	12†	2.29†	4†
Liquid at 600 K (N.D.)	3.8 ± 0.1	4.7 ± 0.8	3.71 ± 0.02	8.6 ± 0.5	2.29 ± 0.02	4.3 ± 0.3

† These are the values of the input parameters used in a near-neighbour model to give the best fit to the total x-ray pattern.

(N.D.=Neutron Diffraction) (from ref. 41)

viscosity as compared with, say, molten $SrCl_2$ or $BaCl_2$, are instead attributed to the close packing of Cl^- in the melt, providing tetrahedral sites for the Zn^{2+} ions, and restricting the mobility of the latter. Table 2.2, reproduced from this reference, compares Zn-Zn, Cl-Cl and Zn-Cl distances and coordination numbers obtained by various techniques; the results of Biggin and Enderby (41) seem to indicate that liquid zinc chloride most closely resembles the gamma form of the solid which has layers of cubic close-packed chlorine atoms, with zinc in tetrahedral holes between alternate layers. A computer simulation of molten zinc chloride (see ref. 41) based on an ionic model was considered to confirm the neutron diffraction results.

It must be pointed out that X-ray evidence (42) suggests that the alpha, beta and gamma forms owe their structure to the presence of small amounts of hydroxyl groups (due to the aqueous preparative methods) and thus are not true polymorphs.

2.4 Transport and physico-chemical properties

2.4.1 General

Janz et al (43) have systematically reviewed determinations of electrical conductance, density, viscosity and surface tension in molten zinc chloride and its mixtures up to 1975. Each reference was critically evaluated, and the most reliable data selected on the basis of the experimental technique employed, and staistical analysis of the results. Since 1975 only a handful of determinations appear to have been carried out.

Of most interest are those due to Ejima et al (44,45,46), who attempted to relate changes in transport properties of zinc chloride-alkali chloride mixtures (M=Li,Na,K,Cs) to composition changes. The results for various properties are considered briefly below.

2.4.2 Electrical conductance

For the pure zinc chloride measurements of specific conductance (K) carried out by numerous workers are found not to agree closely over a wide temperature range, possibly due to variations in melt purity (47). The conductance does not obey the Arrhenius equation, that is, a plot of ln K versus 1/(absolute temperature) is curved. This is evidently due to structural changes resulting in rapid conductivity increases as the temperature rises. For the alkali chloride binary mixtures, the conductivity variations do not show any marked maxima or minima, as is found, for example, at the 50:50 mole% composition in $KCl-AlCl_3$ melt (48,49), corresponding to the relatively abrupt changes in component activity at this point (figs. 2.1 and 2.2).

2.4.3 Density

Janz et al (43) have recommended the data of Bloom and Weeks (49) for the pure zinc chloride. For the alkali chloride binary mixtures, Ejima et al (44) supplemented the data of the latter authors to obtain consistant results over the entire composition ranges. The excess molar volume and partial molar volume exhibited "very complicated" behaviour with both temperature and composition. From the variation in thermal expansion

Figure 2.1. Typical conductivity isotherms obtained for the KCl-$ZnCl_2$ melt. (from ref. 48).

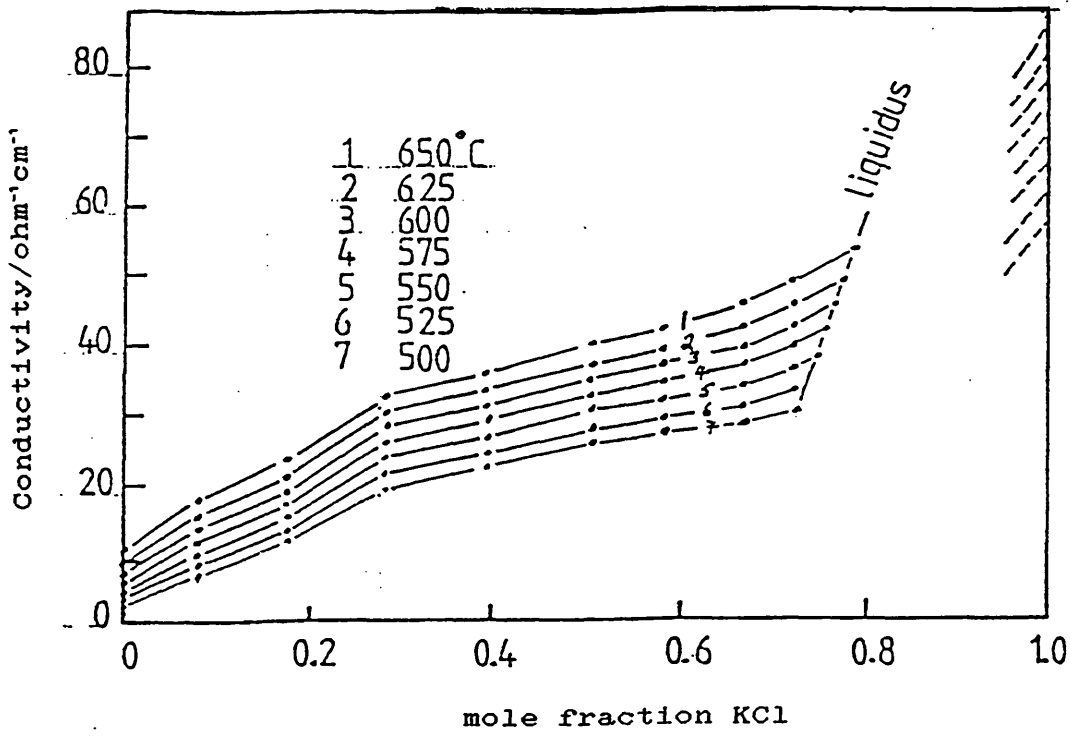
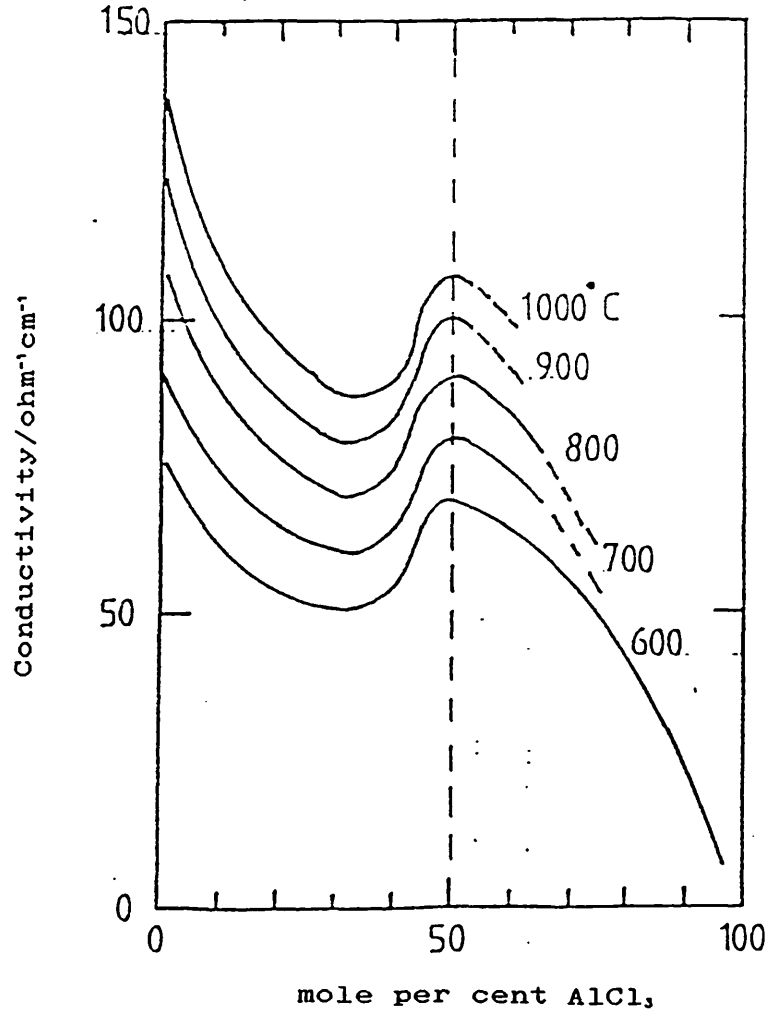


Figure 2.2. Typical conductivity isotherms obtained for the KCl-$AlCl_3$ melt. (from ref. 49).



coefficient with increasing alkali chloride content, a change from associated liquids to ionic melts was inferred at the 50:50 mole% composition.

2.4.4 Viscosity

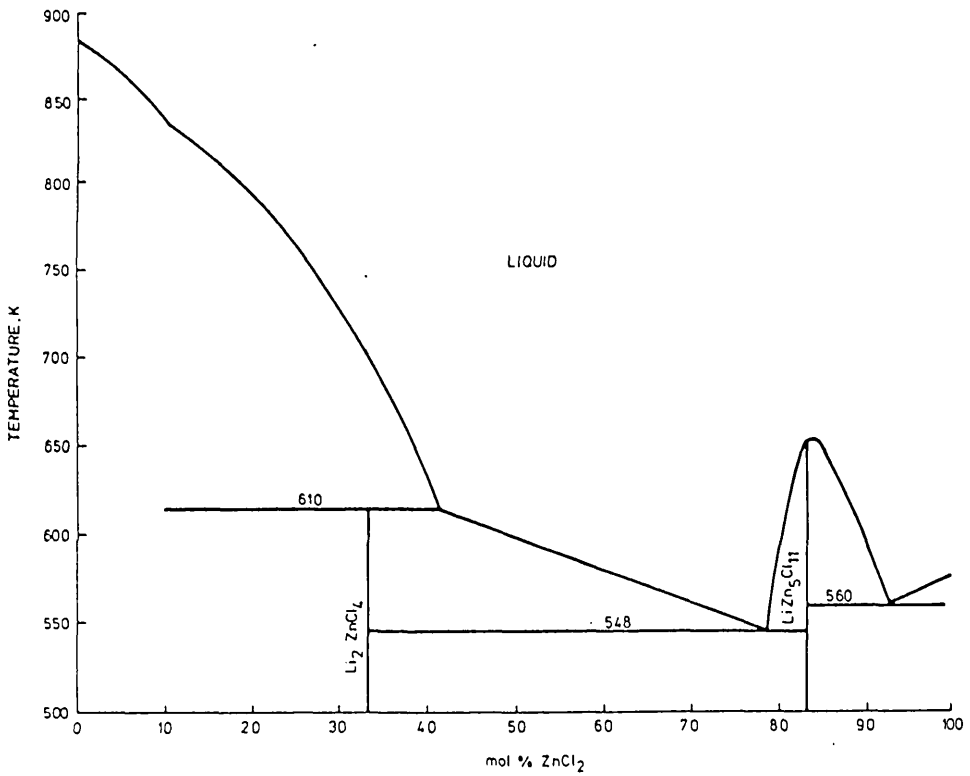
Ejima et al (45,46) have also obtained results for the viscosities of the $ZnCl_2$-MCl systems (M=Li,Na,K,Cs). In contrast to lithium and sodium-based melts, potassium and cesium binary mixtures after an initial decrease with MCl content, showed maxima in viscosity and activation energy at the 66mole% MCl compositions, which the authors correlated with the formation of $ZnCl_4^{2-}$, due to the greater Cl^- donor ability of KCl and CsCl. However, Bloom (2) has observed that there appears to be little or no relationship between complex formation and viscosity. For instance, there is no obvious correlation between viscosity and conductivity minima in the KCl-$CdCl_2$ system.

The viscosity of pure zinc chloride, like the conductivity, exhibits a curved Arrhenius plot (45).

2.4.5 Phase diagrams

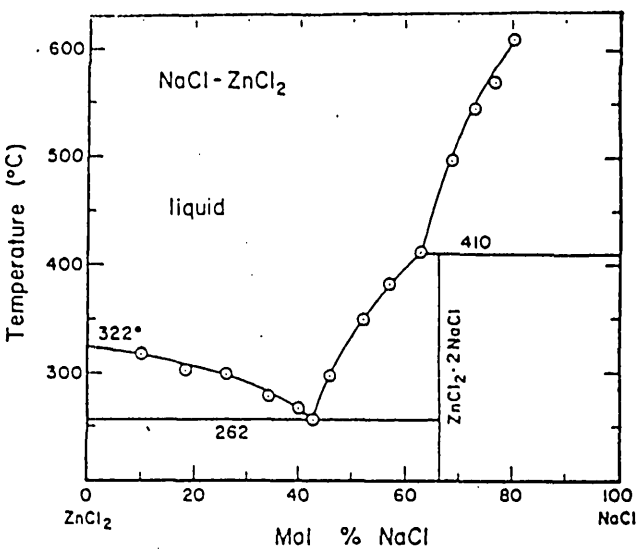
Phase diagrams for MCl-$ZnCl_2$ systems are reproduced in figure 2.3. These are taken from Janz (43), apart from the LiCl and KCl-based binaries, which are more recent assessments (50,51). The usual trend towards greater complexity as the alkali metal cation increases in size (2) can be observed. The KCl-$ZnCl_2$ system, for example, forms three eutectic mixtures, with respective zinc chloride contents (mole%) and melting points: 31.5, 432°C; 54, 230°C; 72, 262°C (37).

Figure 2.3. Phase diagrams for $MCl-ZnCl_2$ systems.



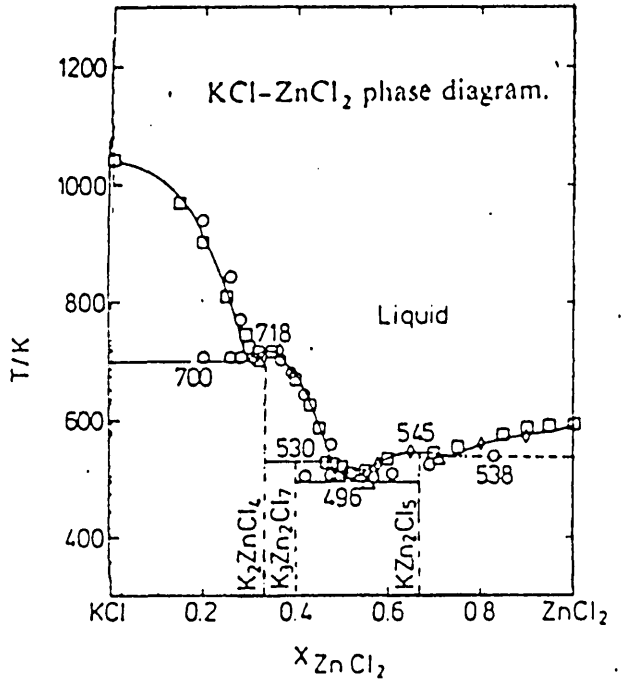
$LiCl-ZnCl_2$ Phase Diagram

(from ref. 51)

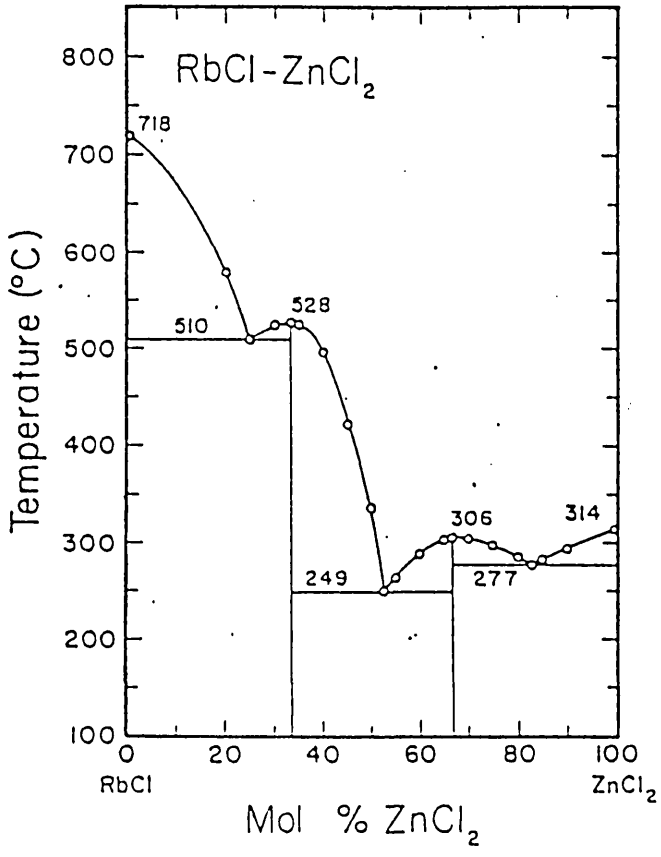


Temperature-composition phase diagram for $NaCl-ZnCl_2$.

N. N. Evseeva and A. G. Bergman, Izv. Sekt. Fiz.-Khim. Anal., Inst. Obshch. Neorg. Khim., Akad. Nauk S.S.S.R., 21, 208 (1952).

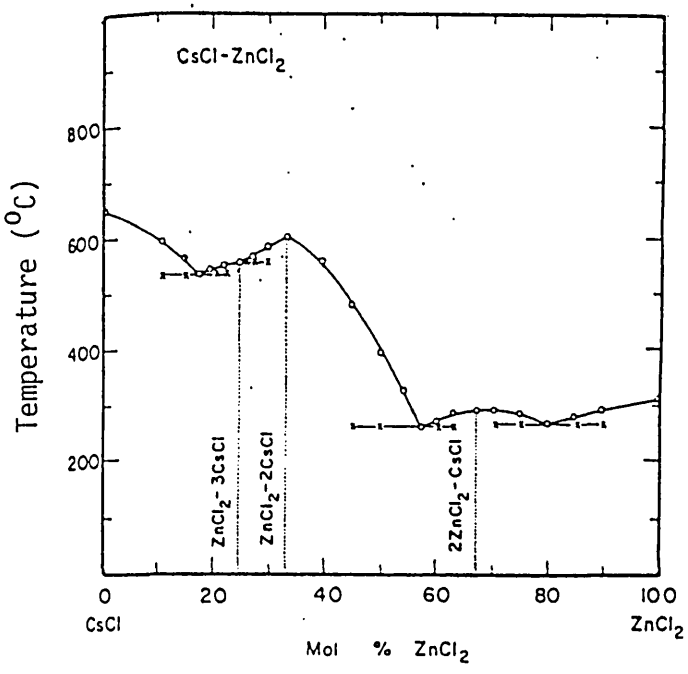


(from ref. 50).



Temperature-composition phase diagram for RbCl-$ZnCl_2$.

F. B. Markov, I. D. Panchenko and T. S. Kostrenko, Ukr. Khim. Zh., 22, 287 (1956)



Temperature-composition phase diagram for CsCl-$ZnCl_2$.

B. R. Markov, I. D. Panchonko, and T. G. Mostenko, Ukrain. Khim. Zhur., 22, 287–91 (1956).

Figure 2.3 continued. Phase diagrams for MCl-$ZnCl_2$ systems.

The LiCl-KCl-$ZnCl_2$ system is reported to have a miscibility gap (51).

2.4.6 Vapour pressure

The vapour pressure of zinc chloride, both pure and in its mixtures with alkali chlorides (M=Na,K), has been determined as a function of temperature by Moss (52) and Bloom et al (53). At 500°C, for example, the vapour pressure of pure zinc chloride is roughly 1mm Hg. Robertson and Kucharski (54) determined vapour pressure relations for KCl-$ZnCl_2$ and CsCl-$ZnCl_2$ mixtures. The vapour pressure decreases with increasing size of alkali metal cation, and was apparently not significant for CsCl mole fractions >0.48, up to 800°C, showing the greater chloride ion donating ability of the cesium cation, which produces a corresponding decrease in $ZnCl_2$ activity.

In the KCl-$ZnCl_2$ system, complex vapour phase species have been postulated, e.g. $KZnCl_3$ and $ZnCl_2$ dimers (52). The latter species is also thought to occur in the vapour of pure zinc chloride (53).

2.5 Electrochemical studies

2.5.1 Formation and concentration cells

These cells have frequently been used with molten chloride electrolytes. For obtaining accurate thermodynamic data, the formation cell is preferred over other types (e.g. concentration cells) as these cells do not give rise to unknown junction potentials. The simplest configuration of formation cell involves a metal electrode and a chlorine electrode dipping into the melt.The only recent and reliable values of emf for the

cell: $Zn/ZnCl_2(+MCl)/Cl_2,C$ (M= K,Rb,Cs) would appear to be those of Robertson and Kucharski (54). These authors used a cell which minimised loss of zinc chloride by volatilisation. The salts were purified by dehydration under vacuum, followed by fusion under hydrogen chloride gas, which was then bubbled through the melt. The chlorine electrode was pre-saturated with the gas. Stable, reproducible potentials were obtained after saturating the melt with chlorine gas; in the case of zinc chloride-melts, this could take up to one day. The results were corrected for the lowering of the chlorine partial pressure by zinc chloride vapour (significant above 500°C).

The authors also compared their results for $E°(ZnCl_2)$ with values calculated from thermochemical data (5,55-57). The results agree well with one set of thermochemical data (57), but considerable differences are observed between the other sets of E° data (fig. 2.4).

Figure 2.5 shows a plot of zinc chloride activity versus mole fraction for the $MCl-ZnCl_2$ systems, derived from cell data at varying temperatures, where M=Li (58), Na (59,60), K,Rb,Cs (54) (see also below). A consistant trend of increasing negative deviation from ideality with increasing cation radius can clearly be seen, though more data at similar temperatures are required for a better comparison.

Formation cells of type:

Na/Na^+-conductor/$ZnCl_2$+NaCl/Cl_2,C where the reactive sodium metal must be isolated from the melt, have also

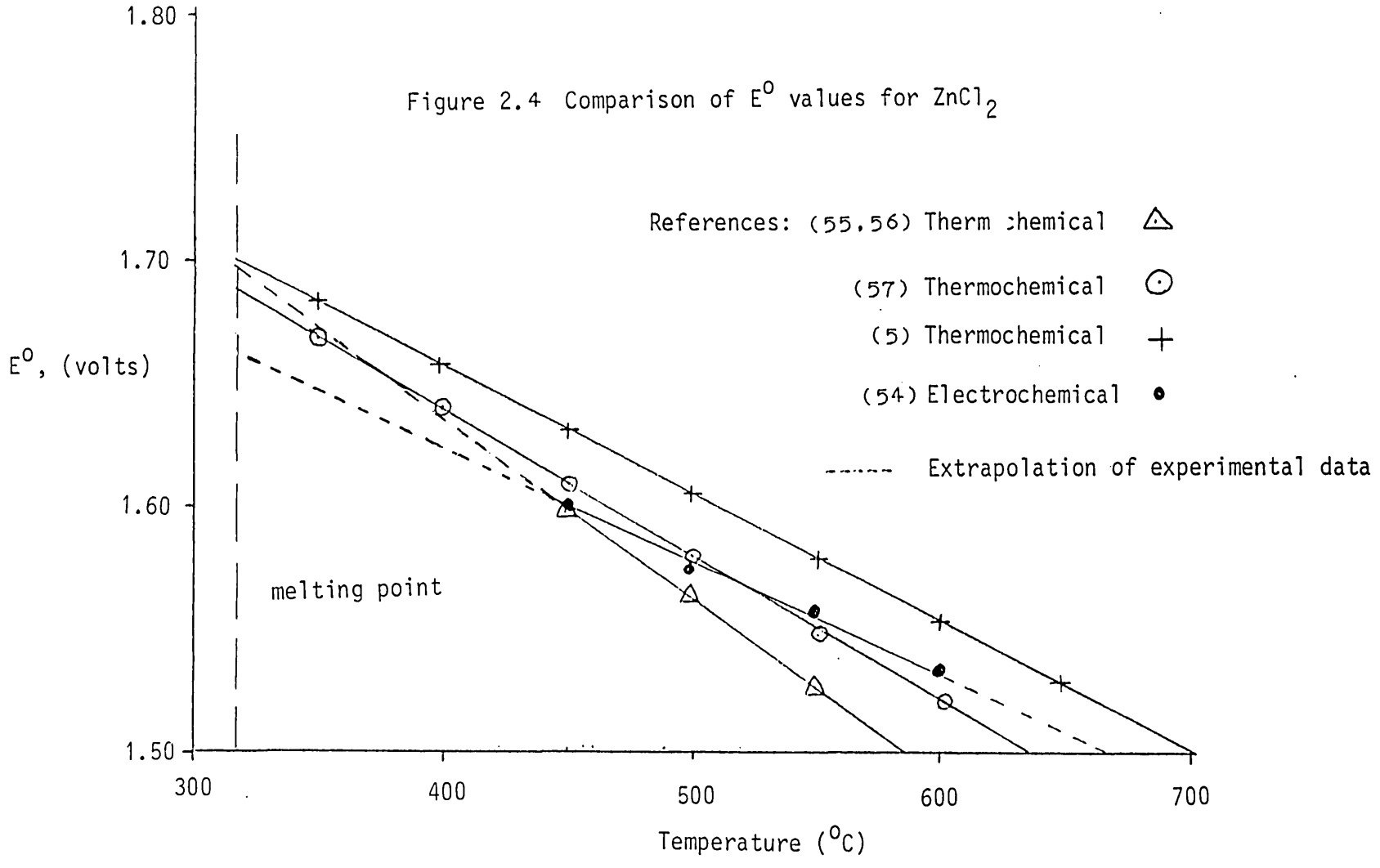


Figure 2.4 Comparison of E^o values for $ZnCl_2$

been studied. For example, Flinn and Stern (61) have investigated the membrane potential of sodium beta-alumina in HCl-treated $ZnCl_2$-NaCl melts, and concluded that the sodium ion selectivity of the beta alumina was similar to that of pyrex glass, i.e. virtually 100% sodium ion conduction. However in the same paper it was also shown that zinc ions could be incorporated into the sodium beta alumina if electrolysis was carried out, reducing the conductivity. The zinc was not removed by reverse electrolysis.

Again in the HCl-treated NaCl-$ZnCl_2$ system, Dudley and Inman (60) determined the activity of sodium chloride using the formation cell formulated above. Figure 2.6 shows the variation of sodium chloride activity with composition, and also the change in zinc chloride activity calculated by the Gibbs-Duhem integration. The cell emf was found to vary with temperature according to the Nernst equation, $E=E^{\circ}-(RT/F)\ln a_{NaCl}$, indicating a reversible cell reaction. This study demonstrates that the change in sodium chloride activity is not so abrupt as in the analogous aluminium chloride system (10), though considerable deviation from ideality does occur.

The latter results may be compared with those of Lesourd et al (59). These researchers employed the cell: $Zn/ZnCl_2$+NaCl/pyrex/$NaNO_3$/AgCl,Ag. Figure 2.5 shows these results for the activity of zinc chloride. It can be seen that the values of Lesourd et al indicate a greater positive deviation from ideality than do the formation cell results of Dudley and Inman (60). The latter values

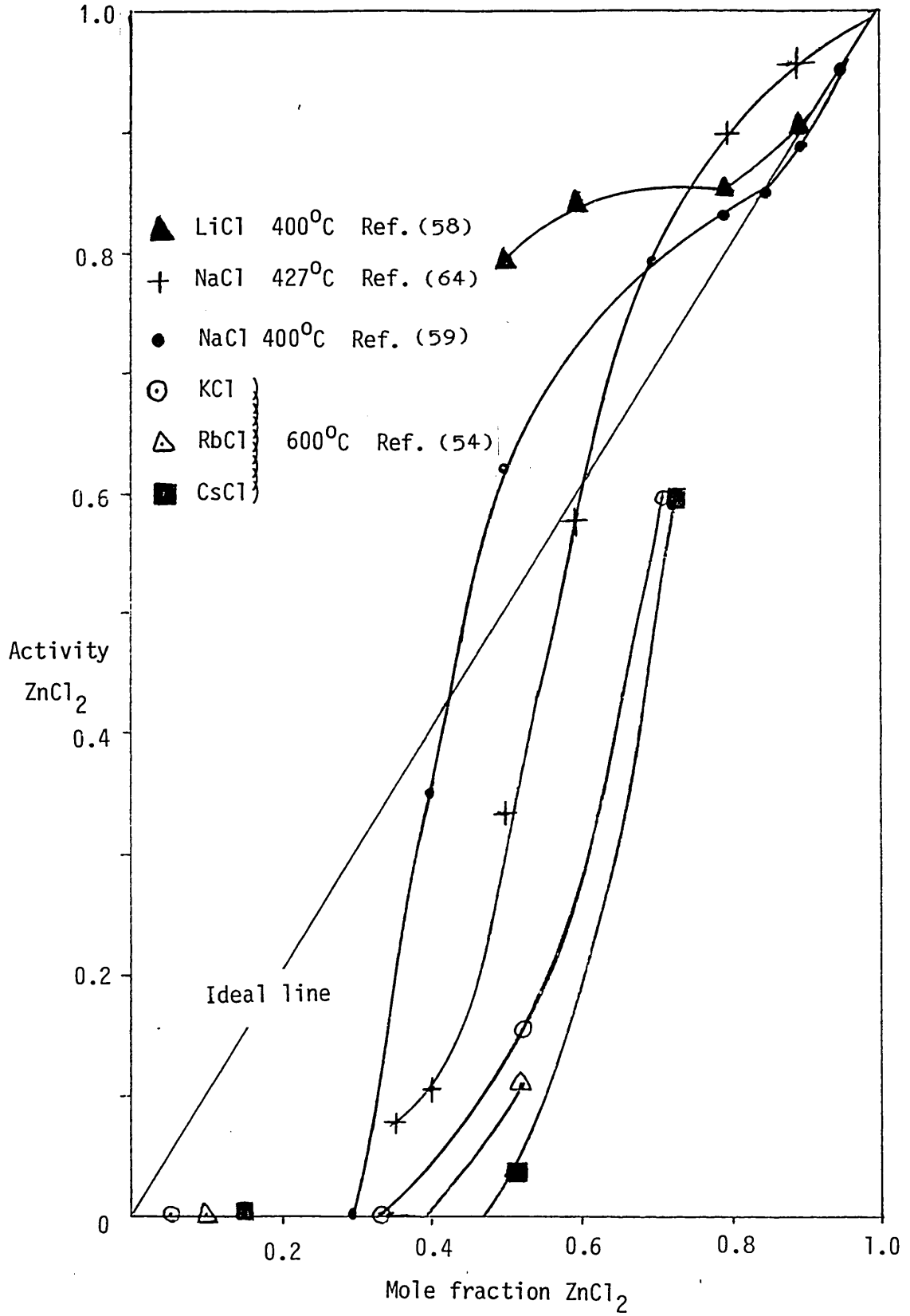


Figure 2.5 Activity of zinc chloride in the MCl - $ZnCl_2$ systems.

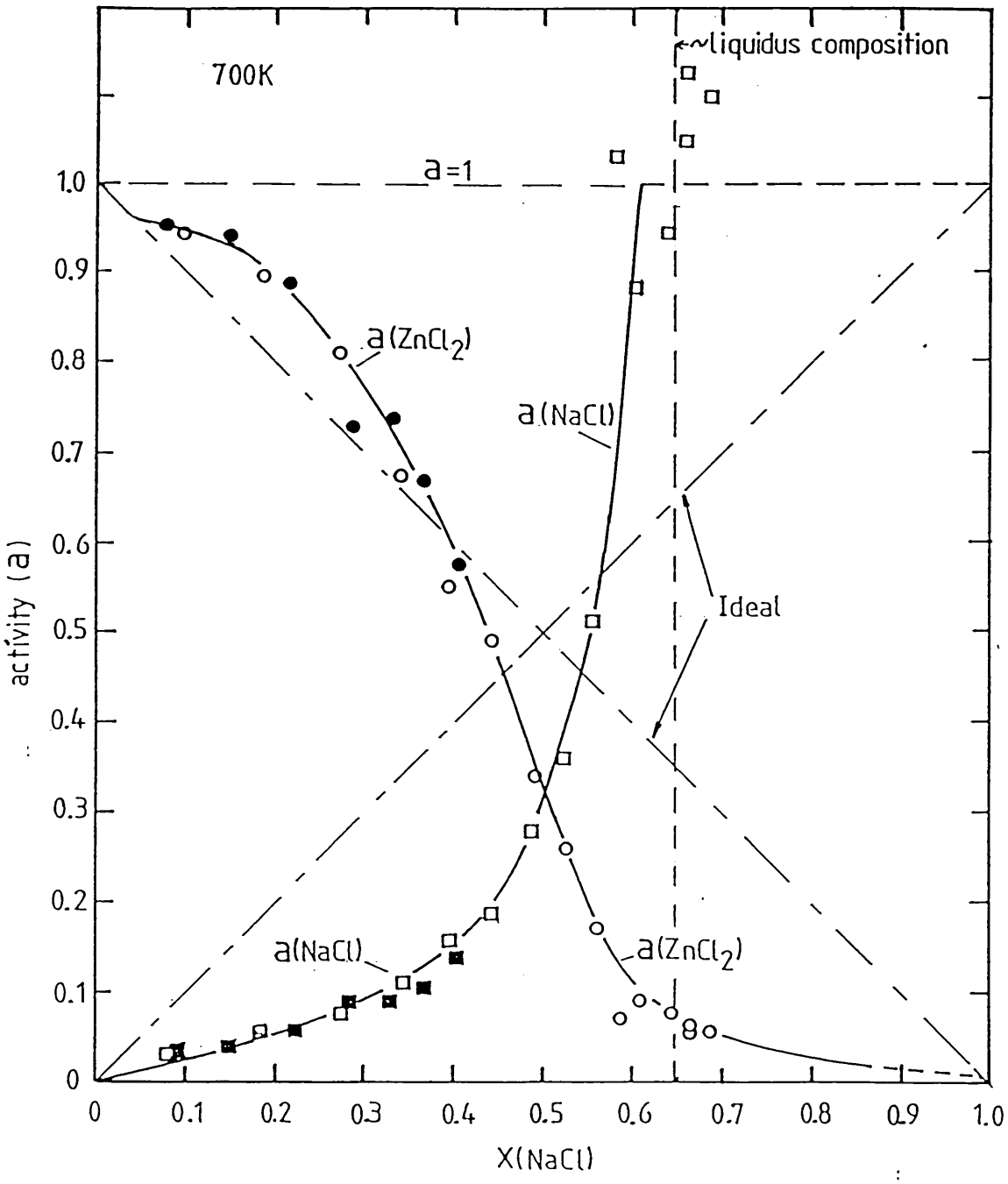


Figure 2.6. Activities of sodium chloride and zinc chloride as a function of melt composition in the sodium chloride -zinc chloride system at 700K.

(from ref. 64)

are however to be preferred, since the interpretation of the cell emf as reported by Lesourd et al involves a number of free energy terms of questionable accuracy, and also a possibly significant liquid junction potential.

The latter workers (58) also reported results for the equivalent cell containing LiCl in place of NaCl; this system showed a greater positive deviation in the 0-0.5 mole fraction alkali chloride region (fig.2.5).

Matsunaga and Hosokawa (62) studied the dependance of zinc electrode potential in the concentration cell:

$Zn/ZnCl_2$(reference)+NaCl/$ZnCl_2$(x)+NaCl/Zn

A pyrex membrane was used to separate the two solutions, acting as a sodium ion conductor. A chlorine electrode was also coupled with the reference half-cell, and the variation in chloride ion activity with composition was deduced, at 450°C. The single ion activity, however, cannot be readily compared with thermodynamic activities of melt components.

The reversibility of a pyrex membrane to sodium ions in sodium chloride-zinc chloride melts was demonstrated by Bartlett and Crowther (63) in the cell:

Na/pyrex glass/$ZnCl_2$+NaCl/Zn. At low sodium chloride concentrations (<0.1 mole kg^{-1}) (where the solute presumably obeys Henry's law) a linear dependence of the potential on sodium chloride concentration was found, with the slope as predicted by the Nernst equation. Micropolarisation tests confirmed the reversibility of the electrode.

Finally, the results of Dudley and Inman (64) for the

cell W,Na(l)/beta alumina/$ZnCl_2$-NaCl/Zn(l),W may be considered. The emf for this cell should conform to:

$$E=E^{\circ}-(RT/2F)\ln\{(NaCl)^2/(ZnCl_2)\} \qquad (2.2)$$

This potential corresponds to the difference of two formation cells involving the production of sodium chloride and zinc chloride respectively. Thus from their results for the sodium chloride formation cell (60) the authors could predict the emf of the above cell. However, stable emfs were not achieved with this cell. This was attibuted to the slow formation of a layer on the zinc electrode, due to residual moisture, and causing a drift of emf with time; a large emf drop (50mv) was observed on forming a fresh liquid zinc surface. Thus the melt purity may affect the reversibility of the zinc electrode.

2.5.2 Voltammetric studies

A number of reports deal with the voltammetric behaviour of solutes in zinc chloride melts, and also with the electrochemical reactions of electrode materials. For example, Susic and Mentus (65) reported that a platinum electrode in molten zinc chloride formed a passive layer of $PtCl_2$ at anodic potentials. At cathodic potentials, deposited zinc appeared to alloy with the platinum. Similar results were obtained in $ZnCl_2$-NaCl and LiCl-KCl-$ZnCl_2$ melts. A glassy carbon electrode however showed only reactions due to the decomposition of the melt (zinc deposition and chlorine evolution).

Minh and Welch (83) studied the reduction of hydrogen chloride dissolved in LiCl-KCl-$ZnCl_2$, while Perry and

McDonald (37) investigated the behaviour of hydrogen chloride in KCl-$ZnCl_2$. Large discrepancies were apparent between the calculated diffusion coefficients of hydrogen chloride betwen this study and that of Minh and Welch, probably due to uncertainty in the solubility of HCl in these melts, rather than differences in melt composition.

Rubel and Gross (66) compared the electrochemical oxidation of Pt, Ni, Mo and W electrodes in AgCl-KCl and $ZnCl_2$-KCl (49-51 mole%) melts. The results for platinum agree with those of Susic and Mentus (65) above, i.e. in both melts the metal could be oxidised to a passivating layer of the chloride, and a zinc alloy was formed at relatively cathodic potentials in the latter melt. Nickel could be anodically dissolved as Ni(II), and deposited from the solutions. Molybdenum formed soluble Mo(III) in both melts, and could also be deposited. Tungsten also formed the +3 state in AgCl-KCl, but in the zinc chloride melt, soluble W(VI) was produced, possibly as an oxychloro- complex, as a soluble oxide layer was postulated to form initially on the electrode, presumably due to oxygen contamination of the latter melt. Tungsten metal could apparently be electro-deposited from this solution. Tungsten metal has however frequently been used as an "inert" electrode in chloride melts (67).

Topol et al (68) performed cyclic voltammetric studies on a number of solute species in a $ZnCl_2$-NaCl-KCl melt (60-20-20 mole%). The following oxidation states were accessible within the electrochemical window of the melt: Ag(0), Ag(I), Cu(0), Cu(I), Cu(II), Ni(0), Ni(II), Bi(0),

Bi(III), Sb(0), Sb(III), Cr(0), Cr(II), Cr(III), Fe(II) and Fe(III). Additionally metallic Cu, Al, Be, and Mg were capable of displacing zinc from the melt and were oxidised to the respective chloride solutions. The solubilities of $NiCl_2$, $CrCl_3$, $CuCl_2$, and $FeCl_3$ were less than 15wt% at 320°C.

In comparison other workers (62) also found reversible one-electron reductions for $CrCl_3$ and $FeCl_3$ dissolved in $ZnCl_2$-NaCl (53-47 mole%) at 300°C; however chromium(II) could not be reduced to metal before zinc deposition, though metallic iron could be deposited from the iron(III) solution.

Electrochemical reactions have also been reported for germanium and indium (69), and chromate(VI), cadmium and mercury (70) in relatively basic alkali chloride-zinc chloride melts. The mercury(I) state was not stable in the equimolar NaCl-$ZnCl_2$ melts, but the Cd^{2+}_2 ion appeared to have a transient existence before disproportionating to metal and Cd^{2+}.

The lower oxidation states of bismuth can be stabilised in chlorozincate melts, as in chloroaluminates (14) (see chapter 1).

2.5.3 Chronopotentiometric studies

Two such studies have indicated the existance of the Zn^{2+}_2 ion in solutions of metallic zinc in pure zinc chloride. The solubility as determined by Vetyukov and Francis (71) was low, 0.187 mole% at 525°, and 0.326 mole% at 600°C. A two electron transfer reaction was found, consistant with the presence of the subvalent ion.

Van Norman et al (72) reported similar results, but gave a considerably lower solubility, 0.019 mole% at 500°C.

2.6 Solute behaviour

There is little to be found concerning the change of solute behaviour with melt composition in zinc chloride-based melts. However Smith et al (73) have studied the rather complex changes in d-d absorption spectra of nickel(II) in the $CsCl-ZnCl_2$ system. In pure zinc chloride, some nickel ions were suggested to replace zinc in the network structure and were thus four-coordinate; however an octahedral species was also present, favoured by increasing temperature. Addition of small amounts of CsCl resulted in a complex tetrahedral-octahedral equilibria: but, at the 50:50 mole% composition, a single entity was present, with distorted tetrahedral coordination of nickel by a mixture of Cl^- and $ZnCl_4^{2-}$ ions. In CsCl-rich melts, the $NiCl_4^{2-}$ ion was formed.

In comparison, analogous coordination equilibria of nickel(II) were found by Angell and Gruen (74) in $KCl-ZnCl_2$ melts. In this melt, a shift towards octahedral coordination occurs in the presence of the more acidic potassium cation. In contrast to nickel, cobalt(II) had only tetrahedral coordination in this melt.

2.7 Overall summary

This survey reveals that knowledge of zinc chloride-based melts is fragmentary, and in some cases, inconsistant. This may be perhaps due to experimental difficulties associated with the hygroscopic nature of

pure zinc chloride and the high vapour pressure. Though the structure of the melts has been comparatively well-studied, controversy still exists over the degree of covalency exhibited by the systems.

From the point of view of this thesis, it was evident that a confirmatory check of the component activities in the NaCl and KCl-based melts was desirable. It is also apparent that though a number of solute species have been studied at one particular composition in a particular melt, the effect of variation in composition, on, to take one example, the disproportionation of cadmium(I) (70), is unknown.

CHAPTER THREE

EXPERIMENTAL

3.1 Melt preparation

3.1.1 Zinc chloride

A 500g batch of purified zinc chloride was manufactured using recommended techniques (36). (Apparatus shown in figure 3.1). Analar grade "anhydrous" $ZnCl_2$ was vacuum-treated at room temperature for about five days, until a pressure of about 15 microns was obtained. The temperature was then gradually raised to 200°C over several days until the original pressure was regained. HCl (dried over a molecular sieve) was then passed over the solid salt and the temperature raised until the $ZnCl_2$ melted, at which point HCl was bubbled through the melt for two hours using a porous frit. Pure argon was then substituted for the HCl, and the melt purged. The melt was then filtered through a porous frit. This was achieved by breaking a thin glass bubble at the bottom of the melt container with a glass rod, and allowing the melt to flow into an outer container and through the frit, where the melt was collected in a Pyrex beaker and quickly solidified. The solid was then transferred to a drybox, the latter with a water content < 40ppm, broken into coarse lumps and stored.

Pre-electrolysis to remove electroactive impurities (e.g. heavy metals) appeared to be unnecessary, no waves due to such impurities being detectable by cyclic voltammetry.

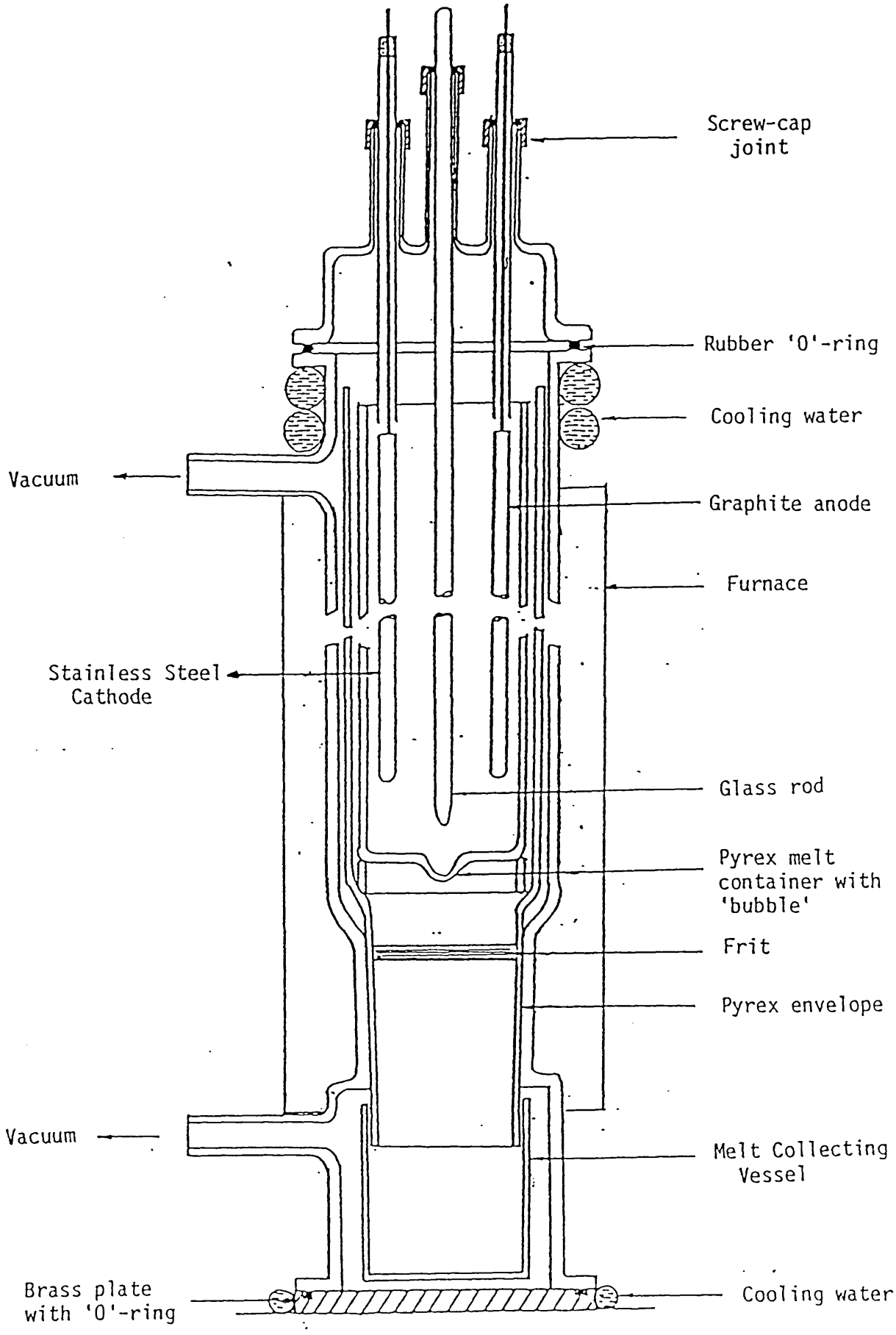


Figure 3.1 Melt Purification Apparatus

3.1.2 Sodium chloride and potassium chloride

These salts were dried by simple vacuum melting and cooling under dried argon of the respective Analar compounds. The purified salts were then stored in the drybox.

3.1.3 Lithium chloride-potassium chloride eutectic

After mixing the salts in the desired proportions (49 mole% LiCl) the purification process was analogous to that used for zinc chloride.

3.2 Vacuum and gas supply system

The vacuum system was evacuated by means of an Edwards oil diffusion pump backed by an Edwards 2SC 20A rotary pump. Pressures inside the system were monitored by means of a mercury manometer and an Edwards GS B2 Pirani gauge, and it was possible to achieve pressures of less than 10 microns with this arrangement.

High purity argon could be admitted into the system, the flow being controlled by a needle valve, and was dried by a molecular sieve and deoxygenated by passing over heated copper wool at 400°C before entering the electrochemical cell.

3.3 Furnace and temperature control

A vertical furnace was used, consisting of an alumina tube wound with 18 swg Kanthal wire and capable of operating up to temperatures up to 800°C. To allow use of the small electrochemical cell, a cylindrical aluminium container was constructed to fit snugly into the alumina tube, into which the cell fitted with a clearance of about one mm. This ensured that the cell was adequately

insulated against temperature variations.

Temperature control was with a PID 15 Eurotherm controller which monitored a Pt/Pt-13%Rh thermocouple placed within the furnace tube, and regulating the temperature to plus or minus 1°C.

3.4 Electrochemical cell

The cell consisted of a flat-bottomed Pyrex tube, 20 cm long and 5.4 cm diameter. At the top of the tube was an 8.5 cm o.d. glass flange. The cell head was made of Pyrex with a corresponding flange. Incorporated in the cell head were three SQ13 joints and one "Sovril 15" screw-thread joint through which electrodes, etc. could be incorporated. Two ball-joints on either side of the cell acted as gas inlet and outlet.

Vacuum-tight seals were obtained by means of screw-caps which compressed a PTFE washer, backed by a silicone rubber sleeve,on to the screw-thread joints. Finally a PTFE annulus provided a seal between the glass flanges. A diagram is shown in figure 3.2.

Before use, the cell and all glass components in contact with the melt were soaked in a 1:1 mixture of nitric and sulphuric acids for at least 24 hours. After rinsing with distilled water the components were dried overnight at 150°C. The cell was then assembled and evacuated overnight at 400°C in the furnace before filling with dry argon, cooling, and transferring to the drybox where the solid melt components were weighed into the inner container (a Pyrex Beaker). After reassembling the cell it was transferred to the pre-heated furnace and

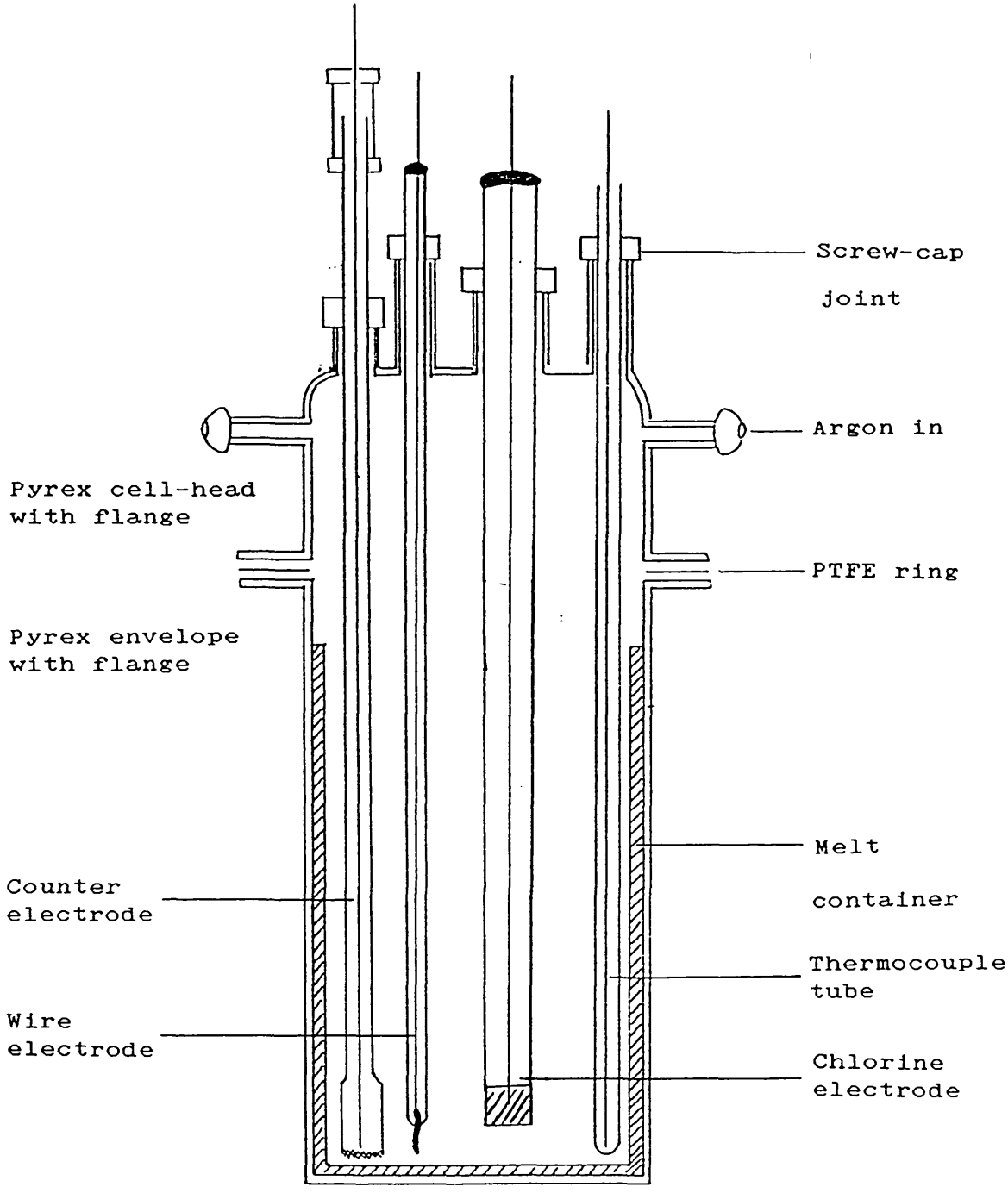


Figure 3.2. Electrochemical cell and miscellaneous electrodes.

connected to the argon/vacuum line. Residual argon was removed by evacuation and a fresh argon flow initiated through the cell before proceeding with the desired experiment.

The melt temperature was measured via a chromel-alumel thermocouple contained in a glass sheath and dipping into the liquid.

3.5 Electrodes

The following electrodes were employed for cyclic voltammetry, A.C. impedance measurements, and for cell emf measurements.

(i) Vitreous carbon microelectrode (fig. 3.3a)

A length of vitreous carbon rod (3mm dia.) was vacuum-sealed into a 6mm o.d. Pyrex tube and the working surface polished with emery paper and then on diamond polishing wheels of 5 micron, 3 micron, and finally 1 micron. Electrical contact was via a stiff copper wire pressed against the rod and immersed in a layer of graphite powder. The electrode construction was completed by filling the Pyrex tube with argon to prevent corrosion of the copper wire, and sealing with epoxy resin. A similar electrode with a 1.5mm diameter conical indentation was also prepared.

(ii) Tungsten microelectrode (fig. 3.3b)

A 2cm length of 1.5mm diameter tungsten wire was spot-welded to a length of copper wire and the tungsten sealed into a 6mm o.d. Pyrex tube. This was achieved by first sealing the tungsten into a section of 3mm o.d. tubing, and melting the larger diameter tubing around the

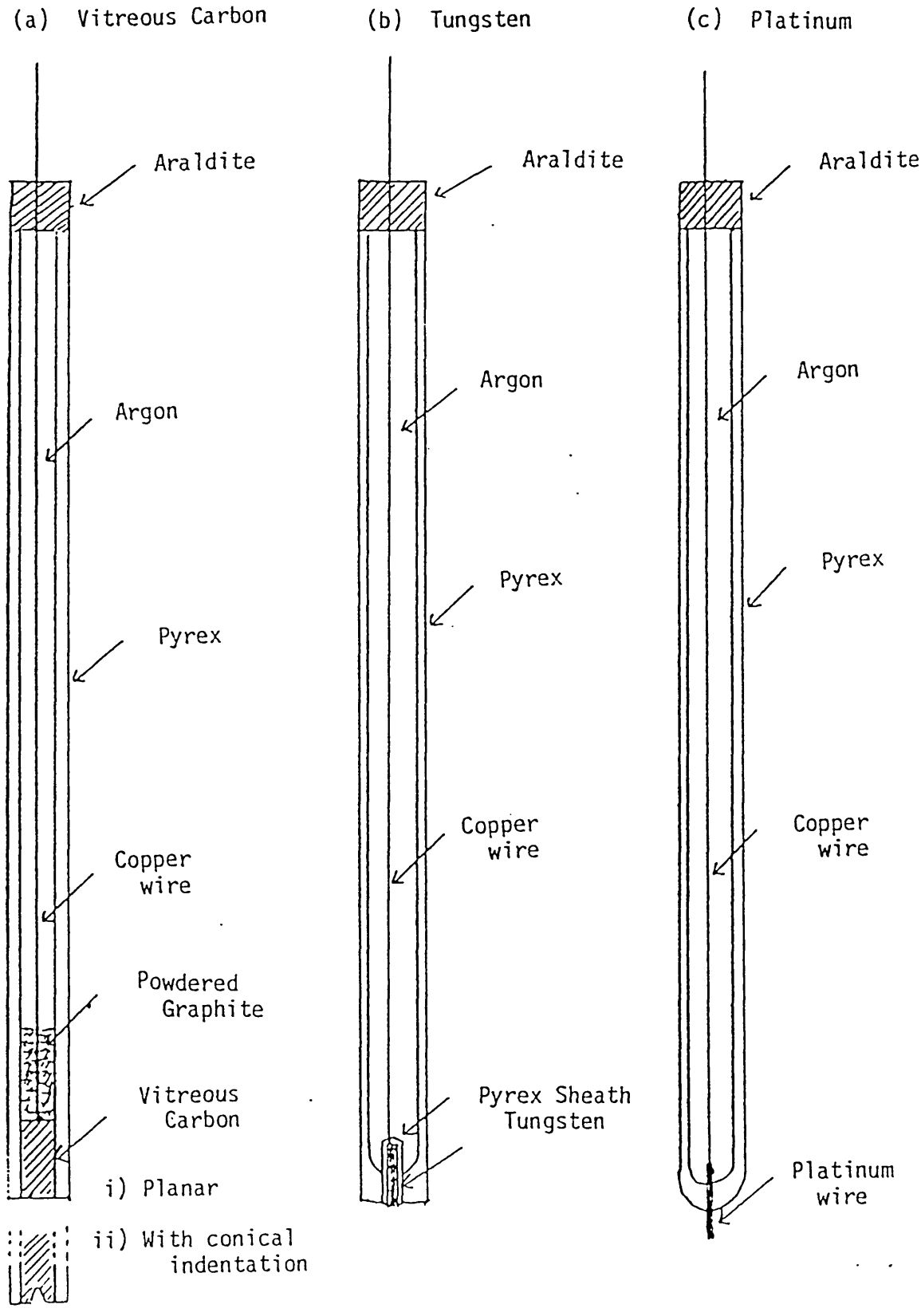


Figure 3.3 Electrodes

smaller bore tube. The tungsten surface was then polished down to 1 micron and the electrode filled with argon and sealed with epoxy resin.

(iii) Platinum wire (fig. 3.3c)

The details for the construction are analogous to those described for the tungsten electrode, except that a 2cm length of 1mm diameter platinum wire was sealed directly into a 6mm o.d. Pyrex tube and a 1cm length of this wire was left exposed below the seal. The platinum was flame-polished before use.

(iv) Gold sphere (fig. 3.4a)

This consisted simply of a length of gold wire with a small sphere at one end, the other being welded to a length of copper wire which was sheathed in a Pyrex tube.

(v) Graphite rod (fig. 3.4b)

A length of 1.5mm diameter graphite rod was inserted into a 6mm o.d. Pyrex tube with a fritted compartment at one end. At the opposite end of the tube the graphite passed through an SQ13 joint fitted with a screw cap and silicone rubber sleeve, which compressed a silicone rubber washer on to the joint providing an air-tight seal. Electrical contact was made directly to the graphite rod.

Before use, the rod was boiled in concentrated HCl and then distilled water, heated for several days at 150°C, and finally at 200°C under vacuum overnight.

(vi) Silver/silver chloride reference (fig. 3.4c)

Essentially this was a 6mm o.d. Pyrex tube with a thin bulb blown at one end which contained the silver chloride solution (0.1m AgCl in LiCl-KCl eutectic). Into this

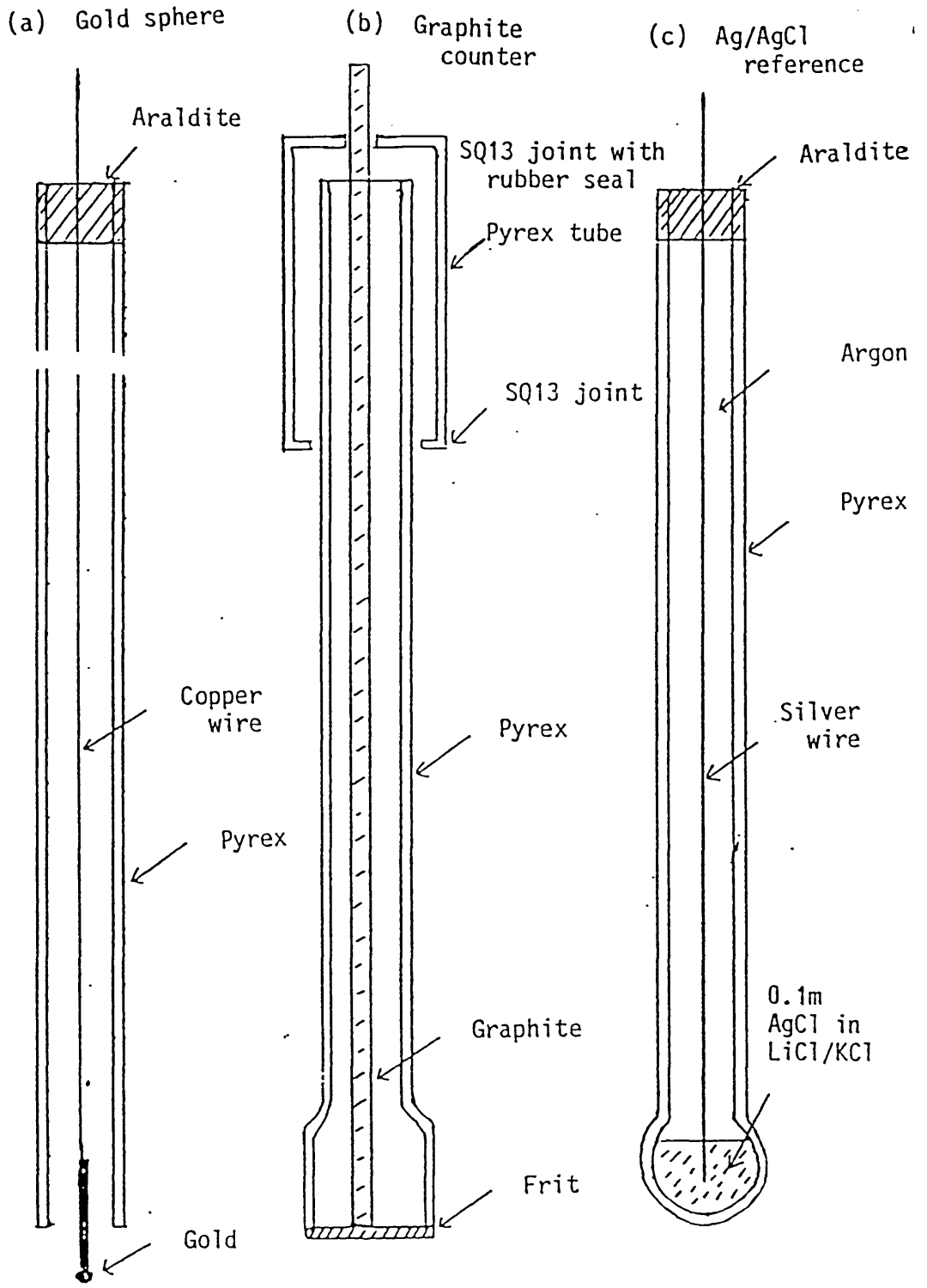


Figure 3.4 Electrodes

solution a silver wire was dipped, to which electrical contact was made. Finally the electrode was sealed with argon and sealed with epoxy resin.

(vii) Zinc rod

This was simply a length of 7mm zinc rod, suspended by a length of platinum wire, which provided electrical contact with the rod. Before use the zinc was briefly dipped into concentrated HCl to remove any oxide, rinsed and dried under vacuum.

(viii) Zinc microelectrode (fig. 3.5a)

This electrode (used in the formation and concentration cells) consisted of a vitreous carbon microelectrode (see above) with a B10/19 joint incorporated. This enabled the electrode to be inserted into a fritted compartment which effectively isolated it from the bulk electrolyte and cell atmosphere. Zinc was deposited on the vitreous carbon surface by a short constant potential electrolysis (see chapter 5).

(ix) Chlorine electrode (fig. 3.5b)

For this electrode, an 8mm Pyrex tube with a cylindrical section of porous graphite sealed into one end was prepared; this end was then ground down to expose the graphite surface. At the opposite end, a side arm with a "Rotaflo" tap was provided to act as the chlorine inlet. Electrical contact to the porous graphite was via a graphite rod which was fixed with epoxy resin into the latter end. Graphite powder was also present to ensure electrical contact.

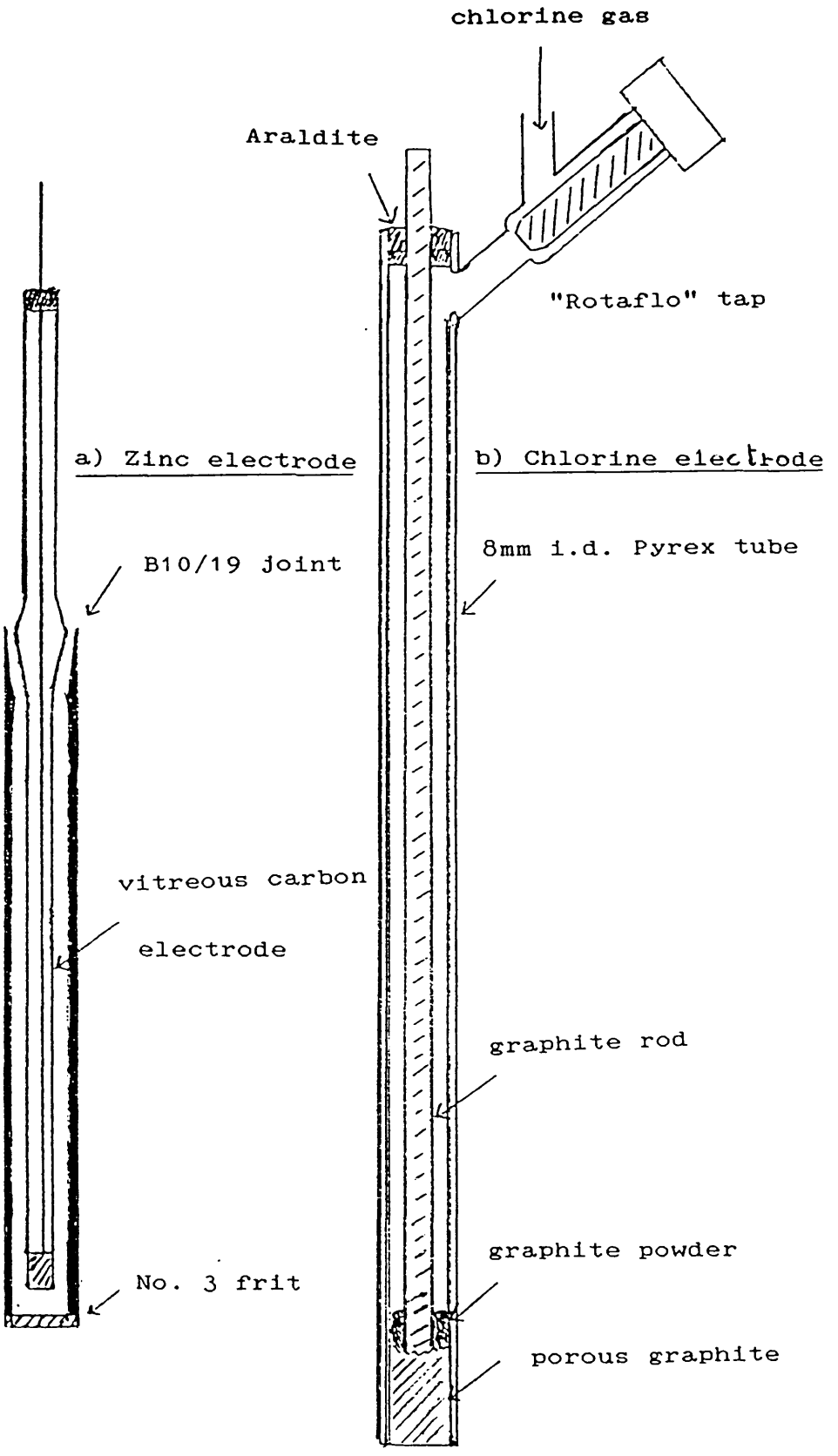


Figure 3.5. Electrodes for formation cell

3.6 Pulse generating equipment

The following set-up was employed where it was necessary to provide a constant current pulse for a specified time, and to measure the potential between two electrodes as a function of time.

The apparatus is shown as a block diagram in figure 3.6. A PARC model 175 sweep generator in conjunction with a Wenking model PCA 72L potentiostat was used to generate a constant potential (range plus or minus 10.99 V) across a resistor connected between the reference and working electrodes outputs of the sweep generator. A constant current (to within 0.01 ma) was then obtained between the working and counter electrode outputs, which were connected across the cell with resistor in series. A 180 ohm resistor was conveniently employed in the present work. The applied current was measured by a Weston 6400 DVM, to within 0.01 ma.

To generate a pulse, a timing circuit with a relay was used to connect the cell to, and isolate it from, The current generating system after the requisite time interval. The emf was then recorded on a Bryans 26000 A3 X-Y recorder as a function of time, the recorder being calibrated by a Fluke 8860A DVM (input impedance 10 M ohm) which simultaneously measured the cell emf. The timer could also be used to activate the trigger of a Datalab DL 905 transient recorder and thus obtain a digital record of the voltage/time transient.

This set-up enabled the potential/time decay curve to be recorded with an accuracy of up to 1 mV/cm and 0.1 sec.

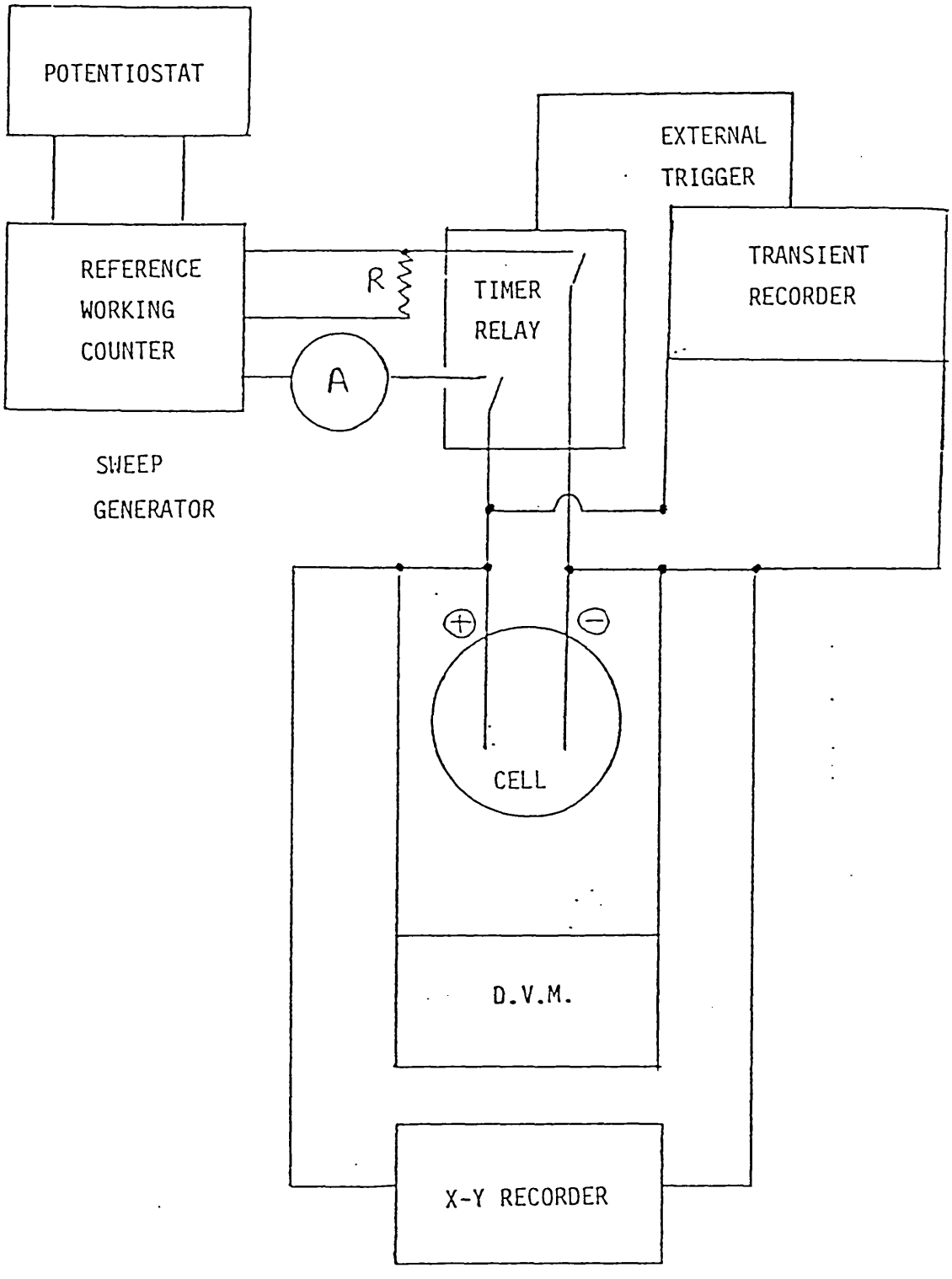


Figure 3.6 Apparatus for current pulse e.m.f. measurements.

/cm on the X-Y recorder, but greater sensitivity was obtained with the transient recorder, which was capable of measuring the potential/time curve over a 1 ms interval after a pre-set delay, with 10-bit resolution.

3.7 Cyclic voltammetry

A PARC model 175 sweep generator with a range of sweep rates from 1 mVs^{-1} to 1000 Vs^{-1}, in steps of 1 mVs^{-1}, was employed, coupled with a Wenking model PCA 72L potentiostat (range ± 10.99 V).

A three electrode system was used, with a microelectrode (vitreous carbon, tungsten, platinum or gold) as the working electrode. The counter electrode was generally a graphite rod, enclosed in a fritted compartment to prevent mixing of reaction products with the bulk melt. For reference, a zinc electrode was used (either bulk zinc or electrodeposited in situ on vitreous carbon) or a platinum wire quasi-reference electrode.

The current-potential curves (voltammograms) were recorded with a Bryans A3 X-Y recorder.

3.8 A.C. impedance

The A.C. signal was provided by a Solartron 1170 Frequency Response Analyser, capable of producing frequencies from 13 M Hz to 5 Hz, with a maximum amplitude of ± 1.5 V. The values of complex and real impedance for a given frequency were read directly from a digital display.

A large area counter electrode was employed, to avoid complications introduced by electrode processes occurring at this electrode.

3.9 X-ray diffraction

X-ray powder diffraction was carried out on a Phillips chart-recording diffractometer using nickel-filtered Cu Kα radiation, the finely-powdered samples being mounted on thin glass slides. The diffraction angles (values of 2 θ) were converted into "d"-spacings via Bragg's law, $n\lambda = 2d\sin\theta$. The resulting "d"-spacings (in Angstrom units) were matched with listed compounds in the JCPDS index (75).

3.10 Optical microscopy

Optical micrographs were obtained using a Reichert polarising microscope in conjunction with a Reichert camera attachment. Standard Polaroid fast black and white film was employed.

3.11 Electron microscopy

This was carried out on a JEOL JSM 35 instrument. The sample was carbon-coated by vacuum sputtering to prevent charging under the electron beam. The major elements were analysed quantitatively using energy dispersive analysis of the emitted X-rays (EDAX). A data-analysing package compared the X-ray intensities and energies with those of a standard. Corrections were automatically applied for atomic weight, absorbtion, and fluorescence (so-called ZAF corrections).

3.12 Electron spectroscopy for chemical analysis

THis technique (ESCA) was performed on an "Escalab II" spectrometer. X-ray photoelectron spectra were recorded using both Al Kα and Mg Kα exciting radiation, the peaks corresponding to electron binding energies being

normalised with respect to a peak due to the carbon 1s orbital at 285eV (the carbon is normally present as a minor contaminant from, e.g. adsorbed organic material, and is used as a calibrant). The binding energy peaks and peaks due to Auger transitions were assigned to an electron sub-shell of a particular element using standard tables (76). A data analysis package was used to expand and deconvolute peaks, etc.

Sample preparation consisted simply of mounting the substance on a metal stud, in the drybox if necessary.

3.13 Atomic absorption

This technique was carried out with a Perkin-Elmer 2380 double-beam instrument. Samples were prepared by dissolution in the appropriate acid (usually HCl) and the absorption intensities for a particular element compared with those of a series of standard solutions, containing the same concentrations of major matrix constituents.

3.14 Materials

Listed below are the grades and manufacturers stated purity or impurity content of the solid reagents and electrode materials employed in this study. The reagents obtained from Johnson Matthey additionally were supplied with certified analyses.

Also reported below are the purification methods applied to the gases used in this study.

Table 3.1-Reagents and Electrode materials

Reagent	Manufacturer	Grade/Form	Purity
Vitreous Carbon	Sigri Elektro-Graphit, GMBH W. Germany	3mm rod Sigradur-G	-
Graphite	Johnson Matthey	Spectrotech 3mm rod	-
Graphite	Union Carbide	Porous block Grade 60	-
Chromium metal	Johnson Matthey	325 mesh powder	>99.0%
Chromium(II) chloride	Cerac Inc. Milwaukee, U.S.A	80 mesh powder	>99.9%
Chromium(III) chloride	Aldritch Chemical Co.	Sublimed flakes	>99.0%
Gallium metal	Johnson Matthey	Specpure ingot	<1 ppm
Gallium(III) chloride	Johnson Matthey	Specpure crystals	<10ppm
Gold	Johnson Matthey	Specpure wire	<15ppm
Lithium chloride	BDH	Analar	>99.0%
Platinum	BDH	Wire	>99.9%
Potassium chloride	BDH	Analar	>99.5%
Silver	Johnson Matthey	Puratronic wire	<10ppm
Silver	BDH	Analar	>99.0%
Sodium chloride	BDH	"	>99.9%

Table 3.1 continued

Reagent	Manufacturer	Grade/Form	Purity
Titanium metal	Johnson Matthey	Specpure powder	<1000 ppm
Titanium(III) chloride	Aldritch Chemical Co.	Flakes	-
Tungsten	Johnson Matthey	Reagent grade 1.5mm wire	>99.9%
Zinc metal	Johnson Matthey	Specpure rod	>99.0%
Zinc chloride	BDH	Analar	>98.0%

Gases were purified in the following ways:

i) Argon

BOC high-purity argon (>99.99%) was passed through a column filled with BDH type 3A molecular sieve (periodically regenerated by heating at 300°C under vacuum) to remove water, and then through heated copper wool (BDH) at 450°C to remove oxygen.

ii) Hydrogen chloride and chlorine

These gases were passed through activated charcoal (BDH) to remove organic matter and then dried by passing through a special acidic molecular sieve (Union Carbide AW300). All glass joints in contact with the gases were lubricated with "Voltalef 90" halogen-resistant grease (BDH). The HCl used was technical grade (>99.6%) and the chlorine of purity >99.5%, both from BOC Special Gases.

CHAPTER FOUR

THERMODYNAMICS OF ZINC CHLORIDE-ALKALI CHLORIDE MIXTURES

4.1 Generation of formation cells by a current pulse method

The simple idea behind this approach was that a formation cell could be generated by electrolysis between two inert electrodes (e.g. vitreous carbon) by a current pulse, thus depositing zinc on one electrode, and evolving chlorine at the other, and setting up the formation cell:

$$C,Zn/ZnCl_2(+ \text{ alkali chloride})/Cl_2,C$$

The cell emf, varying as a function of time as the electrolysis products dispersed, would be extrapolated back to the moment of cessation of electrolysis, and this emf would (for pure zinc chloride) be the standard emf (E°) of the formation cell, i.e. with unit chlorine and zinc activities.

This approach was adopted for two main reasons:

i) The electrode system would be easy to assemble.

ii) The procedure would be simple and quick to obtain results.

Thus this idea was explored by generating formation cells in pure zinc chloride by constant current pulses between a vitreous carbon anode and a zinc cathode, or between two vitreous carbon electrodes. The potential difference was measured between the vitreous carbon anode and either the vitreous carbon or zinc after polarisation, or an unpolarised zinc reference electrode, similar results being obtained in all cases.

4.2 Generation of formation cells-Results and Discussion

4.2.1 Stability of zinc electrode

The stability of the zinc electrode was examined by measuring the potential difference between the electrode and the Ag/AgCl+LiCl+KCl/Pyrex reference electrode in pure zinc chloride melt under argon at 400°C. A constant potential of (83±0.5) mV was obtained, stable for at least 15 minutes. The same potential difference was consistantly obtained after polarising the zinc electrode anodically and cathodically, the potential returning virtually instantaneously to the unpolarised value. These experiments indicated that the zinc electrode was electrochemically reversible and stable in the short term. Passivation by oxidic impurities in the melt which might have occurred in the long term (see 2.5.1 in chapter two) was avoided by the approach described below.

Thus, stable zinc electrodes could also be generated by cathodically polarising vitreous carbon microelectrodes, e.g. with 20 mA for 20 seconds, thus depositing about 0.1 mg of zinc. The potential difference between the vitreous carbon and a pure zinc reference electrode was then typically from 0-1 mV, demonstrating that the surface zinc activity on the vitreous carbon was essentially one.

This experiment demonstrated incidentally that the thermal emfs arising from contact between the connecting wires were never greater than one mV.

4.2.2 Behaviour of planar vitreous carbon electrode

Experiments were performed with this microelectrode, enclosed in a fritted compartment to minimise convection

effects. The effects of current density and pulse time upon the applied potential, and potential-time decay curves after terminating the current pulse, were examined.

i) Variation of applied potential with current density

It was observed that large perturbations in the applied potential occurred at higher current densities. These perturbations could take the form of quite regularly-spaced oscillations, as shown in figure 4.1. The exact form and amplitude of the oscillations were not reproducible in different experiments. The effect was attributed to the formation and loss of chlorine bubbles from the electrode (which could be visually observed), causing a respective increase and fall in the electrode resistance.

ii) Effect of pulse time and current density upon "arrest potential"

After the termination of the current pulse, an instantaneous voltage drop was observed (due to the Ohmic melt resistance), to a potential where a finite rate of potential decrease was found. This latter potential was termed the "arrest potential". At moderately low current densities (0.05-0.35 Acm^{-2}) or if well-defined potential perturbations (amplitude > 0.5V) were not obtained, then a fairly constant "arrest potential" (±5 mV) was obtained at a constant temperature. Additionally if the pulse ended at the "trough" or minimum of an applied potential variation, then similar values of "arrest potential" were obtained. In contrast, if the pulse ended at the "peak" or maximum, then a lower (and less reproducible) value of "arrest

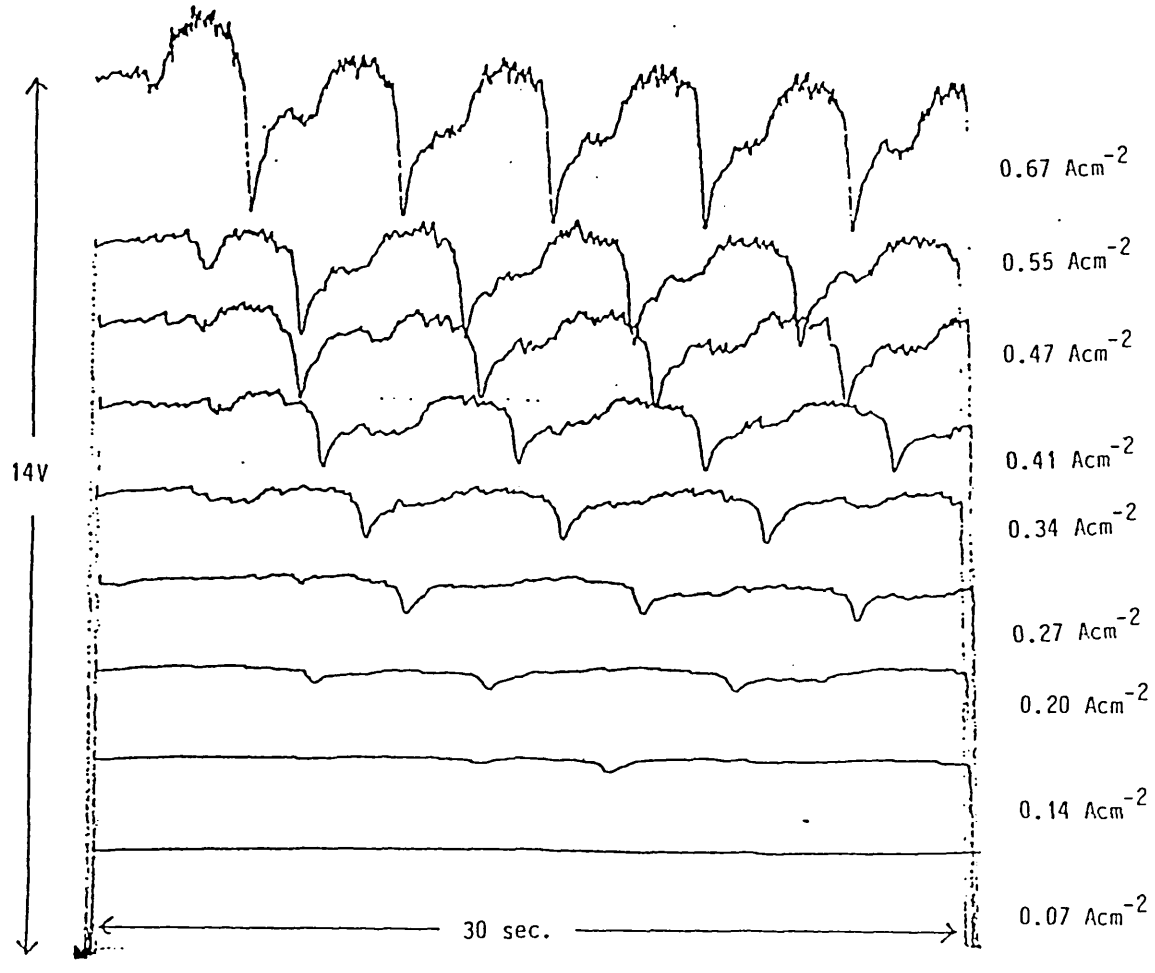


figure 4.1. Variation in potential perturbation with current density on vitreous carbon in pure zinc chloride at 400°C

potential" was obtained, presumably due to low chlorine activities at the anode.

iii) Effect of current density and pulse time upon emf decay curves

Two distinct types of emf/time decay curve were observed. At low current densities, or if the pulse ended at an applied potential maximum, a simple decay curve with a continuously decreasing gradient was found (fig.4.2). Alternatively, if the pulse ended at an applied potential minimum, or if no pronounced potential perturbations were occurring, then an "S"-shaped curve could be obtained (fig. 4.2). The effect of increasing temperature was to increase the gradient of both types of curve.

It was apparent from these curves that chlorine gas was rapidly lost from the electrode, and for this reason the effect of trapping chlorine gas bubbles by means of an indented electrode was examined.

4.2.3 Behaviour of indented vitreous carbon electrode

The electrode was orientated vertically, and was lowered into the melt initially under vacuum so that liquid filled the indentation. Termination of the current pulse at the potential maximum produced an emf decay curve which decreased relatively rapidly in the first 30 seconds, but then stabilised, values between 1.57 and 1.59V being found for different attempts, these values being maintained for over a minute. In contrast, termination of the pulse at a potential minimum produced a curve which showed a more rapid rate of decay, though the "arrest potential" was higher. The decay rates on planar

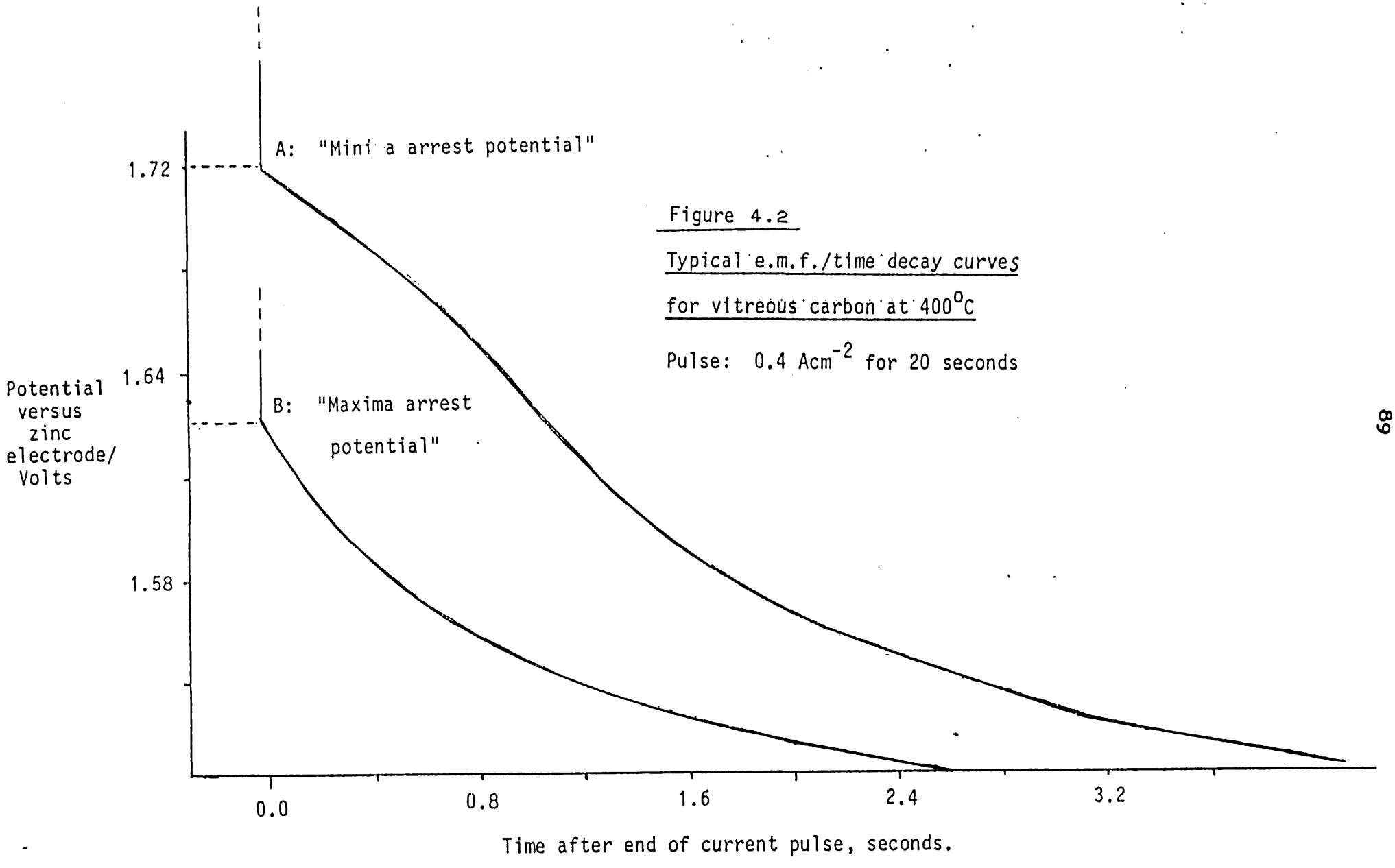


Figure 4.2

Typical e.m.f./time decay curves for vitreous carbon at 400°C

Pulse: 0.4 Acm^{-2} for 20 seconds

electrodes, in comparison, were much greater (fig. 4.3). Hence a significant stabilisation of the chlorine activity near the electrode surface appeared to result from the use of the indented electrode.

The "arrest potentials" obtained at applied potential minima with the indented electrodes were similar to those obtained with planar electrodes, i.e. about 1.72V. This figure is considerably above the reported E° values for zinc chloride at 400°C, which are all below 1.66V (5, 54-57). The most likely explanation of this phenomenon arises from the mechanism of electrolytic chloride oxidation (and chlorine reduction), which has been reported as occurring thus in various molten chloride solvents:

$$Cl^- \rightleftharpoons Cl\cdot(adsorbed) + e^- \qquad (4.1)$$

$$Cl^- + Cl\cdot(adsorbed) \rightleftharpoons Cl_2 + e^- \qquad (4.2)$$

Equation 4.2 is rate-determining (85-88). Hence the potential of the "chlorine" electrode at the " "minima arrest potential" may be determined by the relatively high free energy of combining chlorine radicals (formed in the electrolysis) and is therefore not an equilibrium potential. After a time, as the chlorine atoms combined, equilibrium would be reached between chlorine atoms and molecules, but gaseous chlorine would disperse from the electrode, so that the overall chlorine activity would be less than one, and thus $E<E°$.

This hypothesis explains the variation in "arrest potential" with applied potential. If the current pulse terminates at a maximum in applied potential, i.e. with

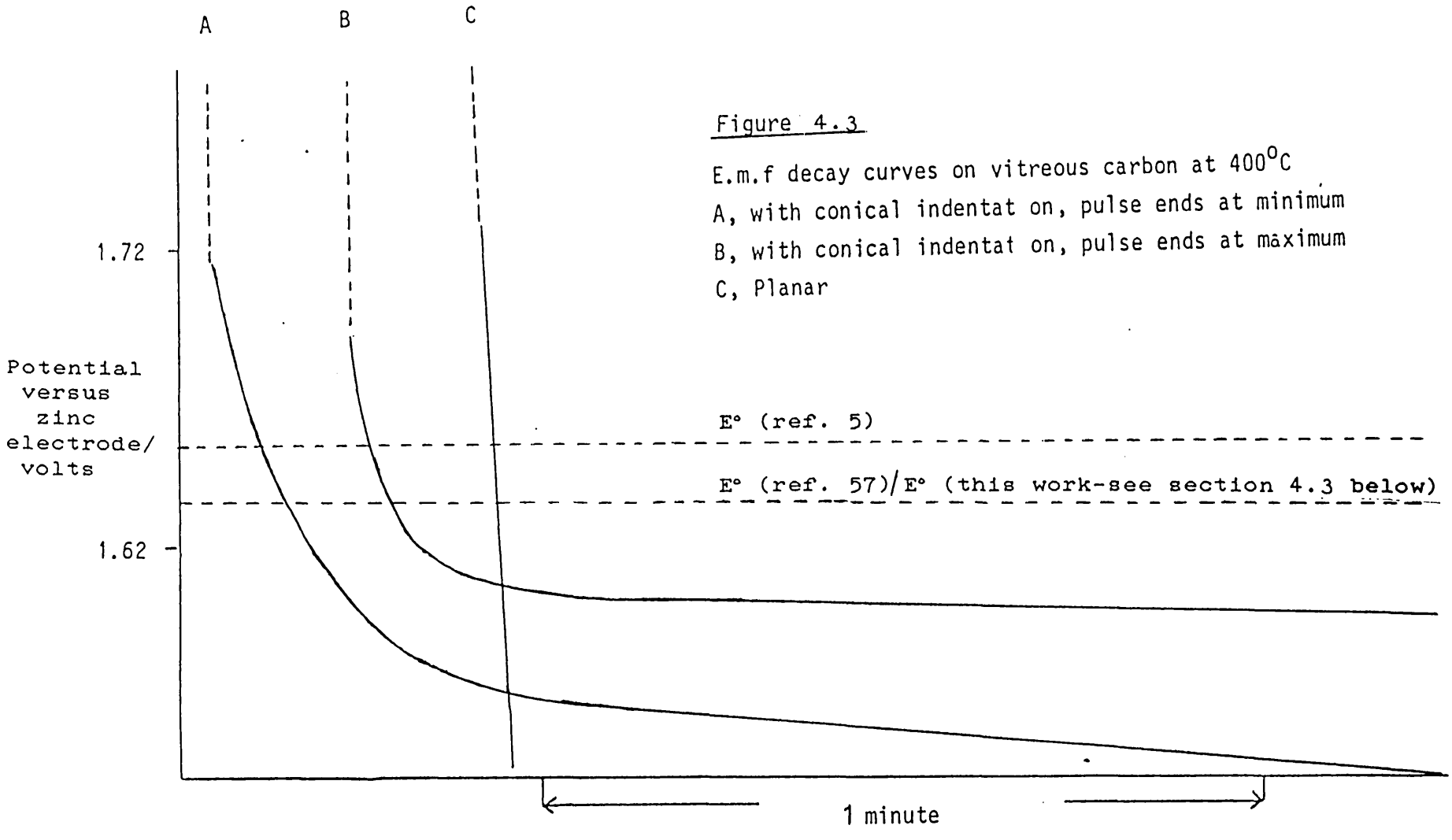


Figure 4.3

E.m.f decay curves on vitreous carbon at 400°C

A, with conical indentat on, pulse ends at minimum

B, with conical indentat on, pulse ends at maximum

C, Planar

chlorine bubbles covering and partly insulating the surface, then a relatively small proportion of the surface is involved in the reaction to form chlorine atoms: thus the relatively low "arrest potential" is determined by the presence of molecular chlorine. If the chlorine bubbles are trapped near the surface, as with the indented electrode, then the potential can stabilise at a value less than, or equal to, E° (fig. 4.3), until the bubbles disperse, e.g. by dissolution.

On the other hand, if the current pulse is cut off at a potential minimum, with presumably a layer of adsorbed chlorine atoms covering the electrode surface and relatively few chlorine molecules, then the relatively high "arrest potential" is determined by the reaction of chlorine radicals; however the potential decays relatively rapidly as few chlorine molecules are formed to buffer the chlorine activity.

The experiments of Murgelescu et al (89) who obtained analogous " arrest potentials" on graphite, corresponding to the E° value (±3mV) in fused silver halides, were conducted at 500°C, and certainly the higher temperature would increase the rate of the chlorine radical combination, thus reducing the effect of the latter reaction in producing anomalously high "arrest potentials".

4.2.4 Generation of formation cells-Conclusions

It was thus concluded that the "pulse method" was not a viable method of determining equilibrium cell emf's, at least at relatively low temperatures, and that some form

of "conventional" formation cell would be necessary. It was also later demonstrated in these formation cell experiments that, particularly for pure $ZnCl_2$, prolonged contact of the melt with chlorine gas (many hours) was necessary to obtain a stable chlorine electrode potential. It is therefore doubtful whether local chlorine saturation could be achieved by short time-scale electrolysis.

However the pulse experiments showed the feasibility of generating reversible zinc microelectrodes in situ by deposition onto vitreous carbon; this idea was employed with the "conventional" formation cells (below) to continually provide a fresh zinc surface and avoid possible passivation problems.

4.3 Conventional formation cells-General

The thermodynamics of pure zinc chloride, and mixtures with NaCl and KCl were investigated using formation cells which coupled a chlorine electrode with a zinc electrode (isolated in a fritted compartment), e.g.

$$C,Zn/KCl+ZnCl_2/Cl_2,C$$

The zinc electrode was formed in situ by electrolysis, using the porous graphite counter as counter (anode). A series of low current density pulses (10-20 $mAcm^{-2}$) were employed, thus depositing about 0.05 mg for each pulse. The quantity of zinc ultimately deposited was negligible in comparison to the quantity of melt in the electrode compartment, usually at least 5g. After each pulse, the potential of the cell was measured as a function of time on the X-Y recorder, and the process repeated until successive pulses gave a constant emf, stable for at

least 10 minutes. It was hoped that this procedure would also aid in saturating the chlorine electrode.

The initial solutions were prepared by melting the weighed components together under argon and quickly cooling. The solidified melt was then transferred to the dry box and ground in a mortar to ensure even mixing. The powdered mixture was then placed in the inner container of the electrochemical cell and in the fritted compartment of the zinc electrode, the cell then being assembled and transferred to the furnace. After each experiment the chlorine saturated melt was cooled and removed to the drybox, where a weighed amount of alkali chloride was added and the above procedure repeated. The concentrations of alkali chloride and zinc chloride were checked by A.A. analysis of small (0.1g) samples.

For each concentration of alkali chloride the cell was subjected to a heating and cooling cycle to ensure that the cell potentials could be reproduced. The potential was very sensitive to temperature changes, but under conditions of thermal equilibrium could be stable to ±0.2 mV.

However, before attempting to measure a "true" cell emf, it was necessary to pass chlorine (flow rate 30 $cm^3 min.^{-1}$) through the melt via the chlorine electrode for an extended period in order to obtain a constant emf, particularly with melts rich in zinc chloride (also noted by Robertson and Kucharski (54)). For the pure zinc chloride, over 24 hours of chlorine bubbling (at 400°C) was necessary before the slow rise in emf

flattened out to a constant value. This relatively long period is evidently necessary to saturate the melts so that the chlorine activity in solution is unity, essential for the interpretation of the formation cell emf. the results in the present work are therefore derived from the maximum obtainable emfs.

Interestingly, the colour of the chlorine-saturated melts changed from pale yellowish-green for pure zinc chloride (easily decolourised by bubbling argon) to a deeper golden-yellow with increasing alkali chloride content, and finally to reddish-yellow for alkali chloride mole fraction = 0.6 (not readily decolourised by bubbling argon). These results probably reflect a change from dissolved molecular chlorine to the relatively stable trichloride ion, e.g.

$$Cl_2 + Cl^- \rightleftharpoons Cl_3^- \qquad (4.3)$$

This latter species has been reported in basic room-temperature chloroaluminates (90), but in acidic melts, molecular Cl_2 was postulated. In NaCl-$AlCl_3$ and CsCl-$AlCl_3$ melts, however, the solubility of chlorine surprisingly did not vary significantly with acidity in the 0.5:0.5 mole fraction region, suggesting that eqn. 4.3 did *not* govern the solubility (91) . In KCl-$PbCl_2$ melts, the predicted change from physical to chemical solubility (eqn. 4.3) was found with increasing alkali chloride content (92).

In the present work, an attempt to characterise the chlorine species in the more basic melts by cyclic voltammetry did not reveal any well-defined waves within

the available potential range.

4.4 Conventional formation cells-Results and Discussion

4.4.1 Pure zinc chloride

The temperature dependance of the cell emf with pure liquid zinc chloride is shown in figure 4.4. and compared with some more recent thermochemical and formation cell determinations by other workers (5,54-57). The values obtained in the present work are in good agreement with the thermochemical estimates (55-57), at least in the 390-490°C range. However, some variation exists in E° values determined by various workers, possibly a result of inadequate saturation of the melts with chlorine in some formation cell estimates, as discussed above. The extent of this variation is shown in table 4.1, where for comparison a temperature of 450°C has been chosen to minimise the extrapolation range when this procedure was necessary. The 11 values vary over 36 mV, with an average E° of 1.606V, which coincides with the value obtained in the present work. This variation can significantly influence the calculation of activities in the alkali halide mixtures, from:

$$RT\ln a_{\text{zinc chloride}} = -2F(E-E^\circ) \qquad (4.4)$$

where E is the emf of the cell containing alkali chloride. For example, a 9 mV variation in E° can reduce the calculated activity by a factor of 0.75. In the present work, the experimentally determined activities will be used, as these are closer to the most recent thermochemical values.

The formation cell emfs in the present work were fitted

Figure 4.4. E° values for pure zinc chloride

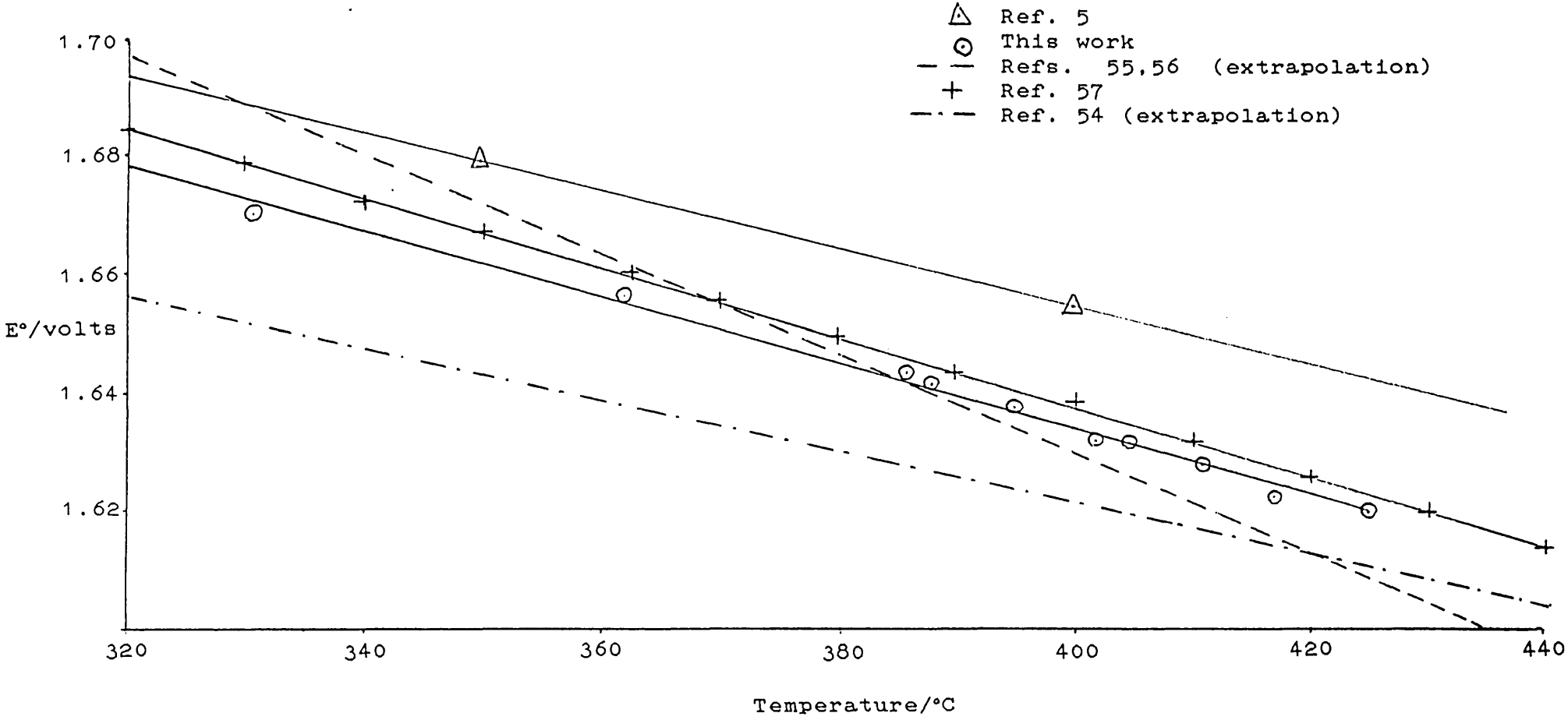


Table 4.1. E° values for pure zinc chloride at 450°C

E°/V	Comments	Reference
1.606	Formation cell (extrapolation)*	This work
1.627	Formation cell	93
1.593	"	"
1.607	"	"
1.607	"	"
1.599	"	"
1.598	"	"
1.599	Formation cell (extrapolation)*	54
1.629	Thermochemical	5
1.608	"	57
1.596	"	55,56

* Values obtained by linear extrapolation of emf variation with temperature.

by a least squares analysis to the equation:

$$E°(V) = 2.0112 - 5.599 \times 10^{-4}\ T(K) \qquad (4.5)$$

(range 604-698K)

The standard deviation was 1.4 mV. This result may be used to calculate standard thermodynamic quantities in the given temperature range, thus:

$$\Delta G° = -388.1 + 0.1081\ T(K) \quad (kJmole^{-1}) \qquad (4.6)$$

$$\Delta H° = -388.1 \quad (kJmole^{-1}) \qquad (4.7)$$

$$\Delta S° = -108.1 \quad (Jmole^{-1}K^{-1}) \qquad (4.8)$$

4.4.2 Sodium chloride-zinc chloride

The Nernst plots for this system are shown in figure 4.5; generally good straight lines were obtained, though for compositions close to pure zinc chloride only a few mV separated the Nernst plots. Consequently the derived activities for these compositions (mole fraction zinc chloride above 0.88) are somewhat less certain than for other compositions. In tables 4.2 and 4.3 the intercepts and gradients for a range of zinc chloride mole fractions obtained from least squares fits are given, together with various thermodynamic quantities derived from the plots. Thus the activities and partial molar free energies, entropies, enthalpies, and excess properties were calculated via the standard equations given in section 1.2 of the first chapter.

To obtain the activity of sodium chloride, the Gibbs-Duhem integration was employed. In terms of activity coefficients, this becomes:

Table 4.2. Least squares analyses of formation cell emf/temperature data for alkali chloride-$ZnCl_2$ systems

Sodium chloride-zinc chloride

Mole fraction zinc chloride	Intercept	Gradient x 10^4	Temperature range/K
1.00	2.011	-5.599	604-698
0.93	2.096	-6.839	642-716
0.88	2.112	-7.037	654-730
0.72	2.100	-6.790	641-717
0.65	2.074	-6.352	633-727
0.56	2.113	-6.843	657-709
0.48	1.991	-4.327	675-721
0.40	2.100	-5.697	662-717
0.33	2.236	-7.350	694-722

Potassium chloride-zinc chloride

0.95	2.048	-6.094	649-692
0.87	2.047	-6.033	655-699
0.80	2.061	-6.155	646-704
0.75	2.078	-6.361	660-693
0.67	2.046	-5.792	665-700
0.60	2.044	-5.595	664-708
0.55	2.049	-5.448	667-709
0.50	2.068	-5.474	662-721
0.43	2.055	-4.737	699-718

Correlation coefficients generally > 0.99

Table 4.3. Selected thermodynamic functions of zinc chloride in zinc chloride-alkali chloride melts at 400°C

Free energy and enthalpy units: kJ/mole; entropy, J/mole/K (x=mole fraction zinc chloride, a=activity zinc chloride)

Sodium chloride-zinc chloride

x	a	$\Delta\overline{G}$	$\Delta\overline{H}$	$\Delta\overline{S}$	$\Delta\overline{G}^E$	$\Delta\overline{S}^E$
0.93	0.96	-0.2	-16.4	-24	+0.2	-25
0.88	0.88	-0.7	-19.6	-28	+0.0	-29
0.72	0.75	-1.6	-17.1	-23	+2.5	-26
0.65	0.65	-2.4	-12.2	-14	+0.0	-18
0.56	0.53	-3.6	-19.7	-24	+3.1	-29
0.48	0.11	-12.6	-29.4	-25	-8.5	+18
0.40	0.06	-15.9	-17.3	-2	-10.8	-10
0.33	0.03	-20.7	-43.4	-34	-14.5	-43

Potassium chloride-zinc chloride

0.95	0.90	-0.6	-0.7	-10	-0.3	-10
0.87	0.80	-1.2	-6.6	-8	-0.4	-10
0.80	0.65	-2.4	-9.8	-11	-1.2	-13
0.75	0.58	-3.0	-13.1	-15	-1.4	-17
0.67	0.48	-4.2	-6.9	-4	-1.9	-7
0.60	0.32	-6.4	-6.4	0	-3.5	-4
0.55	0.19	-9.2	-7.2	+3	-5.8	-2
0.50	0.11	-12.5	-11.2	+2	-8.6	-3
0.43	0.03	-19.7	-8.3	+17	-15.0	+10

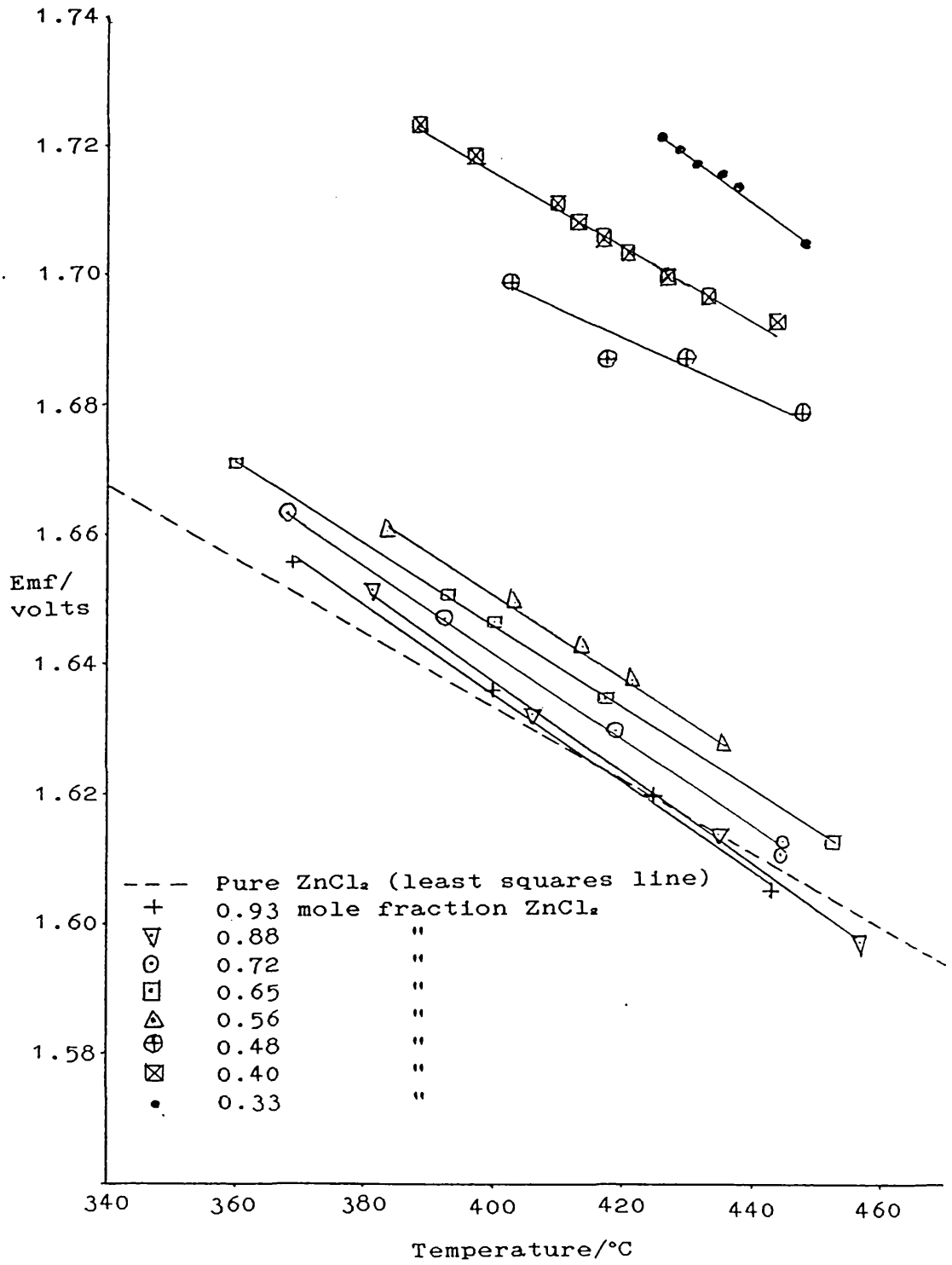


Figure 4.5. The variation of emf with temperature for the formation cell $Zn/ZnCl_2+NaCl/Cl_2$

$$[\ln\gamma_{NaCl}]_{x'_{NaCl}}^{x''_{NaCl}} = -\int_{x'_{NaCl}}^{x''_{NaCl}} x_{ZnCl_2}/x_{NaCl}\, d\ln\gamma_{ZnCl_2} \qquad (4.9)$$

Here x'_{NaCl} corresponds to a chosen standard state. For example, at 400°C, the liquidus in $NaCl/ZnCl_2$ corresponds to the composition x_{NaCl}= 0.62 (43). At this point, a_{NaCl}= 1, and thus γ_{NaCl}= 1.61. Substituting this value into eqn. 4.9, the following is obtained:

$$\ln(\gamma''_{NaCl}/1.61) = -\int_{x'_{NaCl}=0.62}^{x''_{NaCl}} x_{ZnCl_2}/x_{NaCl}\, d\ln\gamma_{ZnCl_2} \qquad (4.10)$$

Thus γ''_{NaCl} can be obtained from the area under a plot of x_{ZnCl_2}/x_{NaCl} versus $\ln \gamma_{ZnCl_2}$, between the limits defined by x_{NaCl}= 0.62 and x''_{NaCl}.

To compare activities of zinc chloride or alkali chloride derived by other workers with the present data at one selected temperature (in this case, 400°C), "b" values were calculated for each given composition, from the expressions (6):

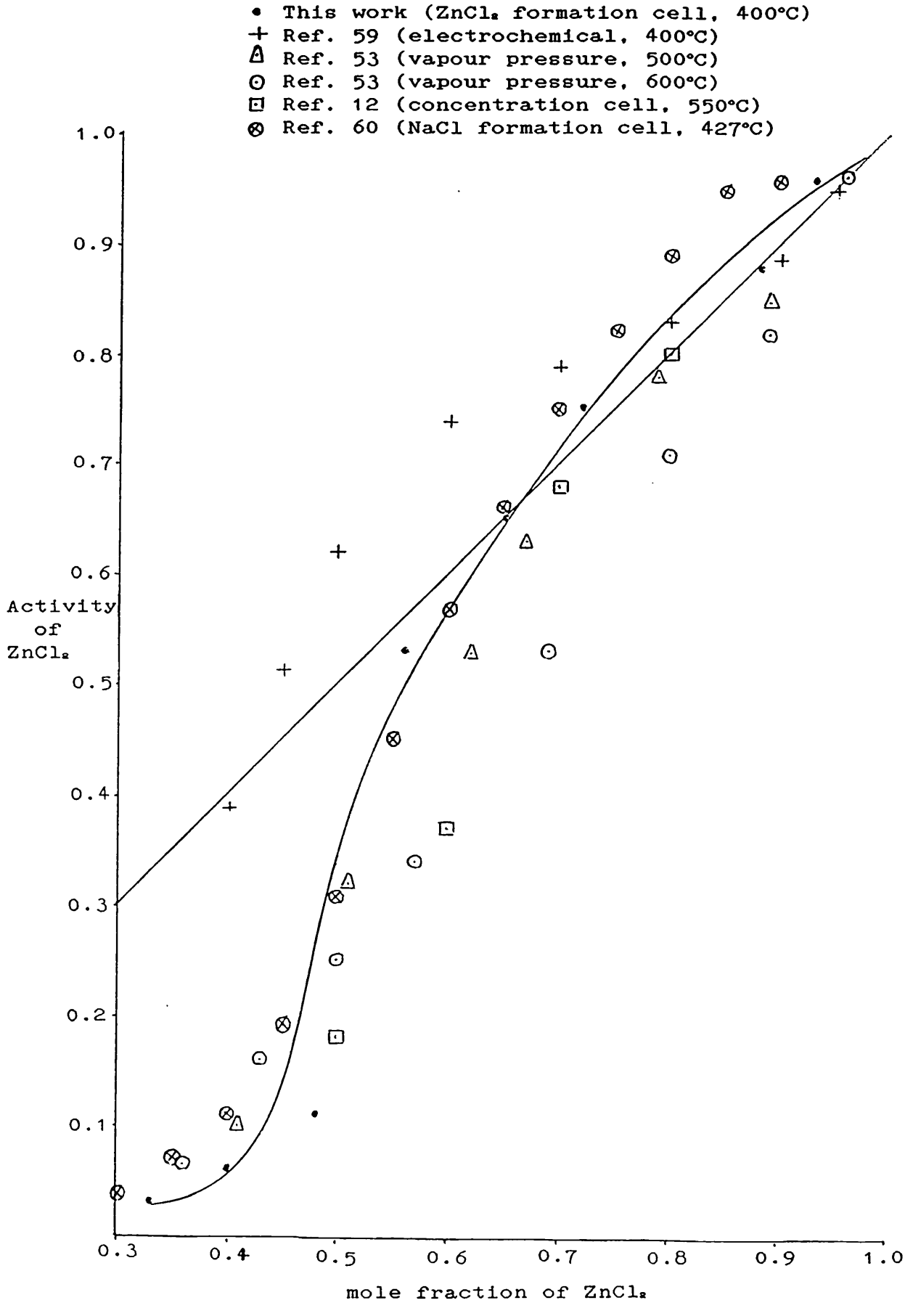
$$RT \ln\gamma_{ZnCl_2} = 2b\, x^2_{KCl}/(1+x_{ZnCl_2})^2 \qquad (4.11)$$

$$RT \ln\gamma_{KCl} = 4b\, x^2_{ZnCl_2}/(1+x_{ZnCl_2})^2 \qquad (4.12)$$

Here "b" is a parameter which represents the change in free energy caused by interaction of ions in the melt, as derived assuming the "regular mixing" model (chapter one). It is assumed that the "b"-values are independent of temperature for a particular composition, and thus activity coefficients may be calculated at any given temperature, if the "b"-value is known.

The activity of zinc chloride (at 400°C) derived from the formation cell emf data in the present work is plotted in figure 4.6. A positive deviation from ideality is

Figure 4.6. Activities of zinc chloride in NaCl-$ZnCl_2$ mixtures
(values corrected to 400°C where required)



indicated for compositions with the mole fraction of zinc chloride < 0.64; below this value the activity decreases relatively rapidly, resulting in large negative deviations for $x_{NaCl} > 0.6$. The activity shows good agreement with the activity of zinc chloride derived by Gibbs-Duhem integration of the sodium chloride activity obtained from the cell Na/beta-alumina/NaCl+$ZnCl_2$/Cl_2,C by Dudley and Inman at 477°C (60), and also with the activity derived from the zinc chloride vapour pressure by Bloom et al (53) and Moss (52). Other comparatively recent investigations of the NaCl-$ZnCl_2$ system have been made by Lesourd et al (59) and by Dijkhuis and Ketelaar (12), both of whom however used cells which may have given rise to unknown junction potentials.

In particular, the results of Lesourd et al (59) appear to show much too great a positive deviation from ideality compared with the results of other workers; their activities derived from the analogous cell containing LiCl likewise show an even greater and probably unjustifiable positive deviation (58) (see chapter two). The discrepancies probably stem from the inevitable use of a number of free energy terms of debatable accuracy in interpretating the potential of the cells in question:

Zn/$ZnCl_2$+MCl/Pyrex/MNO_3/AgCl/Ag (M=Li or Na)

Additionally the emf values show a large scatter.

Returning to the present work, the activity of NaCl at 400°C obtained from the Gibbs-Duhem integration is plotted in figure 4.7. Near the liquidus, positive deviation from ideality is found, but the results did not

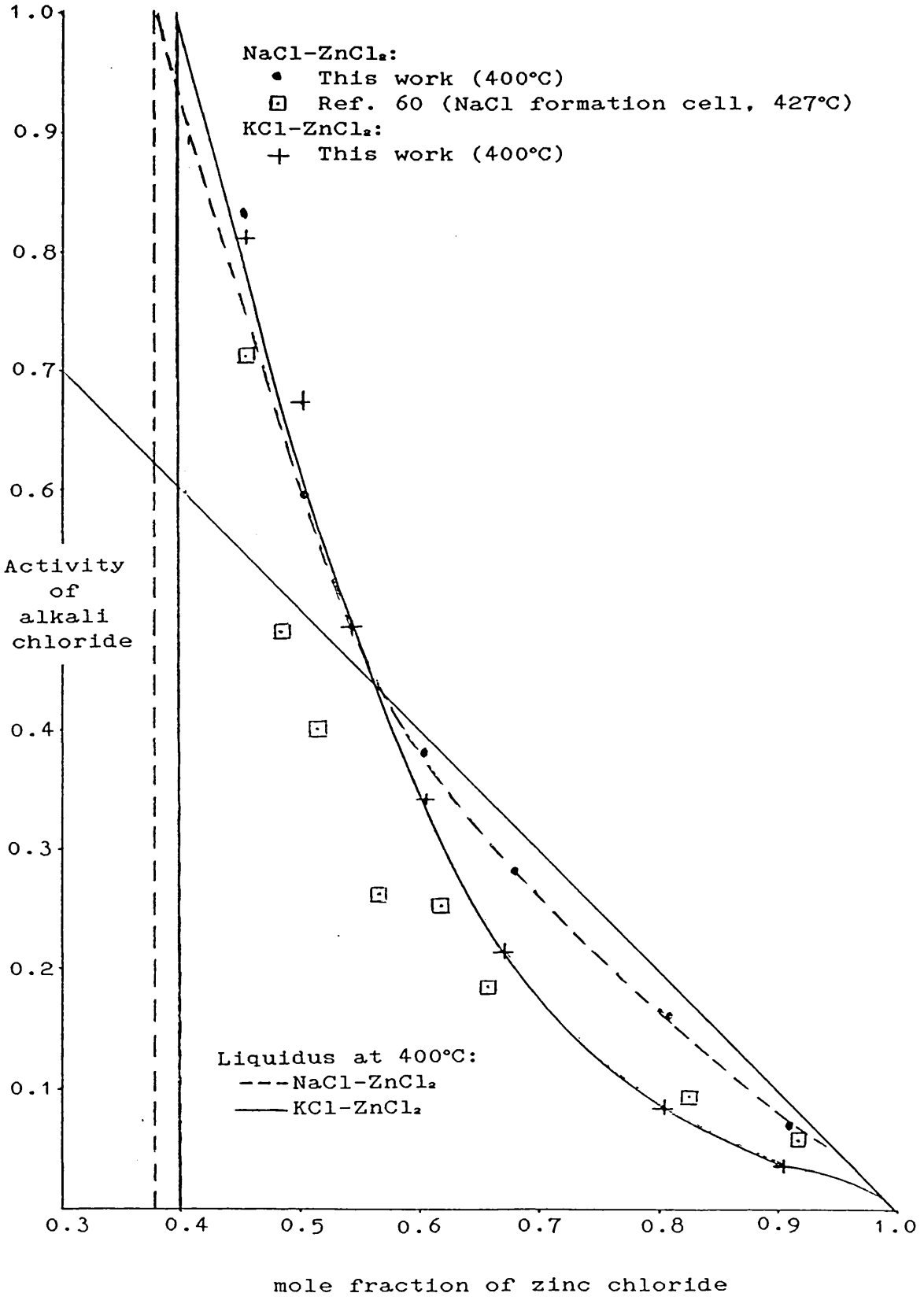


Figure 4.7. Alkali chloride activities in mixtures with zinc chloride

indicate as great a negative deviation as do the extrapolated values of Dudley and Inman for the NaCl formation cell (60).

The partial enthalpies and entropies of $ZnCl_2$ listed in table 4.3 do not show an obvious trend; however it may be pointed out that the values are calculated from the difference between two quantities of similar magnitude and so may be subject to considerable error. For example, a 1% error in the gradients of the Nernst plots can become a 25% uncertainty in the entropy. As a consequence, enthalpies of mixing are best determined calorimetrically; for example, Papatheodorou and Kleppa (7) have reported the integral enthalpies of mixing for the $LiCl/ZnCl_2$ and $CsCl/ZnCl_2$ systems. The "interaction parameter" (117), which is the enthalpy divided by the product of the mole fractions of the components, showed a "sharp" minimum for the CsCl system at the composition corresponding to Cs_2ZnCl_4, suggesting a strong tendency to form the chlorozincate ion. A shallow minimum was however obtained for the LiCl system, agreeing with the expected trend of decreasing interaction with a decrease in basicity of the alkali halide. Finally it may be noted that the formation cell enthalpies of Robertson and Kucharski (54) do not agree well with the calorimetric enthalpies (7), possibly for the reason noted above.

4.4.3 Potassium chloride-zinc chloride

Nernst plots for this system are shown in figure 4.8. Good straight lines were obtained for all compositions, and least squares analyses gave the intercepts and

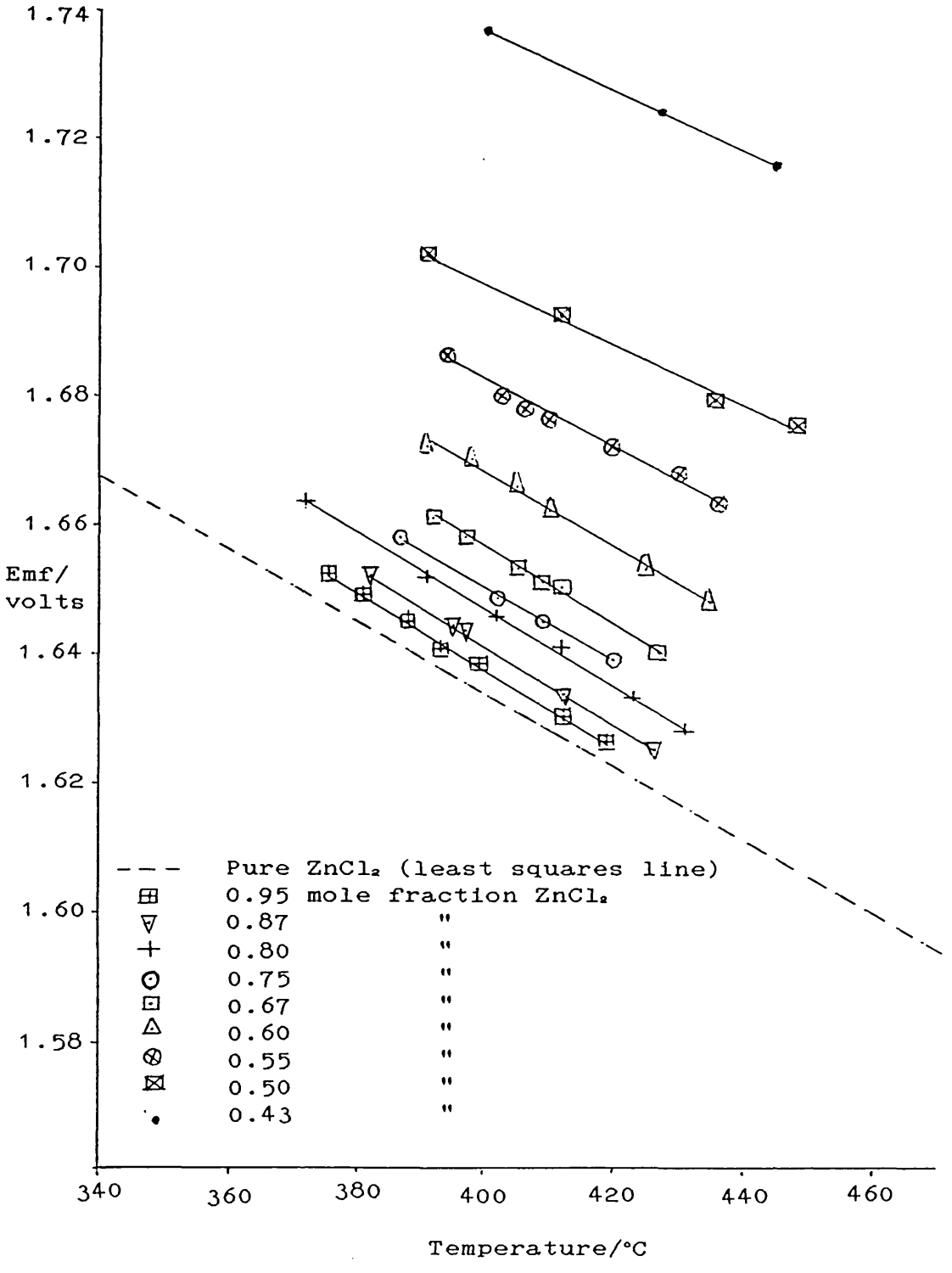


Figure 4.8. The variation of emf with temperature for the formation cell $Zn/ZnCl_2+KCl/Cl_2$

gradients shown in table 4.2. Derived thermodynamic quantities are also reported in table 4.3. The activity of KCl (figure 4.7) was calculated by the Gibbs-Duhem integration, as for NaCl, the standard state being taken at 400°C as $a_{KCl} = 1$ at the liquidus composition where $x_{KCl} = 0.60$ (50), so that $\gamma_{KCl} = 1.67$. This leads to a relationship analogous to that of eqn. 4.10.

In figure 4.9 the activity of zinc chloride is plotted against composition. The values indicate a continuously increasing negative deviation from ideality as the mole fraction of zinc chloride decreases. A reasonable agreement with values obtained for the zinc chloride formation cell by Robertson and Kucharski (54) (extrapolated to 400°C) can be observed, and indeed with the concentration cell results (12), and with the vapour pressure-derived values (52,53). It may be noted that the activities of both KCl and $ZnCl_2$ show generally greater negative deviations than in the NaCl-based system, a reflection of the greater basicity of KCl over NaCl.

The entropies and enthalpies shown in table 4.3 again may not reflect a meaningful trend due to the errors which may be involved (see above).

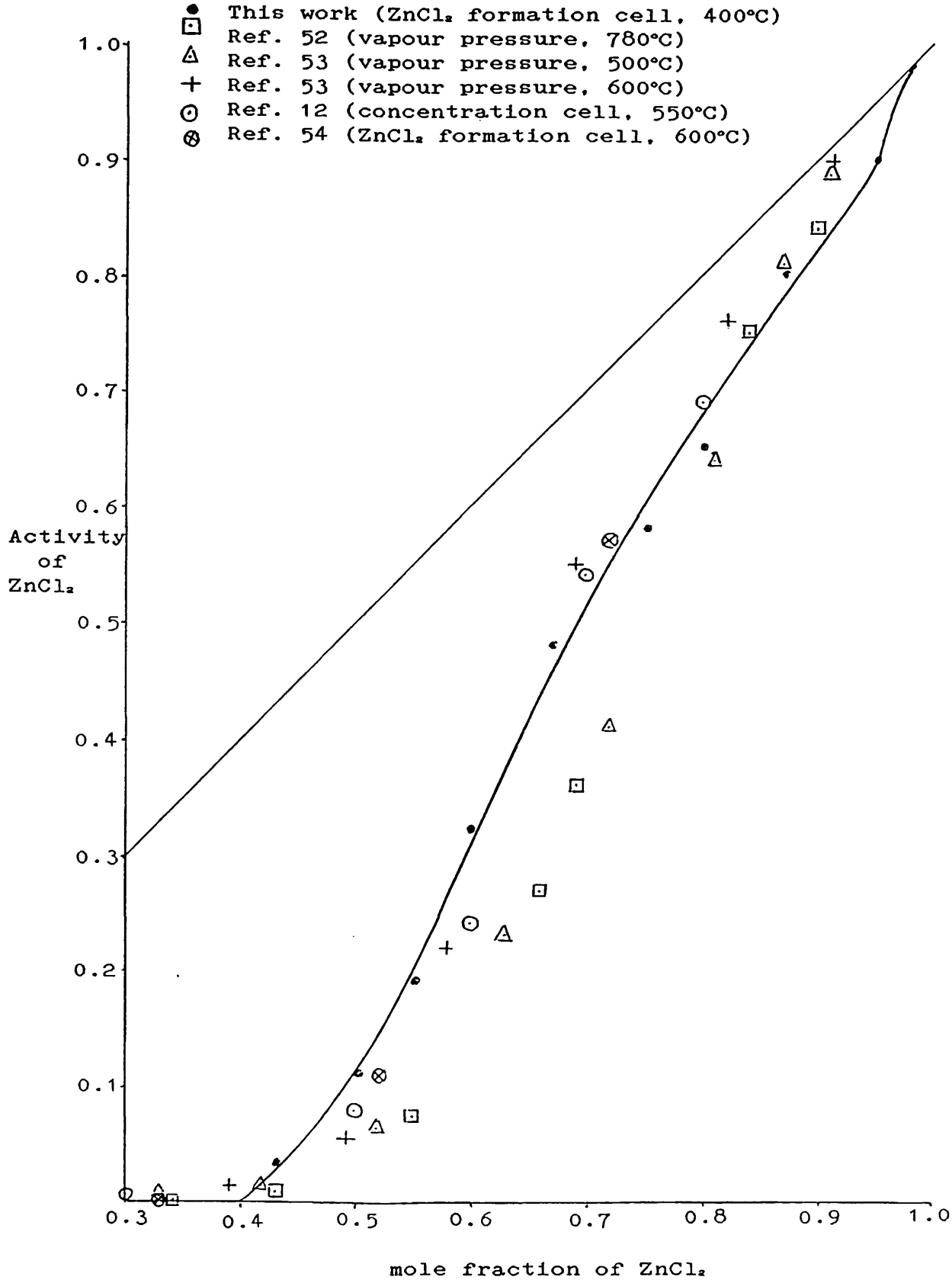
4.5 Concentration cell-General

The concentration cell may be formulated as:

$$Zn/ZnCl_2+KCl(solid)/ZnCl_2+KCl(test\ soln.)/Zn$$

The KCl-saturated reference solution was prepared by mixing powdered KCl and $ZnCl_2$ in the ratio 70:30 mole per cent, and placing in a vertical Pyrex tube of internal diameter 2 cm. with a Pyrex no. 3 frit closing the lower

Figure 4.9. Activities of zinc chloride in KCl-$ZnCl_2$ mixtures
(values corrected to 400°C where required)



end. On heating to the experimental temperature (408°C), a saturated solution of KCl was formed with excess solid present, as indicated by the phase diagram (50).

The reference compartment was placed in the inner container of the electrochemical cell which initially contained a 20 mole per cent $KCl/ZnCl_2$ mixture. The relative weights of melt in the reference and test solution compartments were chosen so as to produce approximately the same melt level.

During the course of the experiment sucessive portions of powdered KCl were added to the test solution through a delivery tube and the solution stirred for ten minutes after each addition by bubbling argon to aid the dissolution of the KCl.

Vitreous carbon microelectrodes were placed in both compartments, and a tungsten wire counter electrode in the solution compartment. The zinc electrodes were formed in situ by depositing metal on the vitreous carbon as described above for the formation cell. The emf between the zinc electrodes was measured immediately after pulsing by a high impedence voltmeter. The asymmetry potential of the cell was determined in a preliminary experiment with pure zinc chloride in both compartments and was found to be 0.4 mV at 408°C.

After the initial heating to 408°C, an equilibration period of about 30 minutes at temperature was required to produce a stable emf. After this period, the cell emf quickly attained a steady value after pulsing and maintained this value for about 10 minutes before

drifting, probably as a consequence of electrode passivation caused by the reaction of trace oxide impurities with the zinc surfaces. On re-pulsing, the same emf was generally obtained (±3 mV).

The reproducibility of the emf was not appreciably altered by bubbling argon through the test solution for 20 minutes, showing that rapid mixing of the reference and test solutions was not occurring.

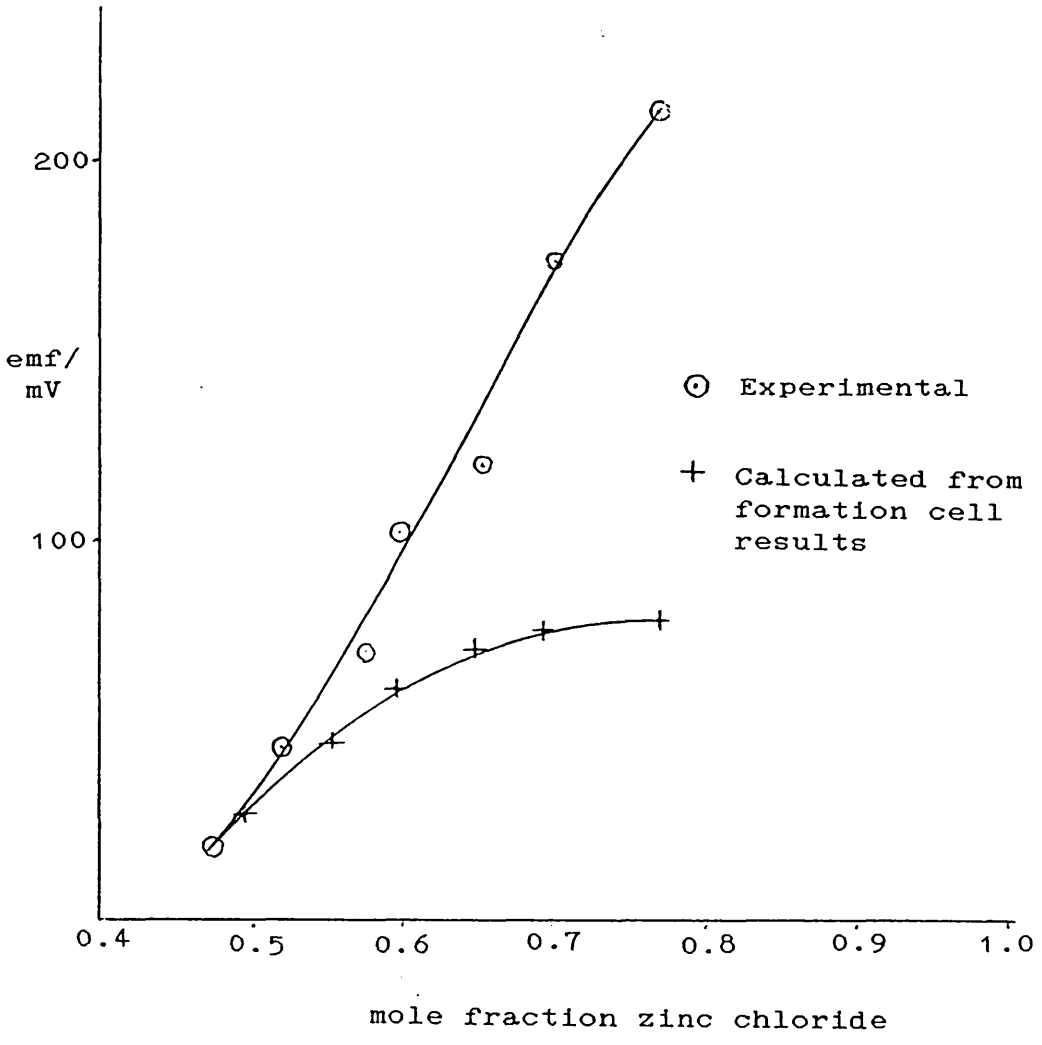
4.6 Concentration cell-Results and Discussion

The emf values for a series of KCl concentrations, from two separate experiments, are plotted in figure 4.10. It may be shown (116) that the emf of such a cell is given by:

$$E = RT/2F \ln[a(I)/a(II)] + L \qquad (4.13)$$

where a(I) and a(II) represent the zinc chloride activities in the test and reference solutions respectively, and L represents the liquid junction potential, which is a function of the transport numbers of zinc and potassium in the two solutions. This latter term is evidently not negligable, since values of a(I) were taken from the formation results and substituted into eqn. 4.13, and the apparent value of a(II), the supposedly constant reference activity, calculated. The values were found to vary by a factor of 100X. Alternatively, a value for a(II) was estimated from the present work, and from literature values (see figure 4.8), giving a result of the order of 10^{-2}. Further, a value of 0.04 may be calculated from eqn. 4.13, taking a(I) as 0.11 at a zinc chloride mole fraction of 0.5 (formation cell result from

Figure 4.10. Variation of emf with composition for the concentration cell $Zn/KCl+ZnCl_2(ref)/KCl+ZnCl_2/Zn$ at 408°C



the present work), and assuming that since this test solution composition is close to that of the reference, the liquid junction potential may be neglected.

Taking the reference solution zinc chloride activity as 0.04 then, theoretical cell emfs may be calculated as a function of composition for the concentration cell. The results are compared with the experimental values of emf in figure 4.10. It can be seen that the calculated emf deviates considerably from the experimental as the composition difference increases between the reference and test solutions. For example, a very considerable 150 mV discrepancy exists for the zinc chloride mole fraction 0.77 in the test compartment.

Thus the above analysis indicates that the liquid junction potential cannot be neglected in the concentration cell. This is perhaps not surprising when the relatively large changes in structure and physical properties between melts rich in zinc chloride and melts rich in alkali chloride are considered, which in turn affect the transport numbers across the junction. The cells accordingly do not seem useful for the determination of accurate thermodynamic data.

4.7 Calculated Solute activities in zinc chloride melts

With the determination of component activities in zinc chloride-based melts, it becomes possible to calculate the activity coefficients of dilute solute species in these solvents by means of the coordination cluster theory (8), as a function of composition (see chapter one). The results should however be taken as merely indicating

general trends, as the theory has not been quantitatively verified, as least in molten salt media. It is also necessary to estimate solute activity coefficients in pure zinc chloride and pure alkali chloride. for the acidic solutes considered in this work, strong interactions with alkali chlorides are expected, leading to low activity coefficients. On the other hand, relative insolubility in pure zinc chloride was found for the trivalent chloride of chromium, implying large activity coefficients. Chromium(II) chloride and titanium(III) chloride were however, comparatively soluble. With these points in mind, calculations were made, using the simplified form of the equation with the exponential term set to one, and taking the coordination number, Z, as 6. The activity coefficient in pure alkali halide was taken as 0.1. For an "insoluble" solute, γ was taken as 100, and γ for a soluble solute in pure zinc chloride as 1 or 0.1. The various cases can now be considered:

i) Solute "insoluble" (γ=100) in pure zinc chloride. Figure 4.11 shows that the activity coefficients increase smoothly as the alkali chloride content increases, implying that the solubility decreases in the same fashion.

ii) γ=1 in pure zinc chloride. Again the activity coefficients increase monotonically with alkali chloride mole fraction.

iii) γ=0.1 in pure zinc chloride. The activity coefficient is relatively constant over the available composition range, increasing slightly near the liquidus.

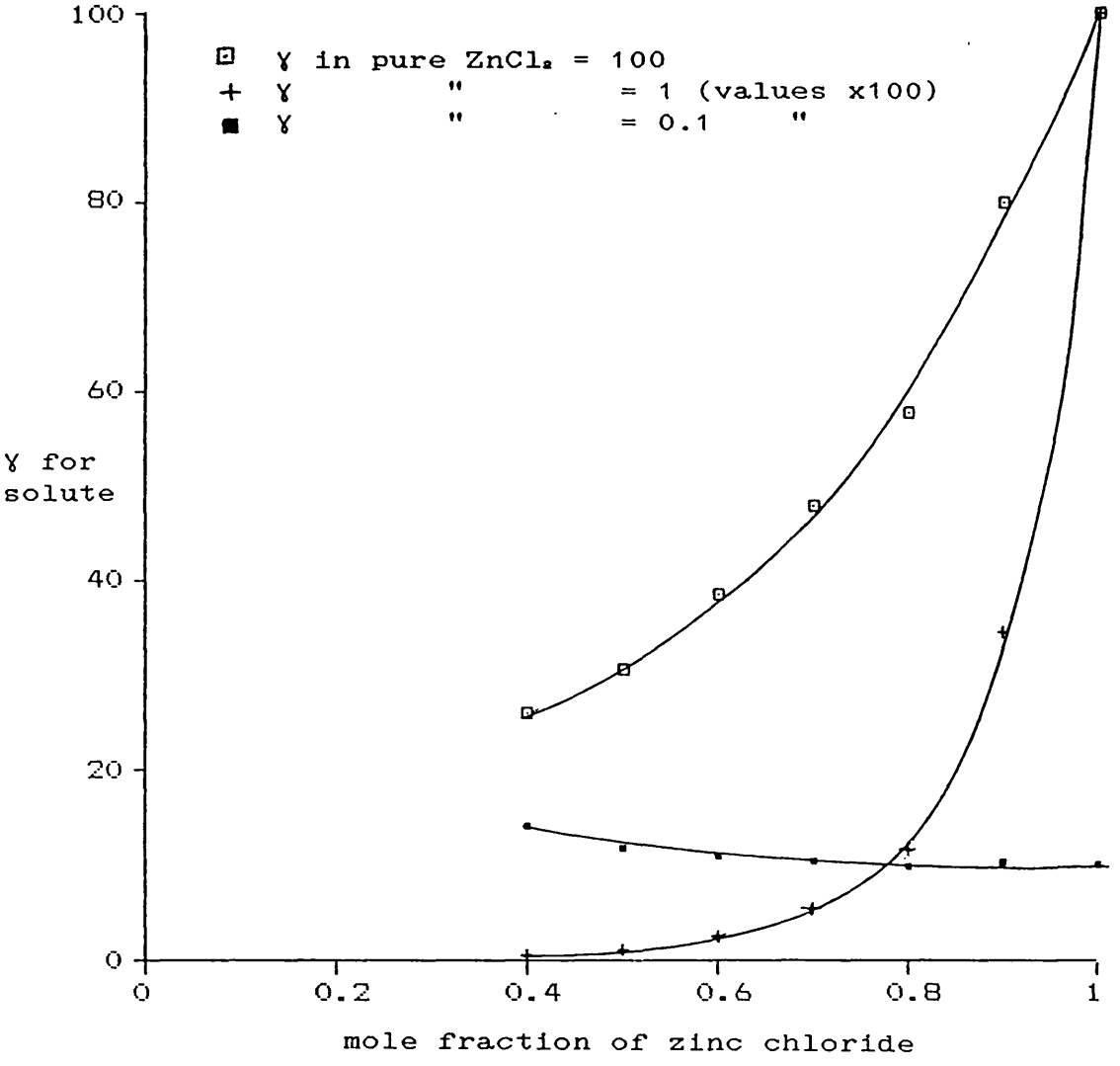


Figure 4.11. Typical coordination cluster theory calculations for a solute in the system AlkCl-$ZnCl_2$ as a function of melt composition (Alk = K or Na)

Thus the calculations suggest that though large changes in solute activity coefficient may occur, these changes will occur relatively smoothly over the composition range investigated. There is, for example, no "sharp" maxima in solute activity coefficient such as occurs in aluminium chloride based melts at the 0.5:0.5 mole fraction composition, a consequence of the less rapid component activity changes in zinc chloride melts, due to the lower Lewis acidity as compared with aluminium chloride.

The implications for solute solubility, for example, are that a solute insoluble in pure zinc chloride but soluble in alkali chloride (e.g. in LiCl/KCl eutectic) would show a continuously increasing solubility as the alkali chloride mole fraction increased in an alkali chloride-zinc chloride mixture.

CHAPTER FIVE

CYCLIC VOLTAMMETRY OF ZINC CHLORIDE-BASED MELTS WITHOUT ADDED SOLUTE SPECIES

5.1 General

As a preliminary to the solute studies, the cyclic voltammetric behaviour of "pure" zinc chloride-based melts (i.e. without added solutes) was examined with various working electrodes. The purpose of this was twofold; firstly to determine the behaviour of the working electrode materials in the melts in order to select the most suitable for the solute studies, and secondly to briefly assess the effectiveness of the purification process, and the results of allowing air and moisture to contact the molten salt.

5.2 Principles of Cyclic Voltammetry

Cyclic voltammetry is a technique which can yield diverse information about the mechanism of an electrochemical reaction from a comparatively simple and rapid experimental procedure. For these reasons it is probably the most useful technique for the characterisation of new systems. Several good reviews of the technique are available (77,78), from which the references to the original papers may be obtained if necessary.

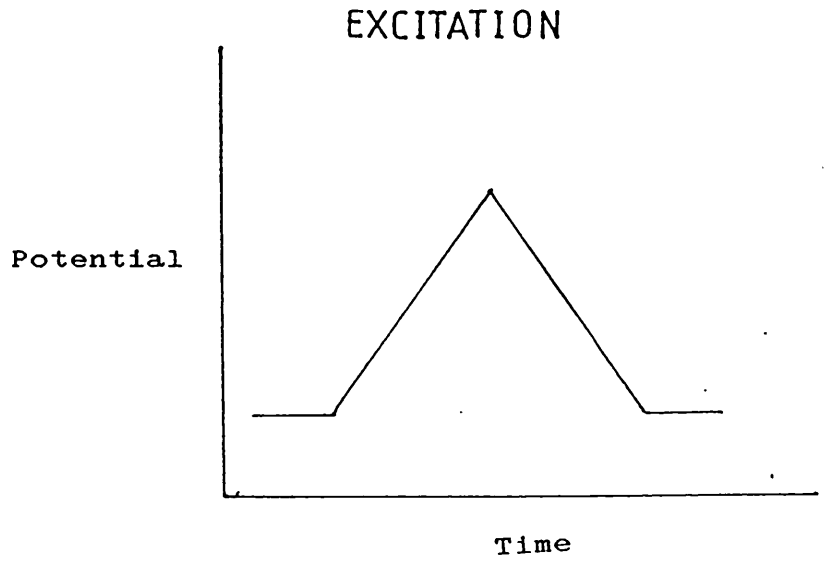
The theoretical basis of this method relies on the application of Fick's laws of diffusion (assuming that transport by migration and convection is negligible), in particular the law which describes linear diffusion to a stationary plane from an essentially infinite bulk of

solution:

$$\frac{dC(x,t)}{dt} = D\,\frac{d^2C(x,t)}{dx^2} \qquad (5.1)$$

where C(x,t) is the concentration of a species at time t and distance x from the electrode. D is the diffusion coefficient and is a function of solution viscosity and temperature, factors which are usually constant during the electrochemical experiment. Analogous equations may be applied for non-planar electrodes. Eqn.(5.1) may be solved to give the surface concentrations at the electrode as a function of time, employing the appropriate boundary and initial conditions. Combining this result with the first law, which states that the flux at the electrode surface is proportional to the surface concentration gradient, allows a relation between the current and potential to be derived, as given below.

In the case of the cyclic voltammetric technique, the potential of the electrode is varied linearly as a function of time, and at some potential limit, the direction of the sweep is reversed. The potential-time relation and the resulting current-potential curve are shown in figure 5.1. The shape of the latter curve is characteristic of a "reversible" reaction (with soluble reactant and soluble product), i.e. a reaction where the rate of the electron transfer is very rapid compared with the rate of diffusion to the electrode. Thus as the potential approaches the formal potential ($E^{\circ\prime}$) of the redox couple, the surface concentration of reactant drops, the flux to the surface increases, and the current increases. As the potential moves past $E^{\circ\prime}$, the region



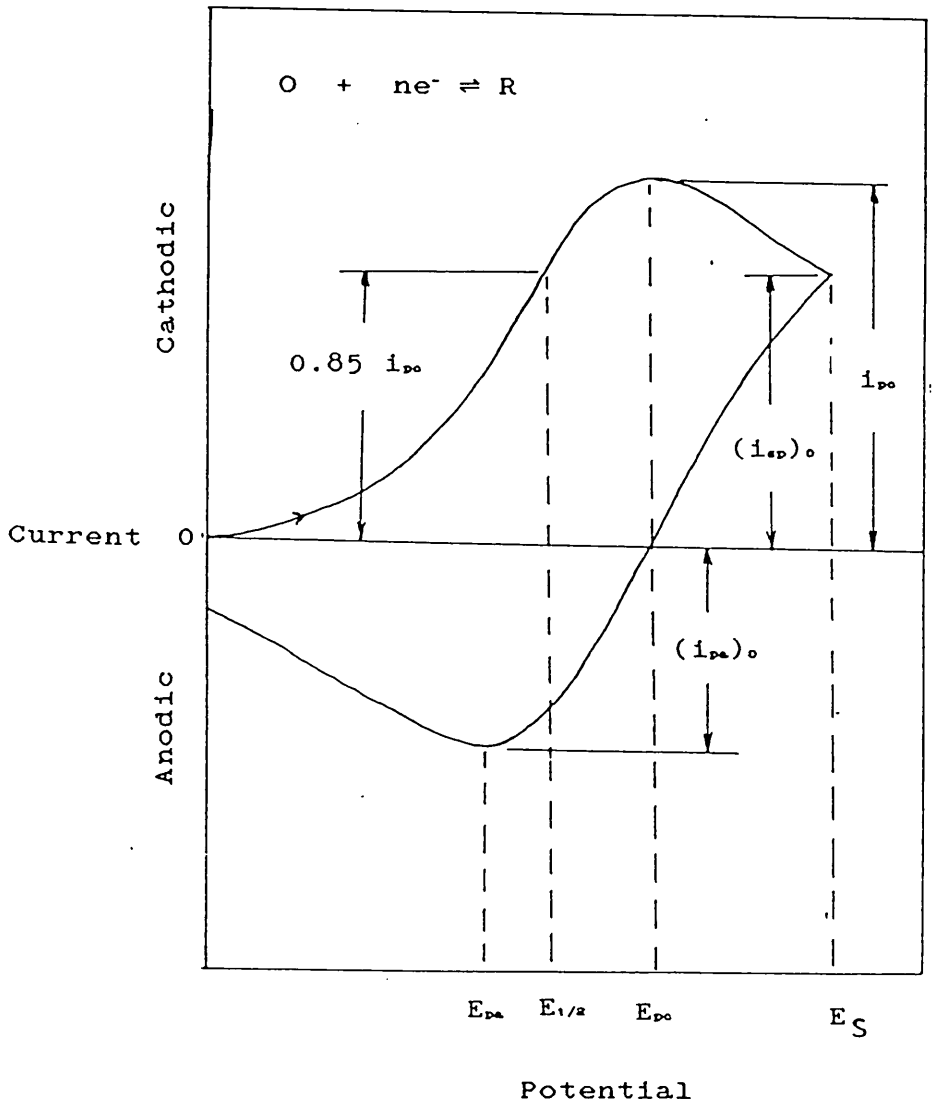


Figure 5.1. Cyclic voltammogram for a reversible reduction process with both reactant and product soluble.

near the electrode is depleted of reactant and the current reaches a maximum and declines. On reversal, analogous changes occur with the product, and a similar peaked curve results.

The useful parameters which may be obtained from the voltammogram are also indicated. For a reversible wave, involving a soluble product, the forward peak current is given by:

$$i_{po} = 0.4463nFAC^*(nF/RT)^{1/2}\nu^{1/2}D^{1/2} \qquad (5.2)$$

where n= number of electrons transferred, A= electrode area (cm^2), C^*= bulk concentration of species O (moles cm^{-1}), ν= scan rate (Vs^{-1}), D= diffusion coefficient of O (cm^2s^{-1}), and the other symbols have their usual meaning. The relation implies that $i_{po}/\nu^{1/2}$ is constant with scan rate.

The peak potential E_{po} is related to a quantity called the half-wave potential $E_{1/2}$ by:

$$E_{po} = E_{1/2} + 1.109(RT/nF) \qquad (5.3)$$

where

$$E_{1/2} = E^{o'} - (RT/nF)\ln(D_o^{1/2}/D_R^{1/2}) \qquad (5.4)$$

and D_o and D_R are respectively the diffusion coefficients of the oxidised and reduced forms of the couple. Usually D_o=D_R approximately, and thus $E_{1/2}$ may be taken as $E^{o'}$, the formal potential of the couple.

The peak potential at $0.5i_{po}$, $E_{p/2}$, is given by:

$$E_{p/2} = E_{1/2} - 1.09(RT/nF) \qquad (5.5)$$

It follows that:

$$E_{po} - E_{p/2} = 2.2(RT/nF) \qquad (5.6)$$

$$= 128 \text{ mV at } 400°C \ (n=1)$$

For an insoluble product (79) the peak current is:

$$i_{pc} = 0.6105nFAC^*(nF/RT)^{1/2}\nu^{1/2}D^{1/2} \qquad (5.7)$$

(reversible electron transfer), and the peak potential is:

$$E_{pc} = E^{o'}+(RT/nF)\ln[a^*/(0.924)^2)] \qquad (5.8)$$

where a^* is the bulk activity of species O, and it can be shown that:

$$E_{pc}-E_{p/2} = 0.77(RT/nF) \qquad (5.9)$$

$$= 45 \text{ mV at } 400°C \ (n=1)$$

It may be pointed out that the treatment for the insoluble product contains the assumption that the deposit activity is instantaneously unity, which may not be the case at the beginning of electrolysis.

For a soluble product, the ratio of anodic to cathodic peak currents (assuming the initial scan is cathodic) is unity for an uncomplicated reversible reaction (i_{pa} measured from the decaying current baseline of cathodic sweep). This may be calculated by the method of Nicholson and Shain (77,78):

$$i_{pa}/i_{pc} = (i_{pa})_o+0.485(i_{sp})_o/i_{pc}+0.086 \qquad (5.10)$$

$(i_{pa})_o$ is the anodic peak current measured from the zero current baseline, and $(i_{sp})_o$ is the current measured at the switching potential.

Again for a soluble product, the peak separation is:

$$E_{pa}-E_{pc} = 2.3(RT/nF) \qquad (5.11)$$

$$= 133 \text{ mV at } 400°C \ (n=1)$$

No such simple relationship can be derived for the insoluble case, since the form of the reverse sweep depends on the deposit morphology, though recently Schiffrin (80) has given a (approximate) current-potential

relation for the entire voltammogram.

If slow electron transfer kinetics and/or coupled chemical reactions are involved in the redox reaction, then peak broadening, peak potential shifts and deviations of the peak current ratio from unity can be expected as the scan rate is changed. Also i_p may not be proportional to $\nu^{1/2}$. The behaviour of these parameters may allow diagnosis of a reaction mechanism.

Caution must however be applied in diagnosis, since "uncompensated solution resistance" can cause peak broadenings and potential shifts with scan rate, identical to those produced by slow electron transfer (irreversibility). The effect is produced by low solution conductivities and may not be totally eliminated by the circuitry of the potentiostat.

5.3 Results and Discussion

5.3.1 Counter and reference electrodes

A graphite rod electrode was generally used as the counter in these studies. After prolonged use, swelling and disintegration were sometimes observed, probably due to chlorine evolution in the pores of the graphite.

For general use as a reference electrode, the platinum wire quasi-reference was employed. The potential remained constant (±5 mV) in purified melts under dry argon, but shifted to more positive potentials, e.g. by up to +0.4 V if air was admitted to the system, probably because of the reduction of atmospheric oxygen at the electrode which set up a redox couple.

The Ag/AgCl glass reference electrode also exhibited a stable potential in purified melts, the potential being approximately 80 mV more positive than the zinc deposition potential.

Finally, the zinc rod electrode also gave a stable potential in purified melts corresponding to the zinc deposition potential as expected (see also discussion in chapter 4 on stability of zinc electrodes).

5.3.2 Working electrodes

Very different results were obtained with the four working electrodes and these will be discussed separately.

i) Tungsten electrode.

Cyclic voltammograms obtained in purified melts (e.g. with 0.15 mole fraction NaCl) with this electrode showed variations according to whether the cathodic melt limit (zinc deposition) was reached. If the limit was not reached, then low currents resulted until the anodic limiting reaction (chlorine evolution) was attained (fig. 5.2). However the anodic background current observed over most of the potential range may indicate oxidation of the tungsten, as noted by Rubel and Gross (66) in these melts.

If the cathodic limit was reached, then additional peaks appeared on subsequent scans, occurring at about + 50 mV and +1.3 V respectively, relative to the zinc deposition potential (A and B in fig. 5.3). These peaks did not occur with the other working electrodes, and were thus thought to be due to a reaction of the tungsten, possibly of an oxide layer on the surface, since the intensity increased in "wet" melts (below).

Figure 5.2. Cyclic voltammogram of purified 15 mole per cent NaCl-$ZnCl_2$ melt at 391°C under argon

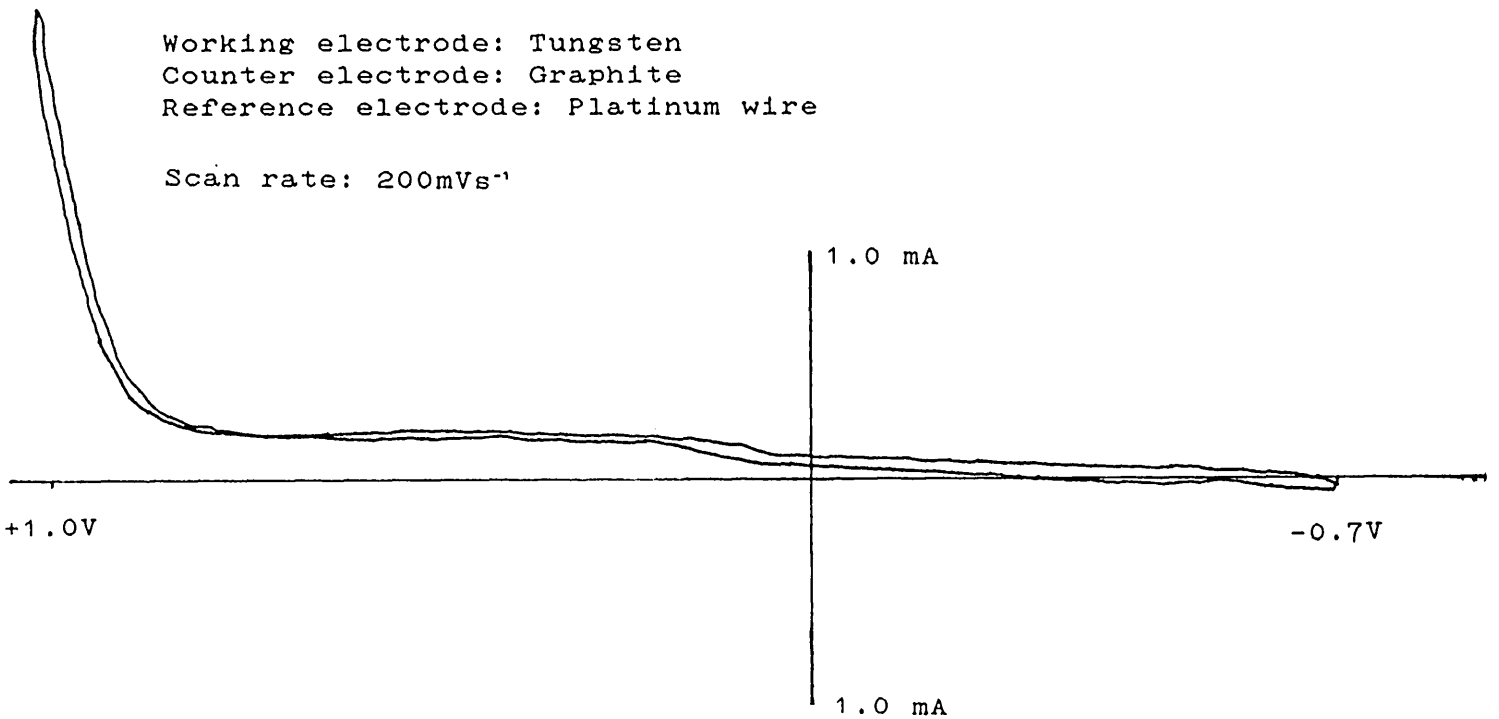
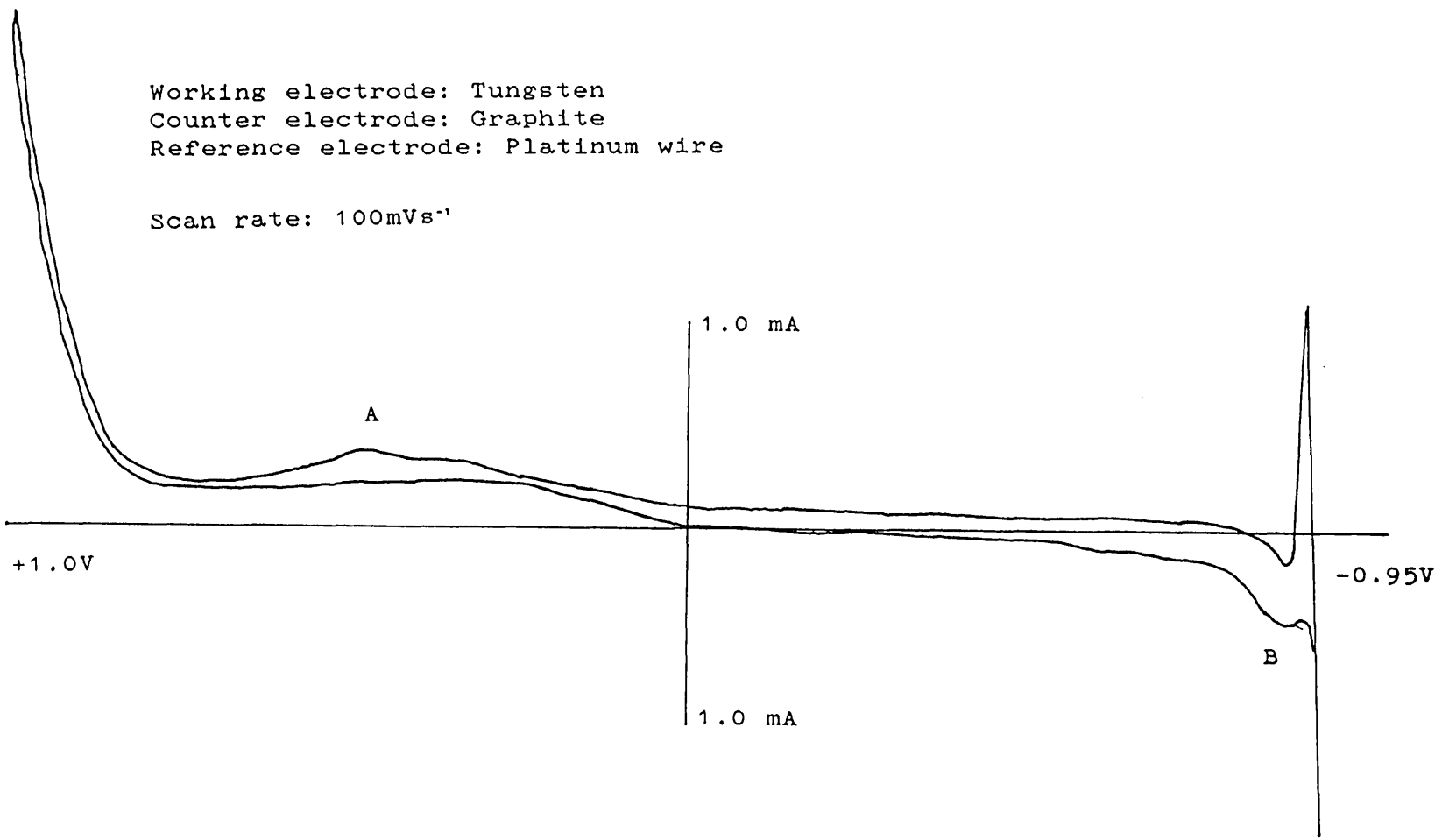


Figure 5.3. Cyclic voltammogram of purified 15 mole per cent NaCl-$ZnCl_2$ melt at 391°C under argon



The effect of exposing a purified melt to the atmosphere was to enhance the intensity of the "additional" peaks (fig. 5.4). This only occurred after several hours exposure, indicating a relatively slow interaction with moisture in the molten state. For comparison a "wet" melt was investigated; this was prepared by mixing in the dry box Analar zinc chloride and sodium chloride from the bottle and melting under dry flowing argon without any purification. Initially copious quantities of water were evolved from a water-white melt; under these conditions the voltammograms exhibited much larger currents (fig. 5.5). After about three hours the evolution of water appeared to cease, and after one day, the glass of the container was etched and opaque. By this time the current was somewhat diminished, and some rather ill-defined peaks could be distinguished (fig. 5.6).

It was also observed that when the "wet" melt was allowed to solidify in its (etched) Pyrex container, the container shattered, whereas with purified melts, even those exposed to air for several days, the still transparent container did not shatter and furthermore the solid melt did not adhere to the glass. These observations are indicative of the reduction of the concentration of oxide ions and related species in the melt (which are known to cause etching of glass) by the purification process.

To conclude, it may be noted that tungsten anodically oxidised in aqueous NaOH to form an oxide layer, produces similar voltammetric peaks in KCl-$ZnCl_2$ melt (81). Also

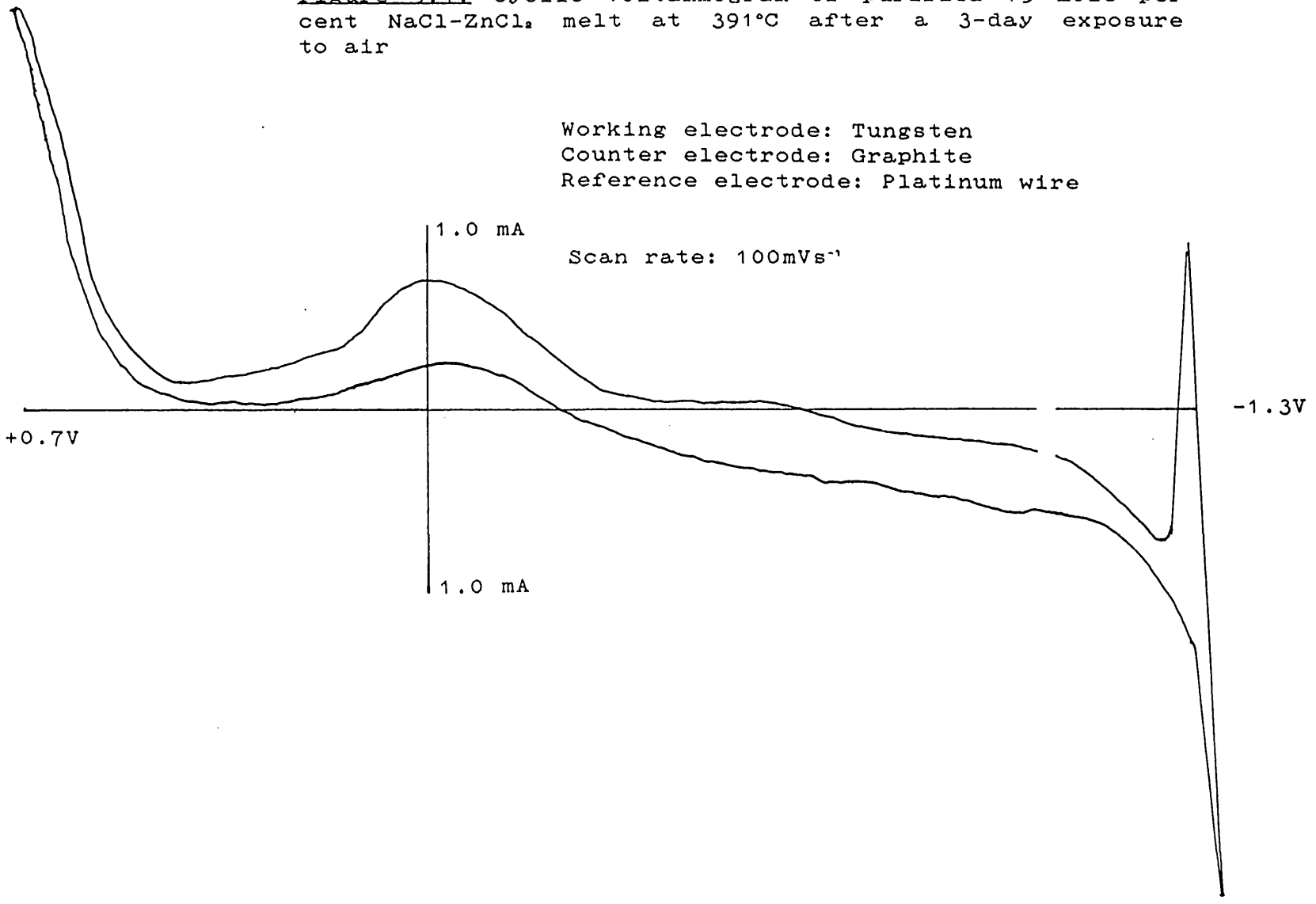


Figure 5.4. Cyclic voltammogram of purified 15 mole per cent NaCl-$ZnCl_2$ melt at 391°C after a 3-day exposure to air

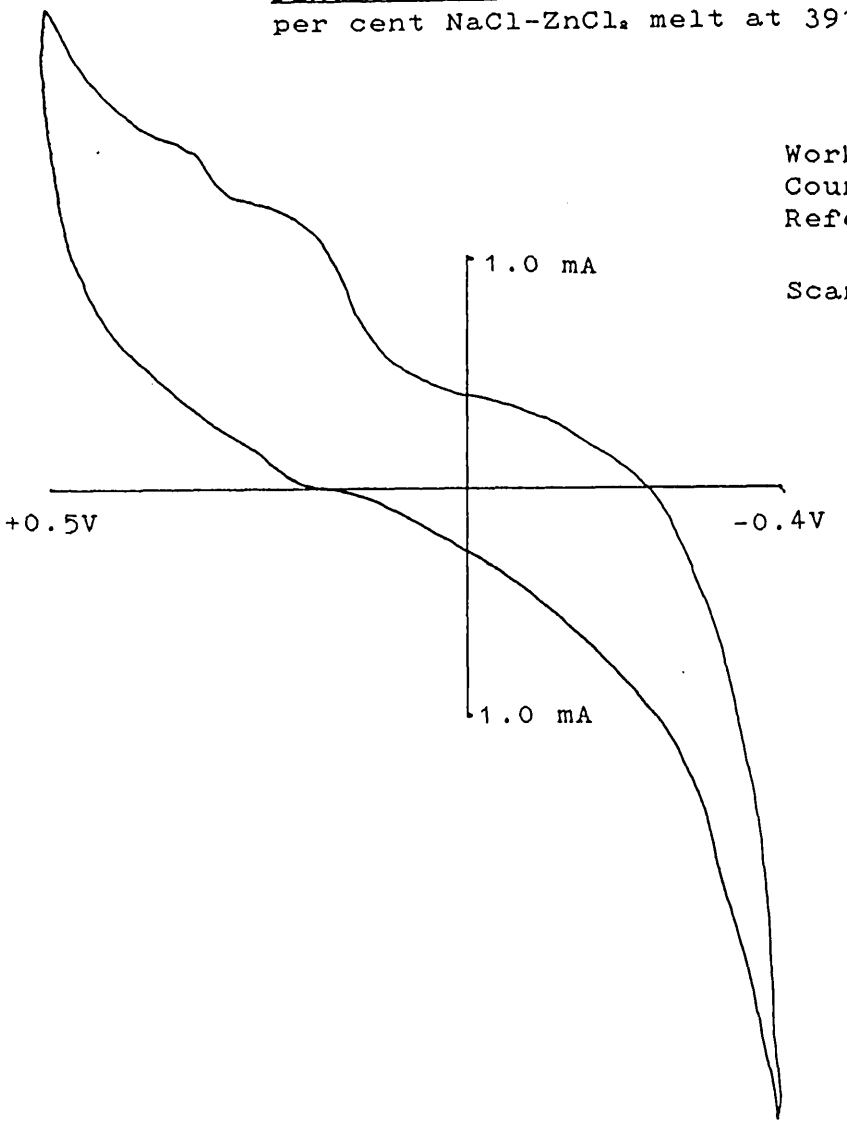


Figure 5.5. Cyclic voltammogram of unpurified 15 mole per cent NaCl-$ZnCl_2$ melt at 391°C

Working electrode: Tungsten
Counter electrode: Graphite
Reference electrode: Platinum wire

Scan rate: 100mVs^{-1}

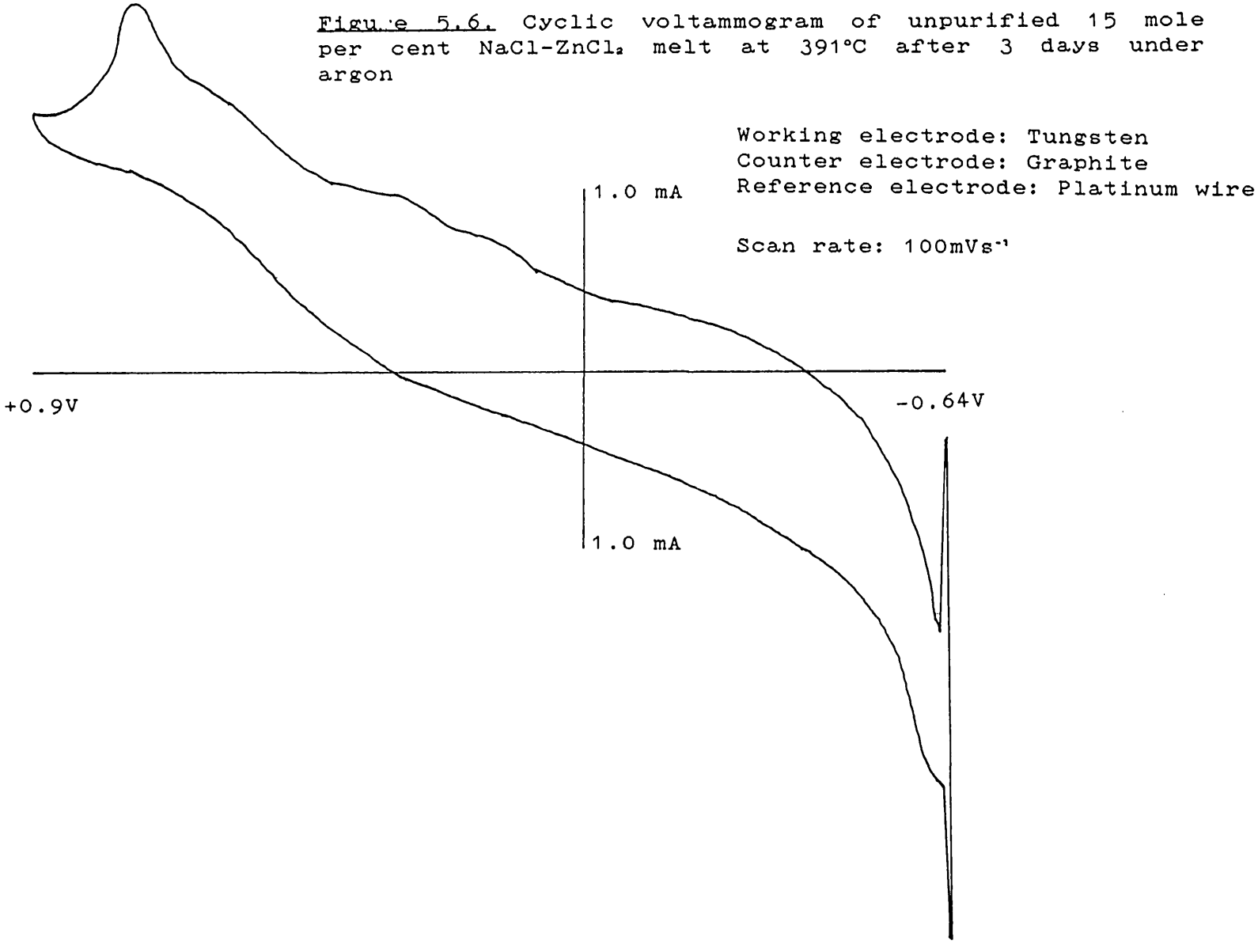


Figure 5.6. Cyclic voltammogram of unpurified 15 mole per cent $NaCl-ZnCl_2$ melt at 391°C after 3 days under argon

Melandres (82) reported "extraneous" peaks when investigating the behaviour of water in LiCl-KCl melts; these peaks were probably manifestations of the same oxide layer.

ii) Vitreous carbon electrode.

In complete contrast to the behaviour of the tungsten electrode, this electrode exhibited no distinct peaks until the melt limits were reached. Thus cyclic voltammograms obtained with purified melts, purified melts exposed to air, and even unpurified melts with copious water evolution, were virtually identical. A typical voltammogram is shown in figure 5.7.

It is of interest that Perry and McDonald (37) failed to obtain peaks on glassy carbon for the reduction of HCl in KCl-$ZnCl_2$ melts, though platinum gave well-defined waves, whereas Minh and Welch (83) surprisingly did obtain waves on glassy carbon in LiCl-KCl-$ZnCl_2$. Osteryoung in contrast reported that waves due to water (or the hydrolysis products, e.g. HCl) could not be obtained in room temperature chloroaluminate melts (84), due to the high overpotential for hydrogen evolution. Hence the evidence suggests that the protonic melt species cannot be reduced on vitreous carbon before the cathodic melt limit is achieved.

iii) Platinum wire electrode.

Tested only in purified melts, the platinum electrode showed low residual currents which confirmed the removal of impurities, but the working range was less than that of tungsten or vitreous carbon (fig. 5.8). As the potential

Figure 5.7. Typical cyclic voltammogram using vitreous carbon working electrode: purified, unpurified or air-exposed 15 mole per cent NaCl-$ZnCl_2$ melt at 391°C

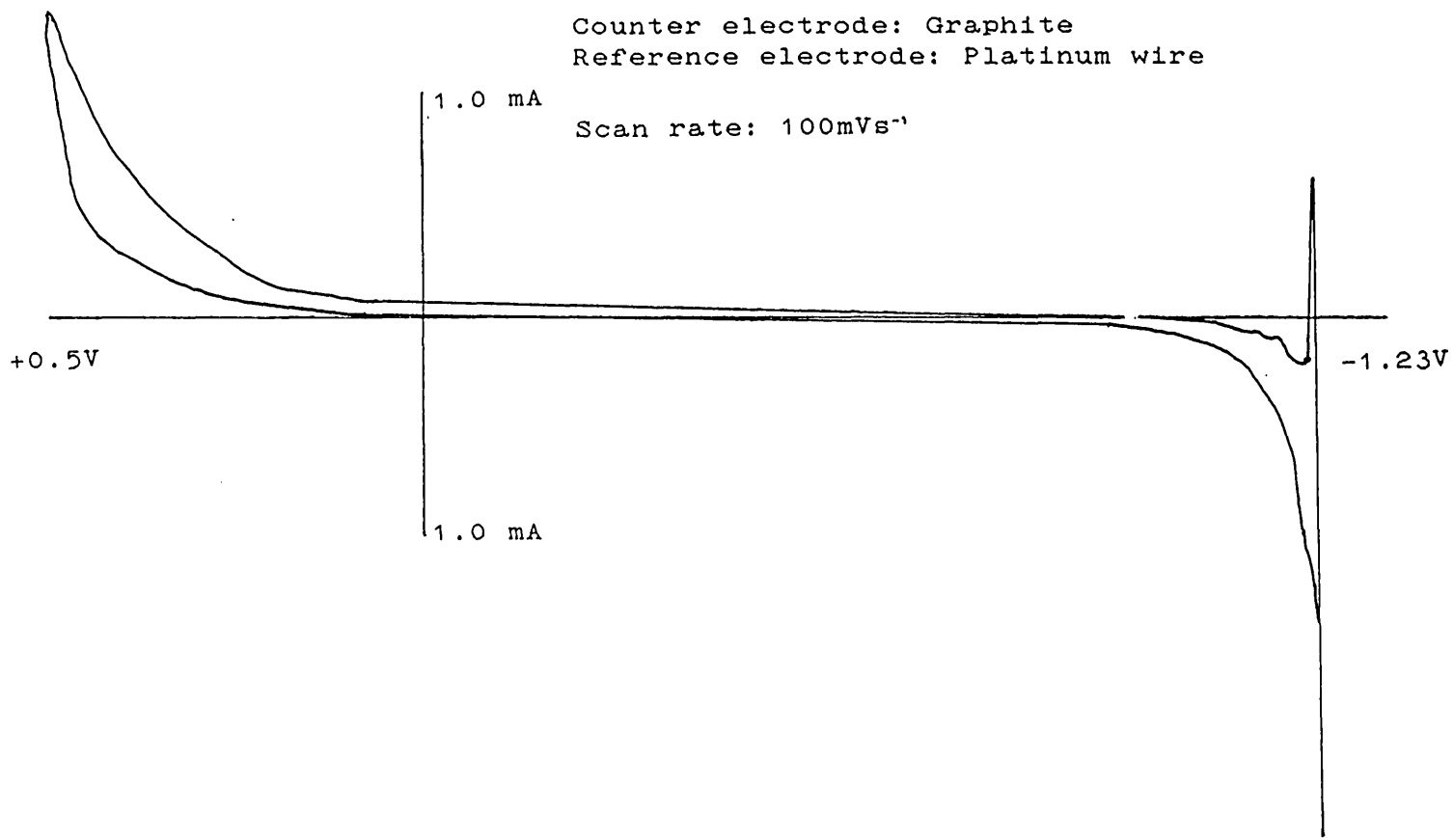
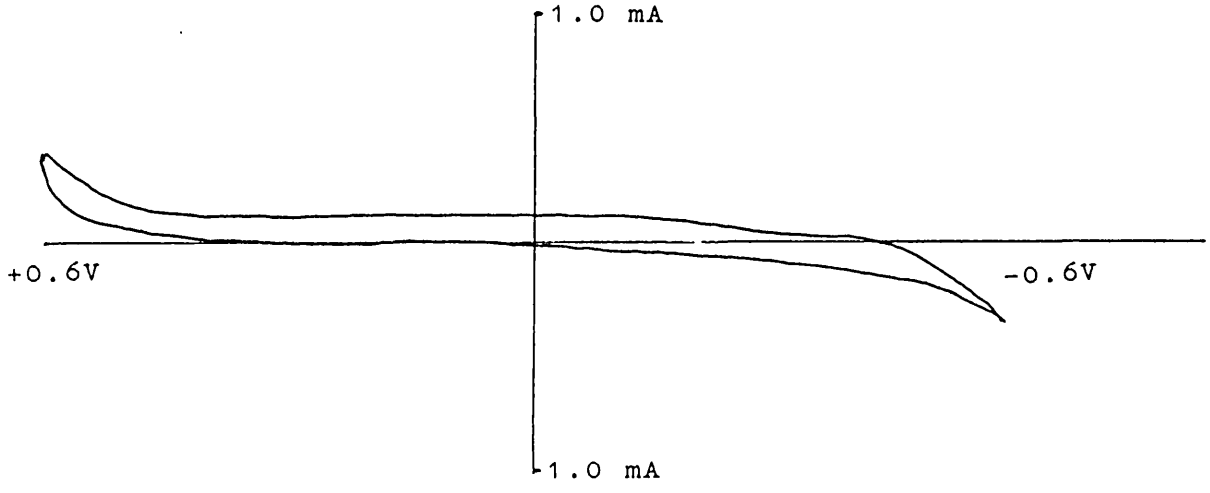


Figure 5.8. Cyclic voltammogram of purified 15 mole per cent NaCl-$ZnCl_2$ melt at 391°C



was lessened in the negative direction a reaction occurred, presumably zinc deposition, the scan becoming "noisy". A sharp stripping peak was not observed, probably due to alloying of zinc with the platinum, as previously reported (65). At a potential of about +1.2V relative to the zinc deposition potential, a reaction was observed which was probably the anodic dissolution of platinum rather than chlorine evolution (65).

iv) Gold electrode.

The range of this electrode (in purified melts) was only about 0.7V, the behaviour being qualitatively similar to that of the platinum electrode. Again a broad stripping peak suggested alloying of deposited zinc,and anodic dissolution of the gold appeared to occur, confirmed by visual observation of a brown colouration around the electrode. A typical voltammogram is shown in figure 5.9.

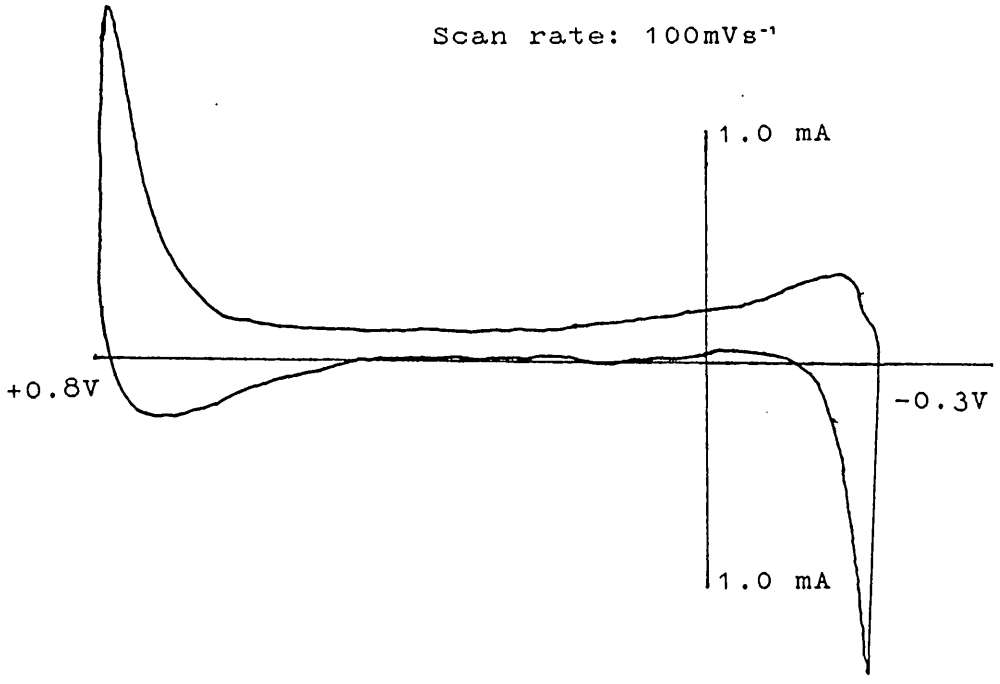
5.4 Conclusions

From this brief study, it was concluded that the low residual currents obtained with tungsten, platinum, and gold electrodes in purified melts demonstrated the success of the purification process in removing electroactive impurities due to the presence of water. It is not however possible to estimate the concentration of electroactive species present, due to the unknown nature of the processes occurring. It has been reported that the same process generally results in less than 500 ppm oxygen content in KCl-$ZnCl_2$ melts (35,37). Generally the residual currents were not significant compared with

Figure 5.9. Cyclic voltammogram of purified 15 mole per cent $NaCl-ZnCl_2$ melt at 391°C under argon

Working electrode: Gold
Counter electrode: Graphite
Reference electrode: Platinum wire

Scan rate: $100mVs^{-1}$



the currents due to the dissolved solute species.

However, the use of the above-mentioned electrodes in the solute studies was considered undesirable, due to the possibility of reactions such as metal dissolution, formation of surface films, and alloying. Hence the vitreous carbon electrode was exclusively used for the solute studies. This electrode has the advantage of low residual currents, and the absence of alloying or dissolution reactions. A possible disadvantage was the inability to detect waves due to contamination by water; however it was considered that any such contamination would probably be detectable by the effect on the solute species, and thus influence the form of the cyclic voltammograms.

CHAPTER SIX

CYCLIC VOLTAMMETRY OF CHROMIUM COMPOUNDS IN ZINC CHLORIDE-ALKALI CHLORIDE MELTS

6.1 Procedure and general observations

This chapter mainly concerns the electrochemical behaviour of chromium(II) solutions in these melts. The solutions were conveniently prepared by the reaction of finely-divided chromium metal with the molten salt, and it was hoped that this procedure would minimise oxygen contamination of the melts. It was not possible to prepare chromium(III) solutions in the more acidic melts, due to the insolubilty of the chloride.

The reaction of chromium metal produced visually a grey suspension, which settled to leave a clear pale green solution, regardless of melt composition. Unreacted chromium metal and chromium(III) oxide, but not zinc metal, were detected in the residue after dissolving the solidified melt in water. However, the green melt solution gave the characteristic strongly reducing blue chromium(II) solution in water, leaving little doubt that chromium dissolution in the melt occurred by displacement of zinc:

$$Cr + ZnCl_2 \longrightarrow CrCl_2 + Zn \qquad (6.1)$$

This is consistant with the fact that the free energies of formation of the respective chlorides differ by only about 10 kJmole^{-1} at 400°C, and thus in the presence of a large excess of zinc chloride, as in the present work, reaction 6.1 will proceed to the right.

The aqueous chromium(II) solutions were conveniently

analysed by A.A. to provide chromium, zinc, and alkali metal melt concentrations.

The redox behaviour of the chromium(II) melt solutions was studied as a function of melt composition, solute concentration, and temperature. The maximum temperature employed in the studies was about 440°C, chosen so as to minimise problems due to volatilisation of zinc chloride, particularly in the more acid melts. It is convenient to consider the more basic melts first, however, as these exhibited readily interpretable electrochemical behaviour. All density and viscosity values needed below (e.g to calculate chromium(II) concentrations and Stokes law radii) are derived from data given in references 44, 45, and 46.

6.2 Cyclic voltammetry of chromium(II) solutions- Results and Discussion

6.2.1 Potassium chloride-zinc chloride melts

a) 0.6 mole fraction KCl and 0.5 mole fraction KCl.

The oxidation of chromium(II) in melts of these compositions was found to be a one-electron reversible process involving soluble reactant and product, for all concentrations of chromium(II) and temperatures studied. In the case of the 0.5 mole fraction KCl mixture, the reaction of chromium metal at 400°C produced a maximum chromium(II) concentration of 0.16M, which appeared to be in equilibrium with excess chromium metal. The maximum concentration was not determined for the 0.6 mole fraction KCl composition. No reduction wave for chromium(II) could be observed before the onset of zinc deposition.

Thus figure 6.1 shows a typical cyclic voltammogram for chromium(II) in a 0.6 mole fraction KCl melt (0.065M at 388°C), while table 6.1 shows the behaviour of the voltammetric parameters with scan rate (ν). Figure 6.2 gives a plot of i_{pa} versus $\nu^{1/2}$. The peak separation, peak positions, and half-peak widths did not vary significantly with scan rate and are consistant with a reversible one-electron transfer (calculated ΔE_p, 131 mV, $E_{pa}-E_{pa/2}$, 125 mV). Also, the i_{pa}/i_{pc} values are nearly constant and close to 1.0 for all scan rates.

The linearity of the plot of i_{pa} against $\nu^{1/2}$ (fig. 6.2), also indicates the absence of chemical reactions coupled to the electron transfer.

For chromium(II) in the 0.5 mole fraction KCl melt, very similar results were obtained, with the exception that the peak separation increased slightly with scan rate (table 6.2). This may indicate a degree of irreversibility in the electron transfer reaction, though the effects of uncompensated solution resistance cannot be ruled out, the effect being enhanced by a drop in melt conductivity, e.g. by increasing the zinc chloride content (see below).

Table 6.2 also shows that below 50 mVs^{-1}, the peak current ratio is somewhat less than one. This was a quite general phenomenon if the melt temperature was above about 400°C, and was attributed to removal of the reaction product by convection due to the relatively long scan times.

Figure 6.3 shows plots of i_{pa} versus $\nu^{1/2}$ for

Figure 6.1. Typical cyclic voltammogram for the oxidation of chromium(II) (0.065M) in 0.6 mole fraction KCl-$ZnCl_2$ at 388°C

Working electrode: vitreous carbon
Reference electrode: zinc

Scan rate: 1000 mVs^{-1}

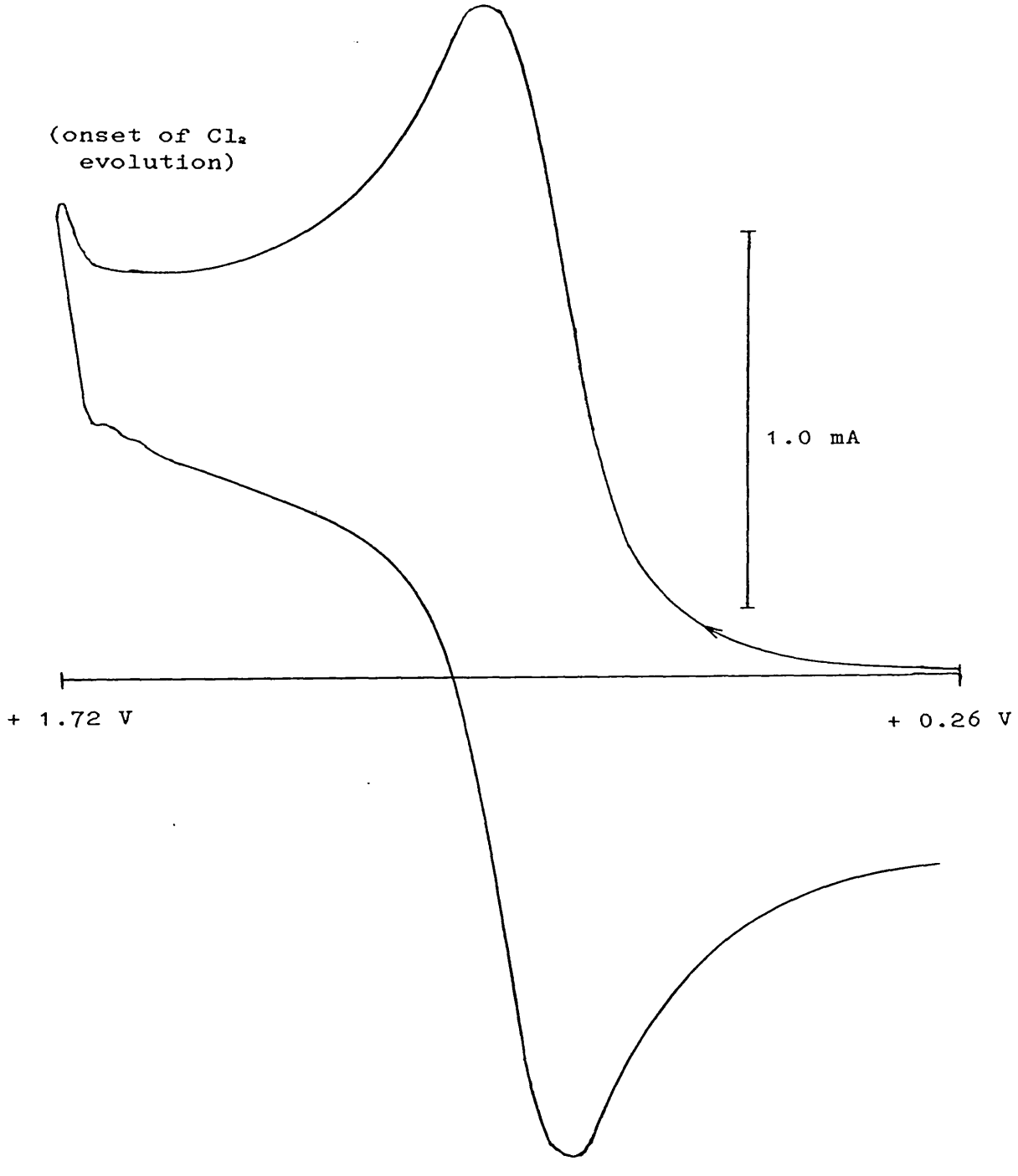


Table 6.1. Voltammetric Parameters for 0.065M chromium(II) in 60/40 mole p.c. KCl/$ZnCl_2$ at 388°C

Scan rate/ mVs^{-1}	I_{pc}/I_{pa}	ΔE_p/ mV	$I_{pa}/\nu^{1/2}$/ $mA/(Vs^{-1})^{1/2}$
1000	1.10	130	1.78
500	1.08	"	1.80
200	1.05	"	1.82
100	1.08	"	1.82
50	1.02	"	1.82
20	1.03	"	1.86
	$E_{pa}-E_{pa/2}$/mV	E_{pa}/V	$E_{1/2}$/V
1000	130	1.01	0.95
500	130	"	"
200	130	"	"
100	130	"	"
50	130	"	"
20	130	"	"
5	130	"	"

Table 6.2. Voltammetric Parameters for 0.15M chromium(II) in 50/50 mole p.c. KCl/$ZnCl_2$ at 412°C

Scan rate/ mVs^{-1}	I_{pc}/I_{pa}	ΔE_p/ mV	$I_{pa}/\nu^{1/2}$/ $mA/(Vs^{-1})^{1/2}$
1000	1.07	180	4.22
500	1.06	190	4.30
200	1.02	170	4.47
100	0.99	165	4.67
50	0.95	160	4.90
20	0.87	150	5.23
5	0.82	140	6.19
	$E_{pa}-E_{pa/2}$/mV	E_{pa}/V	$E_{1/2}$/V
1000	140	1.15	-
500	140	1.14	-
200	135	1.13	-
100	130	1.13	-
50	130	1.13	-
20	130	1.12	-
5	130	1.11	1.04

Table 6.2 continued. Voltammetric Parameters for 0.15M chromium(II) in 50/40 mole p.c. KCl/$ZnCl_2$ at 333°C

Scan rate/ mVs^{-1}	I_{pc}/I_{pa}	ΔE_p/ mV	$I_{pa}/\nu^{1/2}$/ $mA/(Vs^{-1})^{1/2}$
1000	1.14	182	2.79
500	1.10	180	2.84
200	1.10	148	2.88
100	1.13	127	2.76
50	1.15	127	2.74
20	1.23	127	2.82
5	1.07	125	3.04
	$E_{pa}-E_{pa/2}$/mV	E_{pa}/V	$E_{1/2}$/V
1000	153	1.09	-
500	149	1.09	-
200	132	1.08	-
100	127	1.07	-
50	127	1.07	-
20	116	1.07	-
5	111	1.07	1.01

Table 6.2 continued. Voltammetric Parameters for 0.15M chromium(II) in 50/50 mole p.c. KCl/$ZnCl_2$ at 293°C

Scan rate/ mVs^{-1}	I_{pc}/I_{pa}	ΔE_p/ mV	$I_{pa}/\nu^{1/2}$/ $mA/(Vs^{-1})^{1/2}$
1000	1.13	135	2.15
500	1.13	137	2.17
200	1.15	127	2.13
100	1.10	111	2.23
50	1.09	111	2.19
20	1.03	85	2.28
5	0.82	85	2.60
	$E_{pa}-E_{pa/2}$/mV	E_{pa}/V	$E_{1/2}$/V
1000	127	1.07	-
500	116	1.07	-
200	116	1.06	-
100	116	1.05	-
50	111	1.05	-
20	106	1.04	-
5	85	1.04	0.99

Table 6.2 continued. Voltammetric Parameters for 0.15M chromium(II) in 50/50 mole p.c. KCl/ZnCl$_2$ at 260°C

Scan rate/ mVs^{-1}	I_{pc}/I_{pa}	ΔE_p/ mV	$I_{pa}/\nu^{1/2}$/ $mA/(Vs^{-1})^{1/2}$
1000	1.11	176	1.52
500	1.12	148	1.50
200	1.09	127	1.54
100	1.02	106	1.62
50	1.00	106	1.61
20	0.93	95	1.66
5	0.57	85	1.76
	$E_{pa}-E_{pa/2}$/mV	E_{pa}/V	$E_{1/2}$/V
1000	153	1.03	-
500	132	1.02	-
200	161	1.01	-
100	106	1.00	-
50	106	1.00	-
20	106	1.00	-
5	106	1.00	0.95

Figure 6.2. Plot of peak current against square root of scan rate for the oxidation of chromium(II) (0.065M) in 0.60 mole fraction KCl-$ZnCl_2$ at 388°C

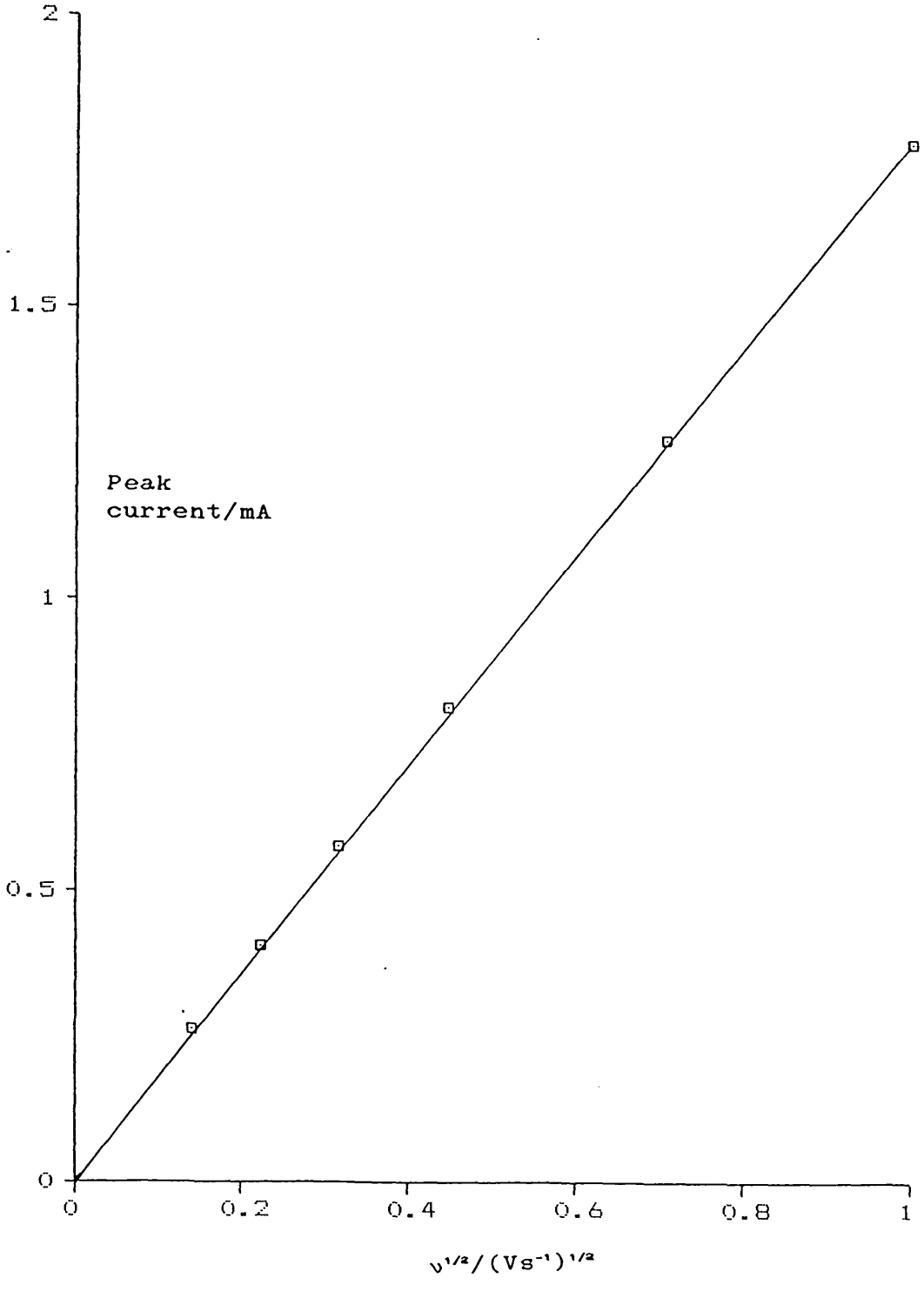
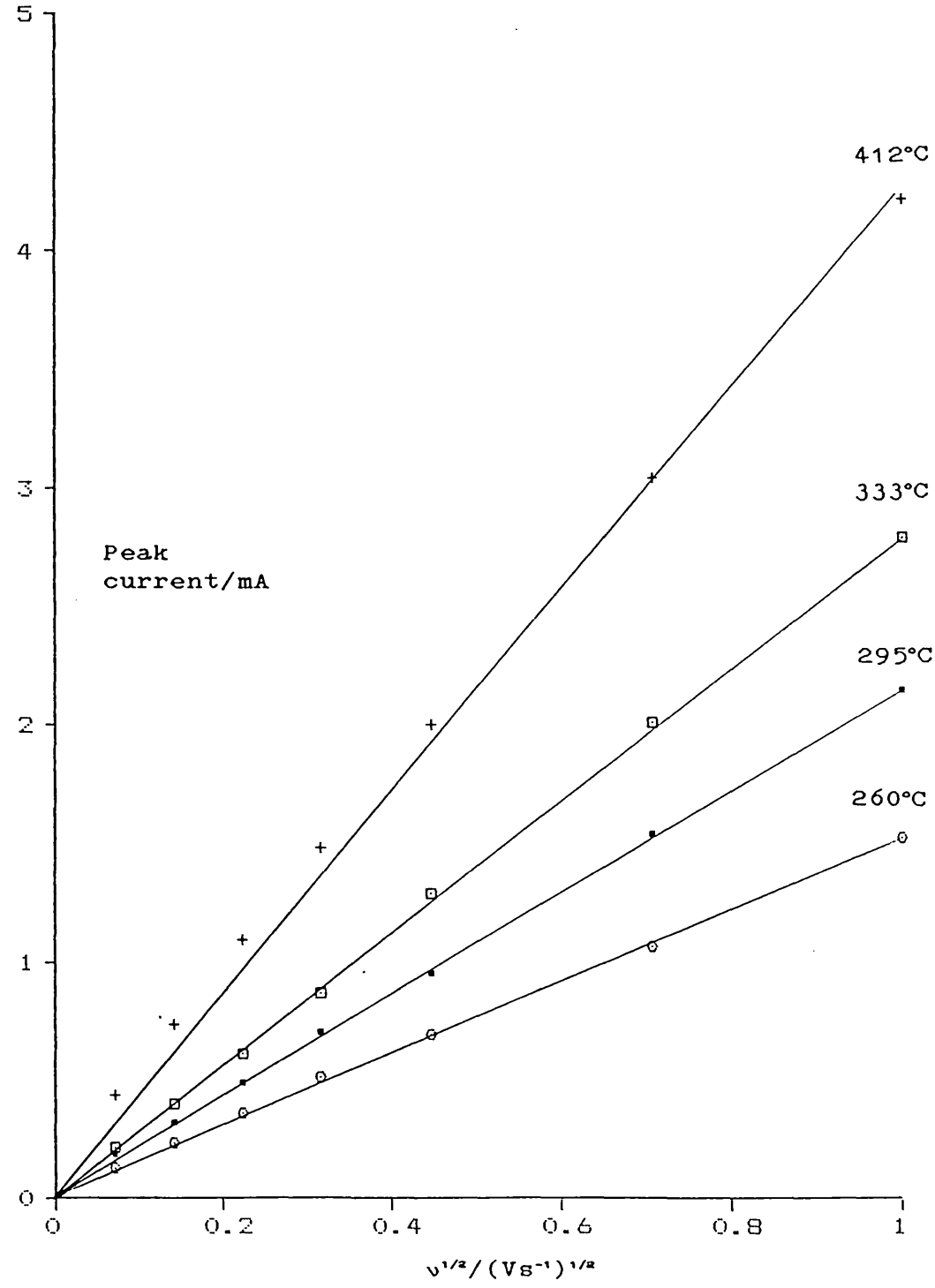


Figure 6.3. Plots of peak current against square root of scan rate for the oxidation of chromium(II) (0.16M) in 0.50 mole fraction KCl-$ZnCl_2$ at various temperatures



various temperatures. It may be noticed that the plots are good straight lines passing through the origin, except at the highest temperature (412°C) where convection effects can be observed at the lower scan rates, and cause the observed currents to be slightly higher than would be predicted from the expected linear relationship.

Diffusion coefficients (cm^2s^{-1} x 10^{-6}) calculated for the four temperatures from the gradients of the peak current/square root(scan rate) plots were as follows: 412°C, 5.0; 333°C, 2.0; 295°C, 1.1; 260°C, 0.5. An Arrhenius plot of lnD against 1/T is shown in figure 6.4. A reasonable straight line was obtained, giving:

$$\ln D = - 4.349 - 5389/T \qquad (6.2)$$

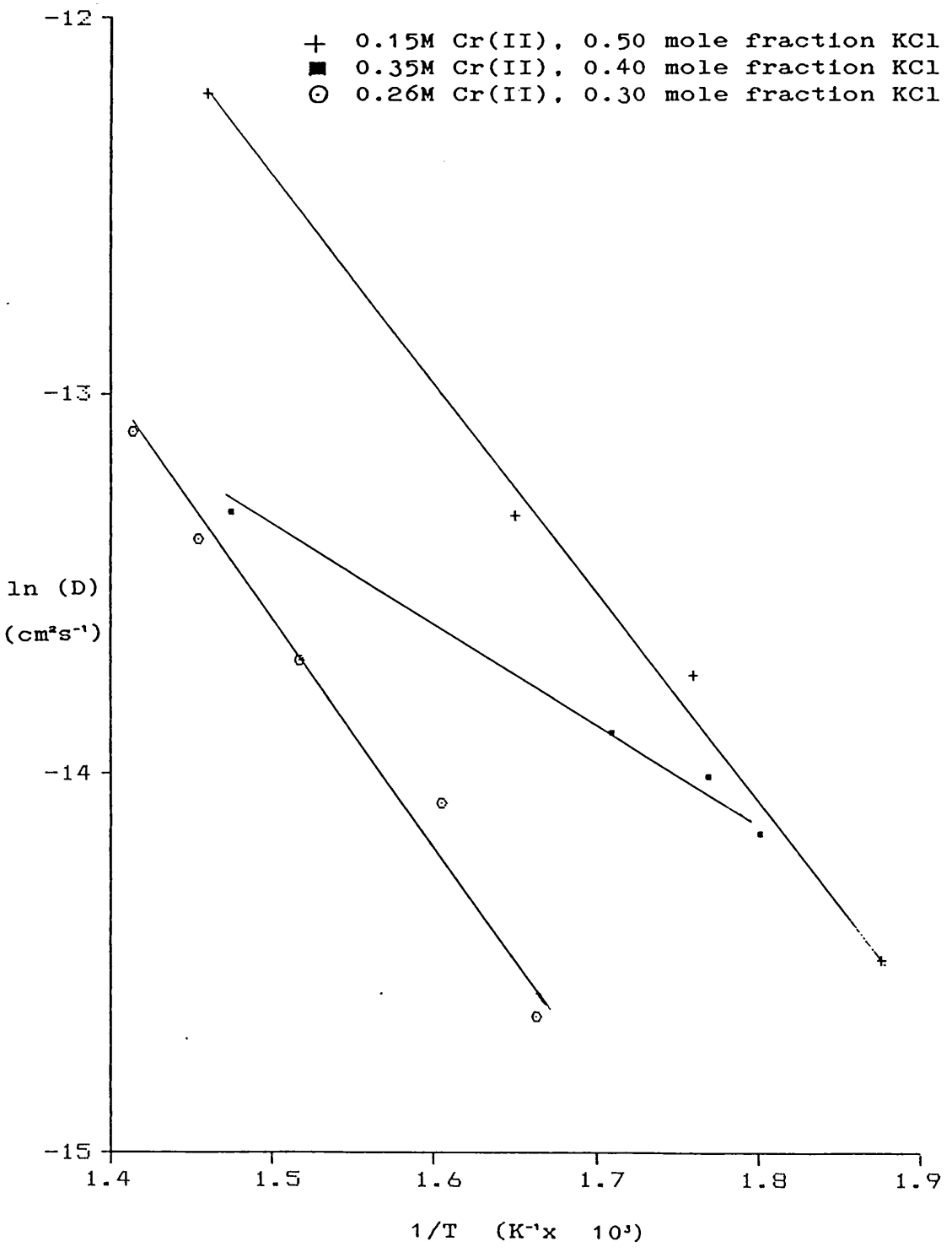
The value of the diffusion coefficient at 412°C may be compared with values obtained in LiCl/KCl eutectic at 397°C for divalent transition metal ions with similar ionic radii: Mn^{2+}, 7.4; Fe^{2+}, 6.9; Co^{2+}, 5.8 (94). As can be seen, the diffusion coefficients are quite similar. Also, Legey (95) has reported a value of $2.0x10^{-5}$ for Cr^{2+} in LiCl/KCl eutectic at 500°C; a value of $1.2x10^{-5}$ can be extrapolated from eqn. 6.2. However Vargas' results (96) give a value of only $1.8x10^{-6}$ at 450°C in this eutectic.

It is interesting to apply the Stokes-Einstein equation to the above results:

$$D = kT/6\pi r\eta \qquad (6.3)$$

where k is Boltzmann's constant, r is the radius of the diffusing ion, and η is the solution viscosity. For the

Figure 6.4. Arrhenius plots for the variation of diffusion coefficient of chromium(II) with temperature in various KCl-$ZnCl_2$ melts



LiCl/KCl eutectic, the viscosity was taken from reference 43. Table 6.3 shows the calculated radii for Cr^{2+} in various melts at various temperatures.

Table 6.3-Stokes radii for Cr^{2+} in KCl/$ZnCl_2$ and LiCl-KCl melts

Melt	Temperature/°C	Viscosity/mPa.s	Cr^{2+} radius/pm
0.6KCl/ $ZnCl_2$	388	7.8	135
0.5KCl/ $ZnCl_2$	412	5.9	169
"	333	12.6	181
"	295	26.1	148
"	260	85.1	90
LiCl/KCl	500	2.4	158

The moderate scatter in the values of the radii despite the relatively large changes in viscosity suggest that a correlation does exist in the form of eqn.(6.3). Furthermore, the values are similar to those obtained for the tetrahedral Fe^{2+} (170 pm) and Ni^{2+} (155 pm) in LiCl/KCl eutectic at 450°C (94), though these values are over twice the "crystallographic" radii for the ions (97), for example, Fe^{2+}, 63 pm for 4-coordination.

The above results are consistant with the presence of a tetrahedral chromium(II) species in the zinc chloride-containing melts, though care must be exercised in the use of the Stokes-Einstein relation, since this is strictly applicable only to spheres moving through an incompressible continuum, but the relation is roughly obeyed by cations in molten salts (98).

Returning to the voltammetric results, these may be compared with results obtained in the LiCl/KCl eutectic, where conflicting reports exist concerning the Cr^{2+}/Cr^{3+} couple. For example, Vargas (96) obtained a reversible wave for Cr^{2+} oxidation ($CrCl_2$ concentration: 0.931M) at 450°C, whereas Levy and Reinhardt (99) reported low i_{pa}/i_{pc} values for the otherwise reversible Cr^{3+} reduction for sweep rates < $100mVs^{-1}$ and a solubility for $CrCl_2$ of only 40 ppm at 500°C. These results they attributed to the slow chemical reaction Cr^{2+} + $+2Cl^-$ ⟶ $CrCl_2$ (solid). Significantly, though, the low solubility was obtained after bubbling argon through a $CrCl_2$ suspension for five hours, and filtering. It is thus likely that the $CrCl_2$ was decomposed to insoluble Cr_2O_3 by oxygen in the argon, no special purification procedures appearing to have been appied to the gas. Laitinen et al (100) obtained results similar to those of the latter authors (99) but noted that $CrCl_2$ was in fact appreciably soluble in the melt, and assumed that the low i_{pa}/i_{pc} values were due to an irreversible chemical reaction following the electron transfer:

$$CrCl_6^{3-} + e^- \rightleftharpoons CrCl_6^{4-} \text{ (rapid)} \qquad (6.4)$$

$$CrCl_6^{4-} \longrightarrow CrCl_4^{2-} + 2Cl^- \text{ (slow)} \qquad (6.5)$$

However, as noted above, the low peak current ratios at relatively slow scan rates in zinc chloride-based melts appeared to be a general phenomenon, regardless of melt composition or solute species, and were attributed to the effects of convection.

To sum up, the behaviour of chromium(II) in the 0.5 and 0.6 mole fraction $KCl/ZnCl_2$ appears to parallel that in the LiCl/KCl eutectic, and it likely that the same chloro-complexes of chromium(II) and (III) (i.e. the hexachlorochromate(III) and tetrachlorochromate(II) ions formulated in eqns. 6.4 and 6.5 above) exist in these melts given the relative availability of chloride ion. For example, bulk oxidation of the green chromium(II) solutions in the chlorozincate melts produced a violet solution characteristic of the hexachlorochromate(III) ion postulated to exist in melts such as the LiCl/KCl eutectic (101). However, UV/visible spectroscopy would be necessary to confirm this conjecture.

b) 0.4 mole fraction KCl.

At 400°C, voltammetric parameters for a 0.35M chromium(II) solution in this melt suggested behaviour similar to that observed for the 0.5 mole fraction KCl melt, i.e. a reversible one-electron oxidation involving soluble reactant and product (table 6.4). Thus the plot of i_{pa} versus $\nu^{1/2}$ is linear, apart from deviations introduced by convection at lower scan rates (fig. 6.5).

However, on cooling the solution below about 320°C, a distinct change was observed in the reverse (cathodic) sweep of the voltammograms at scan rates < 50 mVs^{-1}, the waves becoming narrower, with in increase in current over the expected reversible value, leading to relatively high values of i_{pa}/i_{pc} (table 6.5). On further cooling to 282°C, inflections could be observed in the cathodic peaks, corresponding to relatively abrupt increases in

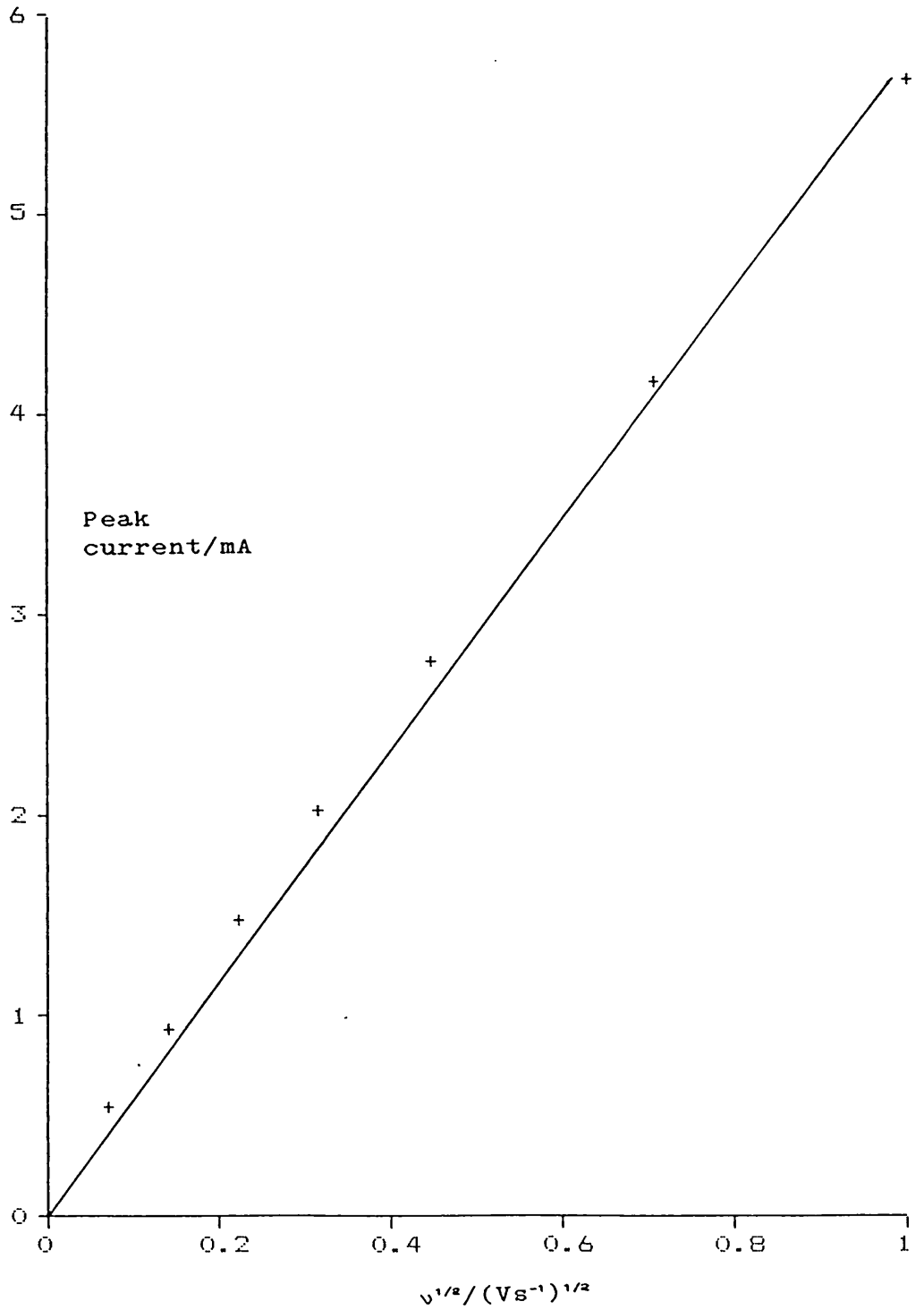
Table 6.4. Voltammetric Parameters for 0.35M chromium(II) in 40/60 mole p.c. KCl/$ZnCl_2$ at 400°C

Scan rate/ mVs^{-1}	I_{pc}/I_{pa}	ΔE_p/ mV	$I_{pa}/\nu^{1/2}$/ $mA/(Vs^{-1})^{1/2}$
1000	1.09	200	5.67
500	1.06	190	5.89
200	1.02	170	6.18
100	1.01	150	6.41
50	1.00	143	6.61
20	1.03	125	6.58
5	0.87	115	7.75
	$E_{pa}-E_{pa/2}$/mV	E_{pa}/V	$E_{1/2}$/V
1000	156	1.136	-
500	161	1.126	-
200	156	1.105	-
100	151	1.095	-
50	148	1.095	-
20	145	1.090	-
5	140	1.090	1.028

Table 6.5. Voltammetric Parameters for 0.35M chromium(II) in 40/60 mole p.c. KCl/$ZnCl_2$ at 312°C

Scan rate/ mVs^{-1}	I_{pc}/I_{pa}	ΔE_p/ mV	$I_{pa}/\nu^{1/2}$/ $mA/(Vs^{-1})^{1/2}$
100	1.10	110	4.59
50	1.02	105	4.71
20	0.98	120	5.03
10	1.23	150	5.13
5	1.32	130	5.61
	$E_{pa}-E_{pa/2}$/mV	E_{pa}/V	$E_{1/2}$/V
100	130	1.069	-
50	125	1.064	-
20	125	1.062	-
10	114	1.060	-
5	104	1.058	1.003

Figure 6.5. Plot of peak current against square root of scan rate for the oxidation of chromium(II) (0.35M) in 0.40 mole fraction KCl-$ZnCl_2$ at 400°C



reduction current (fig. 6.6). At 1 mVs^{-1} scan rate, an inflection could also be seen prior to the anodic peak.

To anticipate results discussed in the later sections of this chapter, it will be noted here that the form of the voltammograms was shown to be due to the deposition of chromium(III) chloride on the electrode, and subsequent stripping of this material, and is evidently strongly dependant on scan rate.

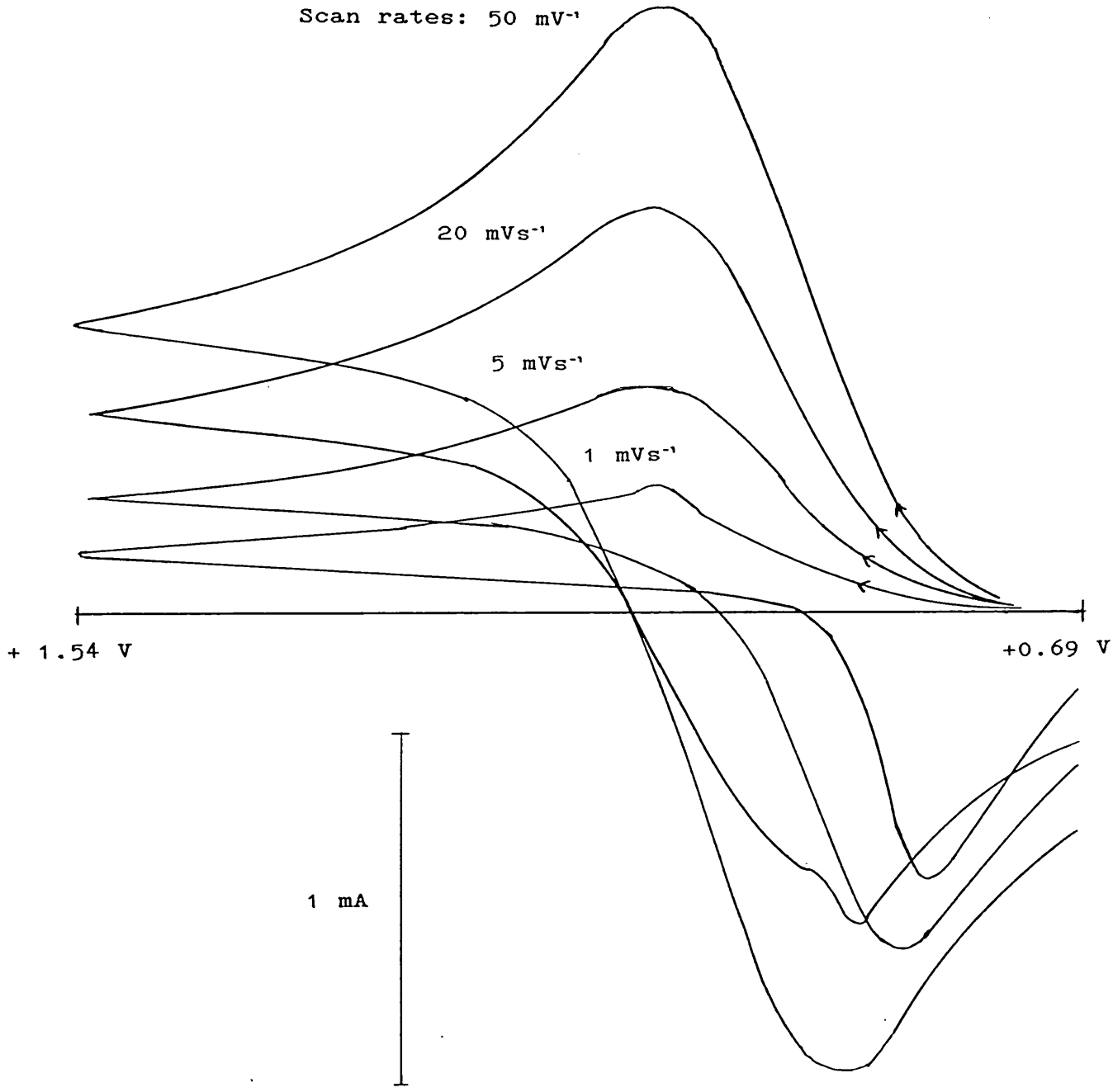
for a more concentrated chromium(II) solution (0.52M) in an 0.39 mole fraction KCl melt at 400°C, the voltammograms exhibited very narrow cathodic stripping peaks, up to at least 1 Vs^{-1}, and inflections were observed prior to the anodic peak, up to 100 mVs^{-1} (fig. 6.7). The i_{pc}/i_{pa} values were consequently relatively high, up to 2.8 (table 6.6). However, the plot of i_{pa} versus $v^{1/2}$ shown in figure 6.8 did not show deviations from linearity any more pronounced than those observed for the reversible oxidations in the more basic melts. On the other hand, a significant shift in peak potential with increasing scan rate, together with peak broadening, was noted, indicating an irreversibility effect (table 6.6).

The appearence of the anodic inflections may be rationalised by noting that, for a reversible reaction, the electrode surface concentration ratio of chromium(III) to chromium(II) is governed by the Nernst equation:

$$C_{Cr(III)}/C_{Cr(II)} = \exp[F(E-E^{\circ\prime})/RT] \qquad (6.6)$$

where E is the applied potential and $E^{\circ\prime}$ is effectively the half-wave potential. It can be seen that the surface concentration ratio is governed only by the applied

Figure 6.6. Typical cyclic voltammograms for the oxidation of chromium(II) (0.35M) in 0.40 mole fraction KCl-$ZnCl_2$ at 282°C



Working electrode: vitreous carbon
Reference electrode: zinc

Figure 6.7. Typical cyclic voltammogram for the oxidation of chromium(II) (0.52M) in 0.39 mole fraction KCl-$ZnCl_2$ at 400°C

Working electrode: vitreous carbon
Reference electrode: zinc
Scan rate: 100 mV^{-1}

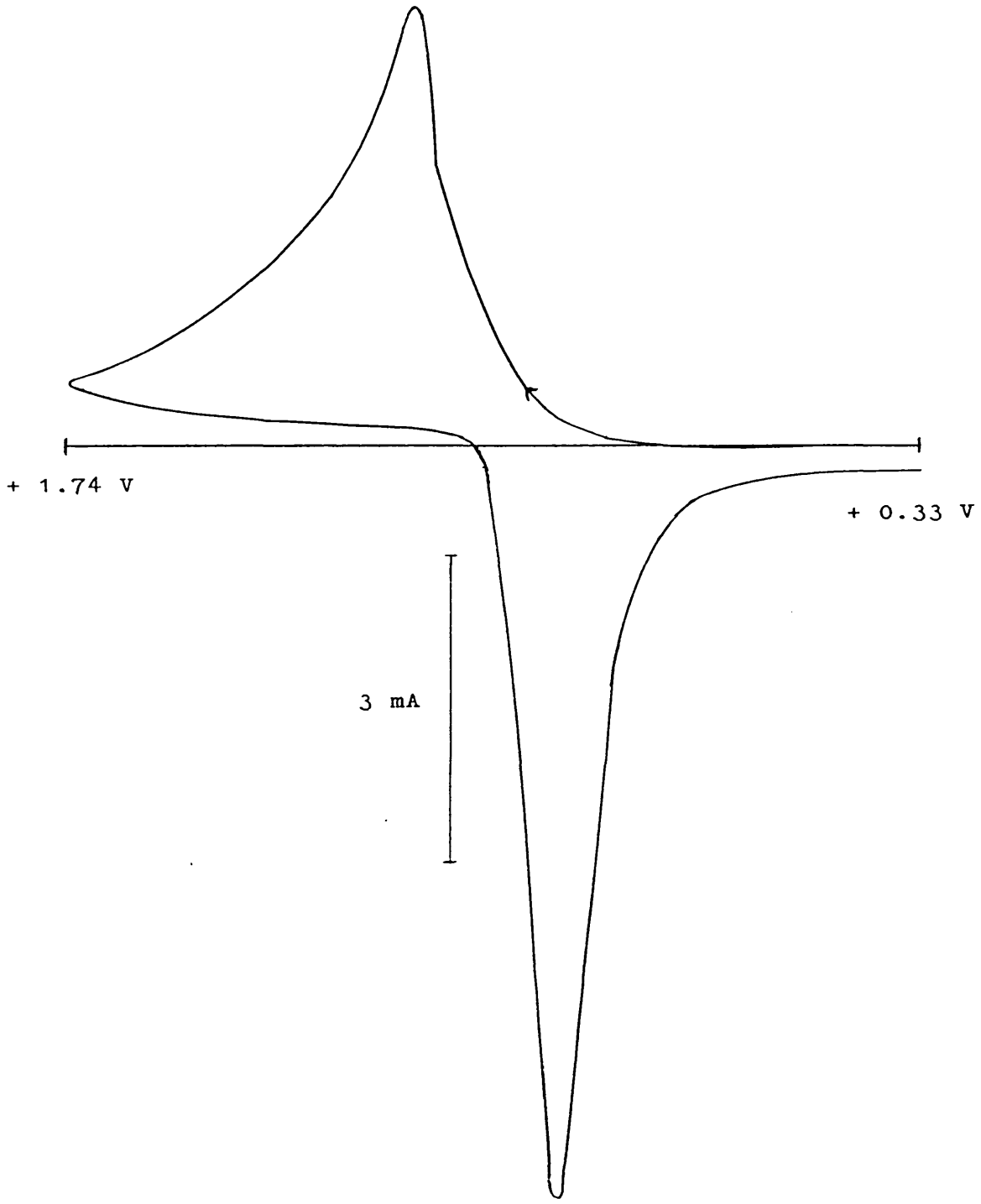


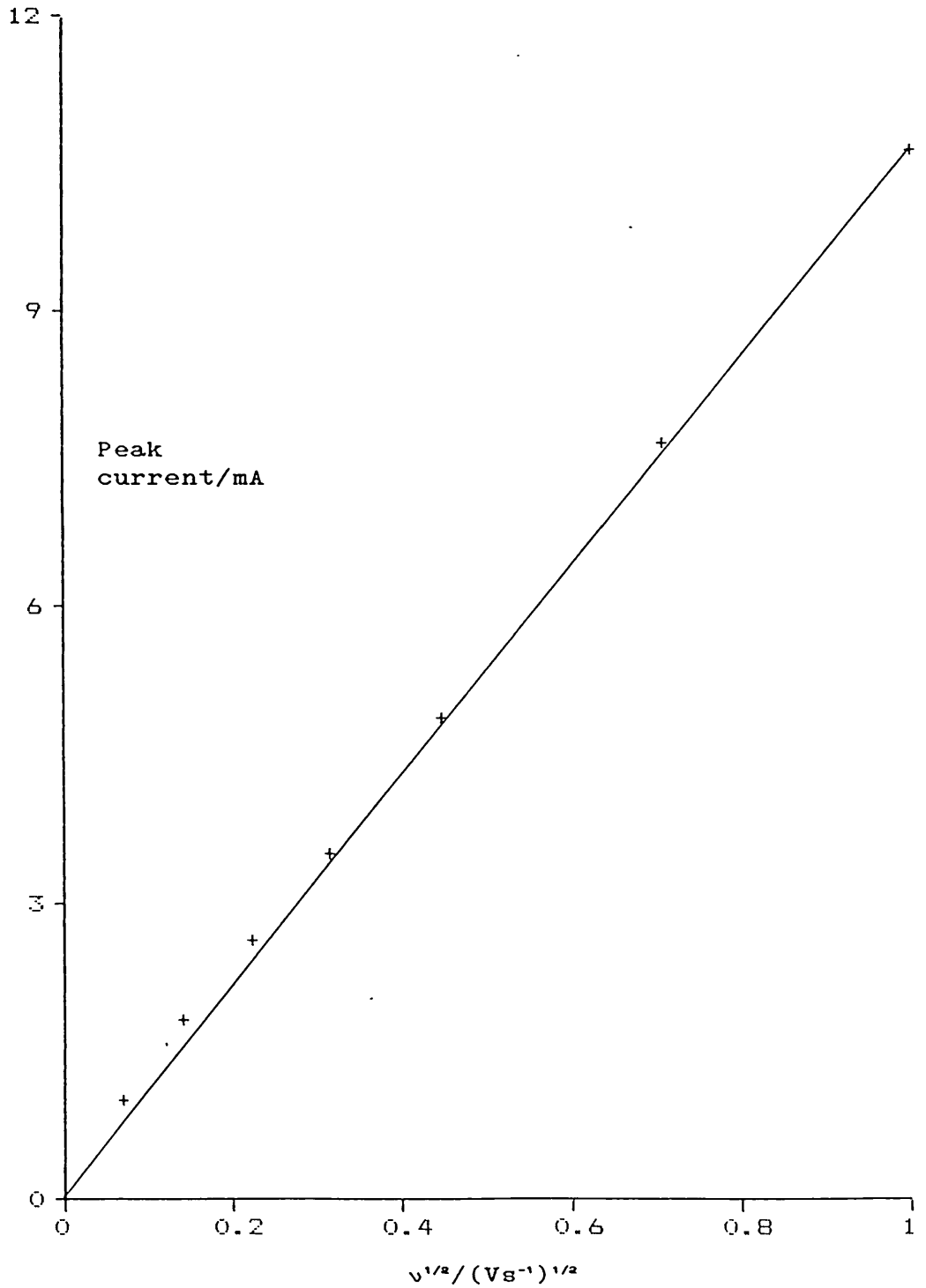
Table 6.6. Voltammetric Parameters for 0.52M chromium(II) in 39/61 mole p.c. KCl/$ZnCl_2$ at 400°C

Scan rate/ mVs^{-1}	I_{pc}/I_{pa}	ΔE_p/ mV	$I_{pa}/\nu^{1/2}$/ $mA/(Vs^{-1})^{1/2}$
1000	1.60	371	10.62
500	1.93	294	10.82
200	2.51	330	10.90
100	2.60	329	11.07
50	2.72	282	11.74
20	2.72	232	12.81
5	2.80	174	14.14
	$E_{pa}-E_{pa/2}$/mV	E_{pa}/V	
1000	177	1.302	
500	146	1.252	
200	162	1.213	
100	188	1.172	
50	146	1.146	
20	118	1.131	
5	94	1.103	

Table 6.7. Voltammetric Parameters for 0.26M chromium(II) in 40/60 mole p.c. KCl/$ZnCl_2$ at 319°C

Scan rate/ mVs^{-1}	I_{pc}/I_{pa}	ΔE_p/ mV	$I_{pa}/\nu^{1/2}$/ $mA/(Vs^{-1})^{1/2}$
1000	1.11	193	3.63
500	1.12	174	3.62
200	1.10	146	3.73
100	1.09	130	3.71
50	1.08	125	3.81
20	1.08	125	3.64
5	1.04	120	3.78
	$E_{pa}-E_{pa/2}$/mV	E_{pa}/V	$E_{1/2}$/V
1000	146	1.075	-
500	138	1.076	-
200	125	1.063	-
100	120	1.056	-
50	120	1.053	-
20	120	1.051	-
5	120	1.051	0.096

Figure 6.8. Plot of peak current against square root of scan rate for the oxidation of chromium(II) (0.52M) in 0.39 mole fraction KCl-$ZnCl_2$ at 400°C



potential, and thus when the solubility of chromium(III) at the electrode surface is exceeded, deposition should occur at a fixed potential, regardless of scan rate. This "critical potential" should correspond to the anodic inflection point on the voltammograms. However, it was also observed that the anodic inflection appeared only at relatively slow scan rates, and shifted anodically with increasing scan rate (see also below). This was undoubtedly partly a consequence of the irreversibility effects observed with the "soluble product" voltammograms, but also probably a result of a kinetic step in the nucleation and growth of the crystals of chromium(III) chloride, as is found, say, in the deposition of chromium metal from LiCl/KCl eutectic (96).

Considering the cathodic part of the voltammogram, it was evident that the form was strongly dependant on chromium(II) concentration and scan rate. At slow scan rates, a greater quantity of material can be deposited, the longer deposition time more than compensating for the reduced currents (since for two given scan rates, the current will decrease as the *square root* of the ratio of the scan rates, but the scan time will increase with the reciprocal of the ratio). Also, the deposit will have less tome to nucleate and grow. These effects can be observed in figure 6.6, as a transition from a rounded "soluble product" peak at higher scan rates, to a more angular stripping peak at lower scan rates.

An idea of the solubility of chromium(III) in these melts can be got by analysing the surface concentration.

For a Nernstian reaction involving a soluble product, it is readily deduced from the surface concentration relations (77,78) that:

$$C^{\circ}_{Cr(III)} = \Theta C^{\circ}_{Cr(II)}/[1+\exp(F(E-E_{1/2}))] \qquad (6.7)$$

where $C^{\circ}_{Cr(II)}$ is the bulk concentration of chromium(II), and Θ is $(D_{Cr(II)}/D_{Cr(III)})^{1/2}$. To a first approximation, Θ may be set to one. For 0.52M chromium(II) at 400°C, an anodic inflection (at 5 mVs^{-1}) occurred at about the "soluble product" peak potential, and so from eqn. 6.7, the surface concentration of chromium(III) at this potential was about 0.75 the bulk concentration of chromium(II), that is, 0.39M. With the less concentrated 0.35M chromium(II) solution at 400°C, eqn. 6.7 predicts that the saturation concentration of roughly 0.39M chromium(III) cannot be attained, since the maximum chromium(III) concentration is the bulk concentration of chromium(II), 0.35M, and thus soluble product behaviour is expected, as was in fact found.

Simlarly, the 0.35M solution at 312°C exhibited narrow cathodic peaks, but no anodic inflections, giving a predicted value for the saturated chromium(III) concentration of between 0.26 and 0.35M (since the potential corresponding to saturation and deposition of chromium(III) chloride is presumed to be anodic of the oxidation peak); whereas a 0.26M solution showed only soluble product behaviour at 319°C (down to 5 mVs^{-1} scan rate), as indicated by the parameters in table 6.7, which is consistant with the concentration range given above.

Typical values of diffusion coefficient calculated for the 0.35M chromium(II) solution are given in table 6.8, together with viscosities and Stokes' radii at various temperatures.

Table 6.8-Diffusion coefficients and Stokes radii for Cr^{2+} in 0.4 mole fraction KCl/$ZnCl_2$ melt

T/°C	D/cm^2s^{-1}	Viscosity/mPa.s	Cr^{2+} radius/pm
405	17 x10^{-7}	5.1	587
312	9.4 "	14.9	308
292	8.2 "	19.7	258
282	7.1 "	22.9	251

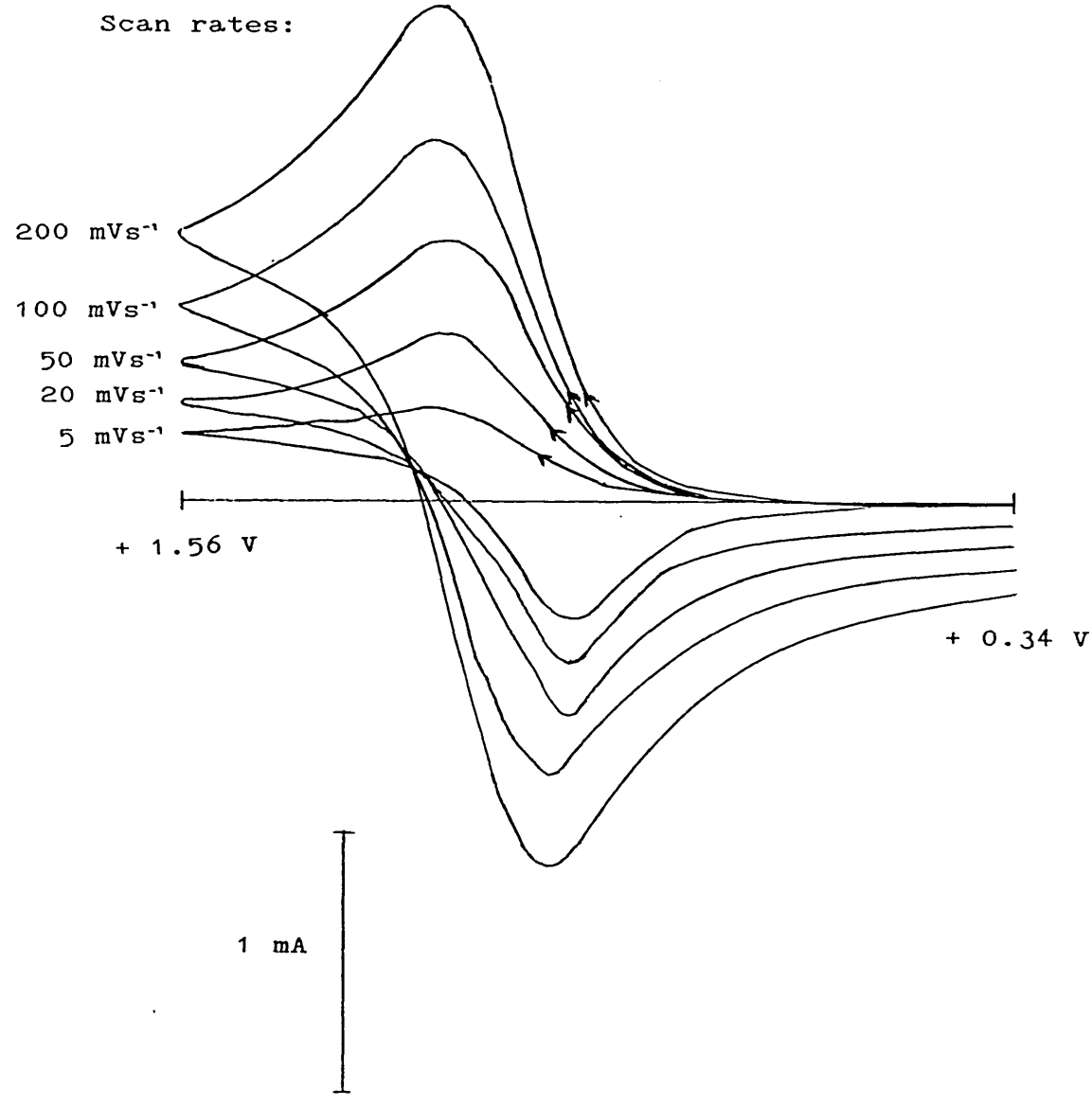
Generally the diffusion coefficients are lower and the radii higher than the values in the 0.5 and 0.6 mole fraction KCl melts, though the viscosities are quite similar. This may point to coordination by larger structural entities, e.g. $ZnCl_4^{2-}$. The diffusion coefficients vary with temperature according to the Arrhenius relation (fig. 6.4).

c) 0.3 mole fraction KCl.

In this more acidic melt, evidence of deposition of chromium(III) chloride was manifested in the voltammograms for the relatively dilute 0.26M chromium(II) solutions, up to at least 434°C. For example, at 414°C, the cathodic peaks showed evidence of inflections and of being narrower than the normal "soluble product" peak, for scan rates below 100 mVs^{-1} (fig. 6.9). For these scan rates, the peak current ratio was significantly greater than one (table 6.9), due to the increase in the cathodic peak. However a plot of i_{pa} versus $\nu^{1/2}$ was linear, with

Figure 6.9. Typical cyclic voltammograms for the oxidation of chromium(II) (0.26M) in 0.30 mole fraction KCl-$ZnCl_2$ at 414°C

Working electrode: vitreous carbon
Reference electrode: zinc



slight deviations at lower scan rates due to convection (fig. 6.10). On cooling to 386°C, an inflection could also now be seen in the anodic peak (5 mVs^{-1}), and on further cooling to 328°C, inflections appeared for scan rates up to 100 mVs^{-1} (fig. 6.11). At this latter temperature, the values of peak current ratio were significantly greater than one (table 6.10) and the plot of i_{pa} versus $\nu^{1/2}$ deviates considerably from linearity at scan rates < 200 mVs^{-1}, indicating that the peak height no longer follows the soluble product relation (fig. 6.12).

For a more concentrated 0.58M chromium(II) solution, in a 0.27 mole fraction KCl melt at 400°C, well-defined anodic inflections could be observed up to at least 1 Vs^{-1} (fig. 6.13). The narrow half-peak widths, which decreased with scan rate, indicating some irreversibilty, are close to the expected value (45 mV) for a 1-electron transfer involving an insoluble product, as shown in table 6.11. Evidently for this composition, the system approximates to the voltammetric insoluble product model, the precipitation of chromium(III) chloride occurring well cathodic of the half-wave potential. It was of interest to see if the entire voltammetric wave conformed to the equation for reversible deposition as derived by Schiffrin (80), and successfully applied to the reduction of Ni^{2+} in LiCl/KCl eutectic at 400°C. The model assumes, as is usual, that the electrode is instantaneously covered with a deposit of unit activity, which may not be the case in the present instance. The

Figure 6.10. Plot of peak current against square root of scan rate for the oxidation of chromium(II) (0.26M) in 0.30 mole fraction KCl-$ZnCl_2$ at 414°C

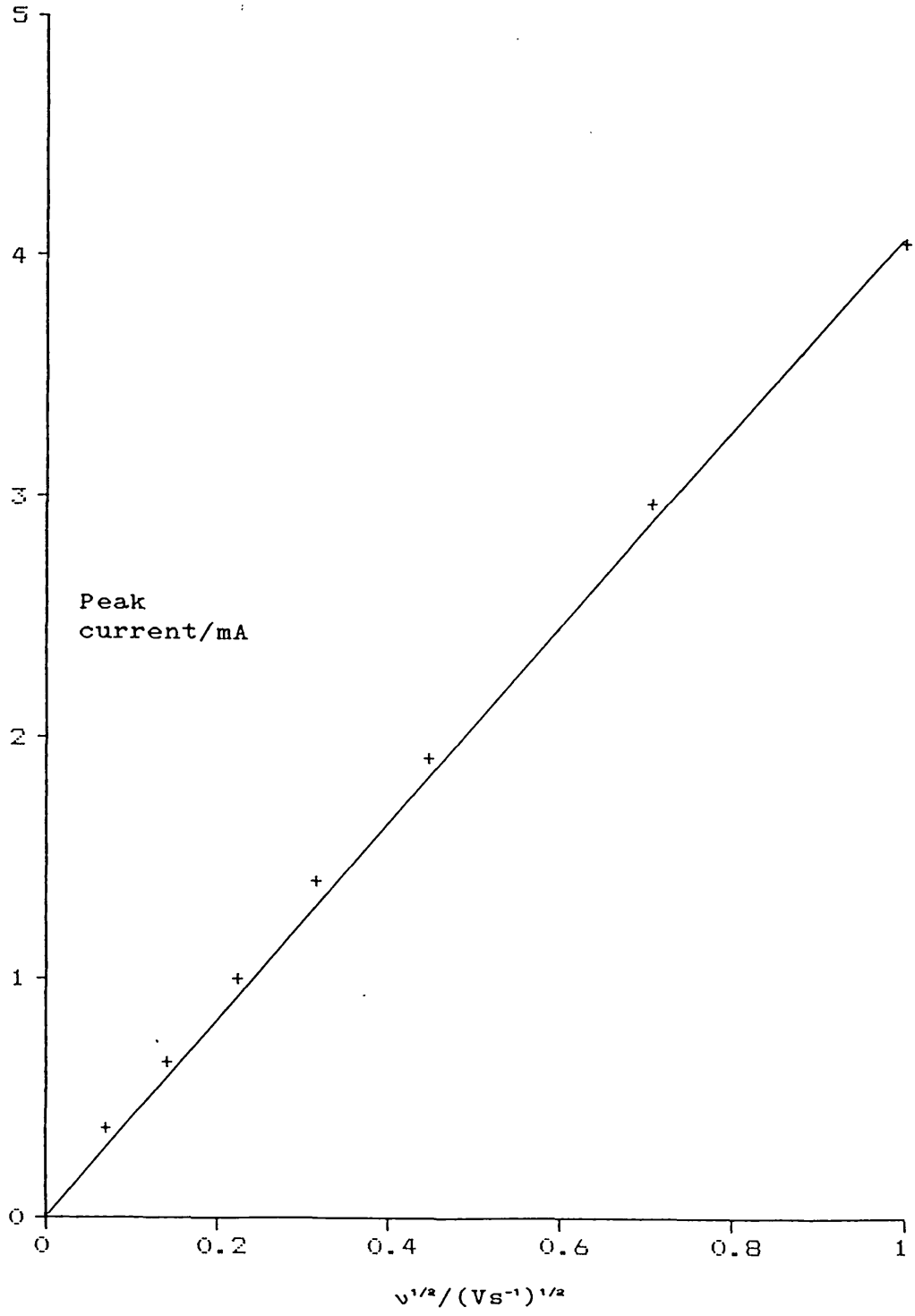


Table 6.9. Voltammetric Parameters for 0.26M chromium(II) in 30/70 mole p.c. KCl/$ZnCl_2$ at 414°C

Scan rate/ mVs^{-1}	I_{pc}/I_{pa}	ΔE_p/ mV	$I_{pa}/\nu^{1/2}$/ $mA/(Vs^{-1})^{1/2}$
1000	1.11	198	4.05
500	1.09	192	4.20
200	1.07	161	4.28
100	1.08	177	4.43
50	1.16	177	4.47
20	1.29	177	4.61
5	1.59	193	5.30
	$E_{pa}-E_{pa/2}$/mV	E_{pa}/V	$E_{1/2}$/V
1000	161	1.184	-
500	156	1.162	-
200	151	1.150	-
100	146	1.150	-
50	143	1.140	-
20	145	1.121	-
5	146	1.121	1.058

Table 6.10. Voltammetric Parameters for 0.26M chromium(II) in 30/70 mole p.c. KCl/$ZnCl_2$ at 328°C

Scan rate/ mVs^{-1}	I_{pc}/I_{pa}	ΔE_p/ mV	$I_{pa}/\nu^{1/2}$/ $mA/(Vs^{-1})^{1/2}$
1000	0.98	270	2.30
500	1.16	276	2.32
200	1.50	270	2.61
100	1.73	281	2.81
50	1.95	260	2.73
20	1.40	208	3.34
5	1.37	140	3.93
	$E_{pa}-E_{pa/2}$/mV	E_{pa}/V	
1000	156	1.148	
500	151	1.138	
200	135	1.137	
100	134	1.123	
50	99	1.100	
20	73	1.090	
5	42	1.065	

Figure 6.11. Typical cyclic voltammograms for the oxidation of chromium(II) (0.26M) in 0.30 mole fraction KCl-$ZnCl_2$ at 328°C

Working electrode: vitreous carbon
Reference electrode: zinc

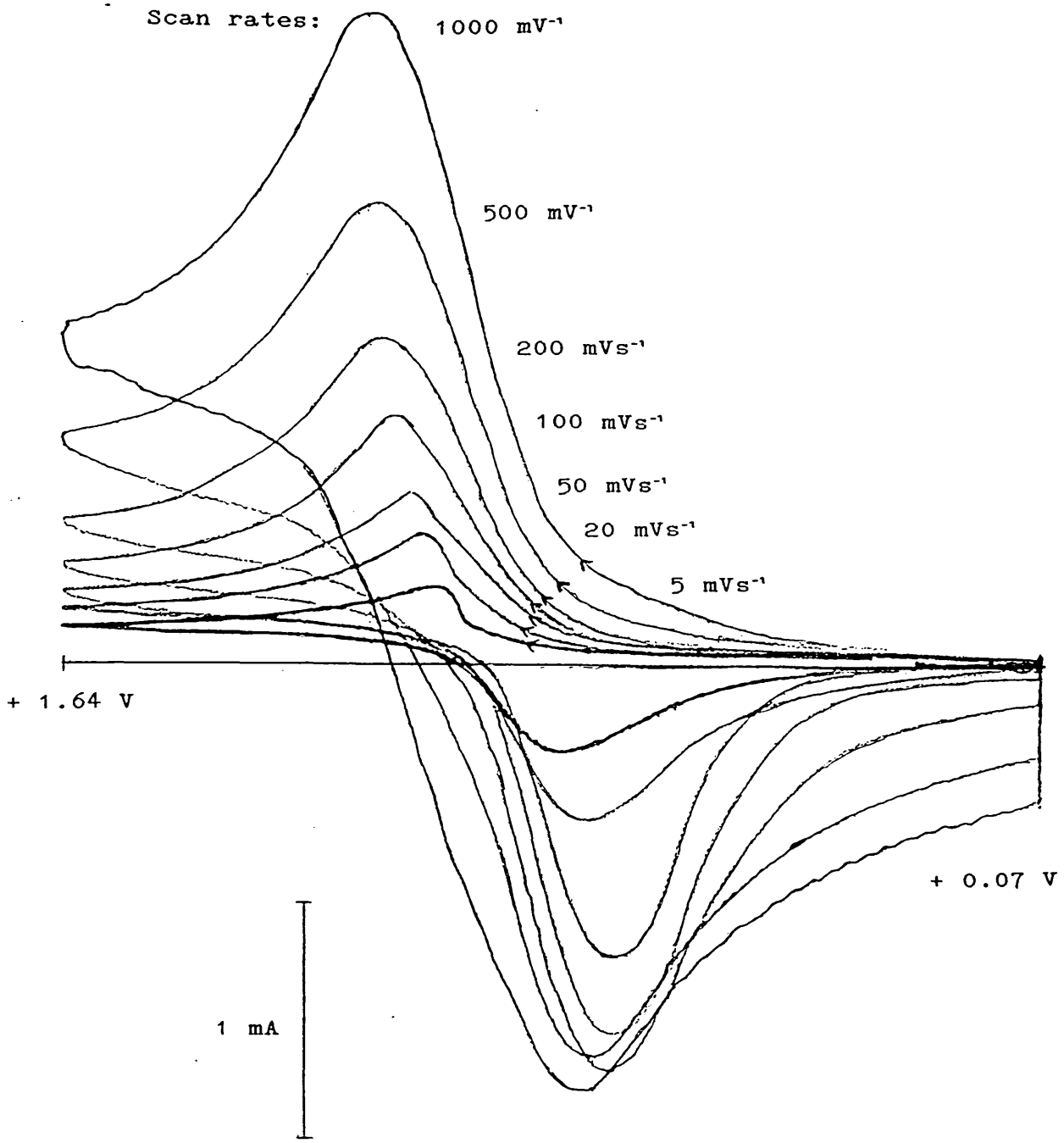


Figure 6.12. Plot of peak current against square root of scan rate for the oxidation of chromium(II) (0.26M) in 0.30 mole fraction KCl-$ZnCl_2$ at 328°C

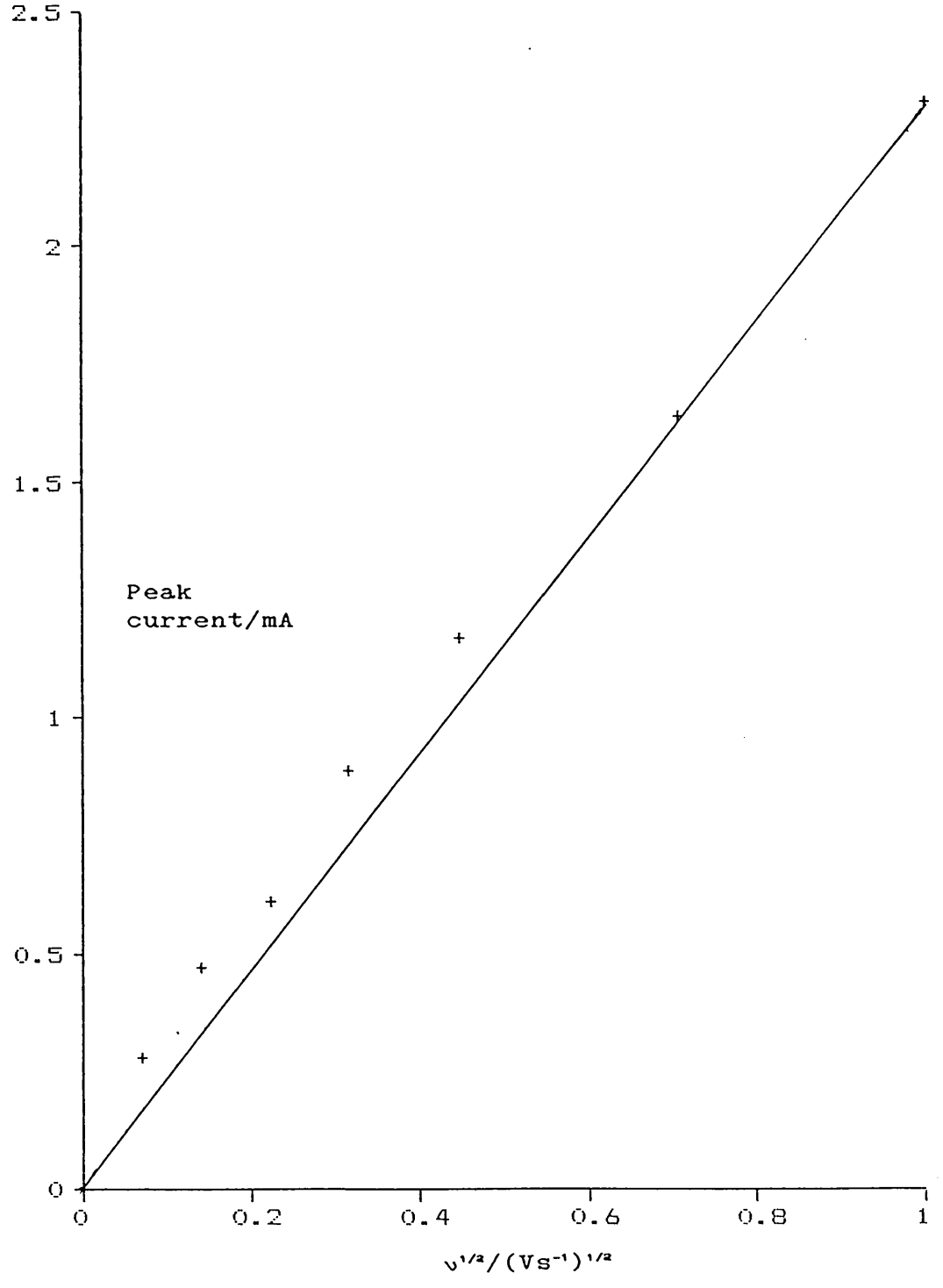


Figure 6.13. Typical cyclic voltammograms for the oxidation of chromium(II) (0.58M) in 0.29 mole fraction KCl-$ZnCl_2$ at 400°C

Working electrode: vitreous carbon
Reference electrode: zinc

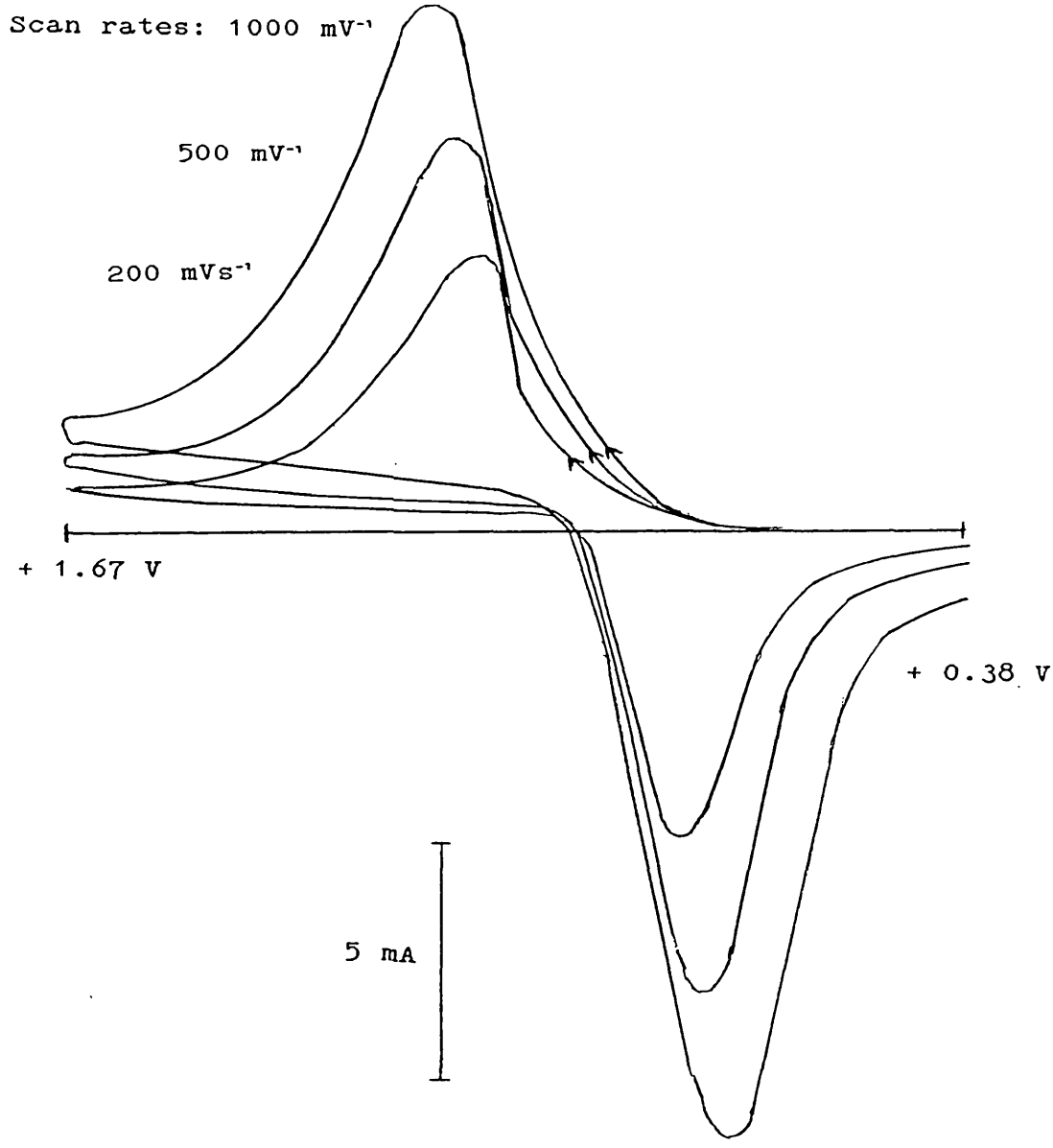


Table 6.11. Voltammetric Parameters for 0.58M chromium(II) in 27/73 mole p.c. KCl/ZnCl$_2$ at 400°C

Scan rate/ mVs^{-1}	I_{pc}/I_{pa}	ΔE_p/ mV	$I_{pa}/v^{1/2}$/ mA/(Vs^{-1})$^{1/2}$
1000	1.35	441	11.33
500	1.35	364	12.18
200	1.28	290	13.28
100	1.24	259	13.85
50	1.22	221	14.00
20	0.92	220	15.49
5	0.64	172	17.67
	$E_{pa}-E_{pa/2}$/mV	E_{pa}/V	
1000	152	1.446	
500	90	1.110	
200	63	1.078	
100	54	1.044	
50	39	1.044	
20	40	1.044	
5	36	1.015	

current for the voltammetric wave is:

$$i = 1.8484 i_p[\Phi(V^{1/2}) - e^{-Vs}\Phi(V-Vs)^{1/2}.H] - 1.6381[e^{-Vs}.e^{(V-Vs)}.erf(V-Vs)^{1/2}].H \quad (6.8)$$

where i_p is the peak current, $\Phi(x)$ is the Dawson integral (102), erf(x) is the standard error function, $V = (nF/RT)E$, (E = applied potential), $Vs = (nF/RT)Es$, (Es = switching potential), and H = 0 if E < Es, else H = 1 if E > Es.

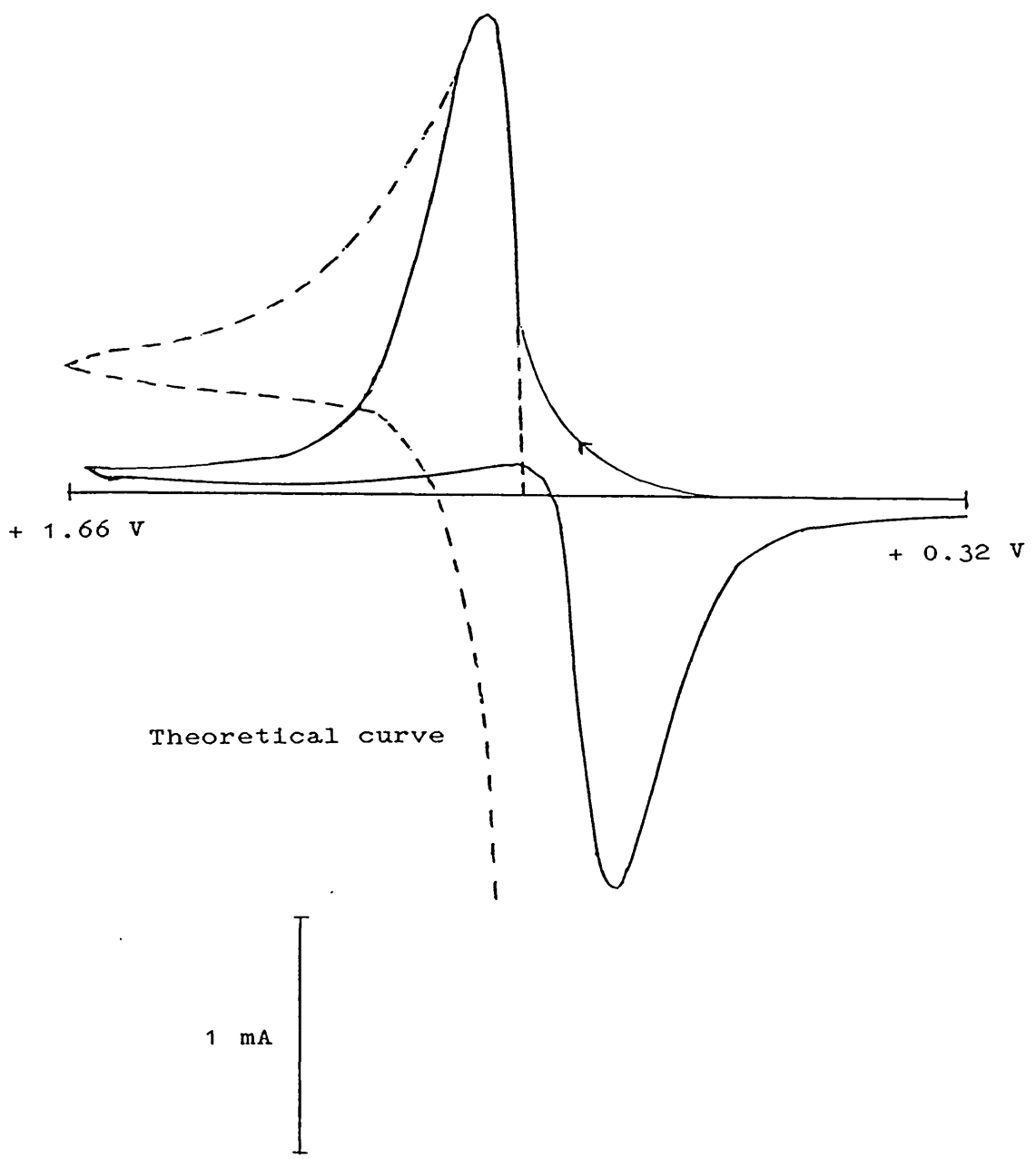
The origin of the potential coordinate E is the potential, E_r, at which electrolysis starts; this is given by (80):

$$E_p - E_r = 0.8450\ RT/nF \quad (6.9)$$

where E_p is the peak potential. At 400°C, E_r is 49mV cathodic of E_p. Values of i were calculated from eqn. 6.8 using a computer program to evaluate the integrals; the results were checked against standard tables (102). The peak current i_p was measured from the voltammograms.

The results of a typical calculation are shown in figure 6.14. and compared with the experimental voltammogram for 20 mVs^{-1} scan rate. The deviation at the beginning of the sweep may be due to non-unit activity of the deposit, which is also observed for metal deposition (80). Considerable deviations from the model equation are indicated for potentials past the peak potential, the current falling off too quickly. Also, it may be noted that the stripping peak is significantly cathodic of the predicted potentials. This latter result in particular was characteristic of deposits obtained under varying conditions. Thus the deposition does not

Figure 6.14. Cyclic voltammogram for the oxidation of chromium(II) (0.58M) in 0.29 mole fraction KCl-$ZnCl_2$ at 400°C: Comparison with reversible case



appear to be purely diffusion-controlled and this process and the subsequent stripping are not totally reversible.

Diffusion coefficients were calculated for the 0.26M chromium(II) solution. (assuming that the anodic peaks conformed to the standard "soluble product" relation as indicated by the linear $i_{pa}/v^{1/2}$ plot of fig. 6.10). The results are shown in table 6.12.

Table 6.12-Diffusion coefficients and Stokes radii for Cr^{2+} in 0.3 mole fraction $KCl/ZnCl_2$ melt

T/°C	D/cm^2s^{-1}	Viscosity/mPa.s	Cr^{2+} radius/pm
434	21 x10^{-7}	4.0	632
414	19 "	5.0	544
386	15 "	7.0	459
350	9.6 "	11.5	413
328	4.4 "	16.0	625

Further increases in the Stokes radii may be noted, and a decrease in diffusion coefficient below the values for the more basic melts at similar temperatures. The diffusion coefficients conform reasonably to the Arrhenius relation, as shown in figure 6.4.

A rough estimate of the solubility of chromium(III) based upon eqn. 6.7 can be made. For 0.26M chromium(II) at 386°C, an anodic inflection may be seen about 10 mV anodic of the half-wave potential (5 mVs^{-1}). This yields a solubility of 0.14M.

d) 0.21 mole fraction KCl.

In this yet more acidic melt, only relatively dilute solutions of chromium(II) gave the "soluble product" voltammograms, for example, a 0.023M solution at 400°C

(table 6.13 and fig. 6.15). The peak shifts and broadening with increasing scan rate indicate some irreversibility or uncompensated solution resistance. Unfortunatly at these low concentrations ,the anodic part of the voltammograms was perturbed by background current evidently due to the onset of chlorine evolution; this effect was probably responsible for the rather low values of i_{pc}/i_{pa} found in table 6.13.

With a 0.081M solution at 412°C, evidence of insoluble product deposition appeared in the form of narrow cathodic stripping peaks for scan rates of 20 mVs^{-1} or below (fig. 6.16). This voltammetric behaviour is manifested as high peak current ratio values in table 6.14.

For a much more concentrated 0.57M solution at 414°C, insoluble product formation was apparent for scan rates at least up to 1 Vs^{-1}, as might be predicted. The general form of the voltammograms was similar to that of the 0.58M solutions in the 0.27 mole fraction KCl melt. Results are presented in figure 6.17 and table 6.15.

The diffusion coefficients calculated for the 0.081M and 0.023M Cr^{2+} solutions were surprisingly high, considering that the melt viscosity had increased, for example, 6.8 $x10^{-6}$ cm^2s^{-1} at 414°C for the 0.081M solution. This figure gives a Stokes radius of 67 pm (with η as 11 mPa.s), a value which must approximate to the "crystallographic" radius of chromium(II). The value must be cautiously interpreted, but assuming the validity of the Stokes-Einstein relation (eqn. 6.3) this implies

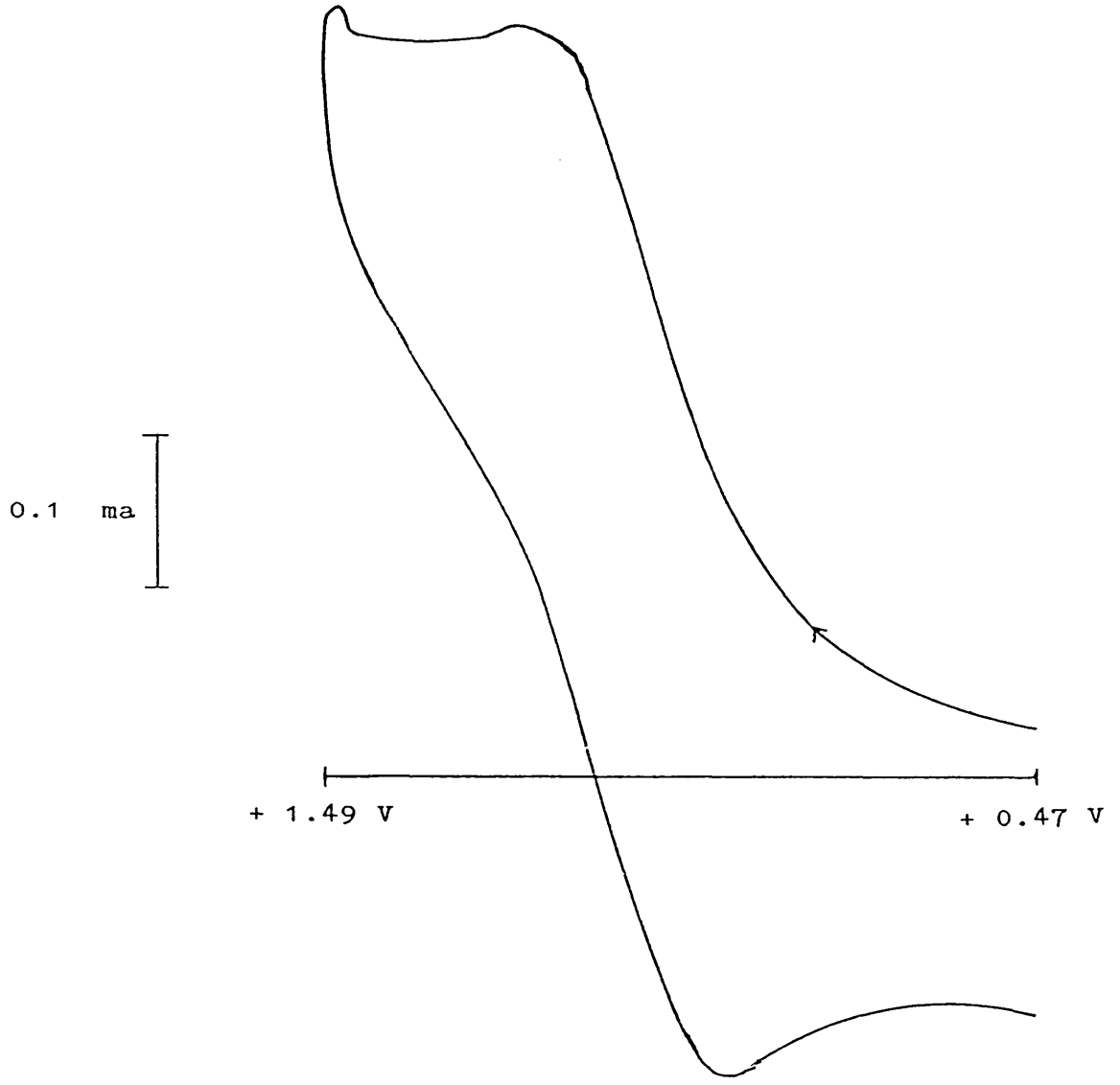
Table 6.13. Voltammetric Parameters for 0.023M chromium(II) in 21/79 mole p.c. KCl/$ZnCl_2$ at 400°C

Scan rate/ mVs^{-1}	I_{pc}/I_{pa}	ΔE_p/ mV	$I_{pa}/\nu^{1/2}$/ $mA/(Vs^{-1})^{1/2}$
1000	1.01	292	0.65
500	0.96	269	0.68
200	0.88	232	0.71
100	0.84	211	0.74
50	0.75	193	0.80
20	0.66	183	0.90
5	0.63	181	1.06
	$E_{pa}-E_{pa/2}$/mV	E_{pa}/V	$E_{1/2}$/V
1000	213	1.220	-
500	200	1.201	-
200	195	1.181	-
100	191	1.175	-
50	190	1.165	-
20	182	1.157	-
5	178	1.142	1.077

Table 6.14. Voltammetric Parameters for 0.081M chromium(II) in 21/79 mole p.c. KCl/$ZnCl_2$ at 414°C

Scan rate/ mVs^{-1}	I_{pc}/I_{pa}	ΔE_p/ mV	$I_{pa}/\nu^{1/2}$/ $mA/(Vs^{-1})^{1/2}$
1000	1.18	172	2.37
500	1.15	163	2.31
200	1.12	160	2.60
100	1.01	134	2.78
50	1.00	131	2.65
20	1.04	134	2.79
5	2.92	172	3.10
	$E_{pa}-E_{pa/2}$/mV	E_{pa}/V	$E_{1/2}$/V
1000	172	1.203	-
500	163	1.192	-
200	147	1.190	-
100	142	1.184	-
50	140	1.161	-
20	135	1.142	-
5	131	1.139	1.074

Figure 6.15. Typical cyclic voltammogram for the oxidation of chromium(II) (0.023M) in 0.21 mole fraction KCl-$ZnCl_2$ at 400°C



Working electrode: vitreous carbon
Reference electrode: zinc
Scan rate: 500 mV^{-1}

Figure 6.16. Typical cyclic voltammograms for the oxidation of chromium(II) (0.081M) in 0.21 mole fraction KCl-$ZnCl_2$ at 412°C

Working electrode: vitreous carbon

Reference electrode: zinc

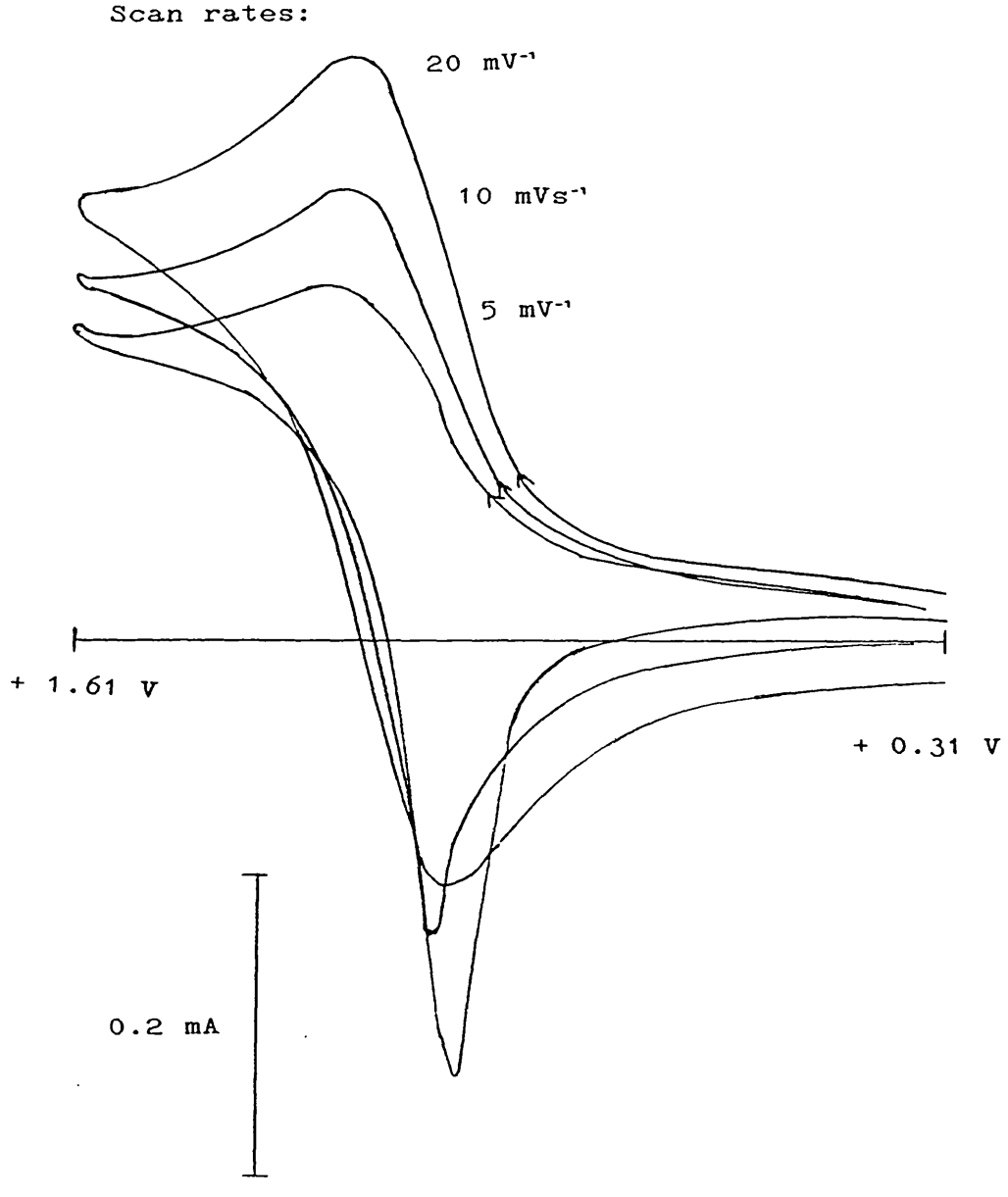


Figure 6.17. Typical cyclic voltammograms for the oxidation of chromium(II) (0.57M) in 0.21 mole fraction KCl-$ZnCl_2$ at 414°C

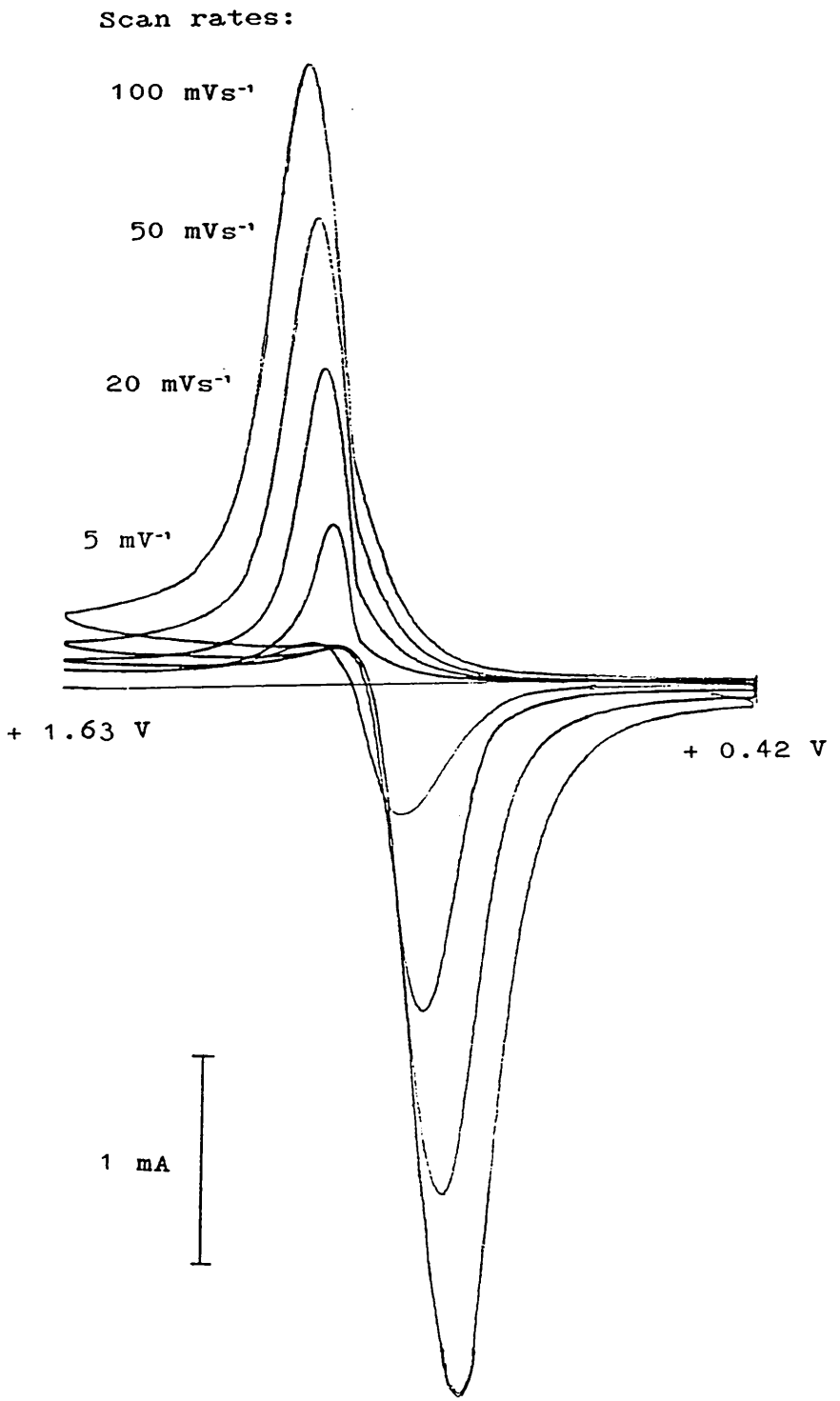


Table 6.15. Voltammetric Parameters for 0.57M chromium(II) in 20/80 mole p.c. KCl/$ZnCl_2$ at 400°C

Scan rate/ mVs^{-1}	I_{pc}/I_{pa}	ΔE_p/ mV	$I_{pa}/\nu^{1/2}$/ $mA/(Vs^{-1})^{1/2}$
1000	1.43	396	7.80
500	1.34	332	8.16
200	1.24	275	8.79
100	1.29	230	9.48
50	1.33	220	9.50
20	1.29	204	10.32
5	1.15	181	11.48
	$E_{pa}-E_{pa/2}$/mV	E_{pa}/V	
1000	180	1.321	
500	153	1.280	
200	117	1.236	
100	83	1.215	
50	37	1.201	
20	35	1.172	
5	35	1.150	

Table 6.16. Voltammetric Parameters for 0.74M chromium(II) in pure zinc chloride at 400°C

Scan rate/ mVs^{-1}	I_{pc}/I_{pa}	ΔE_p/ mV	$I_{pa}/\nu^{1/2}$/ $mA/(Vs^{-1})^{1/2}$
1000	1.46	882	1.81
500	1.52	774	1.90
200	1.61	600	1.89
100	1.47	509	2.27
50	1.44	425	2.30
20	1.41	341	2.65
5	1.36	255	3.09
	$E_{pa}-E_{pa/2}$/mV	E_{pa}/V	
1000	225	1.384	
500	195	1.380	
200	151	1.287	
100	122	1.231	
50	100	1.182	
20	82	1.146	
5	55	1.100	

that the uncomplexed, "bare" ion exists in these acidic melts, presumably due to lack of strongly coordinating species. A similar situation can exist for cations in acidic chloroaluminate melts (103).

From eqn. 6.7, it is evident that the chromium(III) solubility in this system must be less than, or equal to, 0.081M at 412°C.

e) 0.06 mole fraction KCl and pure zinc chloride.

Only insoluble product voltammograms could be obtained in these very acidic melts, which were also distorted by uncompensated solution resistance. In pure $ZnCl_2$, 0.74M solutions gave voltammograms with relatively broad peaks, even at 5 mVs^{-1} scan rate (fig.6.18, table 6.16). Peak shifts and broadening at higher scan rates were also apparent, probably due to the high melt resistance. More reversible voltammograms were obtained with an 0.32M solution through which HCl gas had been bubbled for 1.5 hours, presumably improving the conductivity. Comparison with the calculated reversible insoluble product voltammogram (fig. 6.19) showed a reasonable correspondance for the forward sweep, though the experimental cathodic sweep begins to deviate from the predictions of eqn. 6.8.

In comparison, an 0.72M chromium(II) solution in the 0.06 mole fraction KCl mixture exhibited voltammograms reminiscent of the 0.58M solution in the 0.27 mole fraction KCl melt, with the half-peak width approximating to the reversible insoluble product value (45 mV at 400°C), as shown in table 6.17.

Figure 6.18. Typical cyclic voltammograms for the oxidation of chromium(II) (0.74M) in pure zinc chloride at 400°C

Working electrode: vitreous carbon
Reference electrode: zinc

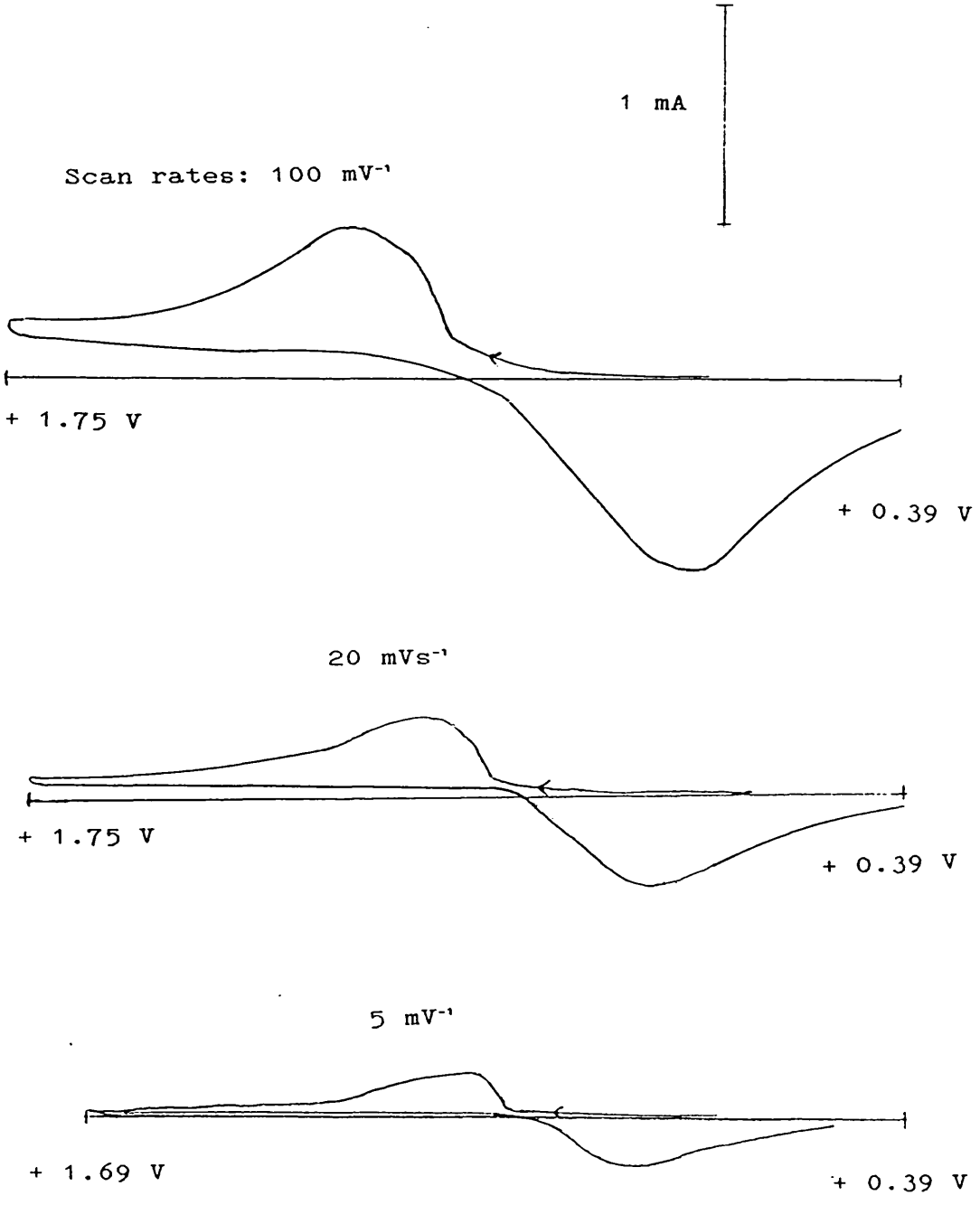
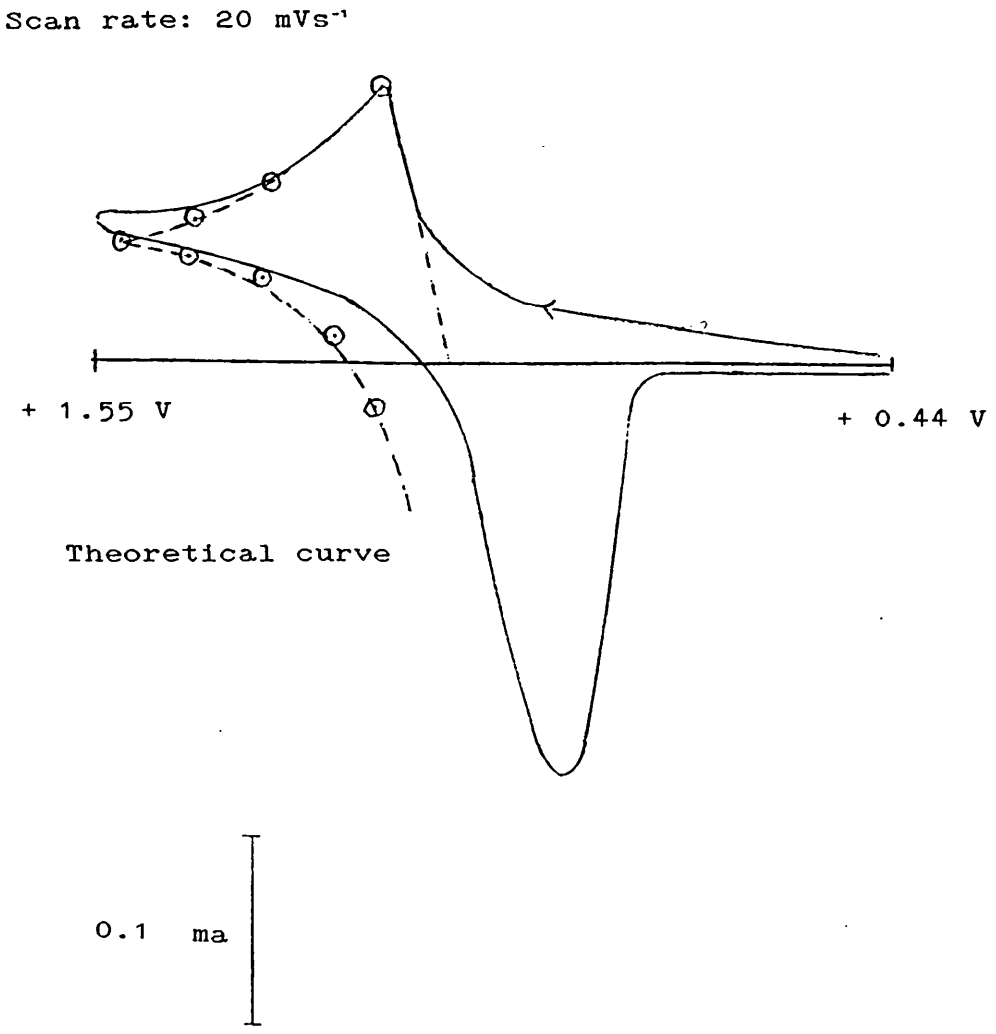


Table 6.17. Voltammetric Parameters for 0.72M chromium(II) in .06/94 mole p.c. KCl/$ZnCl_2$ at 400°C

Scan rate/ mVs^{-1}	I_{pc}/I_{pa}	ΔE_p/ mV	$I_{pa}/\nu^{1/2}$/ $mA/(Vs^{-1})^{1/2}$
1000	1.10	493	6.56
500	1.06	422	6.90
200	0.96	315	7.69
100	0.91	260	8.20
50	0.84	221	8.65
20	0.78	201	9.48
5	0.53	182	10.39
	$E_{pa}-E_{pa/2}$/mV	E_{pa}/V	
1000	125	1.347	
500	112	1.312	
200	93	1.257	
100	75	1.230	
50	58	1.211	
20	52	1.119	
5	45	1.110	

Figure 6.19. Cyclic voltammogram for the oxidation of chromium(II) (0.32M) in "pure" zinc chloride at 400°C (after HCl bubbling): Comparison with reversible case

Working electrode: vitreous carbon
Reference electrode: zinc



6.2.2 Sodium chloride-zinc chloride melts

As the activity of zinc chloride in these melts is greater than that in $KCl/ZnCl_2$ melts for any given temperature and mole fraction of alkali chloride, it was expected that the solubility of chromium(III) would be correspondingly less, and that this would be manifested in the voltammetric results.

a) 0.54 mole fraction NaCl.

At 400°C in this relatively basic melt, essentially reversible "soluble product" voltammograms were obtained for a 0.26M chromium(II) solution, corresponding to the one-electron oxidation to chromium(III), though increasing peak separation and half-peak widths with increasing scan rate were noted as with the KCl melts. Table 6.18 also shows that the peak current ratio was close to one for scan rates greater than 20 mVs^{-1}, and figure 6.20 demonstrates that i_{pa} was proportional to $v^{1/2}$, except at scan rates < 20 mVs^{-1}, the latter effect being attributed to convection.

The diffusion coefficient at 400°C was calculated as 4.4×10^{-6} cm^2s^{-1}, giving a Stokes radius of 225 pm (viscosity coefficient = 5 mPa.s (45,46)). These values are intermediate between those obtained in the 0.5 and 0.4 mole fraction KCl melts.

b) 0.4 mole fraction NaCl.

At 400°C a 0.33M chromium(II) solution in this system showed evidence of product deposition in the form of narrow cathodic stripping peaks and abrupt increases in current in the anodic waves (fig. 6.21). This compares

Table 6.18. Voltammetric Parameters for 0.26M chromium(II) in 54/46 mole p.c. NaCl/$ZnCl_2$ at 400°C

Scan rate/ mVs^{-1}	I_{pc}/I_{pa}	ΔE_p/ mV	$I_{pa}/\nu^{1/2}$/ $mA/(Vs^{-1})^{1/2}$
1000	1.01	200	7.72
500	1.00	195	7.76
200	0.97	173	7.95
100	0.96	164	8.14
50	0.99	161	7.87
20	0.90	154	8.14
5	0.73	152	8.86
	$E_{pa}-E_{pa/2}$/mV	E_{pa}/V	$E_{1/2}$/V
1000	161	1.053	-
500	152	1.050	-
200	145	1.041	-
100	141	1.039	-
50	137	1.037	-
20	132	1.031	-
5	131	1.030	0.968

Table 6.19. Voltammetric Parameters for 0.33M chromium(II) in 40/60 mole p.c. NaCl/$ZnCl_2$ at 400°C

Scan rate/ mVs^{-1}	I_{pc}/I_{pa}	ΔE_p/ mV	$I_{pa}/\nu^{1/2}$/ $mA/(Vs^{-1})^{1/2}$
1000	1.86	281	9.14
500	2.17	272	9.34
200	2.49	269	9.69
100	2.35	260	10.71
50	2.16	232	11.51
20	2.06	204	12.45
5	2.31	177	12.45
	$E_{pa}-E_{pa/2}$/mV	E_{pa}/V	
1000	166	1.067	
500	163	1.067	
200	160	1.067	
100	131	1.024	
50	95	1.104	
20	83	1.101	
5	59	1.101	

Figure 6.20. Plot of peak current against square root of scan rate for the oxidation of chromium(II) (0.26M) in 0.54 mole fraction NaCl-$ZnCl_2$ at 400°C

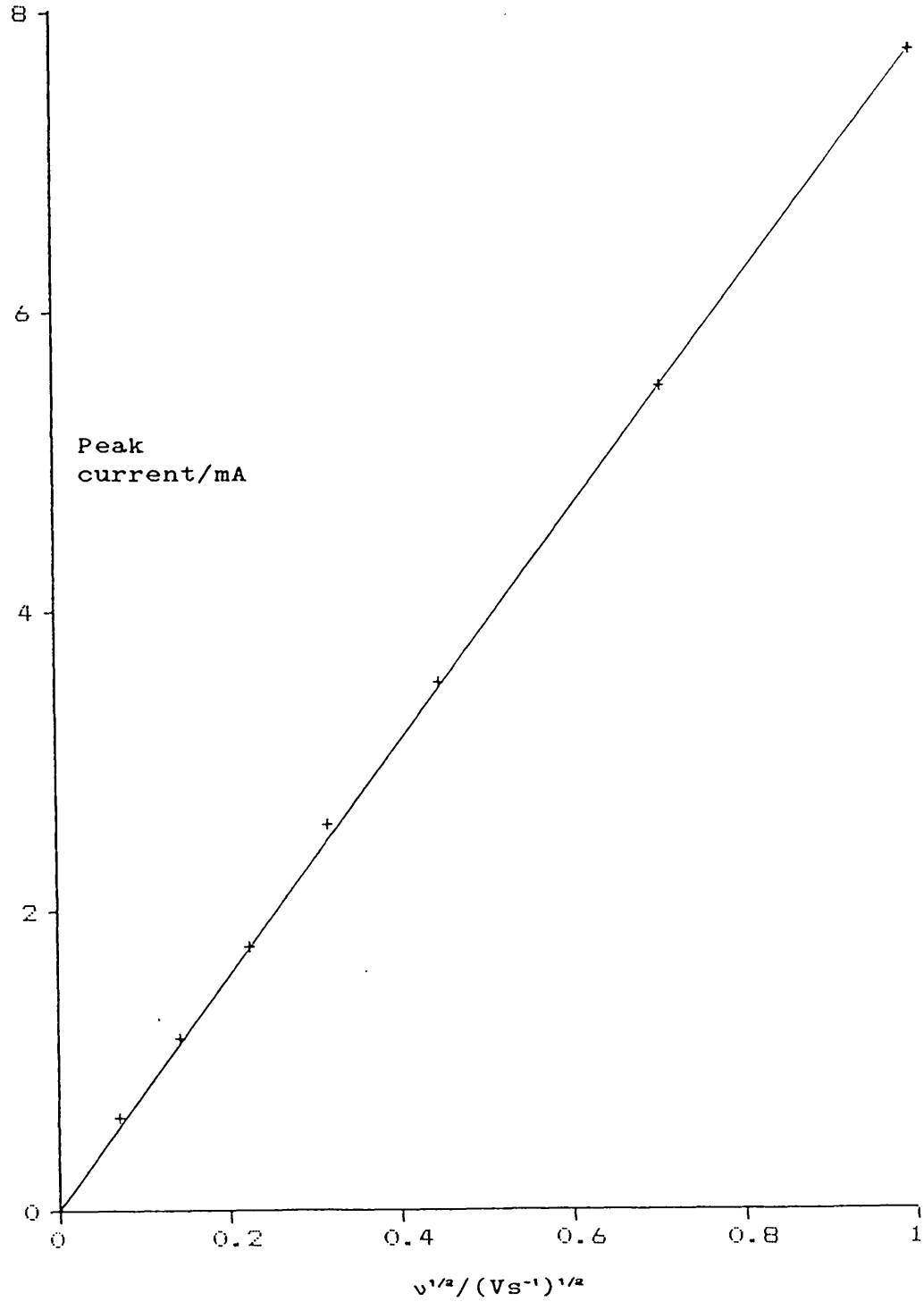
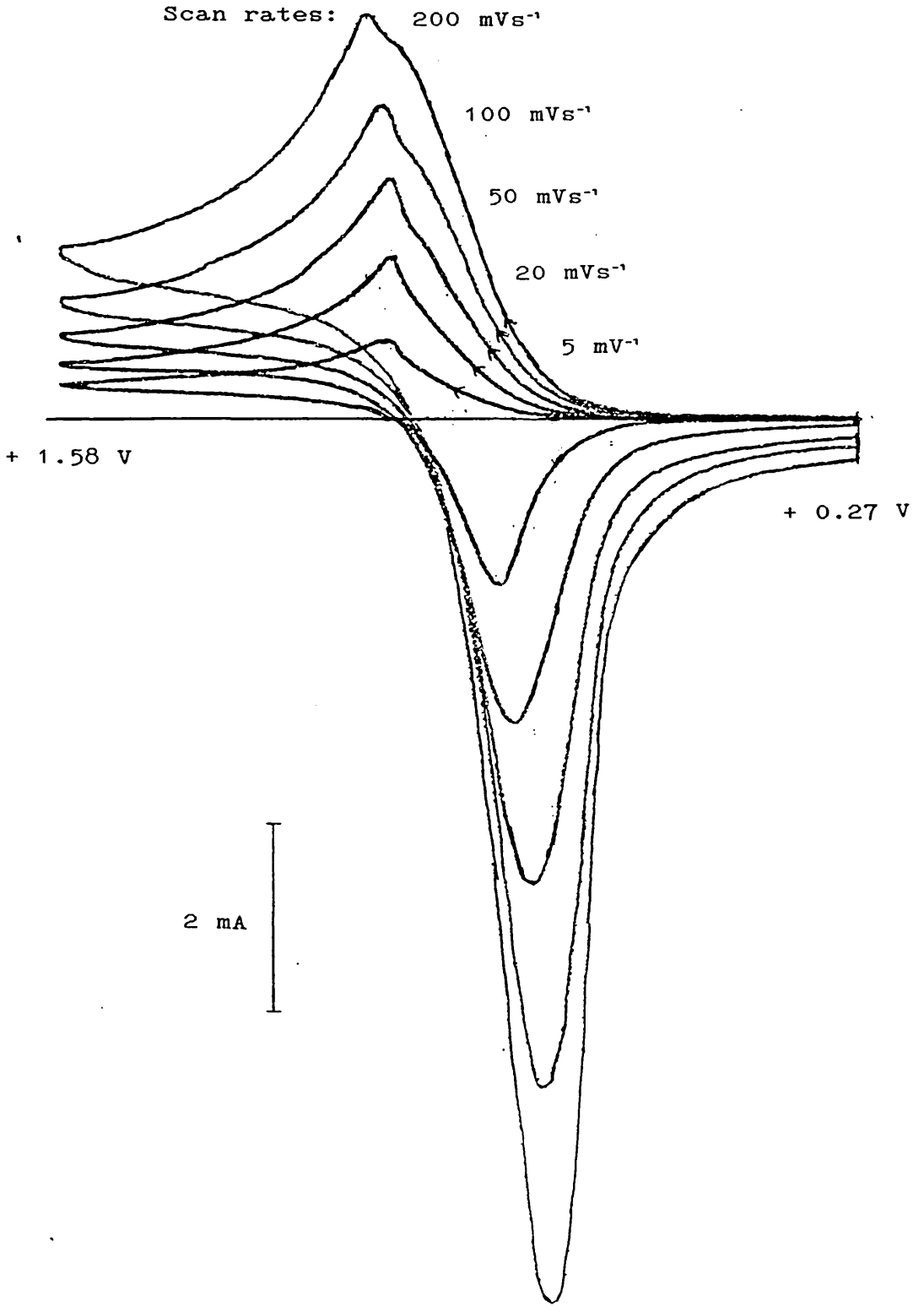


Figure 6.21. Typical cyclic voltammograms for the oxidation of chromium(II) (0.33M) in 0.40 mole fraction NaCl-$ZnCl_2$ at 400°C

Working electrode: vitreous carbon
Reference electrode: zinc



with the 0.35M chromium(II) solution in the equivalent KCl-containing melt, where no evidence of deposition was observed at this temperature.

The voltammetric parameters for the NaCl system were characteristic for the deposition process with the current ratio significantly greater than one, the half-peak width tending to relatively low values at low scan rates, when the effects of irreversibility should have been minimised (table 6.19).

For the more dilute 0.11M chromium(II) solution at 398°C, evidence of deposition was only apparent at low scan rates (< 100 mVs^{-1}) as indicated by the high values of i_{pc}/i_{pa} (table 6.20, figure 6.22). There was no indication of inflections on the anodic peaks. For a yet more dilute 0.075M solution, no evidence of deposition was seen at 388°C, the voltammetric parameters being characteristic of a one-electron transfer with soluble product, apart from a slightly increased peak separation and peak width at higher scan rates (table 6.21).

These results suggest that a significant reduction in chromium(III) solubility occurs on replacing the potassium cation by sodium, precipitation occurring in more dilute solutions, in the $NaCl/ZnCl_2$ melt.

Diffusion coefficients calculated for the solutions were as follows: 0.11M Cr^{2+}, 3.6 $x10^{-6}$ cm^2s^{-1} at 398°C, and 4.1 $x10^{-6}$ cm^2s^{-1} for 0.075M Cr^{2+} at 388°C. These values give Stokes radii of around 250 pm, taking the melt viscosity as 5 mPa.s (45,46). This value is of the same order as those obtained in the equivalent

Table 6.20. Voltammetric Parameters for 0.11M chromium(II) in 40/60 mole p.c. NaCl/$ZnCl_2$ at 398°C

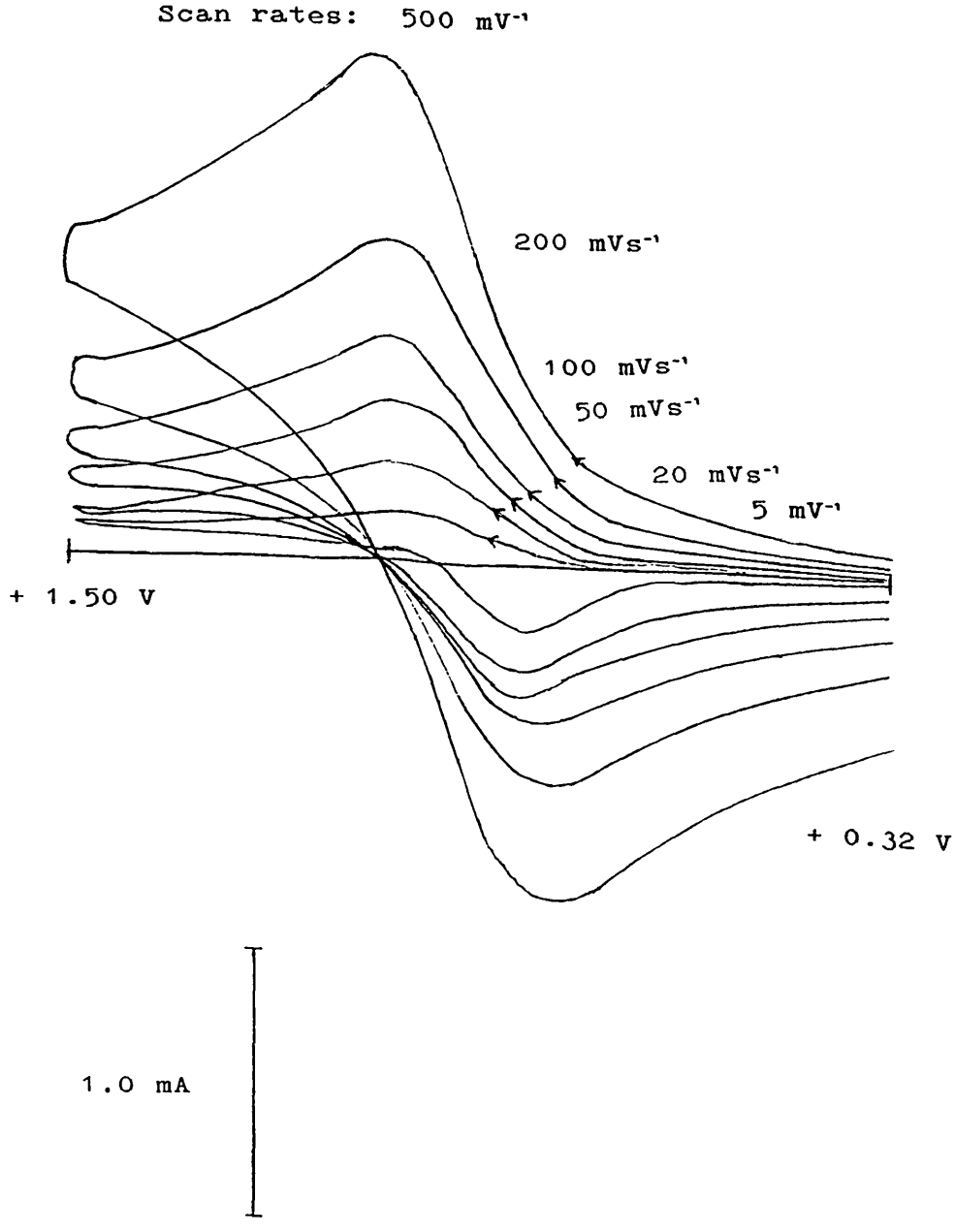
Scan rate/ mVs^{-1}	I_{pc}/I_{pa}	ΔE_p/ mV	$I_{pa}/\nu^{1/2}$/ $mA/(Vs^{-1})^{1/2}$
1000	1.08	252	2.66
500	1.07	245	2.67
200	1.05	205	2.73
100	1.06	199	2.63
50	1.17	168	2.73
20	1.33	168	2.75
5	1.72	157	2.74
	$E_{pa}-E_{pa/2}$/mV	E_{pa}/V	
1000	172	1.068	
500	164	1.053	
200	147	1.041	
100	136	1.132	
50	136	1.114	
20	131	1.104	
5	126	1.100	

Table 6.21. Voltammetric Parameters for 0.075M chromium(II) in 40/60 mole p.c. NaCl/$ZnCl_2$ at 388°C

Scan rate/ mVs^{-1}	I_{pc}/I_{pa}	ΔE_p/ mV	$I_{pa}/\nu^{1/2}$/ $mA/(Vs^{-1})^{1/2}$
1000	1.07	168	1.80
500	1.02	157	1.81
200	1.02	145	1.83
100	0.97	140	1.93
50	0.93	138	1.99
20	0.98	134	2.06
5	0.78	126	2.36
	$E_{pa}-E_{pa/2}$/mV	E_{pa}/V	$E_{1/2}$/V
1000	146	1.131	-
500	138	1.127	-
200	135	1.121	-
100	134	1.118	-
50	130	1.116	-
20	125	1.114	-
5	125	1.109	0.947

Figure 6.22. Typical cyclic voltammograms for the oxidation of chromium(II) (0.11M) in 0.40 mole fraction NaCl-$ZnCl_2$ at 400°C

Working electrode: vitreous carbon
Reference electrode: zinc



KCl-containing melt.

c) 0.3 mole fraction NaCl.

For a 0.10M solution of chromium(II) in this melt at 405°C, the voltammograms were essentially reversible, but with evidence of deposition at 5 mVs^{-1} scan rate, in the form of a narrow cathodic stripping peak (fig. 6.23, table 6.22).

With a more concentrated solution (0.27M) narrow cathodic peaks were observed for scan rates at least up to 500 mVs^{-1}, and inflections in the anodic peaks up to 200 mVs^{-1}, as indicated in figure 6.24 and table 6.23. This compares with the 0.26M solution in the 0.3 mole fraction KCl melt, where deposition was only evident at the slower scan rates, at or below 100 mVs^{-1}, and only in the cathodic peaks.

Diffusion coefficients calculated for the 0.10M solution were 3.4 $x10^{-6}$ cm^2s^{-1} at 405°C, and 5.3 $x10^{-6}$ cm^2s^{-1} at 446°C. These values are about twice as great as the values obtained in the analogous KCl-containing melt at similar temperatures, and the corresponding Stokes radii are respectively 199 and 185 pm. The explanation for the relatively high diffusion coefficients and low Stokes radii may be similar to that postulated for the 0.081M chromium(II) solution in the 0.21 mole fraction KCl melt; i.e. lack of strongly coordinating species.

d) 0.15 mole fraction NaCl.

For a 0.41M chromium(II) solution in this system, purely insoluble product behaviour was observed, as might

Figure 6.23. Typical cyclic voltammograms for the oxidation of chromium(II) (0.10M) in 0.30 mole fraction NaCl-$ZnCl_2$ at 405°C

Working electrode: vitreous carbon
Reference electrode: zinc

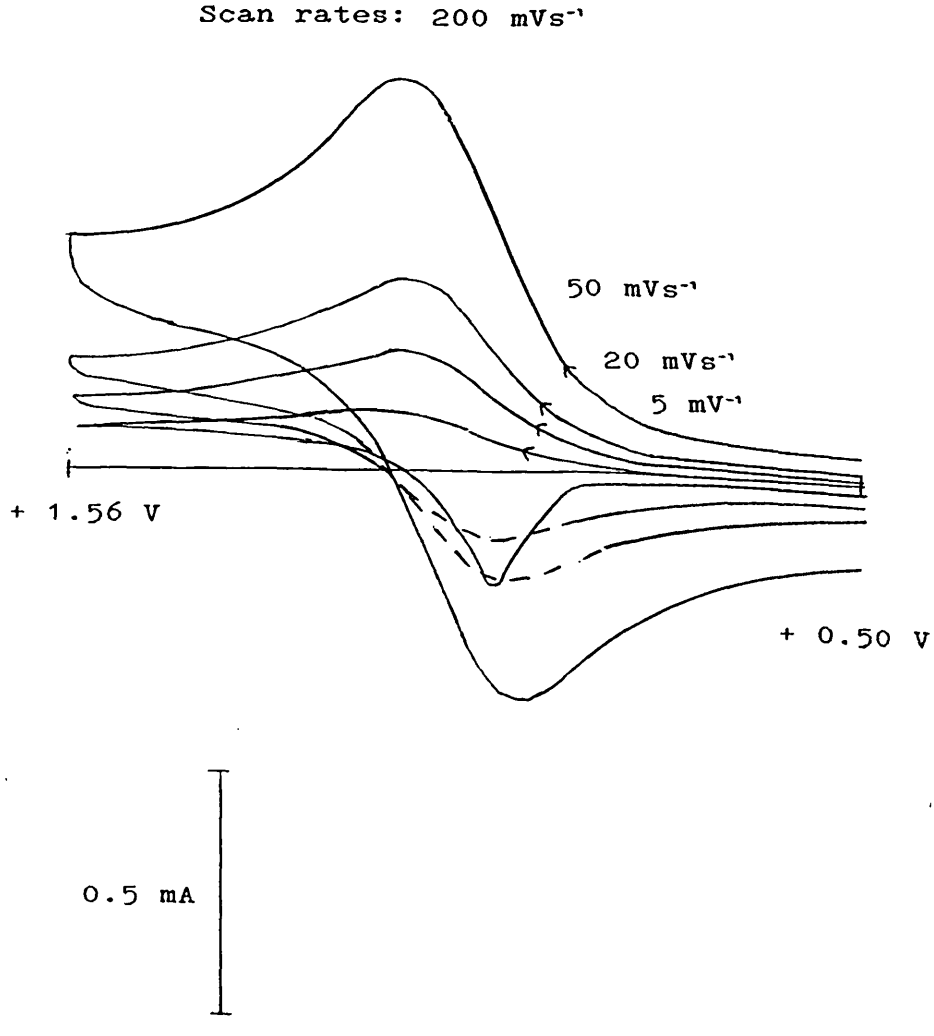


Table 6.22. Voltammetric Parameters for 0.10M chromium(II) in 30/70 mole p.c. NaCl/$ZnCl_2$ at 405°C

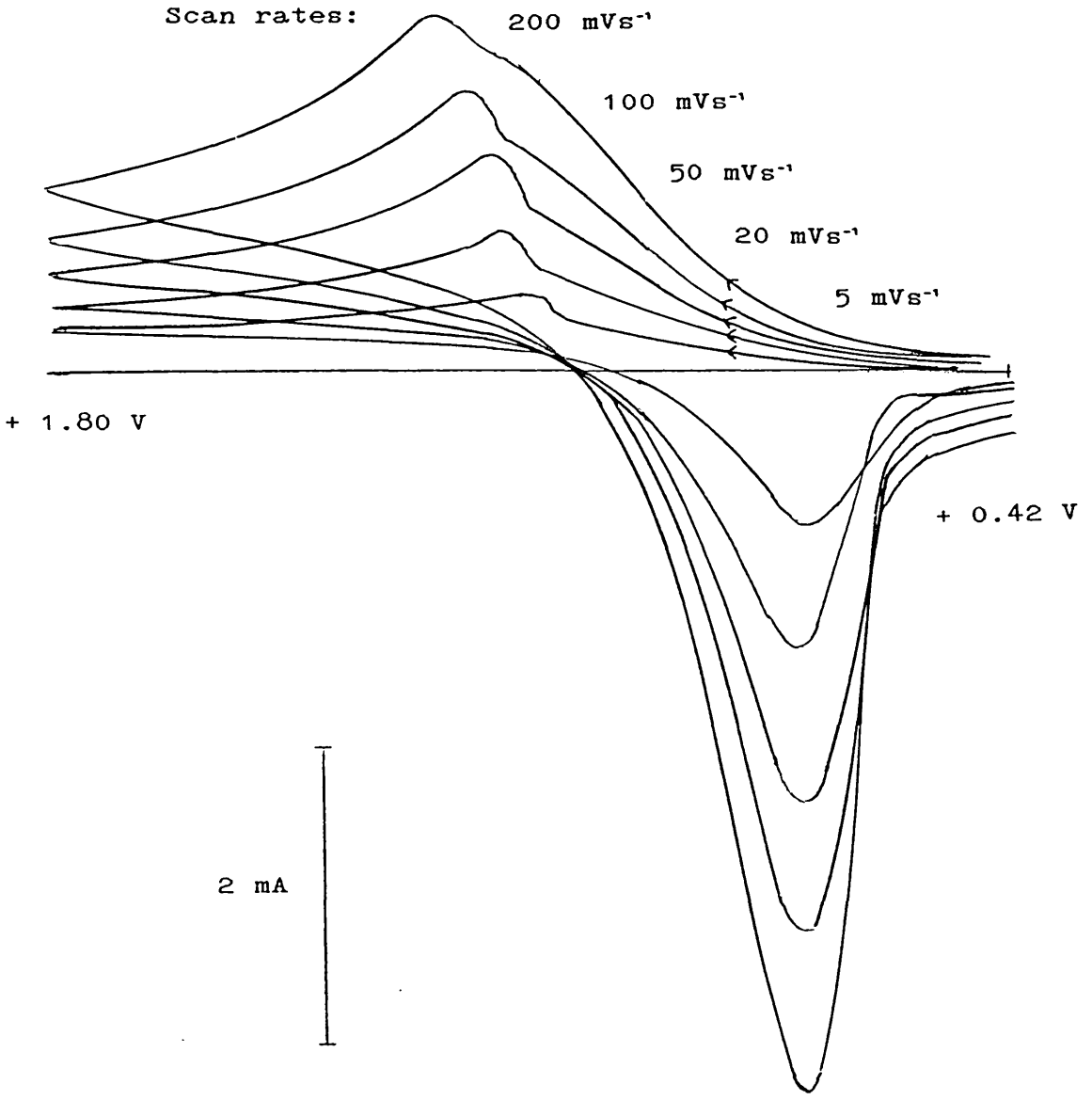
Scan rate/ mVs^{-1}	I_{pc}/I_{pa}	ΔE_p/ mV	$I_{pa}/v^{1/2}$/ $mA/(Vs^{-1})^{1/2}$
1000	0.99	164	1.84
500	0.96	161	1.83
200	0.93	155	1.85
100	0.88	143	1.90
50	0.85	140	1.89
20	0.80	127	1.99
5	1.77	110	2.21
	$E_{pa}-E_{pa/2}$/mV	E_{pa}/V	$E_{1/2}$/V
1000	162	1.147	-
500	160	1.142	-
200	156	1.132	-
100	145	1.121	-
50	141	1.121	-
20	140	1.121	-
5	140	1.121	1.059

Table 6.23. Voltammetric Parameters for 0.27M chromium(II) in 30/70 mole p.c. NaCl/$ZnCl_2$ at 400°C

Scan rate/ mVs^{-1}	I_{pc}/I_{pa}	ΔE_p/ mV	$I_{pa}/v^{1/2}$/ $mA/(Vs^{-1})^{1/2}$
1000	1.07	266	4.77
500	1.02	251	4.86
200	1.02	251	5.47
100	0.97	233	6.14
50	0.93	210	6.76
20	0.98	200	6.78
5	0.78	195	7.81
	$E_{pa}-E_{pa/2}$/mV	E_{pa}/V	
1000	148	1.244	
500	154	1.244	
200	146	1.244	
100	115	1.203	
50	92	1.157	
20	84	1.136	
5	65	1.095	

Figure 6.24. Typical cyclic voltammograms for the oxidation of chromium(II) (0.27M) in 0.30 mole fraction NaCl-$ZnCl_2$ at 400°C

Working electrode: vitreous carbon
Reference electrode: zinc



be predicted for a relatively concentrated solution in this acidic melt (fig. 6.25, table 6.24).

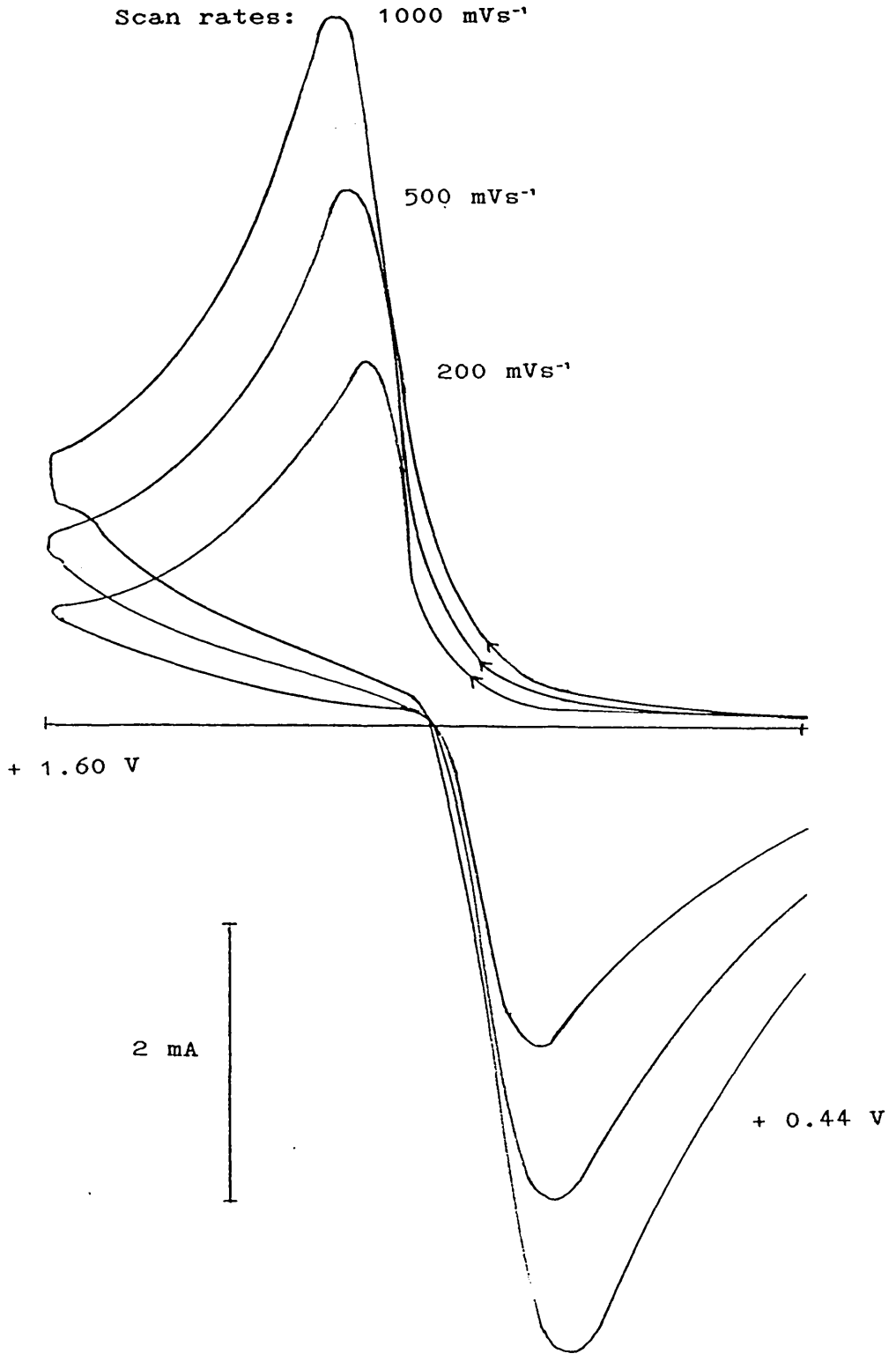
6.2.3 Summary of voltammetric results

The voltammetric evidence suggests that results for sufficiently dilute solutions of chromium(II) conform to the mechanism of a one-electron reversible (or possibly quasi-reversible) oxidation to soluble chromium(III), no other oxidation state being accessible within the redox limits of the solvent (i.e. chloride oxidation or zinc deposition). By increasing the concentration, increasing the melt acidity, or by lowering the temperature, voltammograms diagnostic of insoluble product formation could be obtained. For certain values of these parameters, and by varying the scan rate, voltammograms showing a transition from soluble product formation to product deposition resulted, evidently the form being influenced by the kinetics of the deposition process.

Replacement of the potassium cation by the more acidic sodium cation, other factors being equal, appeared to increase the tendency towards precipitation. These results obviously suggest that an acid-base equilibria is involved in the deposition process. It will be demonstrated below that the deposition product was essentially pure chromium(III) chloride, and evidently this substance is in equilibrium with a complex, formed by reaction with chloride ions. Any factor tending to reduce the chloride ion activity would thus tend to cause precipitation.

There was no hard evidence that would support the existance of chemical reactions coupled to the electron

Figure 6.25. Typical cyclic voltammograms for the oxidation of chromium(II) (0.41M) in 0.15 mole fraction NaCl-$ZnCl_2$ at 400°C



Working electrode: vitreous carbon
Reference electrode: zinc

Table 6.24. Voltammetric Parameters for 0.41M chromium(II) in .15/85 mole p.c. NaCl/$ZnCl_2$ at 400°C

Scan rate/ mVs^{-1}	I_{pc}/I_{pa}	ΔE_p/ mV	$I_{pa}/\nu^{1/2}$/ $mA/(Vs^{-1})^{1/2}$
1000	1.14	434	5.08
500	1.12	370	5.46
200	1.16	289	5.79
100	1.12	213	5.99
50	1.03	191	6.44
20	1.01	112	6.78
5	0.91	102	6.96
	$E_{pa}-E_{pa/2}$/mV	E_{pa}/V	
1000	110	1.161	
500	82	1.125	
200	54	1.083	
100	37	1.031	
50	34	1.030	
20	32	1.030	
5	32	1.029	

transfer in these melts, effects such as increasing peak separation and peak widths with increasing scan rate were best attributed to uncompensated solution resistance due to relatively low melt conductivities, while low peak current ratios at low scan rates appeared to be due to convection effects.

The voltammetric results in the present work may be compared to those of other workers. Topol et al (68) studied the Pt/$CrCl_2$,$CrCl_3$ system in 0.6/0.2/0.2 mole fraction $ZnCl_2$/NaCl/KCl melt at temperatures up to 320°C. They concluded that the solubility of $CrCl_3$ was less than 0.1M, but the redox couple was reversible with an equilibrium potential of +0.959 V w.r.t. zinc at 320°C. This value is similar to the half-wave potential obtained in the present work, i.e. about 1.04 V in relatively basic melts at 400°C, the peak potential then being about 1.10 V, which is similar to the value found by Matsunaga and Hosokawa (62) in the NaCl/$ZnCl_2$ eutectic at 400°C, 1.14 V. The latter authors also reported the couple to be reversible.

Topol et al (68) further claimed that chromium(II) could be reduced to metal at +0.1 V w.r.t. zinc, in contrast to the present work.

The latter authors also found that chromium(II) could be oxidised to an insoluble species in the acidic 0.61/0.39 mole fraction $AlCl_3$/NaCl melt at 208°C, in which chromium(III) chloride is insoluble. However, two sharp stripping peaks were observed, the nature of the processes involved being obscure. In the basic 0.498/0.502

mole fraction $AlCl_3$-NaCl melt at 175°C, chromium(III) chloride is soluble, and the couple is reversible (104).

The deposition of other metal chlorides has been observed, for example in the case of soluble $ZrCl_4$ to insoluble $ZrCl_3$ in basic $AlCl_3$-NaCl (105); the deposition and stripping peaks somewhat resemble those obtaned for chromium in the present work. Further, Gilbert et al (103) have investigated the oxidation of ytterbium(II) in $AlCl_3$-NaCl. As the melt acidity decreased, the precipitation of $YbCl_3$ could be observed as an inflection occuring at progressively lower points on the oxidation wave. The change may be expressed as:

Yb^{3+}(uncomplexed, soluble)+Cl^- $\longrightarrow$ $YbCl_3$(insoluble)

However the analogous change in the present work can probably be expressed as:

$CrCl_3$(insoluble)+Cl^- $\longrightarrow$ Cr^{3+}(complexed, soluble)

6.2.4 Effect of melt acidity on peak potential

Since the chromium(II)/chromium(III) redox couple appears to be uncomplicated by coupled chemical reactions, the peak potentials should be influenced by the melt acidity in a straightforward way. The half-reaction for the Cr^{2+} oxidation is:

$$CrCl_2 + Cl^- \longrightarrow CrCl_3 + e^- \qquad (6.10)$$

and the potential for this reaction is related to the zinc deposition potential, the relevant half-reaction being:

$$ZnCl_2 + 2e^- \longrightarrow Zn + 2Cl^- \qquad (6.11)$$

Combining the half-reactions and applying the Nernst equation yields:

$$E = E^\circ - RT/F \ln[(CrCl_3)/(CrCl_2)]$$
$$+RT/2F \ln(ZnCl_2) \qquad (6.12)$$

Now the second term on the right-hand side can be split into two terms involving activity coefficients and concentrations respectively. If any point on the reversible (soluble product) voltammetric wave is taken, then the concentration ratio of chromium(III) to chromium(III) is fixed and may be incorporated into the E° term. Thus eqn. 6.12 may be re-written as:

$$E = E^\circ - RT/F \ln[(\gamma CrCl_3)/(\gamma CrCl_2)]$$
$$+RT/2F \ln(ZnCl_2) \qquad (6.13)$$

The activity coefficient ratio may remain approximately constant with melt acidity, and if so, a plot of peak potential versus ln $(ZnCl_2)$ should be linear with a slope of RT/2F (+29 mV at 400°C).

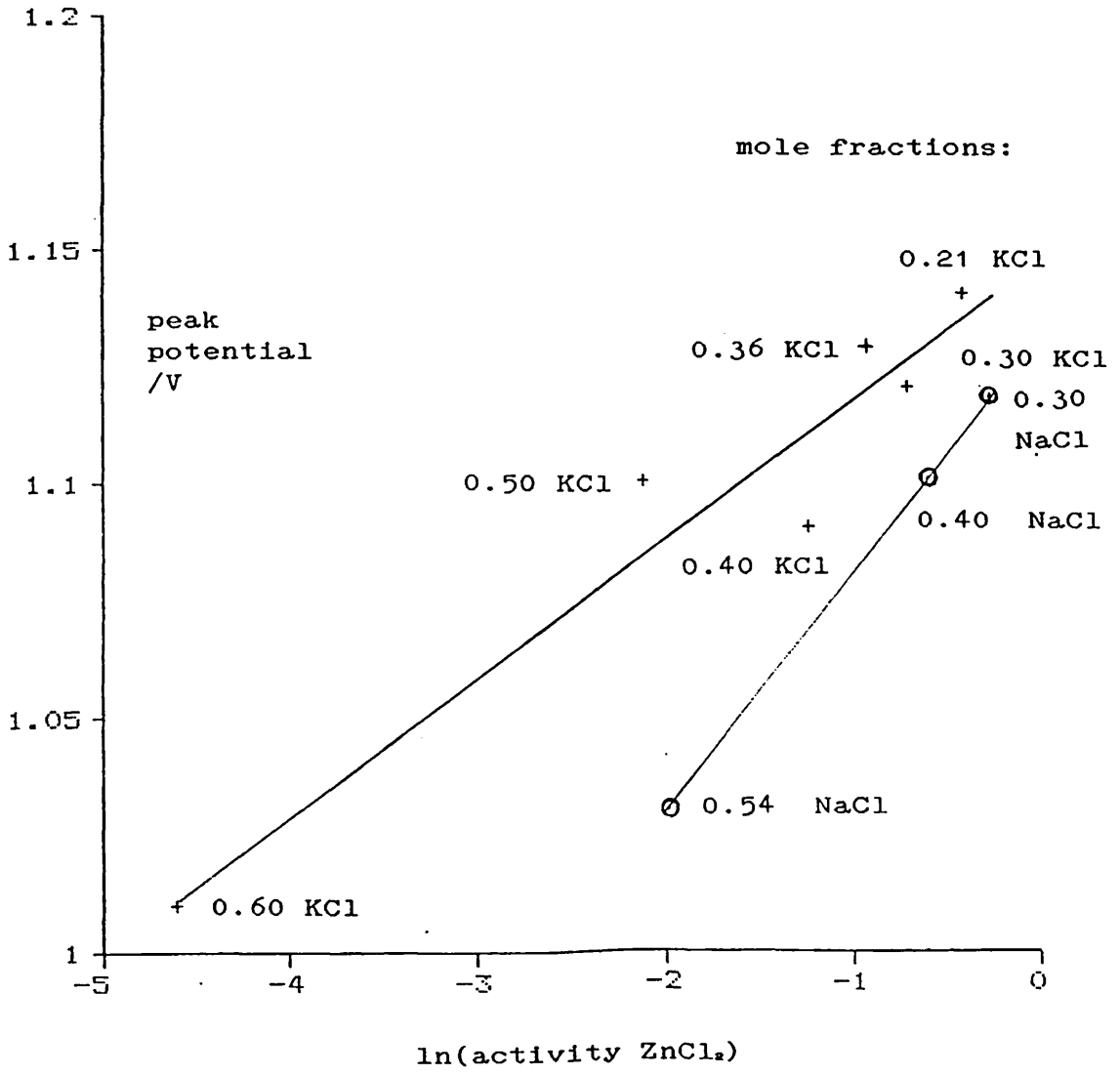
Figure 6.26 shows such a plot for the $KCl/ZnCl_2$ system. Though the points are fairly scattered, the least squares fit produced a line with a slope of +28 mV, in agreement with the theoretical analysis. Errors in the measured peak potential, activity values, and variation in the activity coefficient ratio may account for the scatter. The results for $NaCl/ZnCl_2$ give a higher gradient, +56 mV, but only three compositions were considered (fig. 6.26).

6.3 Characterisation of the anodic oxidation product

6.3.1 Isolation of the product

Having obtained from the voltammograms evidence of a reaction involving deposition, it was natural to attempt to characterise the product. Anodic oxidation of the

Figure 6.26. Variation of the reversible voltammetric peak potential for chromium(II) oxidation with melt acidity in alkali chloride-zinc chloride systems



chromium(II) solutions in KCl/$ZnCl_2$ melts was thus carried out potentiostatically with large area (several cm^2) platinum or vitreous carbon electrodes.

In the relatively basic melts, or where the voltammograms indicated a soluble product, then violet or black solutions were obtained, but no solid material. In contrast, for a solution where the voltammogram was indicative of deposition, a violet-red product could be obtained. For example, in a 0.27 mole fraction KCl melt with 0.5M chromium(II) at 400°C, and the potential held at about 300 mV anodic of the voltammetric peak, overnight electrolysis produced a deposit of about 50 microns thickness.

In order to examine the deposit, it was necessary to raise the electrode from the melt, cool, transfer the cell to the drybox, remove the electrode, and then dissolve the frozen layer of melt from the electrode by using a suitable solvent such as water, ethoxyethane, or propanone. However, a great variation in the reactivity of the deposit was noticed, some preparations reacting readily with water to form a green solid, while others appeared stable, retaining the violet-red colour. Decomposition also occurred in ethoxyethane, but apparently not rapidly in propanone, so that this was the preferred solvent, the melt dissolving quite rapidly. Once washed with fresh solvent, the deposit was stable to water and air indefinitely. The varying reactivity is probably a consequence of the fact that anhydrous chromium(III) chloride is thermodynamically unstable to water, but

kinetically inert, unless traces of chromium(II) are present as catalyst (106). Thus the deposit may be attacked by soluble chromium(II) in the melt layer which dissolves into the solvent. Once this is removed, the deposit is stable.

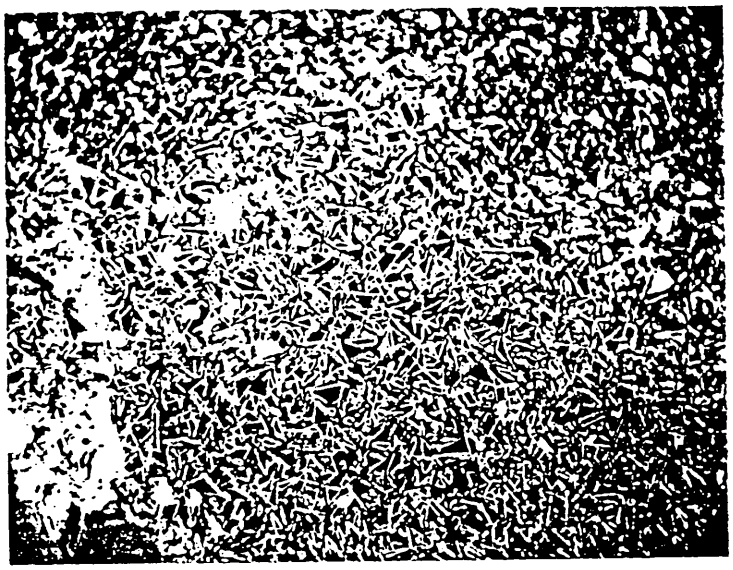
The initial variation in reactivity may be a consequence of the fact that varying amounts of chromium(II) may be present in the melt layer adjacent to the electrode, according to how depleted the layer is after electrolysis.

It was incidentally discovered that application of an A.C. voltage (±1V) to a platinum flag electrode at a frequency of 1000 Hz produced a relatively thick deposit as compared with the D.C. method above.

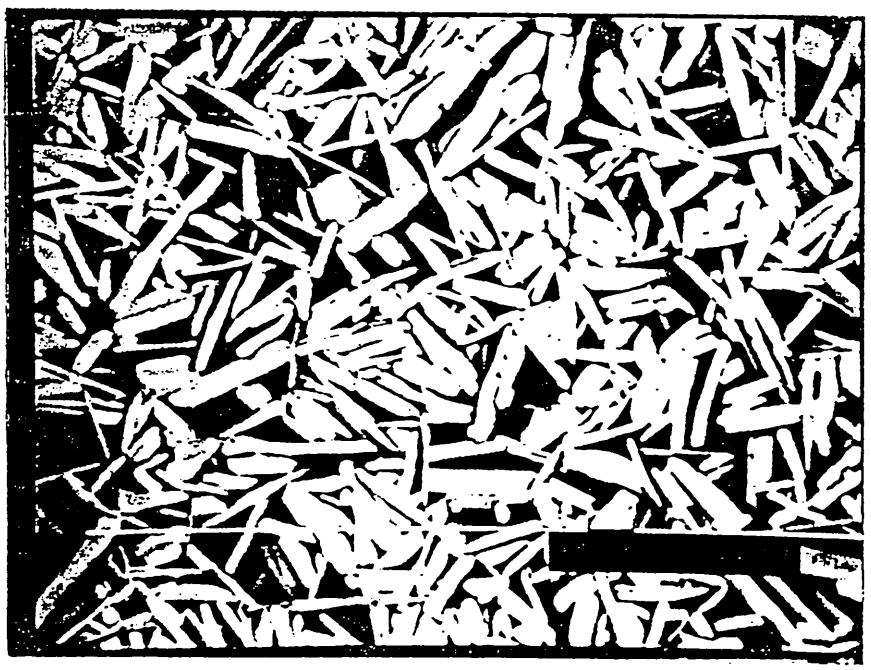
6.3.2 Morphology of the electrode deposit

The violet layer produced by the constant potential electrolysis could be easily detached in fragments for examination. The top surface under the optical microscope appeared to consist of flat plates aligned parallel to the surface of the electrode (fig. 6.27 a)), but under the electron microscope, in back-scattered mode, the surface can be clearly seen to consist of thin plates with the crystal edges orientated vertically with respect to the electrode (fig. 6.27 b)). This observation was confirmed by optical examination of the edge of the layer, which showed the vertical growth of the plates, as in figure 6.27 c). Furthermore, the deposit was easily disintegrated by subjecting a fragment in propanone to an ultrasonic bath for a few minutes, when the individual platelets

Figure 6.27. Morphology of chromium(III) chloride electrode deposit



a) Optical micrograph x88 Surface of deposit.



b) Electron micrograph Surface of deposit.

Figure 6.27. continued.



c) Optical micrograph x256 Edge of deposit



d) Optical micrograph x256

Platelets after ultrasonic dispersion in acetone

could now be seen optically, after allowing the dispersion to dry on a glass slide. The platelets were mostly irregularly shaped, though occasionally perfect hexagons were observed (fig. 6.27 d)). No other crystal phases were observed.

All these observations are consistant with the known crystal structure of chromium(III) chloride, which has a pseudo-hexagonal symmetry (107). This has been described as having "honeycomb" sheets of chromium ions separated by two layers of close-packed chloride ions, held together only by Van der Waals forces (fig. 6.28). As a result, the crystals cleave readily in a direction parallel to the chloride layers, and always form as thin plates.

the vertical growth of the crystal plates from the electrode surface would thus seem to be a consequence of the fact that the crystal edge must be the fastest growing face of the crystal, and of the constraints imposed upon available directions of growth.

There appeared to be no significant differences in morphology with crystals formed from solutions of varying concentration, temperature, etc.

6.3.3 Analysis of the deposit

a) X-ray powder diffraction.

The diffraction pattern of the electrode deposit corresponded closely with the reported patterns of chromium(III) chloride (75), reflections apparently corresponding to both monoclinic and hexagonal forms being obtained. However, it has been reported that the room-temperature form of the chloride has only monoclinic

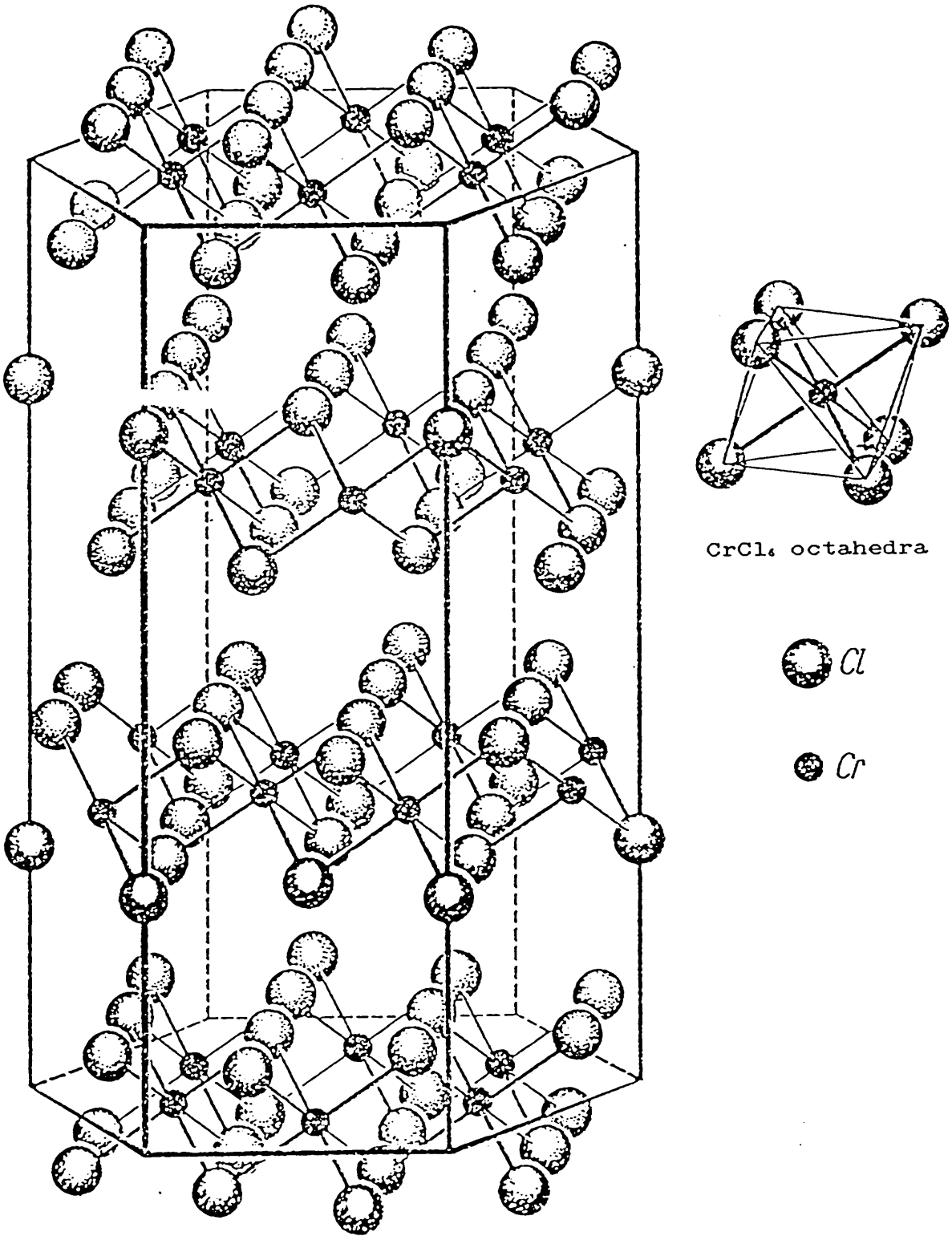


Figure 6.28. Layer structure of chromium(III) chloride (from Gmelin, Cr Tl. B, p.207)

symmetry (107).

Reflections due to metallic platinum were also found for deposits produced on this substrate (table 6.25), indicating corrosion of the electrode.

b) X-ray emission analysis.

Fragments of the electrode deposit from several vitreous carbon electrodes were analysed in the electron microscope by the X-ray emission spectrum. The results of examining about 15 areas on the top surface of each sample indicated an average molar ratio of 2.90±0.25:1 Cl:Cr. The possible chlorine deficiency may result from the presence of oxygen (not detectable) or from the presence of chromium(II). The amounts of zinc and potassium detected were negligable, generally less than 0.002 mole fraction.

c) Chemical analysis.

Analysis of typical samples of the electrode deposit for chromium by a standard technique gave a content of 31.2±0.2 per cent. The figure calculated for $CrCl_3$, 32.8 per cent. It was not possible to obtain an accurate chlorine analysis because only small quantities of sample could be produced.

d) ESCA analysis.

In an attempt to determine whether chromium(II) or other ions had been incorporated into the structure of the chromium(III) chloride electrode deposit, ESCA was employed. This technique measures the kinetic energy (E) of electrons ejected from matter (under high vacuum) after bombardment with X-rays (or other ionising radiation). The binding energies ($E_b = h\nu - E$, where ν is the frequency

Table 6.25. X-ray powder diffraction data for chromium(III) chloride electrode deposit (after detachment)

Electrode material: platinum

Product 'd' spacings	$CrCl_3$		Pt
	Monoclinic	Hexagonal	
1.11 (3)		1.11 (10)	
1.13 (3)			1.13 (12)
1.18 (10)			1.18 (33)
1.39 (10)	1.40 (1)	1.41 (10)	
1.45 (8)	1.45 (6)	1.45 (10)	
1.65 (4)	1.65 (1)	1.65 (20)	
1.72 (10)	1.72 (3)	1.72 (80)	
1.75 (4)	1.75 (3)	1.75 (10)	
1.91 (3)	1.93 (1)	-	
1.96 (28)			1.96 (53)
2.26 (60)			2.27 (100)
2.46 (22)	2.46 (6)	2.46 (100)	
2.81 (4)	-	2.82 (20)	
2.89 (22)	2.90 (14)	-	
2.92 (7)	2.94 (2)	2.93 (30)	
5.79 (100)	5.80 (100)	5.80 (80)	

of the ionising radiation) of the electrons from a particular element are characteristic of the orbital, oxidation state and chemical environment of the atom. The latter two effects are small compared with the first. Because of the low electron energy, only the surface layer of a sample (< 50 angstroms depth) can be examined. Secondary electrons emitted by the Auger process are generally also recorded.

Three samples were studied:

i) detached fragments of an electrode deposit (0.5M Cr^{2+} in 0.27 mole fraction $KCl/ZnCl_2$ at 400°C, washed with propanone).

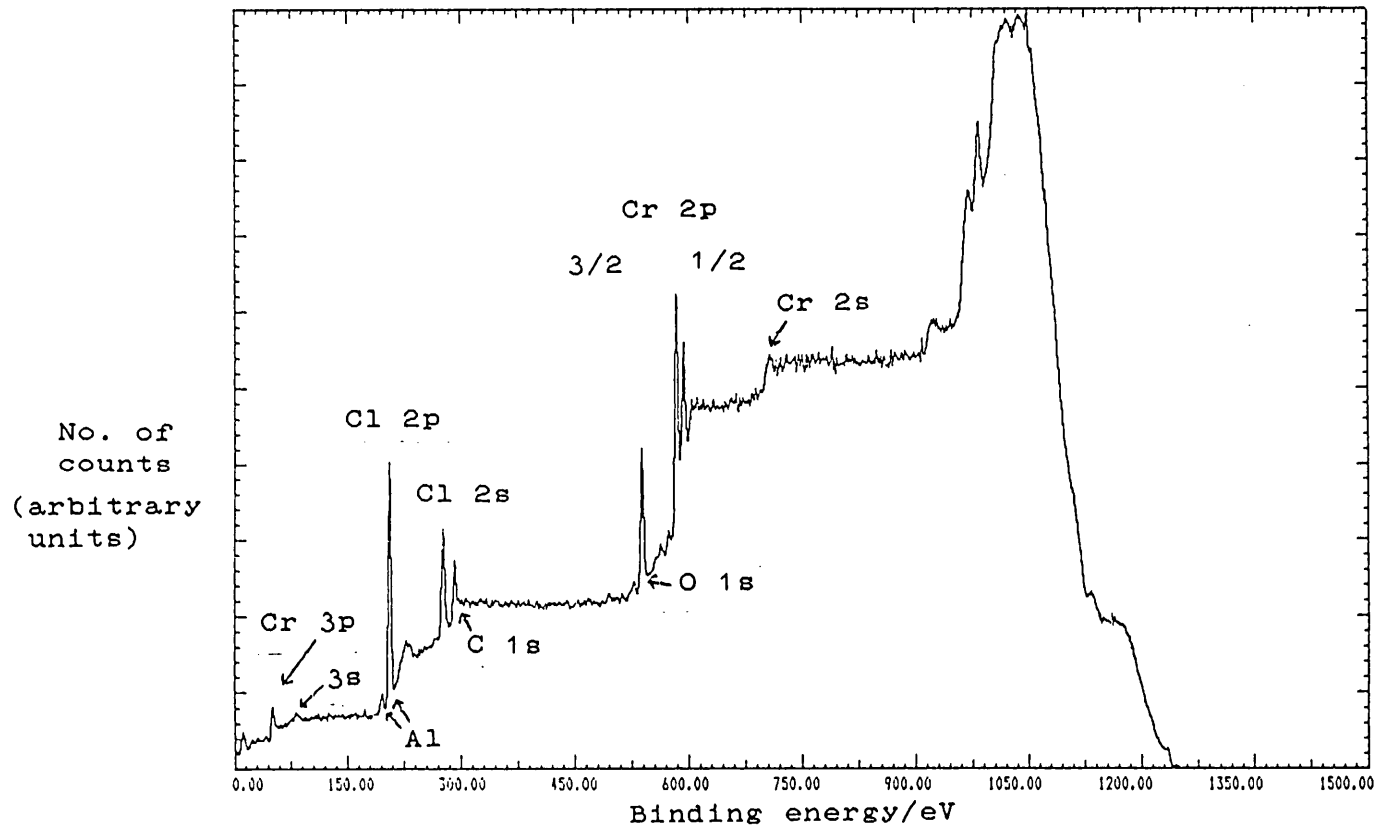
ii) a commercial sample of chromium(III) chloride.

iii) a 50:50 weight per cent mixture of $CrCl_2$ and $CrCl_3$ prepared by grinding the commercial samples in the drybox, and stored under dry argon.

A low resolution plot of electron count versus binding energy applicable to all three samples is shown in figure 6.29. The majority of peaks were readily assigned to chromium 3p, 3s, 2p, and 2s orbitals, and to chlorine 2p and 2s orbitals, using tabulated values of binding energy (76). The peak at 540 eV was assigned to oxygen 1s, and its intensity relative to Cr 2p increased in the order: Cr(II)/Cr(III) mixture > electrode deposit > commercial $CrCl_3$, the peak height ratio being 1.0:0.19:0.08. The order was not unexpected, since some momentary exposure of the sample to air in the port of the spectrometer may have taken place before applying the high vacuum. Thus some hydrolysis of the $CrCl_2$ may have occurred. The electrode

Figure 6.29. X-ray photoelectron spectrum of chromium(III) chloride samples (wide scan)

Exciting radiation: Al Kα



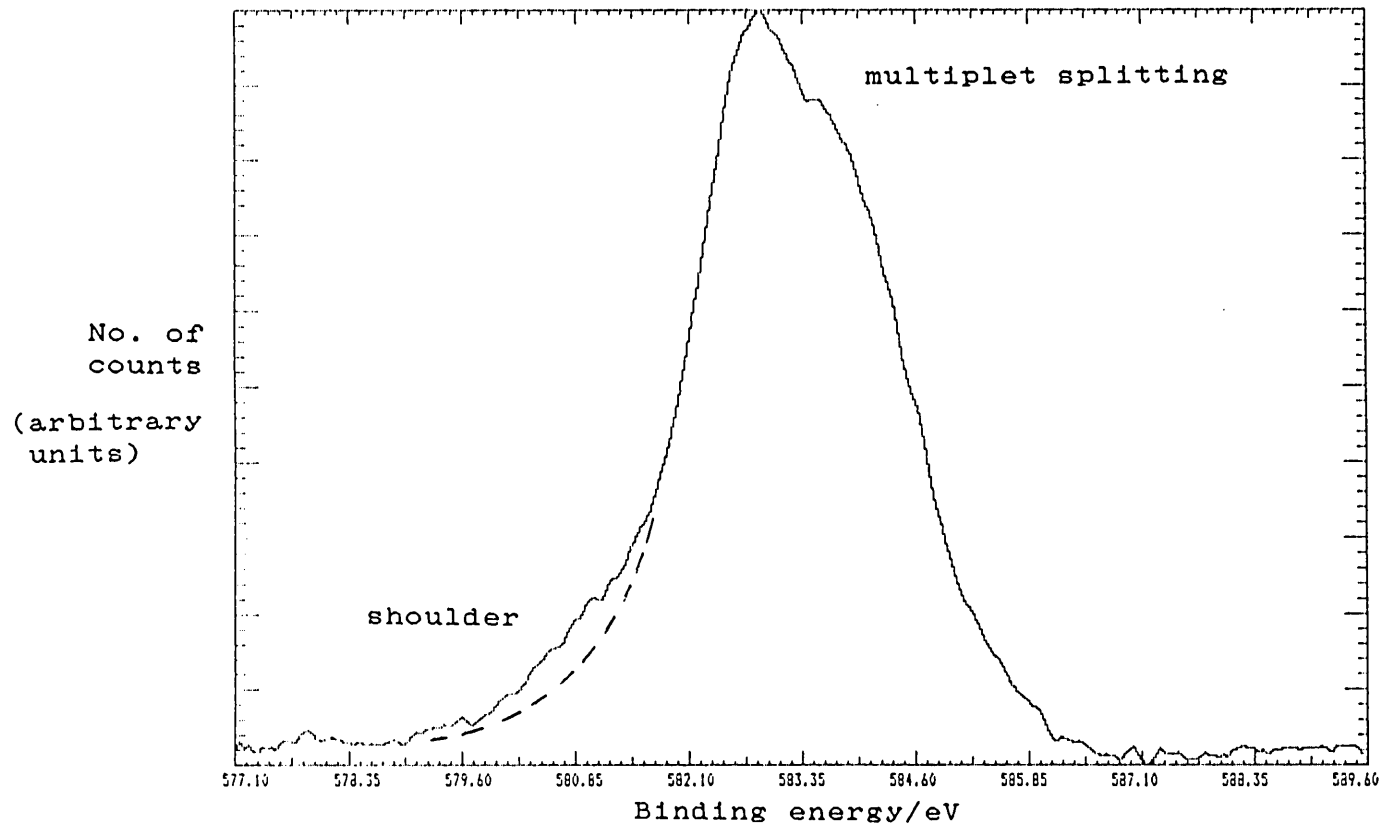
deposit also could have suffered some surface attack during the washing process, thus resulting in oxygen contamination.

The prominent Cr 2p and Cl 2p peaks were examined with higher resolution, and compared between samples. Little difference was found between the Cl 2p peaks, but the Cr 2p peaks showed shoulders on the low binding energy side, in the case of the electrode deposit and the mixed Cr(II)/Cr(III) sample (fig. 6.30). Thus after computer deconvolution of the Cr 2p 3/2 peak for the electrode deposit, a minor peak at 575.7 eV was obtained (normalised to C 1s at 285.0 eV) of area 0.116 of the main Cr 2p 3/2 peak at 577.2(±0.02) eV. The binding energy shift (-1.5 eV) is consistant with the presence of chromium(II), a similar shift being observed between CrF_3 and CrF_2, and for reduction of Cr(III) to Cr(II) in zeolites (109). However, the peak could also be due to oxygen coordination, since the Cr 2p 3/2 peak for Cr_2O_3 occurs at 576.2 eV, and for $NaCr^{III}O_2$ at 576.0 eV (109). (The Cr 2p 3/2 peak is also split due to the effect of unpaired d electrons, the so-called "multiplet" splitting). Thus, as regards the presence of chromium(II), the ESCA analysis must be regarded as inconclusive.

No trace of zinc or potassium was detected in the electrode deposit.

Figure 6.30. X-ray photoelectron spectrum of chromium(III) chloride sample deposited from KCl-$ZnCl_2$ melt:- Cr 2p 3/2 region

Exciting radiation: Mg Kα



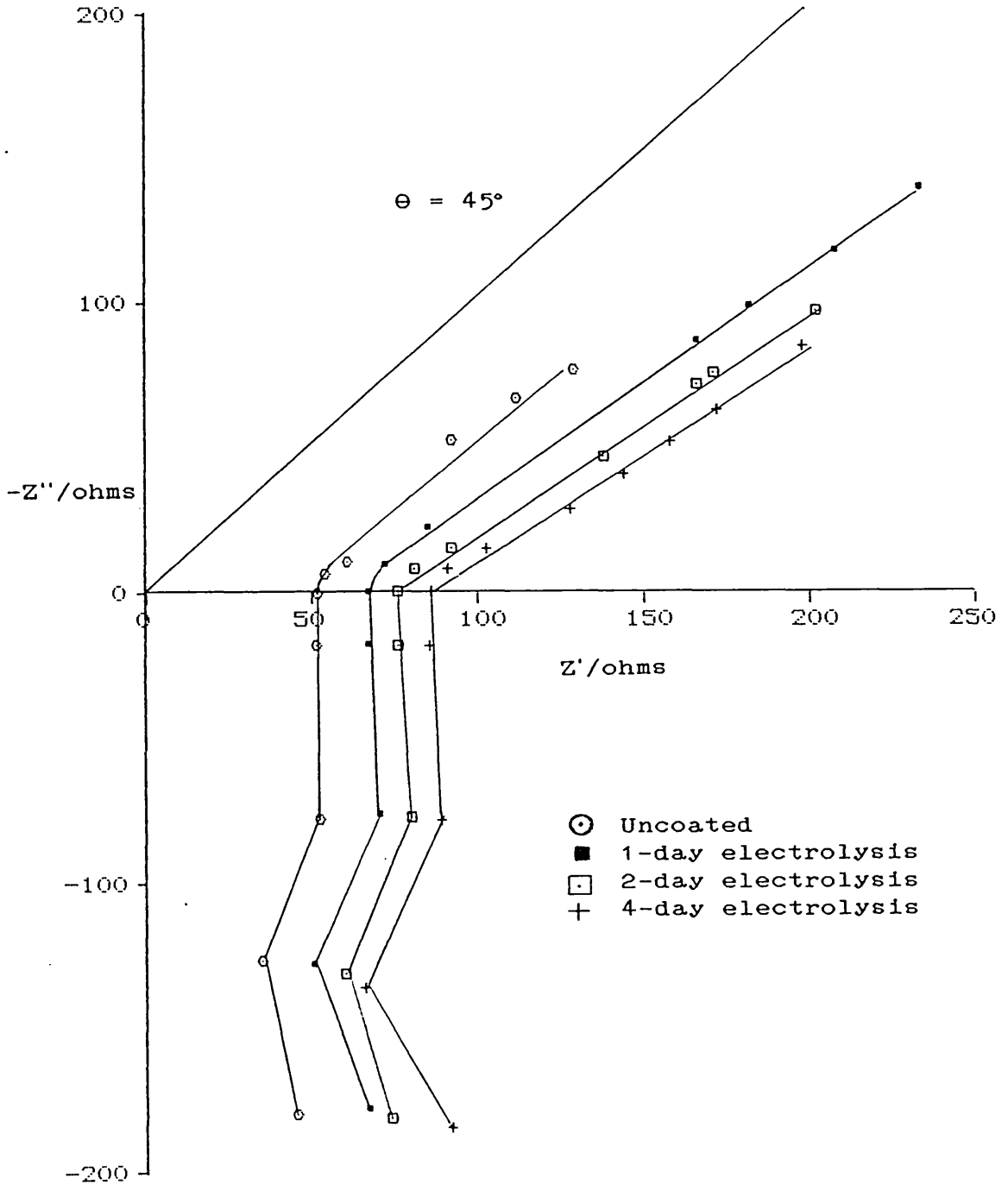
6.4 A.C. Impedance measurements

In order to assess the mechanism of conduction and growth of the chromium(III) chloride deposit, the response of the system to an A.C. signal was examined. Thus the A.C. impedance of the cell between the working and reference electrodes was determined at various stages during the deposition, over the frequency range 13 MHz to 5 Hz (amplitude ±10 mV). A vitreous carbon electrode with a "U"-bend at the working end was conveniently employed to prevent mechanical detachment of the layer during growth. Measurements were taken of the uncoated electrode, and after constant potential electrolysis, the applied potential being removed, and the concentration gradients allowed to equilibrate.

The presence of the chromium(III) chloride layer on the electrode after an experiment was confirmed by visual inspection.

Typical results are shown in figure 6.31 for 0.5M chromium(II) in 0.15 mole fraction $KCl/ZnCl_2$ at 400°, where the complex impedance component $-Z''$ is plotted against the real component Z', as is conventional. Several points may be noted. Firstly, at frequencies higher than about 50 kHz, the plots all drop below the $-Z''$ axis, indicating inductive effects, and exhibit rather complicated behaviour. These high frequency effects were probably a result of the circuit geometry rather than being a property of the electrode process (110). In confirmation, it can be seen that as the electrolysis time increases, and the thickness of the $CrCl_3$ layer grows,

Figure 6.31. Complex plane impedance plots for chromium(III) deposited on vitreous carbon from 0.5M chromium(II) in a 0.25 mole fraction KCl-$ZnCl_2$ melt at 400°C

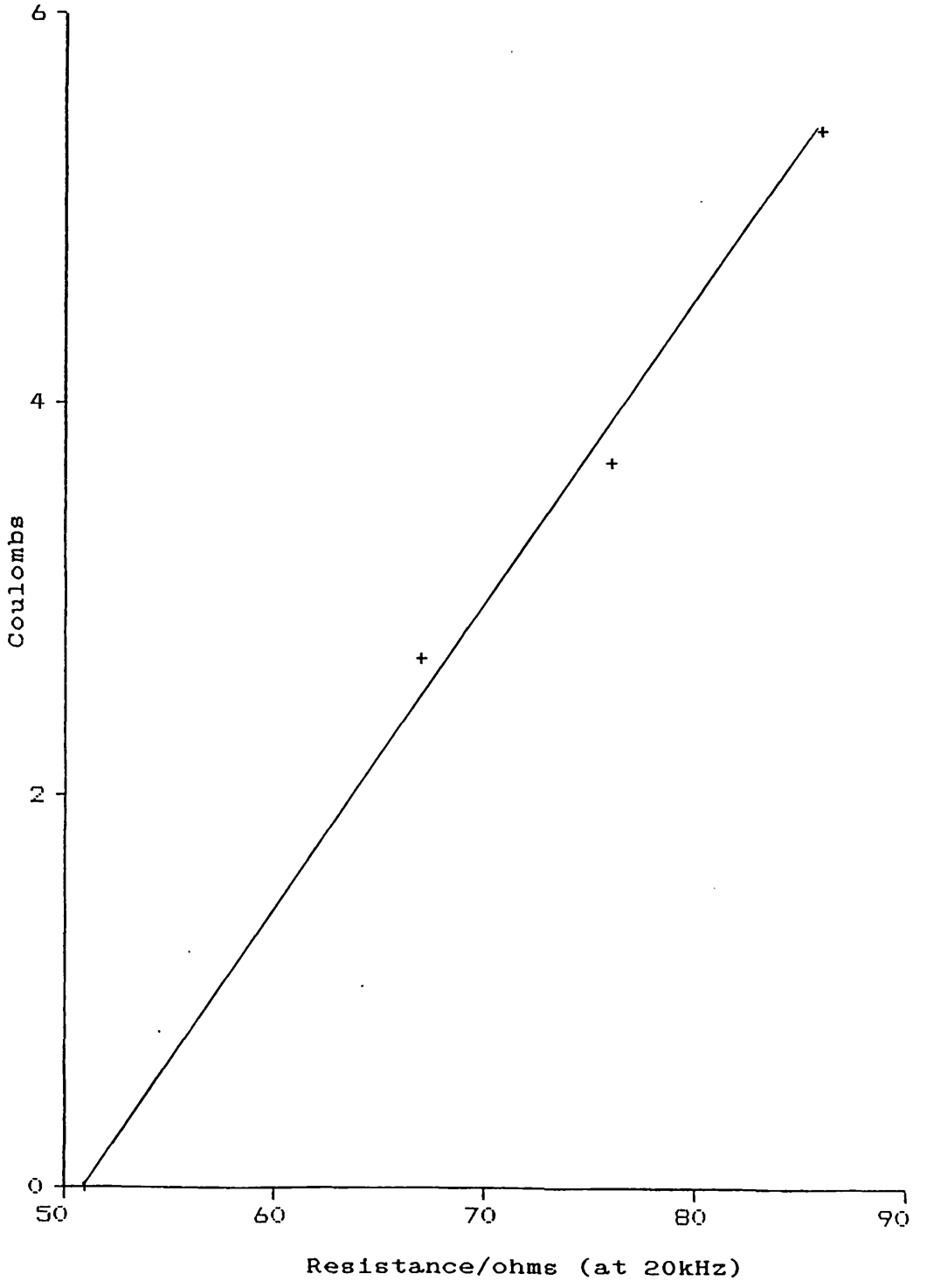


the plots are simply shifted along the real axis, without major changes occurring in the imaginary (capacitive) component.

Also, if the real (resistive) component is plotted against the number of coulombs passed, a good straight line results (fig. 6.32). This implies that the resistance increases uniformly as the deposit grows, a conclusion which is reasonable when the anisotropic morphology of the deposit is considered. Thus the plates of chromium(III) chloride grow vertically from the electrode, and the increase in resistance may be supposed to be due only to the increase in length of the plates, assuming that the accessible surface area of the deposit will not increase significantly, due to the tightly packed nature of the plates. Additionally, the conductivity in a direction perpendicular to the sheet structure is most likely very low, a consequence of the weak interactions between sheets.

A further feature of figure 6.31 is that the lower frequency part of the complex impedance plots ($\omega < 5$ kHz) exhibits a linear relationship between $-Z''$ and Z', with a slope of about 45°. Again, as the deposition time increases, the plots simply shift along the real axis. The linear relationship is characteristic of the Warburg impedance, due to a fast diffusion-controlled electrochemical process (77). If a significant kinetic barrier to electron transfer was present (for example, due to ionic and not electronic conduction through the electrode deposit), then at relatively high frequencies a

Figure 6.32. Plot of real impedance component at 20kHz versus number of coulombs passed during deposition of chromium(III) chloride from a 0.5M chromium(II) solution in 0.25 mole fraction KCl-$ZnCl_2$ melt at 400°



capacitive semi-circle would be found (77), with -Z'' tending to zero as the frequency tended to infinity. There was no indication of this in the present work, and it may therefore be concluded that the presence of the deposit does not hinder the electron transfer (apart from introducing Ohmic resistance), suggesting that electronic conductivity occurs in the layer. Alternatively, it might be supposed that electron transfer takes place at the electrode surface with material which diffuses between the gaps in the chromium(III) chloride plates. This seems unlikely, due to the close-packed nature of the plates and the linear relationship between resistance and deposition time.

A possible mechanism for electronic conductivity in the layer is "electron hopping" between chromium ions via Cr^{2+} ions incorporated into the structure during deposition, leading to semi-conductor type properties, i.e. an increase in conductivity with temperature.

6.5 Overall conclusions and Further work

The electrochemical oxidation of chromium(II) in alkali chloride-zinc chloride melts yields chromium(III), which, depending on Lewis acidity conditions, precipitates as chromium(III) chloride on the electrode, with a characteristic morphology. It is thus concluded that an acid-base solubility equilibrium exists for chromium(III) chloride in these melts, the solubility being enhanced in more basic melts, or by raising the temperature. The substitution of the relatively acidic sodium cation for potassium leads to a significant reduction in solubility.

The system might therefore be used to test the activity coefficient predictions of the "Coordination Cluster" theory (8) (see also chapter one), as a significant change in activity coefficient of chromium(III) evidently occurs with melt acidity.

Cyclic voltammetry indicates that the deposition and stripping process are not completely reversible, but A.C. impedance measurements show that the deposit does not passivate the electrode, and only moderate increases in resistance were observed with increasing layer thickness, linearly related to the charge passed, suggesting uniform growth. These latter results also indicate that the deposit is an electronic conductor.

The relative reversibility of the deposition reaction suggests that a high-temperature secondary battery could be constructed around a solution of chromium(II) in a zinc chloride-based melt, the charging reactions being:

anode: $2Cr^{2+} \longrightarrow 2CrCl_3 + 2e^-$ (6.14)

cathode: $Zn^{2+} + 2e^- \longrightarrow Zn$ (6.15)

and the discharge reactions being the reverse of those above. To develop such a battery, the electrolyte composition would require optimisation for maximum conductivity (i.e. relatively high alkali chloride content), while ensuring that the chromium(III) chloride solubility remained sufficiently low. Further studies to assess the conductivity mechanism and enhance the conductivity of the chromium(III) chloride deposit would also be desirable.

CHAPTER SEVEN

CYCLIC VOLTAMMETRY OF GALLIUM COMPOUNDS IN ZINC CHLORIDE-ALKALI CHLORIDE MELTS

7.1 Procedure and general observations

Solutions of gallium(III) chloride were prepared by mixing the solid substance with the melt components in the drybox, and transferring the sealed electrochemical cell to the furnace, where an argon flow was initiated, and the cell heated to the required temperature. The solutions were colourless, and the chloride appeared to be readily soluble in both acidic and basic melts. Despite the fact that $GaCl_3$ has a low boiling point (below 300°C), there was no evidence of volatilisation of the compound from the melts, and subsequent decomposition, as was found for Ti(IV) (chapter 8), in the form of a thin film of oxide on the cell walls.

The voltammetric results for the gallium(III) solution will now be considered. In this case, it is convenient to start from the acid end, for ease of interpretation.

7.2 Cyclic voltammetry of gallium(III) solutions- Results and Discussion

7.2.1 Potassium chloride-zinc chloride melts

a) Pure zinc chloride.

In this solvent at 400°C, only one wave was observed, for gallium(III) reduction (fig. 7.1). The voltammetric parameters for an 0.09M solution are given in table 7.1. It may be observed that peak broadening and an increase in peak separation occur with increasing scan rate, probably due to melt resistance effects, but at low scan rates, the

Figure 7.1. Typical cyclic voltammograms for the reduction of gallium(III) (0.09M) in pure zinc chloride at 400°C

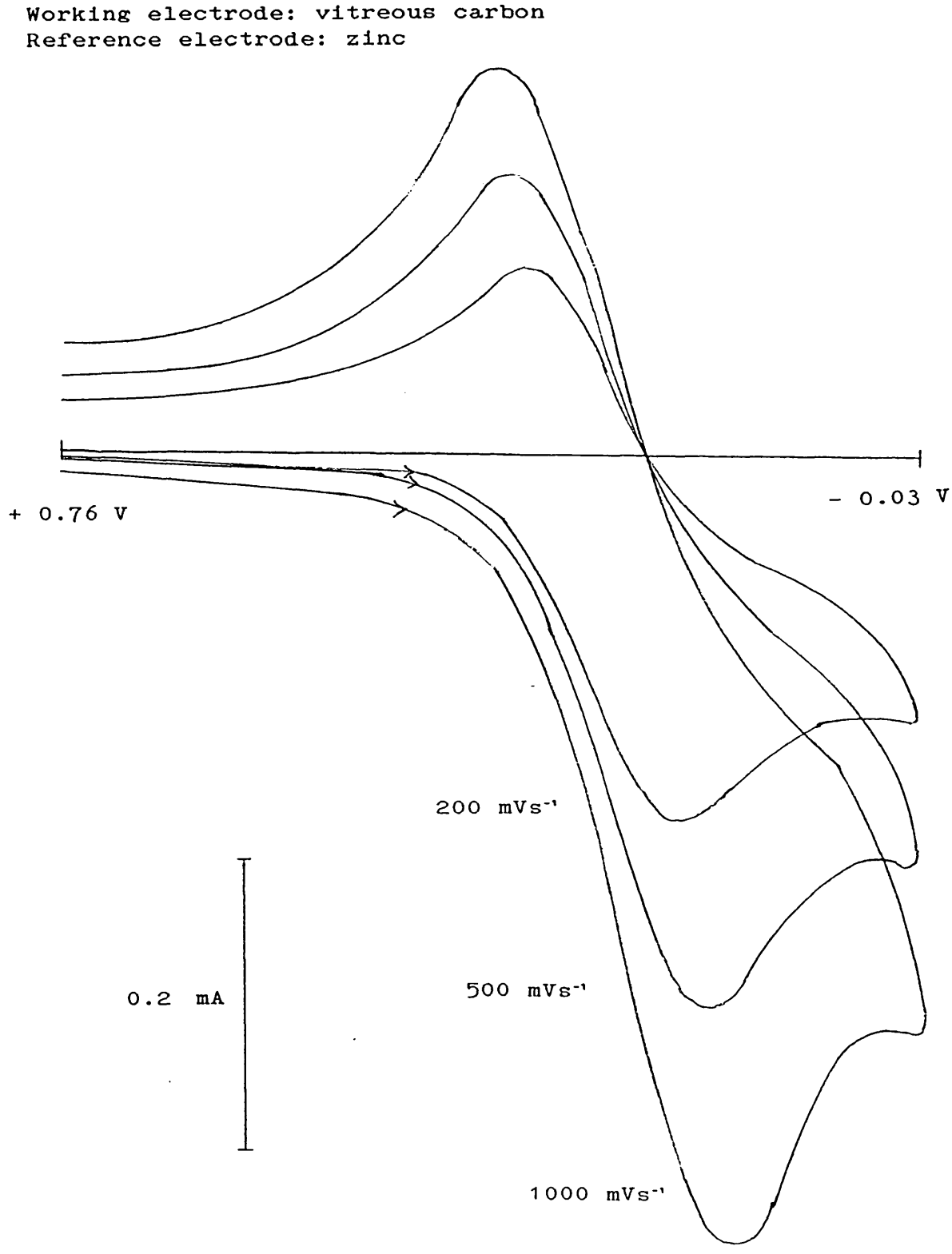


Table 7.1. Voltammetric Parameters for 0.09M gallium(III) in pure zinc chloride at 400°C

Scan rate/ mVs^{-1}	I_{pa}/I_{pc}	ΔE_p/ mV	$I_{pc}/\nu^{1/2}$/ $mA/(Vs^{-1})^{1/2}$
1000	0.94	202	0.53
500	0.95	179	0.53
200	0.95	133	0.55
100	0.92	113	0.59
50	0.95	104	0.63
20	0.89	85	0.64
5	0.82	60	0.70
	$E_{pc}-E_{pc/2}$/mV	E_{pc}/V	$E_{1/2}$/V
1000	84	0.191	-
500	82	0.216	-
200	82	0.244	-
100	80	0.249	-
50	80	0.254	-
20	75	0.261	-
5	70	0.267	0.205

Table 7.2. Voltammetric Parameters for 0.07M gallium(III) in 13/87 mole p.c. $KCl/ZnCl_2$ at 400°C

Scan rate/ mVs^{-1}	I_{pa}/I_{pc}	ΔE_p/ mV	$I_{pc}/\nu^{1/2}$/ $mA/(Vs^{-1})^{1/2}$
1000	0.97	141	2.17
500	0.98	134	2.21
200	0.96	110	2.28
100	0.95	102	2.36
50	0.96	90	2.28
20	0.91	75	2.28
5	0.79	71	2.16
	$E_{pc}-E_{pc/2}$/mV	E_{pc}/V	$E_{1/2}$/V
1000	87	0.234	-
500	90	0.239	-
200	84	0.250	-
100	80	0.260	-
50	80	0.265	-
20	75	0.268	-
5	75	0.268	0.206

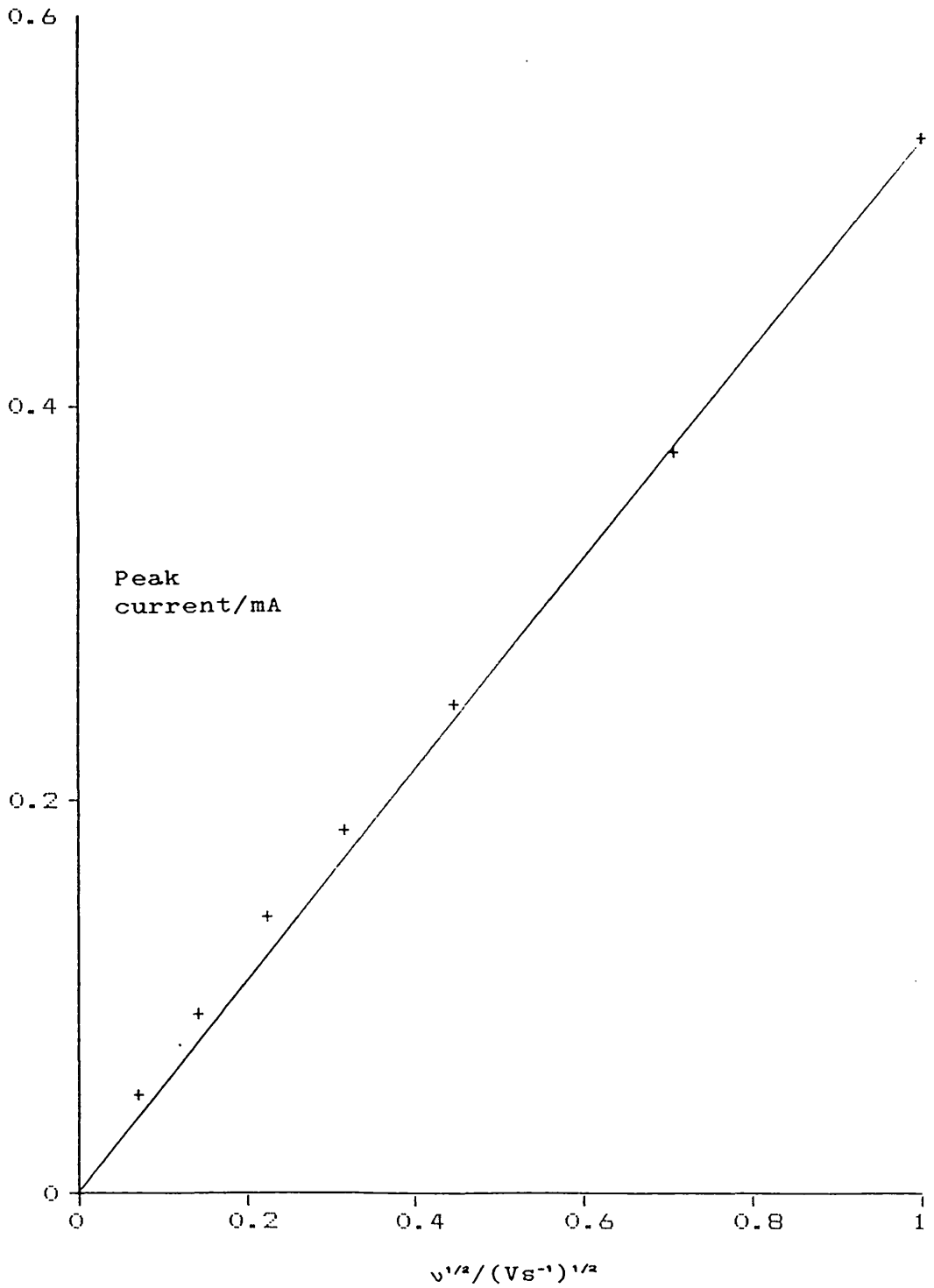
experimental values are close to those calculated for a reversible two-electron transfer involving a soluble product. Thus the calculated peak separation and half-peak width are respectively 67 mV and 64 mV at 400°C, values of 60 mV and 70 mV being found experimentally for the 5 mVs^{-1} scan rate. The peak current ratio values are reasonably constant at around 0.95 (ν > 50 mVs^{-1}) but decrease at lower scan rates, probably due to convection, as noted for chromium(II) in chapter 6. A plot of i_{pc} versus $\nu^{1/2}$ is likewise linear, passing through the origin, except at lower scan rates (fig. 7.2).

The above results imply a (quasi-) reversible reaction to form a stable gallium(I) species, which is consistant with the chemistry of group III elements, though gallium(I) is unstable in all but very acidic solvents, disproportionating to gallium metal and gallium(III):

$$3Ga^{+} \rightleftharpoons Ga^{3+} + 2Ga^{0} \qquad (7.1)$$

Hitherto only a few well-characterised gallium(I) compounds have been prepared, since the oxidation state has virtually no aqueous chemistry (111), but may be stabilised in acidic chloroaluminate melts, as is shown by the existence of the compound $GaAlCl_4$. In $AlCl_3$/NaCl/KCl eutectic, for example, both Ga(I) and Ga(III) show reversible reactions, and the difference between the Ga(III)/Ga(I) and Ga(I)/Ga(0) equilibrium potentials is 0.544 V, giving K for disproportionation as 5 $x10^{-14}$ (eqn. 7.1). In comparison, this value in water is calculated as 3 $x10^{9}$ (112,113). The analogous compound $Ga^{I}Ga^{III}Cl_4$ is one of the best-known

Figure 7.2. Plot of peak current against square root of scan rate for the reduction of gallium(III) (0.09M) in pure zinc chloride at 400°C



examples of gallium(I), and is prepared by interaction of gallium metal and the Lewis acid gallium(III) chloride, the latter substance having an acid-base chemistry similar to that of aluminium chloride (114,115).

Hence in the present work the acidic zinc chloride appears to stabilise the gallium(I) oxidation state in a similar fashion.

b) 0.13 mole fraction KCl.

The voltammetric results for this system at 400°C were qualitatively similar to those obtained for the pure zinc chloride (above). The results are presented in table 7.2, and figure 7.3 for an 0.07M solution.

c) 0.35 mole fraction KCl.

Rather more reversible behaviour was suggested by the voltammetric results for this composition, in the sense that no shift in peak potentials, increased peak separation, or peak broadening was observed with increasing scan rate, up to 1 Vs^{-1} (table 7.3). This may simply be due to the reduced melt resistance. Otherwise the remarks made for the pure zinc chloride composition apply equally well here, though in fact the peak separation and half-peak widths are slightly broader, but still well below the values calculated for a one-electron reduction.

d) 0.4 mole fraction KCl.

A definate change in behaviour was found at this composition. At relatively low scan rates, < 100 mVs^{-1}, the voltammograms tended to retrace their forward paths on the reverse sweep, leading to low values of the peak

Figure 7.3. Typical cyclic voltammograms for the reduction of gallium(III) (0.07M) in 0.13 mole fraction KCl-$ZnCl_2$ at 400°C

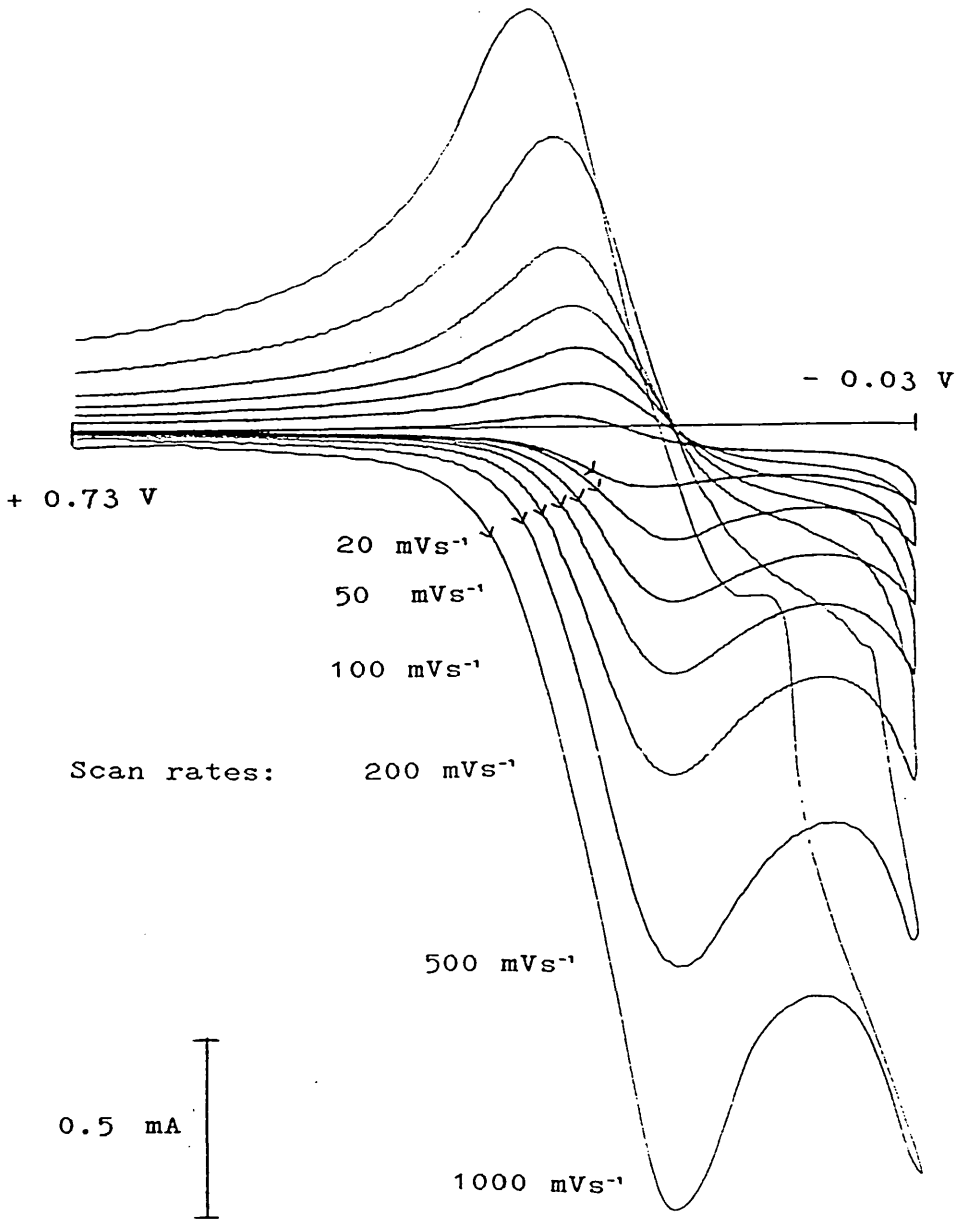


Table 7.3. Voltammetric Parameters for 0.032M gallium(III) in 35/65 mole p.c. KCl/$ZnCl_2$ at 400°C

Scan rate/ mVs^{-1}	I_{pa}/I_{pc}	ΔE_p/ mV	$I_{pc}/\nu^{1/2}$/ $mA/(Vs^{-1})^{1/2}$
1000	1.01	91	2.40
500	1.01	"	2.34
200	0.96	"	2.38
100	0.98	"	2.47
50	1.00	"	2.47
20	0.98	"	2.57
5	0.70	"	2.86
	$E_{pc}-E_{pc/2}$/mV	E_{pc}/V	$E_{1/2}$/V
1000	80	0.241	0.179
500	"	"	-
200	"	"	-
100	"	"	-
50	"	"	-
20	"	"	-
5	"	"	"

Table 7.4. Voltammetric Parameters for 0.060M gallium(III) in 40/60 mole p.c. KCl/$ZnCl_2$ at 400°C

Scan rate/ mVs^{-1}	I_{pa}/I_{pc}	ΔE_p/ mV	$I_{pc}/\nu^{1/2}$/ $mA/(Vs^{-1})^{1/2}$
1000	0.71	90a	2.47
500	0.70	90	2.51
200	0.64	90	2.80
100	0.62	-	2.92
50	0.60	-	3.14
20	0.61	-	3.57
	$E_{pc}-E_{pc/2}$/mV	E_{pc}/V	
1000	60a	0.170a	
500	90	"	
200	100	"	
100	-	"	
50	-	"	
20	-	"	

a. Values in these columns are somewhat uncertain due to distortion of the voltammetric wave.

current ratio as compared with the reversible case (table 7.4,fig. 7.4). Also, if the potential was held constant at a point part-way up the wave, then an appreciable steady-state cathodic current was observed, which did not decay to near-zero, and thus was not diffusion-controlled. It was clear from these results that a chemical reaction is coupled to the electron transfer, which acts to regenerate gallium(III) from gallium(I). Thus the steady-state current noted above occurs because the rate of reduction of gallium(III) (diffusion-controlled) is exactly balanced by the rate of production of gallium(III) (controlled by chemical kinetics).

The chemical reaction in question is almost certainly the disproportionation of gallium(I), brought about by the increase in chloride ion concentration in the melt. Now the Ga^+ ion has been reported to have the same charge/radius ratio as K^+ (114) and may therefore be considered as non-complexing; on the other hand, gallium(III) forms the stable complex ions, $GaCl_4^-$ and $Ga_2Cl_7^-$, for example the former ion in basic chloroaluminate melts (115).

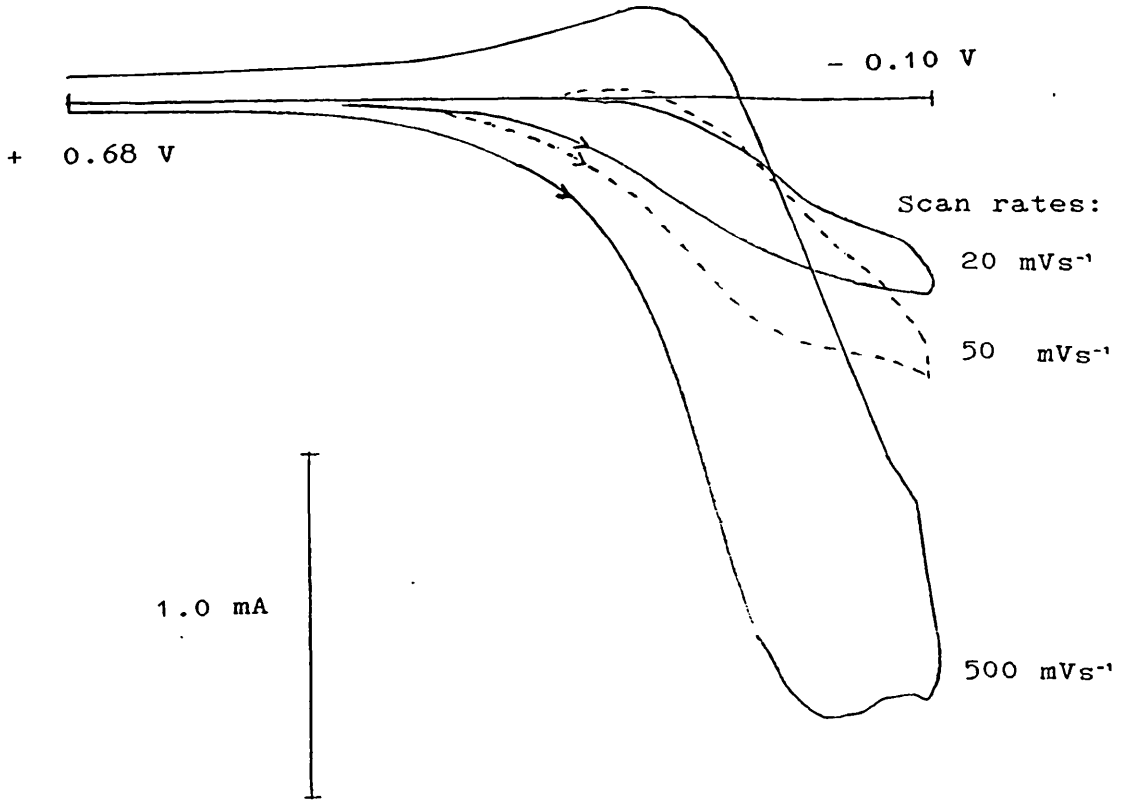
In the basic chlorozincate solvents, the overall disproportionation might therefore better be written as:

$$3Ga^+ + 4Cl^- \longrightarrow GaCl_4^- + 2Ga^\circ \qquad (7.2)$$

At the potentials of the voltammetric wave however, Ga° can be reoxidised and so the net chemical reaction is a regeneration of gallium(III), leading to the observed behaviour.

Figure 7.4. Typical cyclic voltammograms for the reduction of gallium(III) (0.06M) in 0.40 mole fraction KCl-$ZnCl_2$ at 400°C

Working electrode: vitreous carbon
Reference electrode: platinum wire (potentials estimated relative to onset of zinc deposition)



In the $KCl/ZnCl_2$ melt, the voltammetric behaviour was complicated by the proximity of the zinc deposition wave, and the phenomenon was more readily observed in the sodium chloride-based melts (see below).

e) 0.5 mole fraction KCl.

In this melt the gallium(III) reduction wave appeared to have shifted so far cathodic that the wave was only apparent as an inflection on the zinc(II) reduction wave (fig. 7.5). Consequently no voltammetric parameters can be deduced for this composition. On sufficiently cathodic scans a single peak due to zinc stripping was observed (since the peak height was dependant on the switching potential,i.e. on the quantity of zinc deposited).

f) 0.6 mole fraction KCl.

The remarks applied to the 0.5 mole fraction KCl melt above hold for this composition, with the exception that up to three peaks were observed on the reverse scan, the number and relative peak heights depending in a complex fashion on switching potential and scan rate (fig. 7.6). This phenomenon seemed to be a consequence of the codeposition of zinc and gallium metal, since zinc/gallium alloys were found to be produced on bulk electrolysis at these potentials. The three anodic peaks therefore probably represent the oxidation of zinc metal, gallium metal, and a zinc/gallium intermetallic compound. Again this effect was more easily analysed in the $NaCl/ZnCl_2$ melts, as for the disproportionation.

7.2.2 Sodium chloride-zinc chloride melts

The behaviour of gallium(III) chloride in these melts

Figure 7.5. Typical cyclic voltammogram for the reduction of gallium(III) (0.06M) in 0.50 mole fraction KCl-$ZnCl_2$ at 400°C

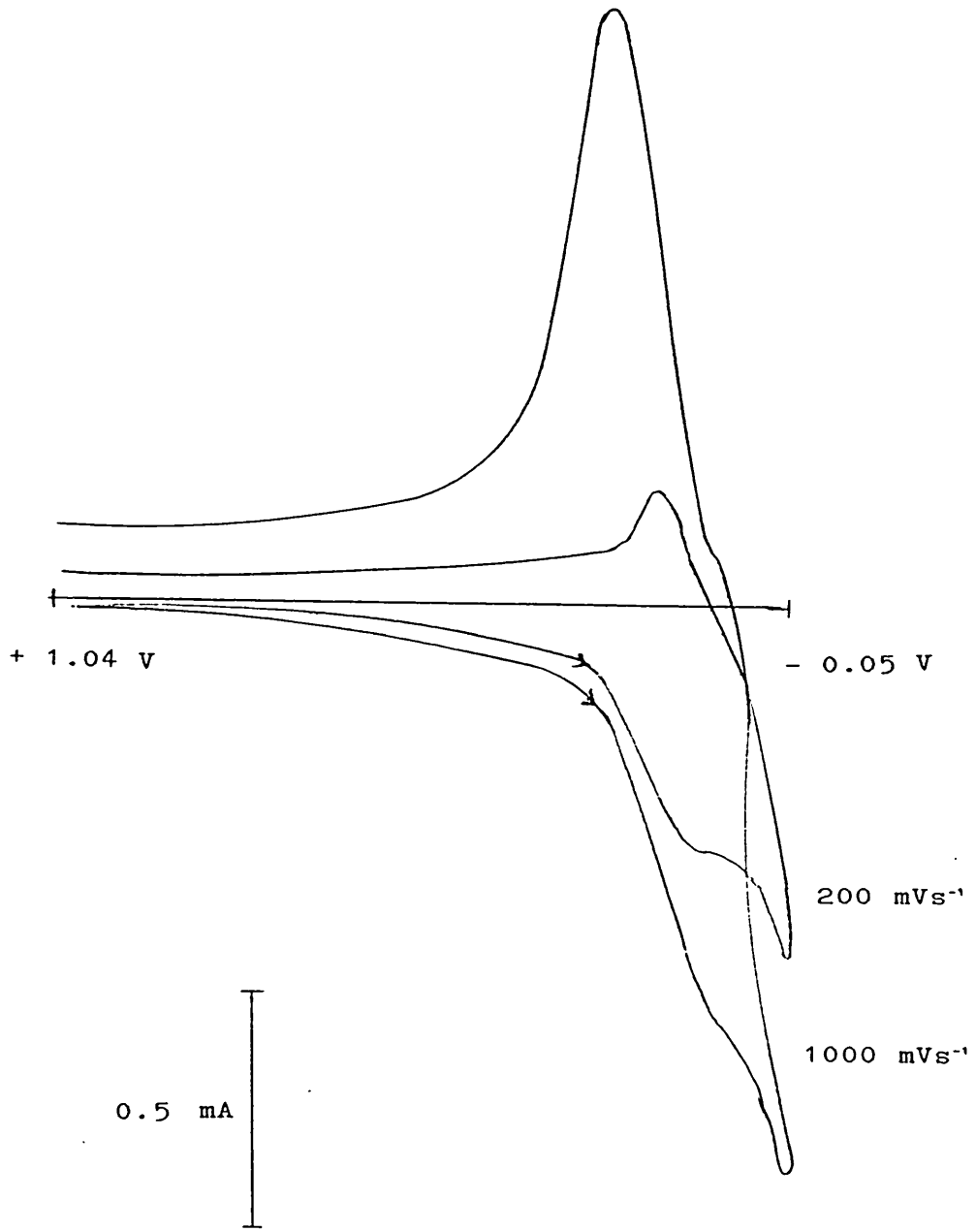
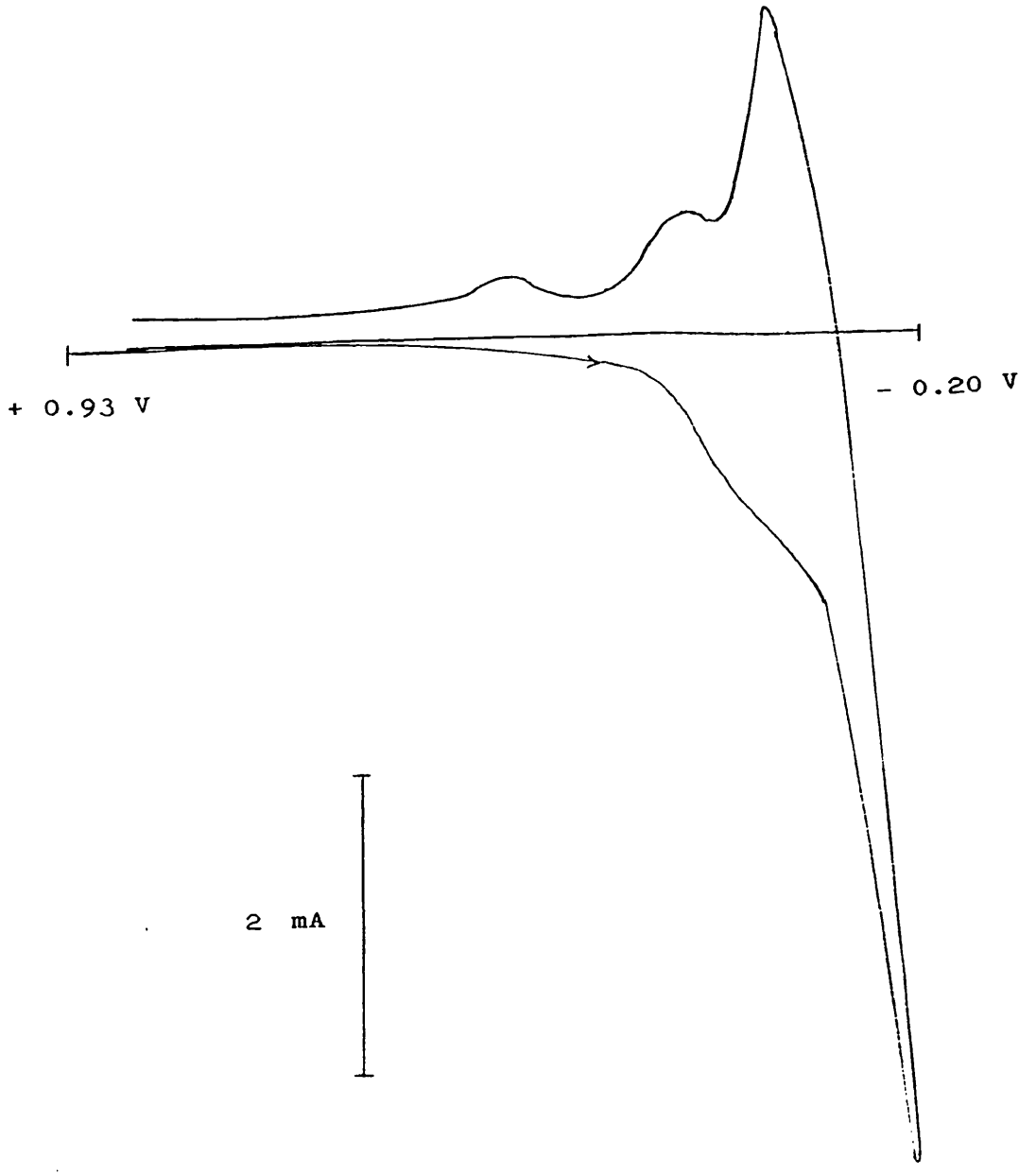


Figure 7.6. Typical cyclic voltammogram for the reduction of gallium(III) (0.06M) in 0.60 mole fraction KCl-$ZnCl_2$ at 400°C

Working electrode: vitreous carbon
Reference electrode: platinum wire (potential estimated relative to onset of zinc deposition)
Scan rate: 200 mVs^{-1}



was studied in the 0.4-0.6 mole fraction NaCl composition range. Since for a given composition, this system is more acidic relative to the KCl-containing melt, it was expected that some evidence of this would be found voltammetrically in the supression of the gallium(I) disproportionation.

a) 0.4 mole fraction NaCl.

At this composition, the voltammograms showed little obvious evidence of disproportionation (fig.7.7); however, the peak current ratio values given in table 7.5 for a 0.13M solution are significantly less than one, and also a cathodic shift with increasing scan rate could be seen for the cathodic peak, while the anodic peak showed initially an anodic shift, but then shifted cathodically at higher ν. These results may be compared with those obtained in the corresponding KCl-containing melt, where clear evidence of disproportionation was apparent at lower scan rates, and at a lower concentration of gallium(I), which would tend to supress the rate of disproportionation.

b) 0.5 mole fraction NaCl.

In this melt, and a 0.11M gallium(III) concentration, the sigmoidal shape of the voltammograms at scan rates less than 50 mVs^{-1} can be clearly seen (fig. 7.8, table 7.6). The melt basicity is evidently now sufficient to cause disproportionation, and the voltammograms resemble those obtained with an 0.4 mole fraction melt. This may be quantified by noting that the zinc chloride activity in the sodium chloride mixture is 0.27, comparable with 0.32 for the potassium chloride mixture (chapter 4).

Figure 7.7. Typical cyclic voltammograms for the reduction of gallium(III) (0.13M) in 0.40 mole fraction NaCl-$ZnCl_2$ at 400°C

Working electrode: vitreous carbon
Reference electrode: platinum wire (potentials estimated relative to onset of zinc deposition)

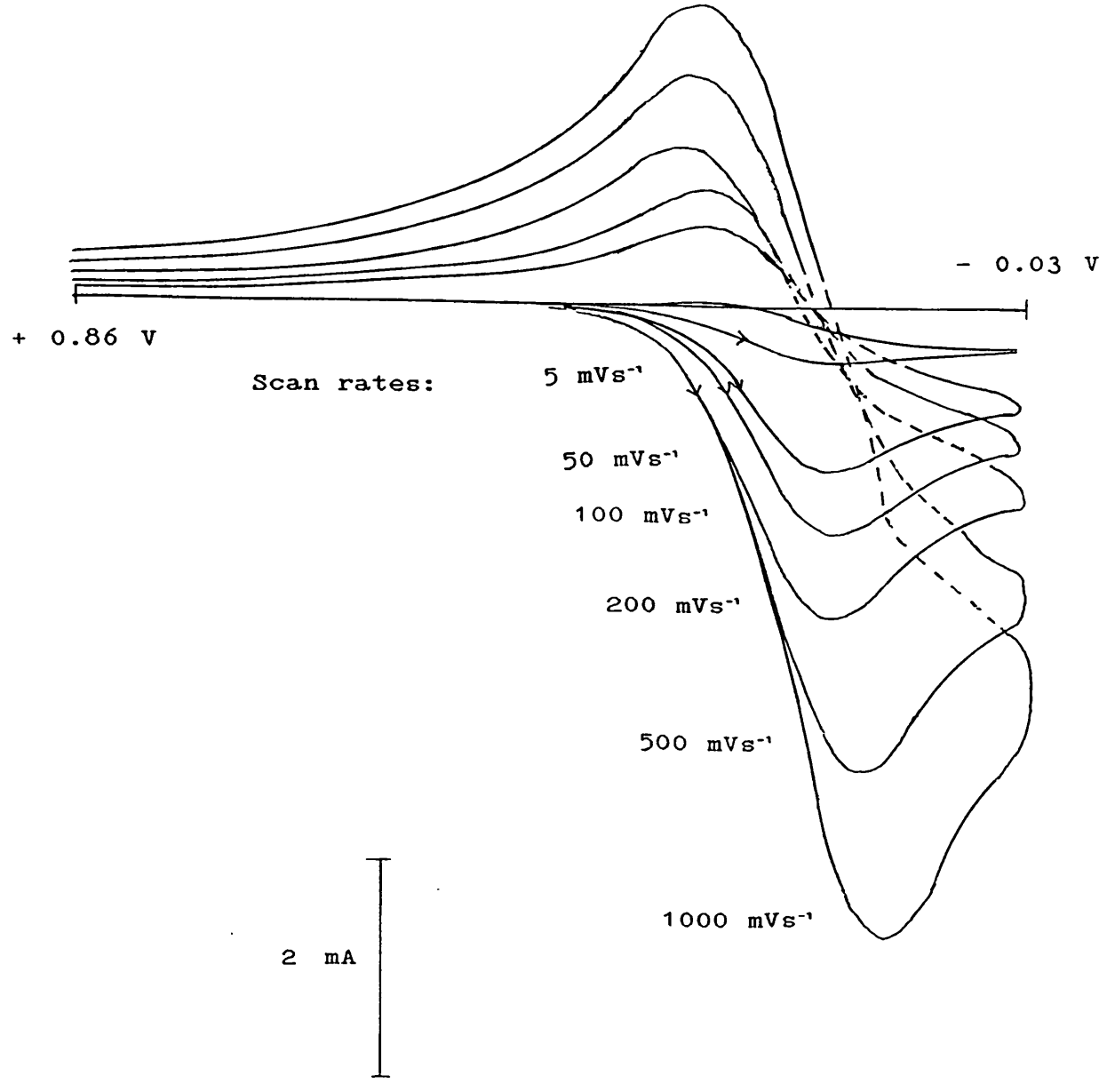


Table 7.5. Voltammetric Parameters for 0.13M gallium(III) in 40/60 mole p.c. NaCl/$ZnCl_2$ at 400°C

Scan rate/ mVs^{-1}	I_{pa}/I_{pc}	ΔE_p/ mV	$I_{pc}/\nu^{1/2}$/ $mA/(Vs^{-1})^{1/2}$
1000	0.92	165	5.81
500	0.92	147	6.10
200	0.92	136	6.43
100	0.90	118	6.72
50	0.91	103	6.70
5	0.59	83	7.51
	$E_{pc}-E_{pc/2}$/mV	E_{pc}/V	
1000	94	0.147	
500	93	0.165	
200	94	0.195	
100	83	0.195	
50	81	0.200	
5	71	0.209	

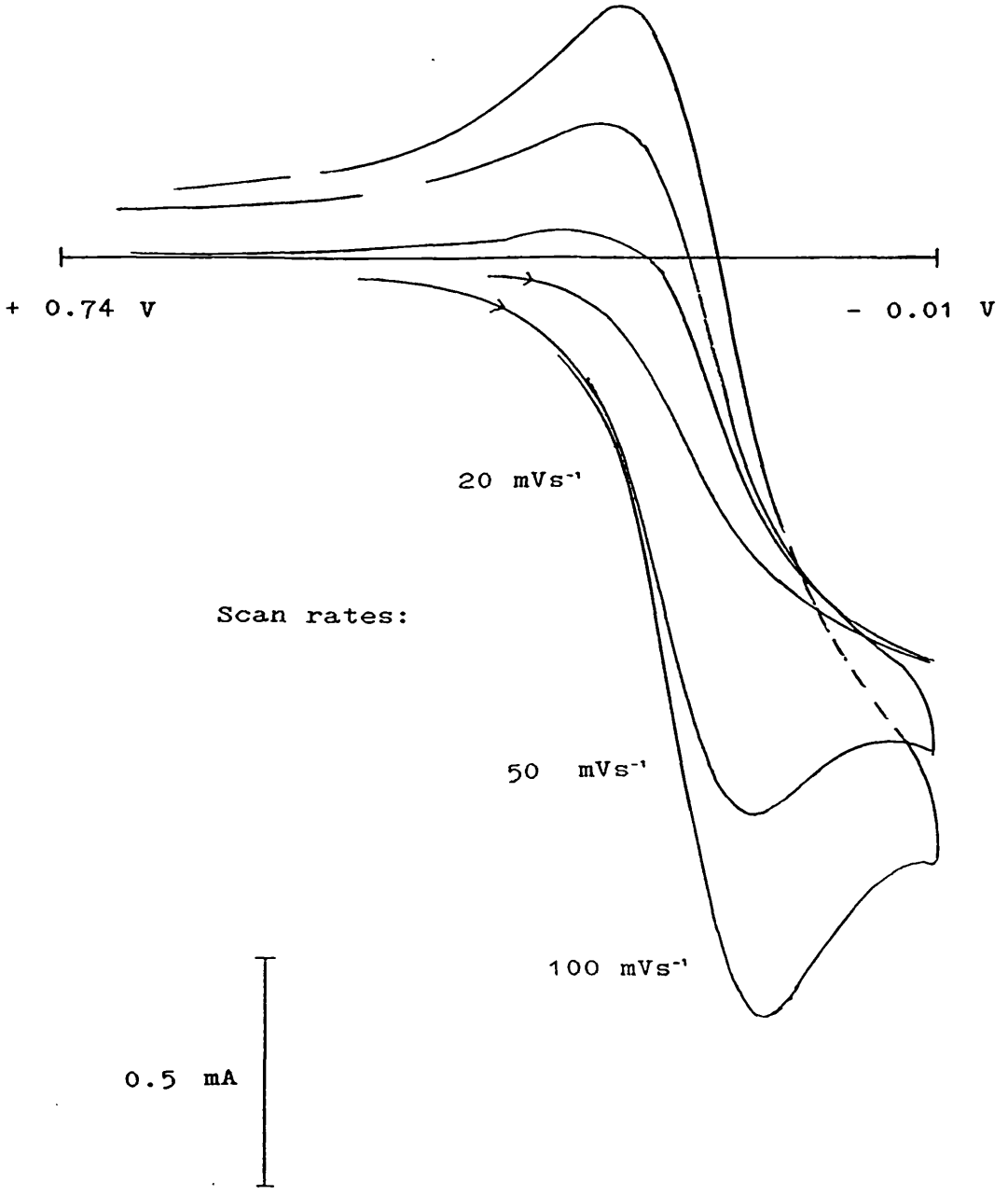
Table 7.6. Voltammetric Parameters for 0.11M gallium(III) in 50/50 mole p.c. NaCl/$ZnCl_2$ at 405°C

Scan rate/ mVs^{-1}	I_{pa}/I_{pc}	ΔE_p/ mV	$I_{pc}/\nu^{1/2}$/ $mA/(Vs^{-1})^{1/2}$
500	0.91	143	4.35
200	0.85	121	4.86
100	0.80	118	5.29
50	0.75	115	5.52
20	0.74	139	6.41
5	0.75	a	10.16
	$E_{pc}-E_{pc/2}$/mV	E_{pc}/V	
500	113	0.133	
200	85	0.147	
100	83	0.153	
50	84	0.159	
20	95	0.153	
5	a	a	

a. These values are uncertain due to sigmoidal shape of voltammogram.

Figure 7.8. Typical cyclic voltammograms for the reduction of gallium(III) (0.11M) in 0.50 mole fraction NaCl-$ZnCl_2$ at 400°C

Working electrode: vitreous carbon
Reference electrode: platinum wire (potentials estimated relative to onset of zinc deposition)



c) 0.6 mole fraction NaCl.

At this composition (but not for 0.55 mole fraction NaCl) the voltammograms began to show additional waves if the sweep was sufficiently cathodic so as to include the zinc deposition wave (fig. 7.9). The effect was best observed at low scan rates, e.g. 20 mVs^{-1}. The gallium(III) reduction wave (A in fig.7.9) was then sigmoidal, and no additional waves appeared if the deposition wave was not included (fig. 7.10). However, if scanning was sufficiently cathodic so that deposition was just apparent, then a narrow peak (F) appeared on the anodic side of the broader wave (E) ascribed to oxidation of soluble Ga^{+}. For reasons detailed below, it is believed that gallium (or a gallium/zinc alloy) is initially deposited rather than pure metallic zinc. It is then possible that the narrow peak F may represent the oxidation of *adsorbed* gallium(I) to soluble gallium(III). A similar phenomenon has been observed for the oxidation of chromium metal to chromium(II) in chloroaluminate melts (104).

Scanning to slightly more cathodic potentials, an inflection (B) can just be discerned on the main zinc deposition wave, and the corresponding stripping wave (C) is well-defined (fig.7.11). This was probably due to gallium metal deposition and stripping.

At yet more cathodic potentials, another stripping peak (D) was manifested, and the gallium stripping peak C split into two (fig. 7.9). The peak D was assigned to zinc stripping, since the height increased indefinitely as the

Figure 7.9. Typical cyclic voltammogram for the reduction of gallium(III) (0.06M) in 0.60 mole fraction NaCl-$ZnCl_2$ at 400°C

Working electrode: vitreous carbon
Reference electrode: platinum wire (potentials estimated relative to onset of zinc deposition)
Scan rate: 20 mVs^{-1}

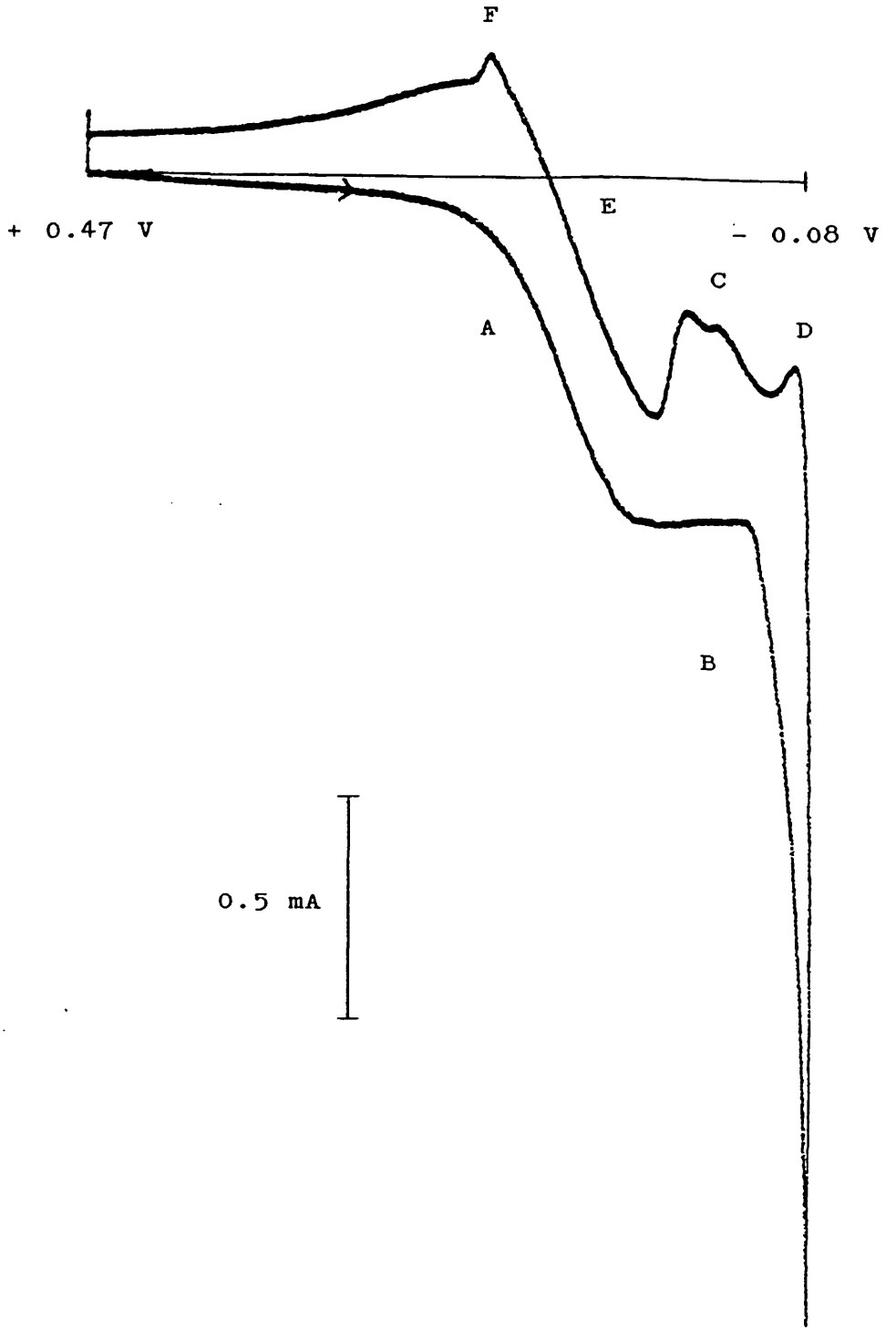


Figure 7.10. Cyclic voltammogram for the reduction of gallium(III) (0.06M) in 0.60 mole fraction NaCl-$ZnCl_2$ at 400°C

Working electrode: vitreous carbon
Reference electrode: platinum wire (potentials estimated relative to onset of zinc deposition)
Scan rate : 20 mVs^{-1}

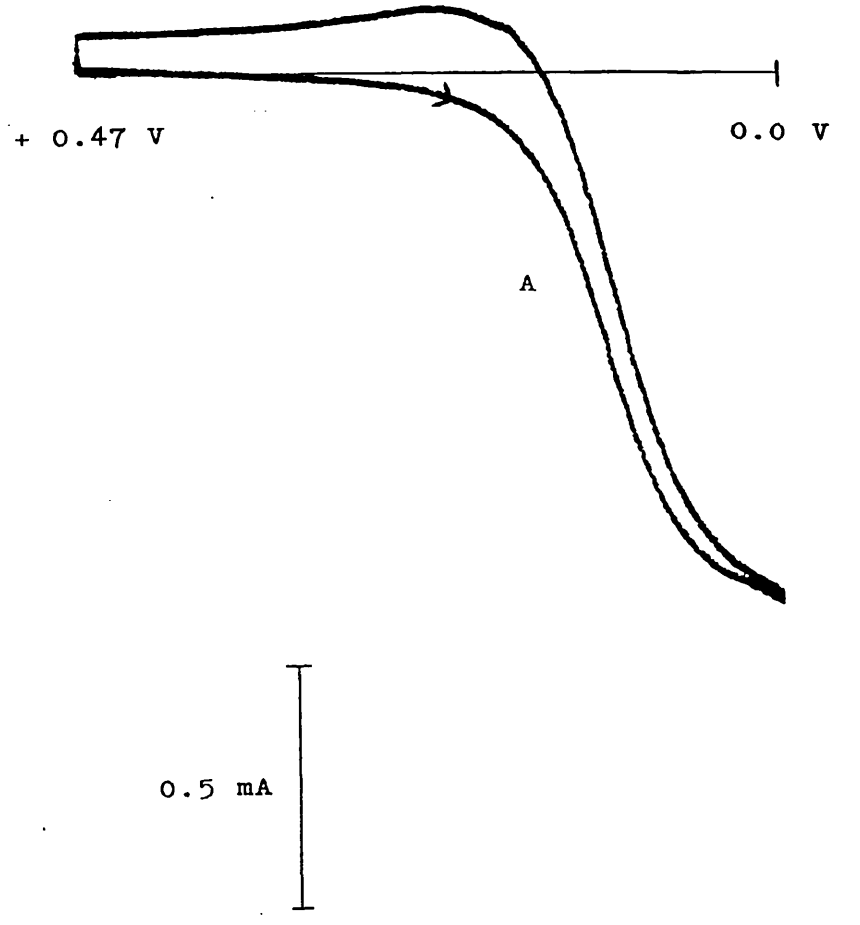
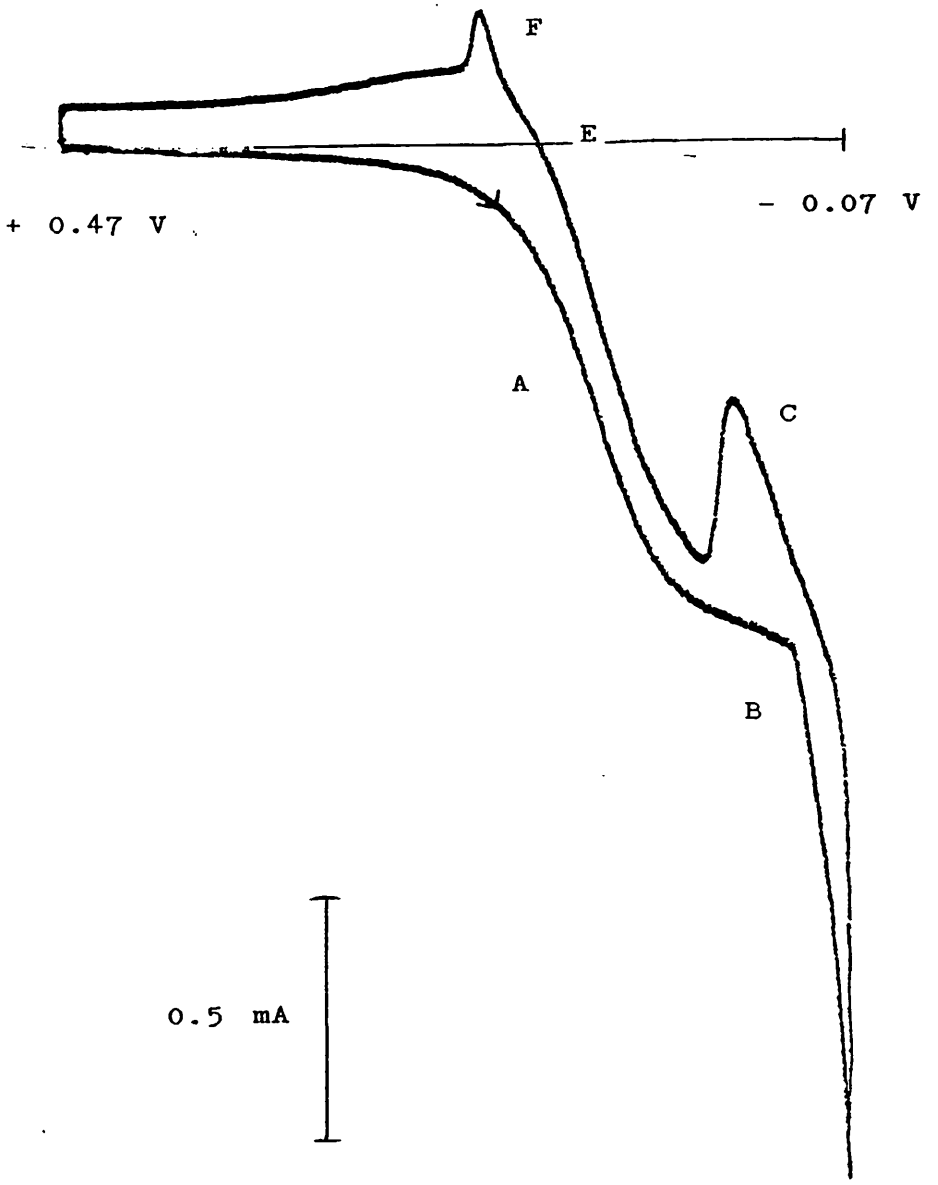


Figure 7.11. Cyclic voltammogram for the reduction of gallium(III) (0.06M) in 0.60 mole fraction NaCl-$ZnCl_2$ at 400°C

Working electrode: vitreous carbon
Reference electrode: platinum wire (potential estimated relative to onset of zinc deposition)
Scan rate: 20 mVs^{-1}



scan was made more cathodic, and more zinc deposited. The splitting of peak C probably indicates the oxidation of a zinc/gallium intermetallic compound formed at the interface between the two metals, followed by the oxidation of metallic gallium.

To confirm that deposition of metallic gallium did indeed take place, a constant potential electrolysis was performed, the potential being held about 20 mV cathodic of the point where deposition started. A 17 per cent weight Ga-Zn alloy metallic bead was recovered (analysis by A.A.).

The reduction and re-oxidation of gallium(III) might therefore be described by the following sequence:

Cathodic sweep:

$$Ga^{3+} + 2e^- \longrightarrow Ga^{+} \qquad (7.3)$$

$$3Ga^{+} \rightleftharpoons Ga^{3+} + 2Ga \qquad (7.4)$$

$$Ga^{+} + e^- \longrightarrow Ga \qquad (7.5)$$

$$Ga + Zn \longrightarrow \text{"GaZn" (intermetallic)} \qquad (7.6)$$

Anodic sweep:

$$\text{"GaZn"} \longrightarrow Ga + Zn^{2+} \qquad (7.7)$$

$$Ga \longrightarrow Ga^{+}(\text{adsorbed}) + Ga^{+}(\text{soluble}) + e^- \qquad (7.8)$$

$$3Ga^{+}(\text{soluble}) \rightleftharpoons Ga^{3+} + 2Ga \qquad (7.9)$$

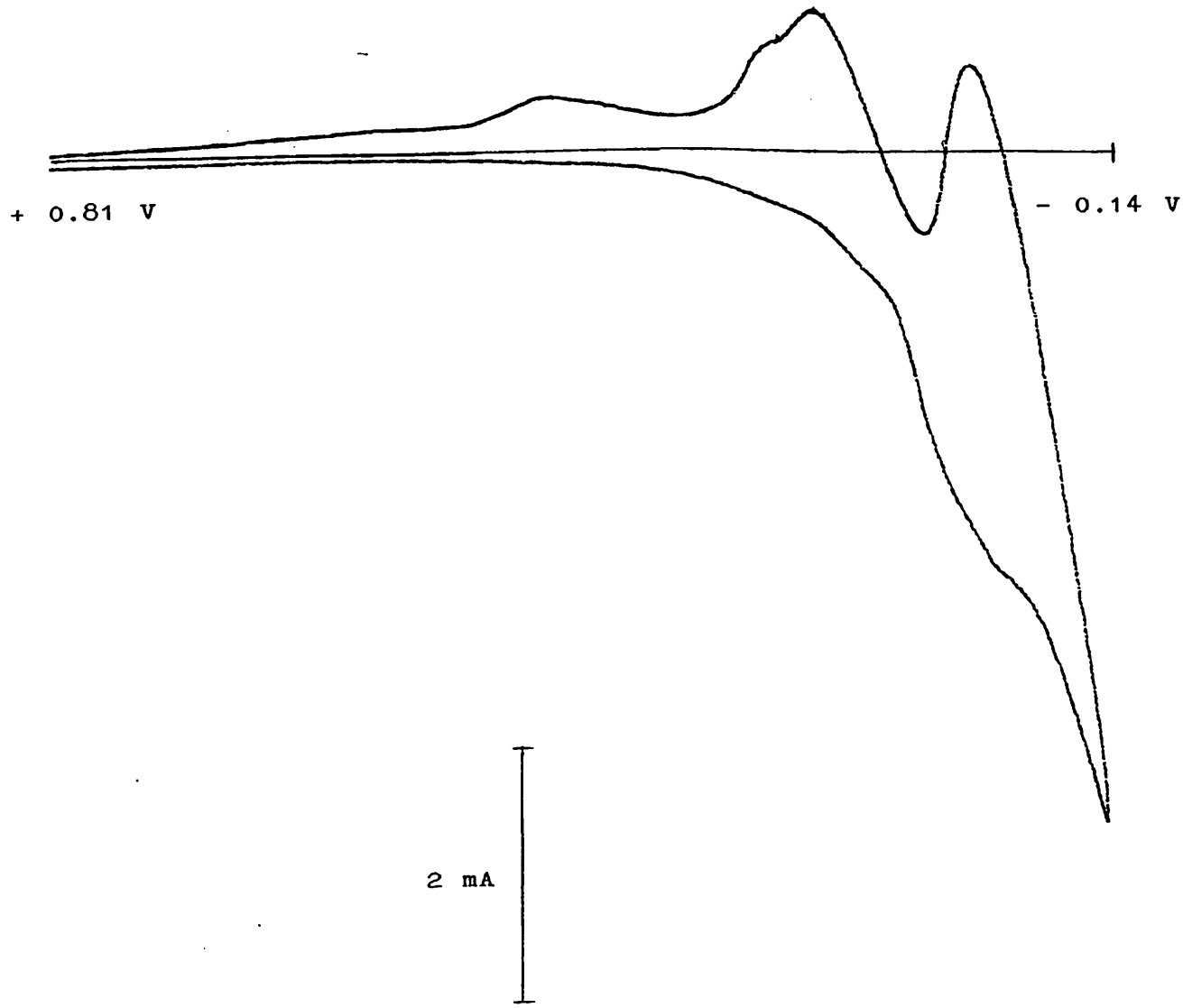
$$Ga^{+}(\text{soluble}) \longrightarrow Ga^{3+} + 2e^- \qquad (7.10)$$

$$Ga^{+}(\text{adsorbed}) \longrightarrow Ga^{3+} + 2e^- \qquad (7.11)$$

With more concentrated solutions of gallium(III) it was found that the reduction wave shifted cathodically and was only observable as an inflection on the zinc deposition wave (fig 7.12).

Figure 7.12. Typical cyclic voltammogram for the reduction of gallium(III) (0.12M) in 0.60 mole fraction NaCl-$ZnCl_2$ at 400°C

Working electrode: vitreous carbon
Reference electrode: platinum wire (potential estimated relative to onset of zinc deposition)
Scan rate: 20 mVs^{-1}



It is interesting to note that the voltammetric behaviour in the acidity region where disproportionation is postulated to occur shows characteristics of the "catalytic" mechanism (77,78), that is, the reaction sequence:

$$O + ne^- \rightleftharpoons R \qquad (7.12)$$

$$R + Z \longrightarrow O \qquad \text{(rate constant } k_f\text{)} \qquad (7.13)$$

For the present purposes, O corresponds to Ga^{3+}; R is Ga^{+}; Z is the species which reacts to regenerate O, i.e. free chloride ion. Eqn. (7.13) is assumed to be first order with respect to R. Theoretical analysis indicates that a "limiting current" will be obtained at sufficiently cathodic potentials, regardless of scan rate, and that at low scan rates, the voltammograms will be sigmoidal, as in the present work. Thus if the net reaction is the regeneration of Ga^{3+}, and the rate-determining step is first order with respect to the latter species, it would be feasible to calculate pseudo-first order rate constants for the regeneration, since a simple relation exists between the "limiting current" and the rate constant.

This type of disproportionation reaction has apparently not been analysed theoretically for a cyclic voltammetric experiment, and indeed only one example of such behaviour attributable to a change in melt acidity appears to be extant. Thus Taoumi (108) reported that indium(I) decomposed in NaCl/KCl melt at 700°C:

$$3In(I) \rightleftharpoons In(III) + 2In \qquad (7.14)$$

In a NaCl/KCl/$ZnCl_2$ (0.38 mole fraction zinc chloride) melt at 550°C, however, In(I) was stabilised.

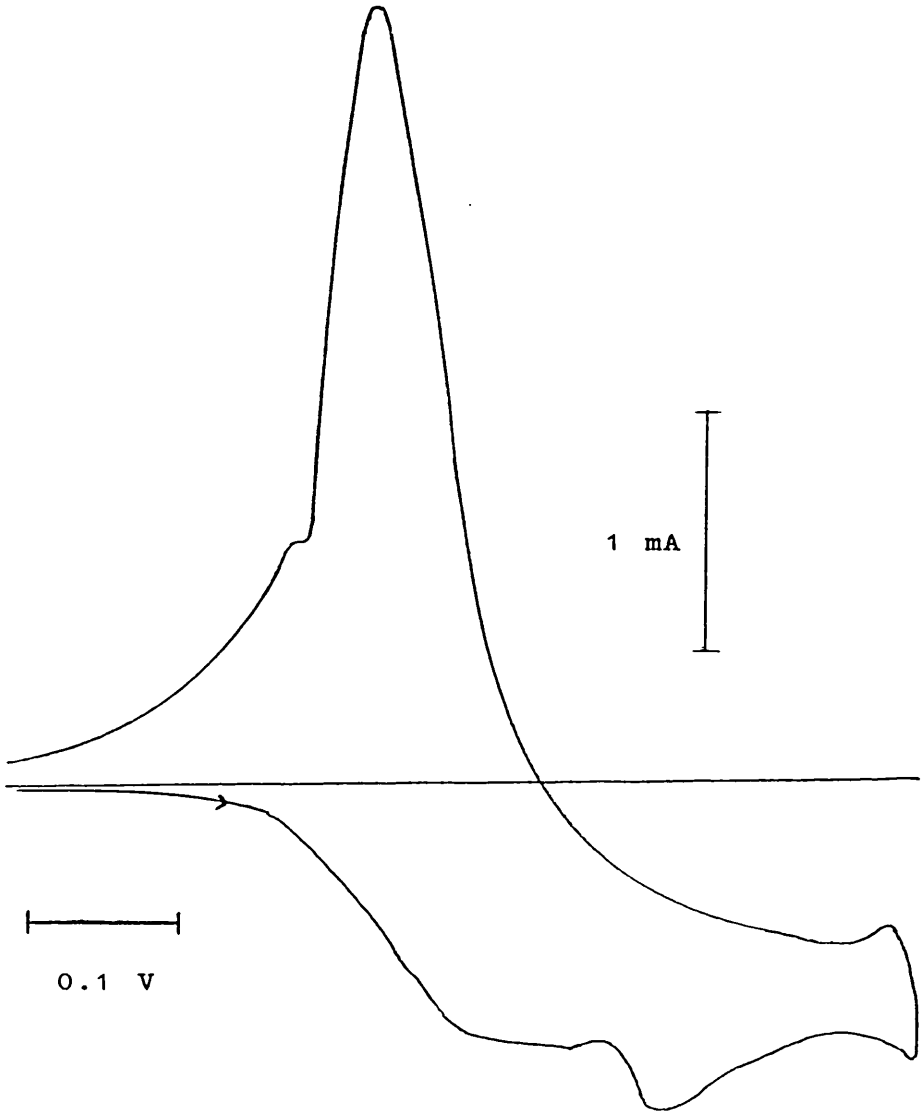
7.2.3 Lithium chloride-potassium chloride eutectic

It was of interest to examine the voltammetric reduction of a gallium(III) solution (0.07M) in this relatively basic melt, since this particular experiment does not seem to have been performed. The solution also contained 0.07M zinc chloride, so that the reduction potentials could be directly compared.

The gallium(III) reduction wave was clearly resolvable into two waves (fig 7.13). The first wave was consistant with a two-electron reversible reduction to soluble gallium(I) (table 7.7), while the second, superimposed on the descending section of the first, showed a relatively sharp increase in current, consistant with a deposition reaction. This wave however shifted cathodically with increasing scan rate, indicating irreversibility. A sharp stripping peak was observed on the return sweep, with an inflection possibly due to intermediate formation of Ga^{+}. Clearly the reduction of gallium(III) proceeds in in two stages via soluble Ga^{+} to gallium metal.

The reduction of zinc(II) began at potentials 0.43 V more cathodic than the Ga^{3+}/Ga^{+} half-wave potentials, which compares with 0.43 V for the difference in equilibrium potentials of Ga^{3+}/Ga° and Zn^{2+}/Zn° at 450°C, as tabulated by Plambeck (128). However, the equilibrium potential for Ga^{3+}/Ga^{+} has not been measured, since the equilibrium constant for Ga^{+} disproportionation (eqn. 7.1) can be estimated as 5×10^{6} (128), indicating that a negligable equilibrium concentration of Ga^{+} would be present in a solution

Figure 7.13. Typical cyclic voltammogram for the reduction of gallium(III) (0.07M) in lithium chloride-potassium chloride eutectic at 400°C



Working electrode: vitreous carbon
Reference electrode: platinum wire
Scan rate: 500 mVs^{-1}

Table 7.7. Voltammetric Parameters for 0.07M gallium(III) in LiCl/KCl eutectic at 400°C

a) First reduction wave.

Scan rate/ mVs^{-1}	$E_{pc}-E_{pc/2}$/mV	$I_{pc}/\nu^{1/2}$/ $mA/(Vs^{-1})^{1/2}$
1000	89	1.56
500	89	1.52
200	91	1.50
100	89	1.53
50	89	1.61
20	85	1.77
5	85	2.21

b) Second reduction wave.

1000	-	1.81
500	-	1.86
200	-	1.96
100	-	2.03
50	-	2.10
20	-	2.32
5	-	2.21

	Difference in peak potentials/mV
1000	136
500	105
200	92
100	87
50	81
20	76
5	76

containing gallium(III) and gallium metal.

It is thus rather surprising in the present work to find no voltammetric evidence for disproportionation, as was found for the more basic zinc chloride-alkali chloride melts with similar gallium(III) concentrations. Evidently, for reasons which are not entirely clear, the rate constant for Ga^{+} disproportionation in the LiCl/KCl melt is low enough to allow this oxidation state to be stable under the conditions of the voltammetric experiment.

7.3 Conclusions and Further work

The voltammetric results clearly show that gallium(III) may be reduced in a reversible two-electron transfer to gallium(I), stable in relatively acidic melts, but reacting to regenerate gallium(III) in more basic melts, most likely via the disproportionation reaction 7.1.

In the present work, substitution of the relatively acidic sodium cation for potassium appeared to significantly stabilise the gallium(I) state, and also increase the separation between the gallium(III) reduction potential and the cathodic melt limit, in melts of comparable alkali chloride mole fraction. At the 0.6 alkali chloride mole fraction compositions, gallium metal could be co-deposited with zinc at sufficiently cathodic potentials, and the form of the stripping wave suggests the production of a zinc/gallium intermetallic compound.

Unfortunatly in the present work, the voltammetric waves were partially obscured in the more basic melts by the proximity of the zinc deposition wave; though the

results suggest that a greater separation could be achieved by the use of a mixture containing a relatively acidic cation such as Li^+ or Ca^{2+}. It might then be possible to analyse the mechanism of Ga^+ disproportionation by varying the gallium(III) concentration and melt acidity, and to calculate rate constants for the reaction.

Conversely, from the point of view of the "pyroredox" process for separating plutonium and gallium (see chapter one), a highly basic melt (i.e. high proportion of alkali chloride, large alkali metal cation) is needed to ensure that gallium metal is not oxidised into the salt phase with the plutonium, since the results described above indicate that gallium metal is thermodynamically unstable with respect to gallium(I) in contact with the more acidic melts.

CHAPTER EIGHT

CYCLIC VOLTAMMETRY OF TITANIUM COMPOUNDS IN ZINC CHLORIDE-ALKALI CHLORIDE MELTS

8.1 Procedure and General observations

Solutions produced by the reaction of titanium metal or titanium(III) chloride with the melts were characterised by cyclic voltammetry. The components were mixed in the drybox in the electrochemical cell, and the cell tranferred to the furnace at the appropriate temperature, as detailed in chapter 3.

The study of the titanium solutions was complicated by a number of factors; firstly, the reaction product of titanium metal, shown to be titanium(III) chloride, was found to have limited solubility in the relatively acidic melts, a finding also applicable to the commercial titanium(III) chloride. Secondly, the melt solutions appeared to decompose on solidification and/or reheating as demonstrated by the decrease in voltammetric peak height of reheated samples. Thirdly, the solutions produced by reaction of titanium metal were never clear, but always black and opaque and did not clear on standing, apparently due to the formation of a fine suspension. Fourthly, a white or pale yellow iridescent film was found to form on the cell walls above the melt, after a solution had been contained for several hours. This was believed to be due to the continuous evolution of volatile titanium tetrachloride, produced by the disproportionation of titanium(III) chloride (118), and subsequent reaction to form the oxide at the cell walls. In this case, the other

disproportionation product, involatile titanium(II) chloride, would presumably have been produced in the melt, possibly accounting for the black suspension noted above (see also below).

As noted above, the reaction of titanium metal with the zinc chloride melts invariably produced the black suspensions, which, on filtering through a Pyrex frit, produced colourless solutions containing soluble titanium. Attempts to obtain "d"-spacings for the black compound by X-ray diffraction of the powdered reaction mixture with pure zinc chloride were unsuccessful, only the diffraction lines for the latter compound being observed, perhaps indicating the amorphous nature of the reaction products.

Dissolution of the above melt mixture in water caused the evolution of hydrogen gas, and a grey suspension with reducing properties was formed (towards, for example, $KMnO_4$). This reacted in air to form yellow solutions, presumably of oxychlorotitanate(IV) salts. However, dissolution of the melt in ethoxyethane produced a precipitate consisting apparently entirely of shiny reddish-violet crystals. After washing with fresh ethoxyethane, chemical analysis indicated a Ti:Cl ratio of 1:3, suggesting that the product was titanium(III) chloride. This observation was consistant with the voltammetric results (below) and so the reaction of titanium metal with zinc chloride may be written:

$$2Ti + 3ZnCl_2 \longrightarrow 2TiCl_3 + 3Zn \qquad (8.1)$$

Similar results were obtained with the alkali chloride mixtures.

The X-ray diffraction pattern of the violet crystals could not be obtained, due to hydrolysis of the extremely hygroscopic substance in the chamber of the diffractometer, despite using a sample holder sealed with polymer film.

It is interesting to note that anodisation of titanium metal in LiCl/KCl eutectic or addition of solid $TiCl_2$ is reported to produce a similar black suspension (119). The substance is evidently an insoluble titanium(II) compound, possibly TiO or $TiCl_2$, but due to the reactive nature it has not been characterised. The involvement of oxygen in the titanium systems is difficult to discount, due to the hygroscopic and air-sensitive nature of the lower oxidation states of titanium.

In contrast to the behaviour of titanium metal, titanium(III) chloride reacted to form clear blue-green solutions, sometimes with a violet precipitate presumably of unreacted $TiCl_3$, and below this a layer of greyish-white TiO_2, the latter substance being identified by X-ray diffraction after dissolving the quenched melt in water.

No simple explanation can be given for the difference in solution colour between titanium metal and titanium(III) chloride, since the voltammetric results did not distinguish between the soluble species present in the two cases. It is possible that electro-inactive oxychloro-species exist in the $TiCl_3$-containing melt, formed by partial hydrolysis of the very hygroscopic compound.

The titanium concentrations of solidified melts were

determined by conventional "wet" chemical methods after dissolution of the solid in hydrofluoric acid.

8.2 Cyclic voltammetry of titanium compounds- Results and discussion

8.2.1 Titanium metal in potassium chloride-zinc chloride

a) Pure zinc chloride.

At 350°c, an 0.60M solution showed only one oxidation wave within the electrochemical window of the melt (fig.8.1). The peak widths and peak separations increased with scan rate, probably due to uncompensated melt resistance, but at relatively low scan rates, the voltammetric parameters were consistant with a one-electron reversible transfer (table 8.1). For example, calculated half-peak width at 350°C, 0.13V, found, 0.14V. The peak current ratios were generally in the range 0.95-1.00, though the $i_{pa}/\nu^{1/2}$ values were rather erratic. This was probably due to the appearence of "noise" at the slower scan rates, on the anodic side of the oxidation wave. The maximum "amplitude" was, however, only about 5 per cent of the peak height.

On heating to 400°C, a significant change was observed, the peak current ratios being significantly less than one up to 1 Vs^{-1} scan rate, and decreasing with decreasing scan rate. Also the noise "amplitude" increased (table 8.2, fig. 8.2). These effects were even further enhanced on heating to 440°C, the noise "amplitude" being up to 50 per cent of the peak height, and the cathodic peaks virtually non-existant (table 8.3).

The behaviour of the peak current ratios with scan rate

Figure 8.1. Typical cyclic voltammograms for the oxidation of titanium(III) (0.60M) in pure zinc chloride at 350°C (reaction product of titanium metal)

Working electrode: vitreous carbon
Reference electrode: zinc

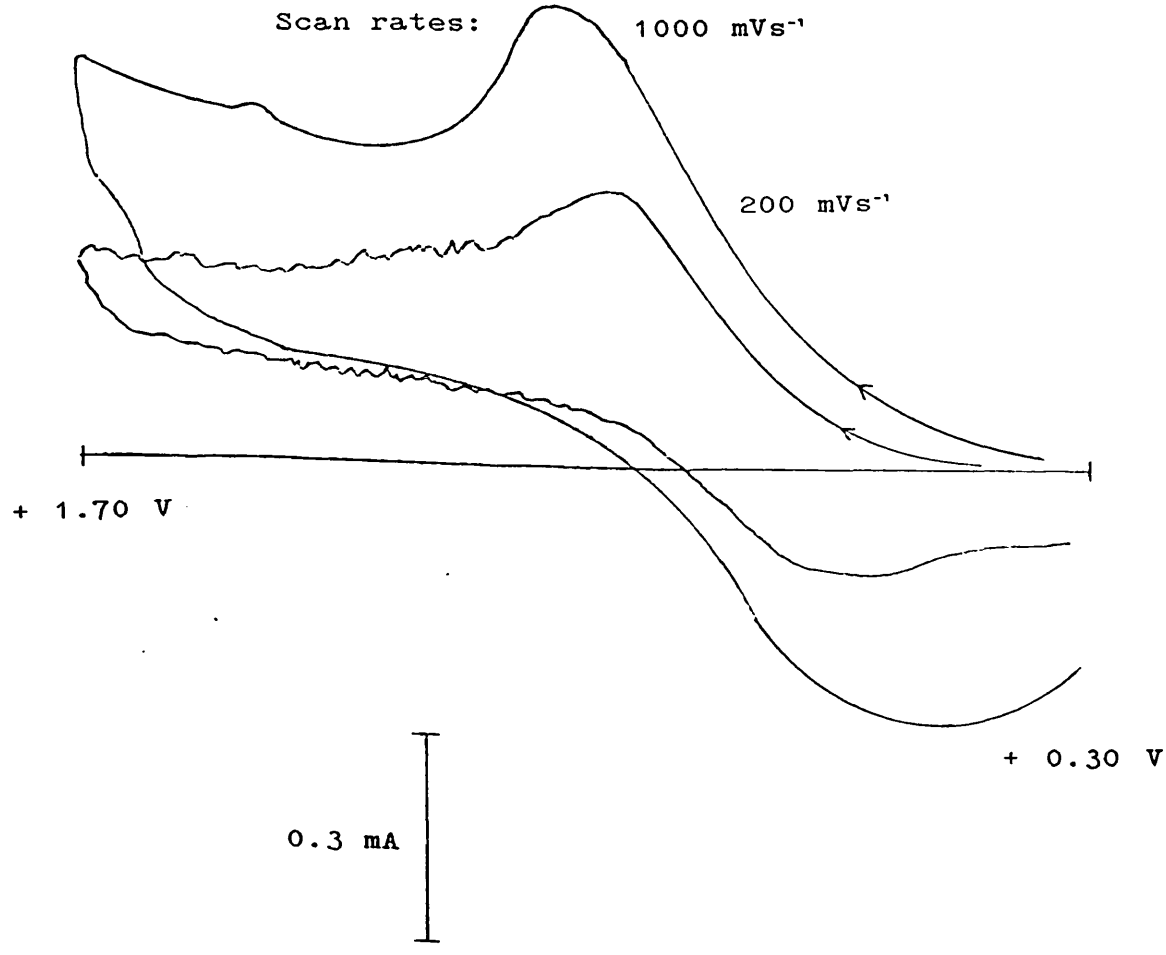


Table 8.1. Voltammetric Parameters for 0.60M titanium(III) in pure zinc chloride 350°C

Scan rate/ mVs^{-1}	I_{pc}/I_{pa}	ΔE_p/ mV	$I_{pa}/\nu^{1/2}$/ $mA/(Vs^{-1})^{1/2}$
2000	0.99	676	0.58
1500	0.95	636	0.63
1000	0.99	579	0.66
500	0.96	475	0.72
200	0.99	344	0.91
100	1.01	244	0.59

	$E_{pa}-E_{pa/2}$/mV	E_{pa}/V
2000	318	1.130
1500	301	1.090
1000	273	1.033
500	221	0.954
200	185	0.931
100	153	0.880

Table 8.2. Voltammetric Parameters for 0.60M titanium(III) in pure zinc chloride at 400°C

Scan rate/ mVs^{-1}	I_{pc}/I_{pa}	ΔE_p/ mV	$I_{pa}/\nu^{1/2}$/ $mA/(Vs^{-1})^{1/2}$
1000	0.76	522	1.41
500	0.74	429	1.37
200	0.69	295	1.35
100	0.63	227	1.32
50	0.63	182	1.33
20	0.63	170	1.40

	$E_{pa}-E_{pa/2}$/mV	E_{pa}/V
1000	238	0.965
500	216	0.897
200	182	0.840
100	159	0.817
50	148	0.806
20	136	0.783

Table 8.3. Voltammetric Parameters for 0.60M titanium(III) in pure zinc chloride at 440°C

Scan rate/ mVs^{-1}	I_{pc}/I_{pa}	ΔE_p/ mV	$I_{pa}/\nu^{1/2}$/ $mA/(Vs^{-1})^{1/2}$
1000	a	a	3.08
500	-	-	3.00
200	-	-	3.07
100	-	-	3.26
	$E_{pa}-E_{pa/2}$/mV	E_{pa}/V	
1000	264	0.956	
500	214	0.864	
200	173	0.793	
100	153	0.773	

a. These values uncertain due to distortion of cathodic peak.

Table 8.4. Voltammetric Parameters for 0.10M titanium(III) in pure zinc chloride at 438°C

Scan rate/ mVs^{-1}	I_{pc}/I_{pa}	ΔE_p/ mV	$I_{pa}/\nu^{1/2}$/ $mA/(Vs^{-1})^{1/2}$
1000	0.92	162	0.62
500	0.86	155	0.60
200	0.77	145	0.58
100	0.67	137	0.62
50	0.65	134	0.57
20	0.61	134	0.65
	$E_{pa}-E_{pa/2}$/mV	E_{pa}/V	
1000	162	0.960	
500	150	0.943	
200	145	0.931	
100	143	0.920	
50	140	0.913	
20	140	0.905	

is, on the face of it, diagnostic of an irreversible chemical reaction following the charge transfer (77,78). However, the "noise" in the voltammetric waves suggests gas evolution due to formation of a volatile titanium(IV) compound (almost certainly $TiCl_4$) since a one-electron oxidation of titanium(III) occurs and thus the decrease in the peak current ratio at lower scan rates probably results from the loss of the oxidation product by volatilisation. A plausible hypothesis was the formation and dissociation of a titanium(IV) complex from an initial titanium(III) complex:

$$TiCl_6^{3-} \longrightarrow TiCl_6^{2-} + e^- \qquad (8.2)$$

$$TiCl_6^{2-} \rightleftharpoons TiCl_4 + 2Cl^- \qquad (8.3)$$

It may be assumed that the equilibrium 8.3 shifts to the right with increasing temperature, as indicated by the increasing amounts of "noise" on the voltammograms. Also, since the formation and growth of gas bubbles undoubtedly involves a nucleation and growth stage, gas evolution ("noise") may not be observed at faster scan rates, as the bubbles will not have time to form.

If a reversible electron transfer is assumed, then at the electrode surface, the concentration ratio of Ti(IV)/Ti(III) will be predictable from the Nernst equation. Thus at some point on the forward sweep, the concentration of $TiCl_4$ should exceed the saturated value and tend to volatilise from the solution, subject to the kinetic limitations indicated above. The effect is analogous to the precipitation of chromium(III) chloride at a critical potential from chromium(II) solutions, as

discussed in chapter six. It is evident that the concentration of $TiCl_4$ at a given potential will increase with the initial titanium(III) concentration. Thus sufficiently dilute solutions should not exhibit "noise" due to gas evolution.

As evidence for the latter prediction, a more dilute solution of titanium(III) (concentration: 0.10M) was examined. At 438°C, this system showed no sign of gas evolution and conformed approximately to the behaviour expected for a reversible system, except that the peak current ratios were significantly less than one, even at 1 Vs^{-1} scan rate, and decreased with decreasing scan rate (table 8.4). Thus it appeared that the oxidation product could be lost even when the voltammograms showed no indication of bubble formation. However, the mechanism cannot be described as a first-order chemical reaction following the electron transfer. This was demonstrated below with solutions in more basic melts, where the effects of uncompensated melt resistance were minimised.

b) 0.1 mol fraction KCl.

A 1.0M solution of titanium(III) in this melt at 412°C showed voltammograms in which the cathodic peak was insignificant compared to the anodic, even at 1 Vs^{-1} (fig.8.3). At lower scan rates "noise" was apparent. Again the anodic half-peak widths (table 8.5) were consistant with a one-electron transfer, though broadening and an anodic peak potential shift were observed at higher scan rates, again probably due to resistance effects.

Figure 8.2. Typical cyclic voltammograms for the oxidation of titanium(III) (0.60M) in pure zinc chloride at 400°C (reaction product of titanium metal)

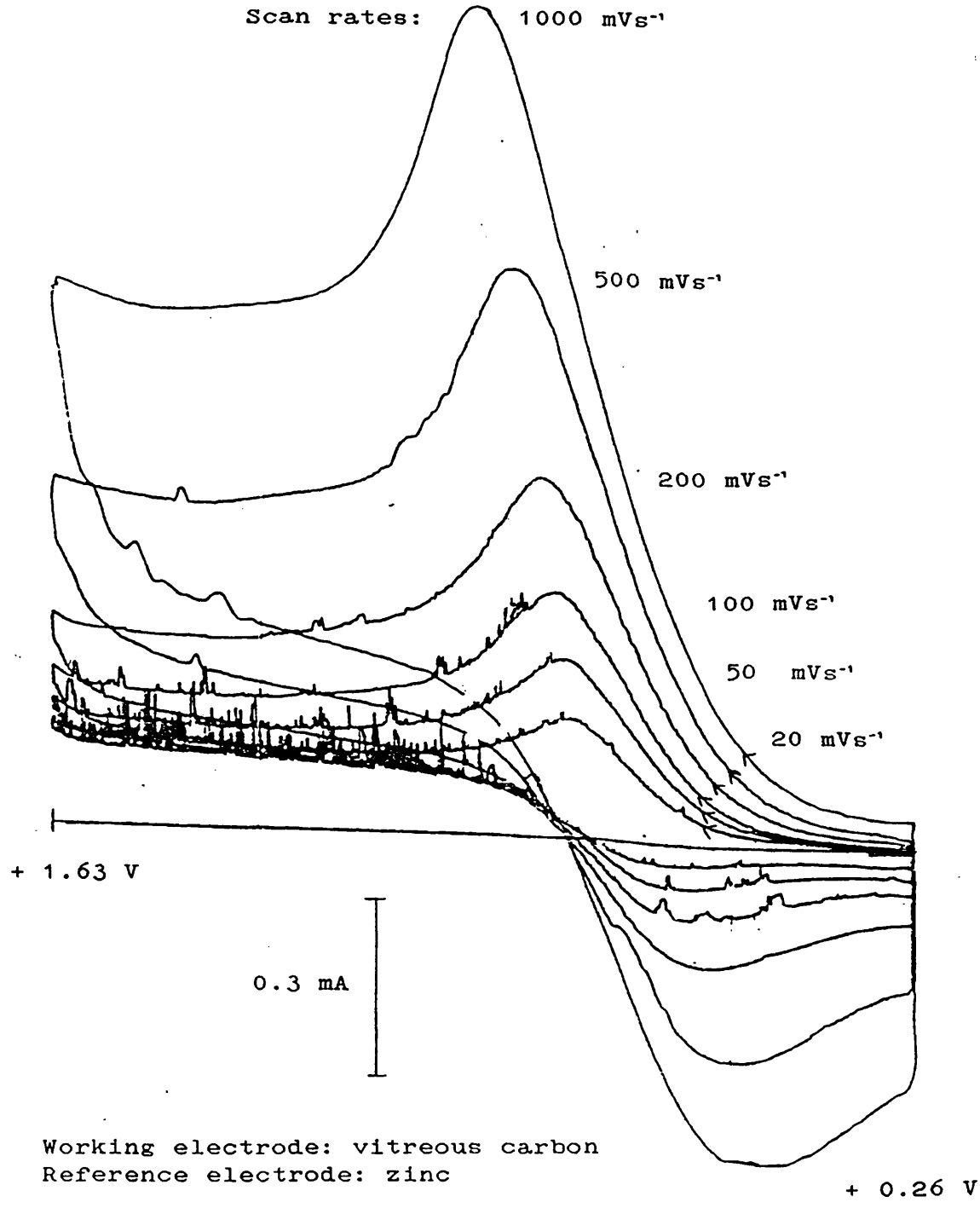


Figure 8.3. Typical cyclic voltammograms for the oxidation of titanium(III) (1.00M) in 0.10 mole fraction KCl-$ZnCl_2$ at 412°C (reaction product of titanium metal)

Working electrode: vitreous carbon
Reference electrode: zinc

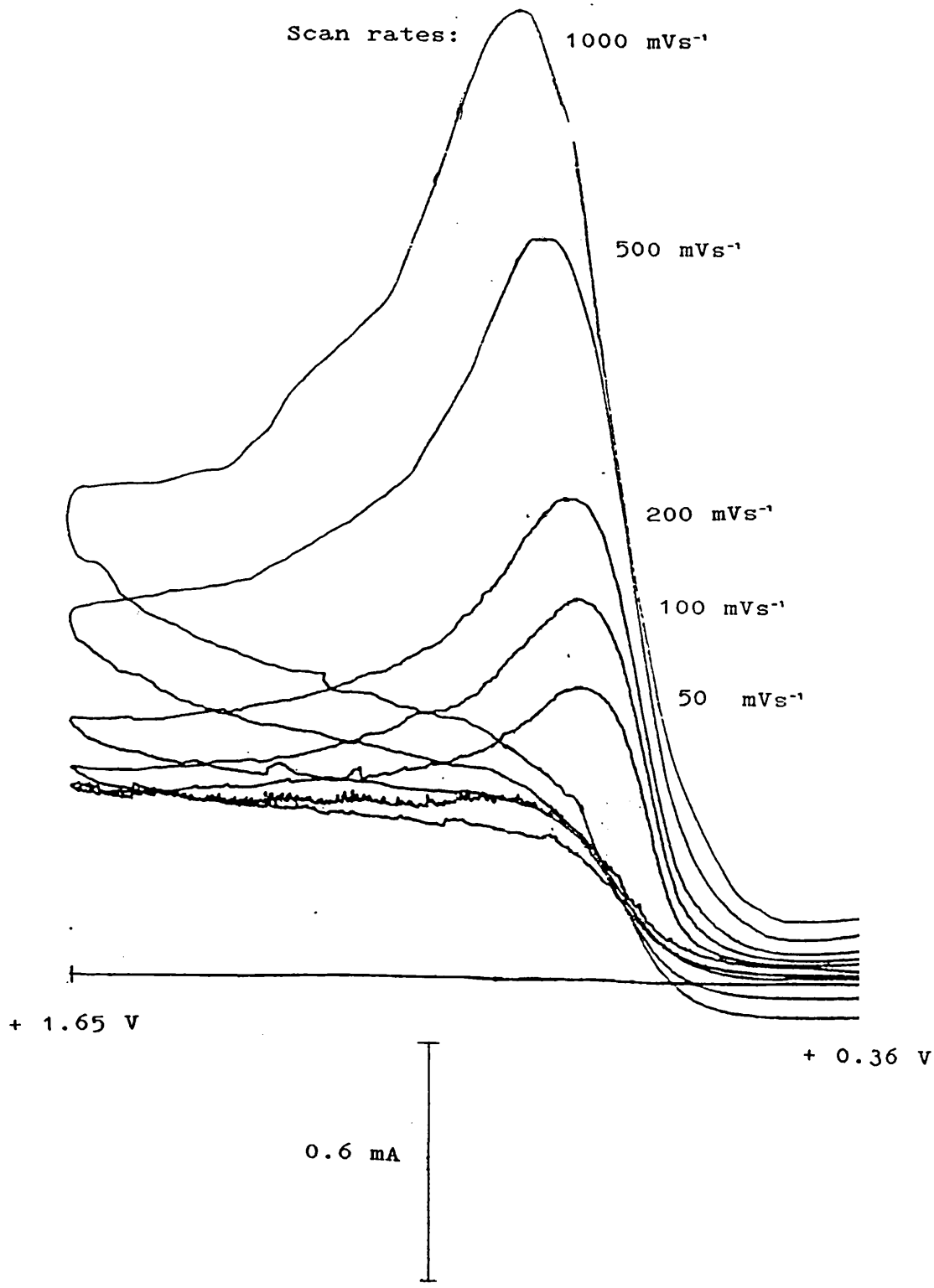


Table 8.5. Voltammetric Parameters for 1.00M titanium(III) in 10/90 mole p.c. KCl/$ZnCl_2$ at 412°C

Scan rate/ mVs^{-1}	I_{pc}/I_{pa}	ΔE_p/ mV	$I_{pa}/\nu^{1/2}$/ $mA/(Vs^{-1})^{1/2}$
1000	a	a	9.37
500	-	-	10.16
200	-	-	9.92
100	-	-	11.66
50	-	-	12.57
20	-	-	14.34
	$E_{pa}-E_{pa/2}$/mV	E_{pa}/V	
1000	192	0.912	
500	161	0.851	
200	132	0.811	
100	127	0.791	
50	125	0.791	
20	101	0.730	

a. These values uncertain due to distortion of cathodic peak.

Table 8.6. Voltammetric Parameters for 0.36M titanium(III) in 30/70 mole p.c. KCl/$ZnCl_2$ at 412°C

Scan rate/ mVs^{-1}	I_{pc}/I_{pa}	ΔE_p/ mV	$I_{pa}/\nu^{1/2}$/ $mA/(Vs^{-1})^{1/2}$
1000	a	a	9.09
750	-	-	9.29
600	-	-	9.19
500	-	-	9.19
300	-	-	9.39
200	-	-	9.09
100	-	-	9.48
50	-	-	10.47
	$E_{pa}-E_{pa/2}$/mV	E_{pa}/V	
1000	146	0.832	
750	136	0.842	
600	133	0.865	
500	130	0.865	
300	128	0.842	
200	123	0.842	
100	120	0.832	
50	b	b	

a. These values uncertain due to distortion of cathodic peak.

b. These values uncertain due to distortion of anodic peak.

c) 0.3 mole fraction KCl.

A 0.36M titanium(III) solution in this system at 400°C again produced voltammograms with little evidence of substantial reduction of the oxidation product. "Noise" was observable even above 1 Vs^{-1} scan rate. However, the anodic peaks showed no variation in peak potential or half-peak width with scan rate, and a plot of i_{pa} versus $\nu^{1/2}$ was linear except for deviations at 50 mVs^{-1} and below, due to peak distortion caused by "noise", and probably also from convection (table 8.6, fig. 8.4). This result was again consistant with a reversible one-electron transfer, until the $TiCl_4$ solubility was exceeded on the forward sweep, and hence lost by volatilisation, rather than a mechanism involving an irreversible chemical reaction, which should involve a cathodic peak shift (77,78).

d) 0.5 mole fraction KCl.

The remarks made above for the 0.36M solution in the 0.3 mole fraction melt apply equally well to a 0.39M solution in this system (table 8.7). However, for a more dilute 0.06M solution at 405°C, well-defined anodic and cathodic peaks were observed, though with the peak current ratio significantly less than one, and with some noise for $\nu < 200$ mVs^{-1} (table 8.8, fig. 8.5). On cooling to 380°C, and then to 338°C, respective increases in the peak current ratio were observed (tables 8.9 and 8.10), suggesting a suppression of the dissociation equilibrium 8.2 above, as noted with the pure zinc chloride.

An even more dilute solution (0.02M) exhibited

Figure 8.4. Typical cyclic voltammograms for the oxidation of titanium(III) (0.36M) in 0.30 mole fraction KCl-$ZnCl_2$ at 400°C (reaction product of titanium metal)

Working electrode: vitreous carbon
Reference electrode: zinc

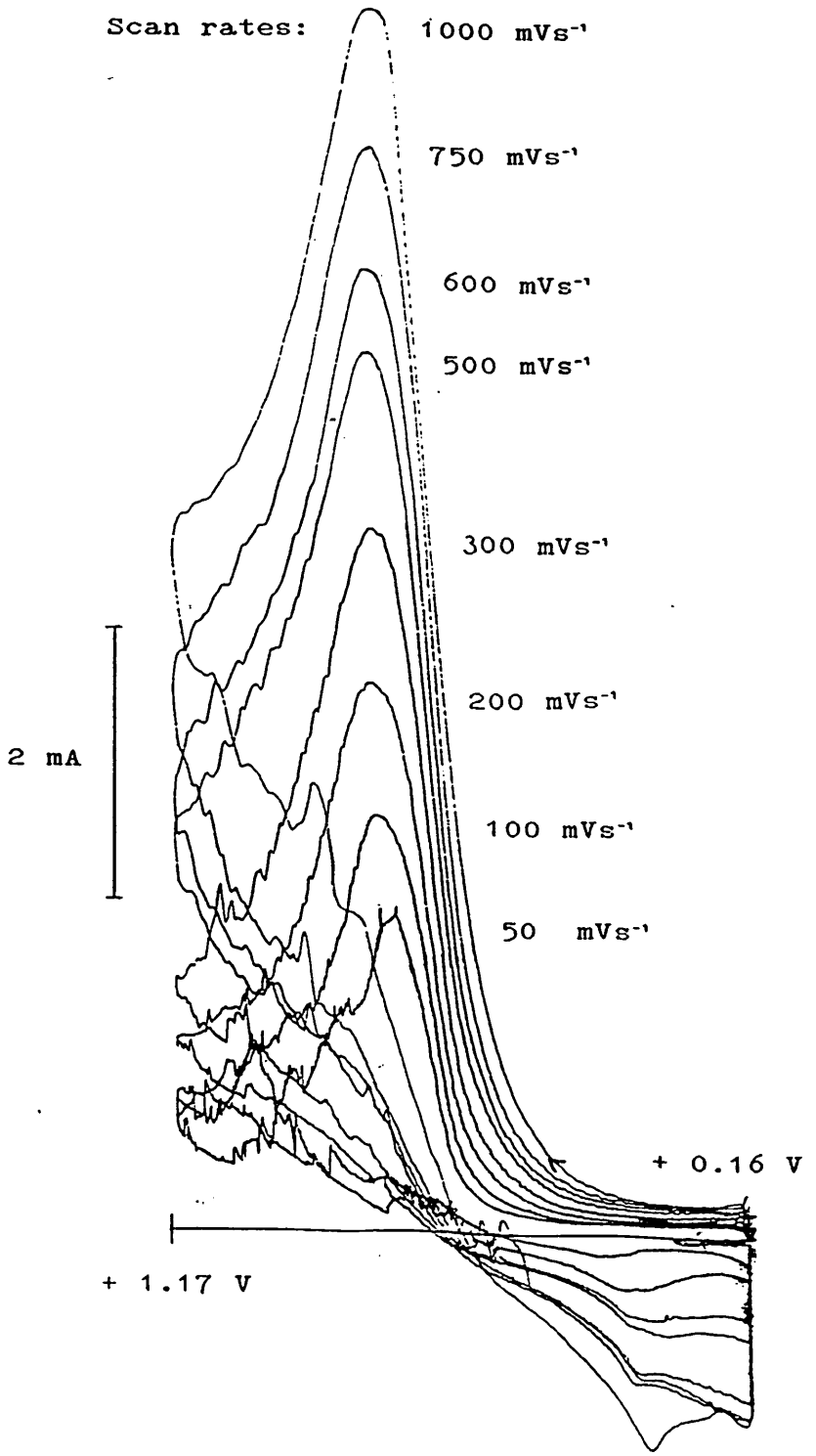


Table 8.7. Voltammetric Parameters for 0.36M titanium(III) in 50/50 mole p.c. KCl/$ZnCl_2$ at 400°C

Scan rate/ mVs^{-1}	I_{pc}/I_{pa}	ΔE_p/ mV	$I_{pa}/\nu^{1/2}$/ $mA/(Vs^{-1})^{1/2}$
1000	a	a	11.50
750	-	-	11.62
600	-	-	11.78
500	-	-	11.74
300	-	-	12.67
200	-	-	13.55
	$E_{pa}-E_{pa/2}$/mV	E_{pa}/V	
1000	124	1.031	
750	124	1.031	
600	124	1.031	
500	124	1.031	
300	124	1.016	
200	134	1.016	

a. These values uncertain due to distortion of cathodic peak.

Table 8.8. Voltammetric Parameters for 0.06M titanium(III) in 50/50 mole p.c. KCl/$ZnCl_2$ at 405°C

Scan rate/ mVs^{-1}	I_{pc}/I_{pa}	ΔE_p/ mV	$I_{pa}/\nu^{1/2}$/ $mA/(Vs^{-1})^{1/2}$
1000	0.60	161	1.71
500	0.57	155	1.66
200	0.52	135	1.68
100	0.51	135	1.68
50	0.46	a	1.89
	$E_{pa}-E_{pa/2}$/mV	E_{pa}/V	
1000	150	1.079	
500	156	1.061	
200	135	1.037	
100	130	1.027	
50	124	1.037	

a. This value uncertain due to distortion of cathodic peak.

Figure 8.5. Typical cyclic voltammograms for the oxidation of titanium(III) (0.06M) in 0.50 mole fraction KCl-$ZnCl_2$ at 405°C (reaction product of titanium metal)

Working electrode: vitreous carbon
Reference electrode: zinc

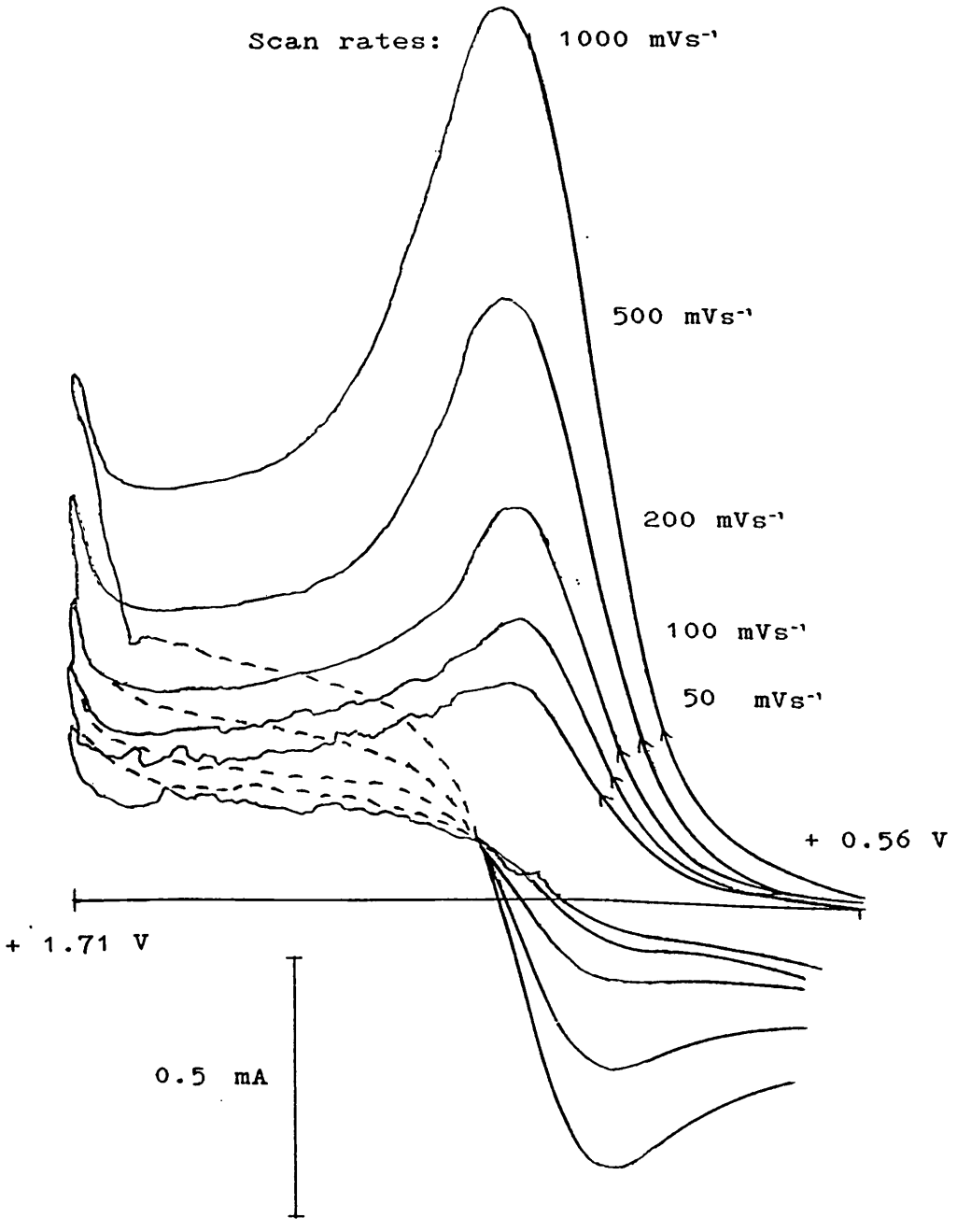


Table 8.9. Voltammetric Parameters for 0.06M titanium(III) in 50/50 mole p.c. KCl/$ZnCl_2$ at 380°C

Scan rate/ mVs^{-1}	I_{pc}/I_{pa}	ΔE_p/ mV	$I_{pa}/\nu^{1/2}$/ $mA/(Vs^{-1})^{1/2}$
1000	0.81	146	1.38
500	0.86	146	1.17
200	0.78	134	1.15
100	0.70	133	1.16
50	0.68	127	1.15
	$E_{pa}-E_{pa/2}$/mV	E_{pa}/V	
1000	180	1.184	
500	149	1.235	
200	149	1.184	
100	154	1.184	
50	149	1.184	

Table 8.10. Voltammetric Parameters for 0.06M titanium(III) in 50/50 mole p.c. KCl/$ZnCl_2$ at 338°C

Scan rate/ mVs^{-1}	I_{pc}/I_{pa}	ΔE_p/ mV	$I_{pa}/\nu^{1/2}$/ $mA/(Vs^{-1})^{1/2}$
1000	0.98	118	1.10
500	0.94	118	1.10
200	0.88	118	1.13
100	0.83	118	1.15
50	0.77	118	1.18
	$E_{pa}-E_{pa/2}$/mV	E_{pa}/V	
1000	132	0.978	
500	132	0.978	
200	139	0.978	
100	134	0.978	
50	139	0.978	

uncomplicated reversible behaviour at 400°C, again demonstrating the effect of concentration (table 8.11).

For this system, attempts were made to calculate rate constants for a presumed irreversible chemical reaction following the charge transfer (E_rC_i mechanism), using the procedure of Nicholson and Shain (120). Thus the values of peak current ratio may be related to a quantity $\log(k_f t)$ from a working curve, where k_f is the rate constant of the chemical reaction, and t is the time in seconds from $E_{1/2}$ to the switching potential. However, in the present instance, calculated values of k_f (table 8.12) were not constant with scan rate, but decreased in a manner approximately proportional to scan rate. This evidence clearly demonstrates that some or all of the assumptions involved in the E_rC_i mechanism are not valid in this case, i.e that the product is converted via a first order chemical reaction to an electrochemically inactive product.

e) 0.6 mole fraction KCl.

A 0.70M solution if titanium(III) at 416°C in this system again exhibited behaviour similar to that observed for the 0.39M and 0.36M solutions in the 0.5 and 0.3 mole fraction KCl melts, the cathodic peaks being insignificant even at 1 Vs^{-1} scan rate (fig.8.6, table 8.13). However, on cooling below 346°C, cathodic peaks became discernable, the peak current ratios being in the range 0.04-0.09 (table 8.14). At 310°C, the ratio had increased by a factor of about 10 (table 8.15). On further cooling to 290°C, inflections began to appear on the

Table 8.11. Voltammetric Parameters for 0.02M titanium(III) in 50/50 mole p.c. KCl/$ZnCl_2$ at 400°C

Scan rate/ mVs^{-1}	I_{pc}/I_{pa}	ΔE_p/ mV	$I_{pa}/\nu^{1/2}$/ $mA/(Vs^{-1})^{1/2}$
1000	1.10	153	0.56
500	1.06	151	0.56
200	1.02	141	0.57
100	0.94	146	0.60
50	0.94	146	0.58
20	0.88	141	0.62
	$E_{pa}-E_{pa/2}$/mV	E_{pa}/V	
1000	167	0.978	
500	167	0.911	
200	162	0.911	
100	164	0.911	
50	164	0.911	
20	165	0.911	

Table 8.12. Calculated rate constants for 0.06M titanium(III) in 50/50 mole p.c. KCl/$ZnCl_2$ at 380°C assuming E.C. mechanism

Scan rate/ mVs^{-1}	I_{pc}/I_{pa}	tau/ s*	rate constant/ s^{-1}
1000	0.81	0.56	1.52
500	0.86	1.12	0.73
200	0.78	2.80	0.32
100	0.70	5.60	0.16
50	0.68	11.20	0.08

* Time from $E_{1/2}$ to switching potential.

Figure 8.6. Typical cyclic voltammograms for the oxidation of titanium(III) (0.70M) in 0.60 mole fraction KCl-$ZnCl_2$ at 416°C (reaction product of titanium metal)

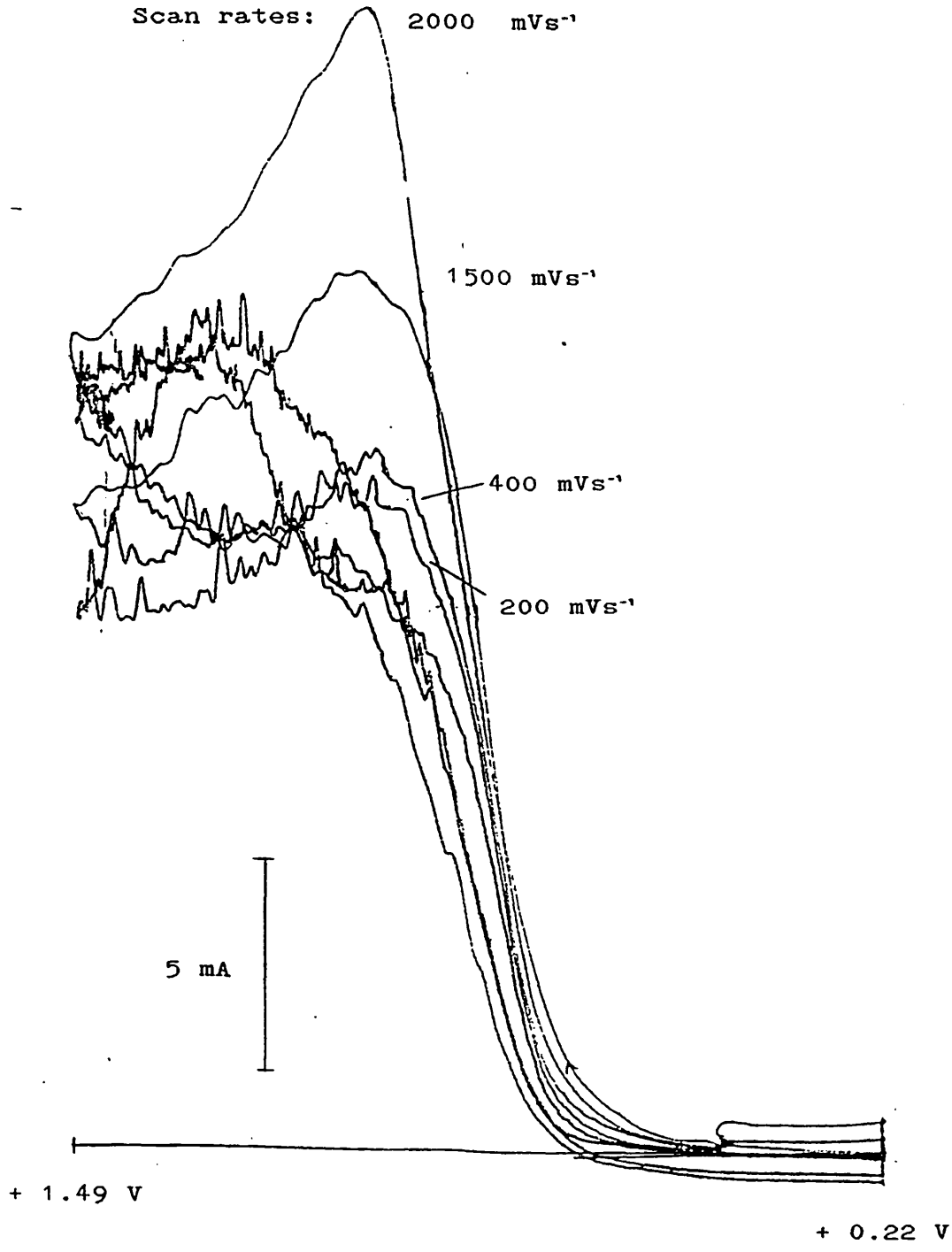


Table 8.13. Voltammetric Parameters for 0.70M titanium(III) in 60/40 mole p.c. KCl/$ZnCl_2$ at 416°C

Scan rate/ mVs^{-1}	I_{pc}/I_{pa}	ΔE_p/ mV	$I_{pa}/\nu^{1/2}$/ $mA/(Vs^{-1})^{1/2}$
2000	a	a	18.77
1000	-	-	20.45
400	-	-	25.19a
200	-	-	29.69a
	$E_{pa}-E_{pa/2}$/mV	E_{pa}/V	
2000	160	1.030	
1000	b	1.040	
400	-	b	
200	-	-	

a. These values uncertain due to distortion of cathodic peak.

b. These values uncertain due to distortion of anodic peak.

Table 8.14. Voltammetric Parameters for 0.70M titanium(III) in 60/40 mole p.c. KCl/$ZnCl_2$ at 346°C

Scan rate/ mVs^{-1}	I_{pc}/I_{pa}	ΔE_p/ mV	$I_{pa}/\nu^{1/2}$/ $mA/(Vs^{-1})^{1/2}$
1000	0.09	319	13.73
750	0.05	310	13.99
500	0.06	310	14.58
300	0.03	a	16.20
200	0.03	-	16.48
100	0.04	-	19.76
50	0.04	-	24.03
	$E_{pa}-E_{pa/2}$/mV	E_{pa}/V	
1000	197	1.179	
750	197	1.169	
500	197	1.169	
300	202	1.143	
200	217	1.107	
100	b	b	
50	-	-	

a. These values uncertain due to distortion of cathodic peak.

b. These values uncertain due to distortion of anodic peak.

Table 8.15. Voltammetric Parameters for 0.70M titanium(III) in 60/40 mole p.c. KCl/$ZnCl_2$ at 310°C

Scan rate/ mVs^{-1}	I_{pc}/I_{pa}	ΔE_p/ mV	$I_{pa}/\nu^{1/2}$/ $mA/(Vs^{-1})^{1/2}$
1000	0.86	492	12.65
500	0.80	452	15.27
200	0.75	378	16.89
100	0.70	368	19.17
50	0.57	283	20.11
	$E_{pa}-E_{pa/2}$/mV	E_{pa}/V	
1000	169	1.179	
500	175	1.231	
200	129	1.174	
100	106	1.170	
50	69	1.156	

Table 8.16. Voltammetric Parameters for 0.70M titanium(III) in 60/40 mole p.c. KCl/$ZnCl_2$ at 290°C

Scan rate/ mVs^{-1}	I_{pc}/I_{pa}	ΔE_p/ mV	$I_{pa}/\nu^{1/2}$/ $mA/(Vs^{-1})^{1/2}$
100	1.03	328	14.03
50	0.76	303	14.81
20	0.49	251	15.68
	$E_{pa}-E_{pa/2}$/mV	E_{pa}/V	
100	104	1.037	
50	90	1.027	
20	59	1.008	

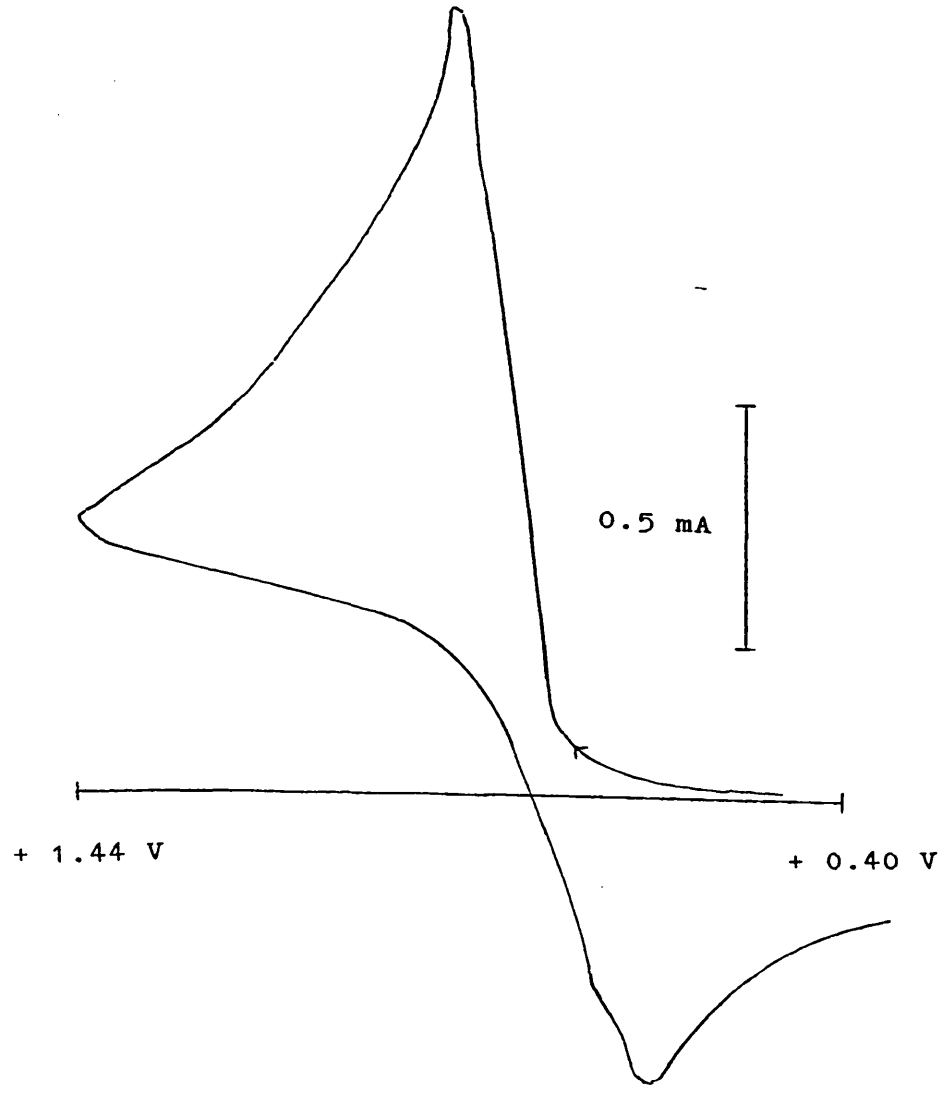
Table 8.17. Voltammetric Parameters for 0.70M titanium(III) in 60/40 mole p.c. KCl/$ZnCl_2$ at 272°C

Scan rate/ mVs^{-1}	I_{pc}/I_{pa}	ΔE_p/ mV	$I_{pa}/\nu^{1/2}$/ $mA/(Vs^{-1})^{1/2}$
100	0.97	350	11.66
50	0.77	255	11.88
20	0.62	262	11.38
10	0.57	115	12.81
5	0.52	87	12.59
	$E_{pa}-E_{pa/2}$/mV	E_{pa}/V	
100	86	0.990	
50	73	0.906	
20	82	0.917	
10	63	0.875	
5	60	0.865	

anodic waves, and cooling to 272°C resulted in voltammograms with narrow anodic half-peak widths, and with inflections also on the cathodic waves, indicative of the deposition and stripping of insoluble product (tables 8.16, 8.17, fig.8.7). Some "noise" was however still evident.

Unfortunatly attempts to isolate the electrode product by constant potential electrolysis at vitreous carbon electrodes were unsuccessful, the product appearing to have decomposed or dissolved when the melt was dissolved away with propanone or ethoxyethane. However, the product in this relatively basic melt was likely to have been potassium hexachlorotitanate(IV). This substance may be prepared from the interaction of $TiCl_4$ and potassium chloride (121), and the stability of the $TiCl_6^{2-}$ ion is markedly dependent on the Lewis acidity of the cation, so that, for example, the analogous sodium or lithium compounds have not been prepared, and interaction of $TiCl_4$ with the LiCl/KCl eutectic below 448°C or with equimolar NaCl/KCl at 700°C (solubility 3.1 mole %) produces the solid potassium compound quantitatively (122,123). At 470°C in the former melt, 0.1 mole % titanium(III) may be oxidised electrochemically to gaseous $TiCl_4$ (124), and more concentrated solutions to solid K_2TiCl_6 (125), actually recovered from the melt, in line with the present work. The existance of a compound such as "$ZnTiCl_6$" is thus unlikely due to the acidity of the zinc cation.

Figure 8.7. Typical cyclic voltammogram for the oxidation of titanium(III) (0.70M) in 0.60 mole fraction KCl-$ZnCl_2$ at 272°C (reaction product of titanium metal)



Working electrode: vitreous carbon
Reference electrode: zinc
Scan rate: 20 mVs^{-1}.

8.2.2 Titanium(III) chloride in potassium chloride-zinc chloride melts

a) 0.25 mole fraction KCl.

In this system, a 0.34M solution of titanium(III) chloride gave an oxidation wave at 0.81 V with respect to the zinc deposition potential, but the corresponding cathodic peak was insignificant in comparison. The peak potential may be compared with 0.82 V for the solution formed by the reaction of titanium metal in the 0.3 mole fraction melt (see below) suggesting that the same species was present in solution. The voltammetric parameters, given in table 8.18, are consistant with a one-electron oxidation, but with the loss of volatile $TiCl_4$ by the process discussed above for the titanium metal solutions.

One further feature of these systems which may be mentioned here is the appearence of two additional waves on the voltammograms. The first, particularly prominant with solutions of titanium(III) chloride, but also occurring occasionally with solutions prepared by reaction of titanium metal, was an anodic wave occurring at about 0.3 V cathodic of the Ti^{3+} oxidation wave; the second, a cathodic wave at about 0.5 V cathodic of the Ti^{3+} oxidation peak. Although the peak positions were relatively constant, the peak heights were very variable between different experiments, one or other, or both, of the waves being absent. Both waves were narrow (half-peak widths, 70 mV and 100 mV respectively at 400°C), and symmetrical (fig. 8.8). The anodic wave increased linearly with the scan rate, whereas the cathodic wave increased as

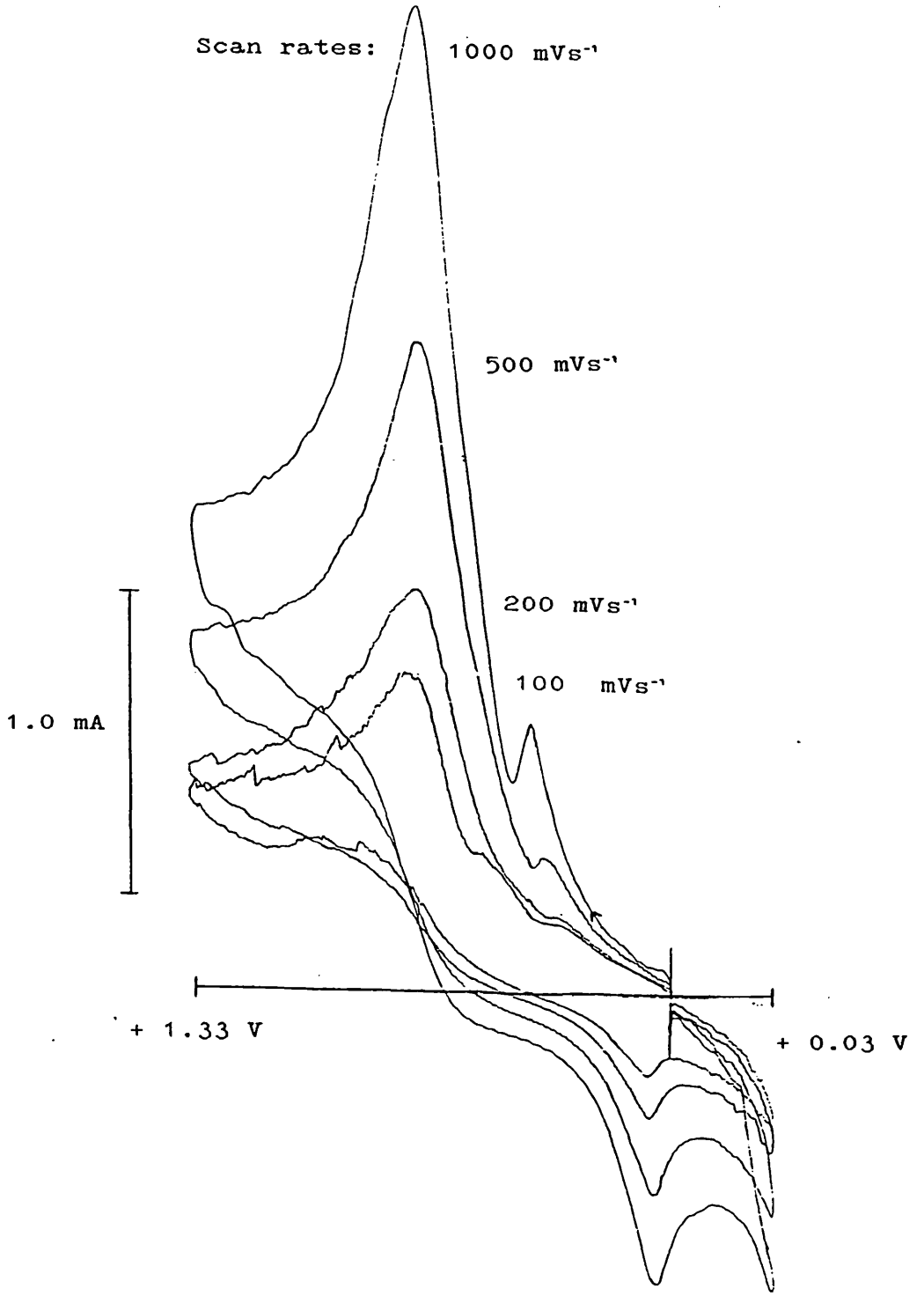
Table 8.18. Voltammetric Parameters for 0.34M titanium(III) in 25/75 mole p.c. KCl/$ZnCl_2$ at 398°C

Scan rate/ mVs^{-1}	I_{pc}/I_{pa}	ΔE_p/ mV	$I_{pa}/\nu^{1/2}$/ $mA/(Vs^{-1})^{1/2}$
1000	a	a	3.25
500	-	-	3.03
200	-	-	2.97
100	-	-	3.31
50	-	-	3.07
20	-	-	3.42
	$E_{pa}-E_{pa/2}$/mV	E_{pa}/V	
1000	123	0.834	
500	118	0.813	
200	118	0.802	
100	131	0.832	
50	105	0.813	
20	105	0.813	

a. These values uncertain due to distortion of cathodic peak.

Figure 8.8. Typical cyclic voltammograms for the oxidation of titanium(III) (0.34M) in 0.25 mole fraction KCl-$ZnCl_2$ at 400°C (reaction product of titanium(III) chloride)

Working electrode: vitreous carbon
Reference electrode: zinc



$v^{1/2}$. This behaviour for the anodic wave is diagnostic of strong adsorption (77,78) of the oxidation product, except that the expected corresponding cathodic peak (at the same potential) was absent.

An additional piece of evidence was that if the potential was held cathodic of the supposed adsorption peak for several minutes, a relatively intense peak was frequently obtained, which decreased in height on subsequent scanning. This suggests that the vitreous carbon electrode was "cleaned" of some species blocking adsorption by being held at these cathodic potentials. Evidently some property of the adsorbed layer prevents the reduction on the reverse sweep.

Moving on to consider the cathodic wave, as noted above, this appears to be diffusion-controlled from the peak height dependence on scan rate. The narrow peak width however suggests a multi-electron transfer or possibly deposition. By varying the switching potential it was shown that the presence of the peak depended on the initial oxidation to form titanium(IV), though the nature of the process is unclear, but might involve oxychloride species. For example, Linga et al (126) reported that even in "purified" n-butylpyridinium chloride/aluminium chloride melt (at 30-60°C), with solutions of $TiCl_4$ an irreversible reduction wave due to an oxychloro-complex of titanium(IV) could be observed, as well as the reversible wave due to $TiCl_4$ reduction. Oxide additions to the melt increased the height of the irreversible wave, which appeared at a more negative potential than the reversible

wave, as does the wave of interest in the present work.

b) 0.44 mole fraction KCl.

The temperature variation of a dilute (0.012M) solution of titanium(III) chloride in the system was investigated. It was found that the peak current ratios were significantly less than one at 382°C, but increased on cooling, so that reversible behaviour was observed at 236°C (tables 8.19, 8.20), the variation being analogous to that observed for the 0.06M solution prepared by reaction of titanium metal in the 0.5 mole fraction KCl melt. The anodic peak potential (1.00 V) was similar to that found in the 0.5 mole fraction melt (1.02 V), again suggesting that a similar species was present.

Voltammetric evidence in the form of "additional" waves was also found for the presence of oxychloro-species, as noted above for the 0.25 mole fraction KCl melt.

8.3 Characterisation of anodic oxidation product

In order to establish the identity of the oxidation product of titanium(III) in these melts, constant potential electrolysis was performed at a large area (5 cm^2) vitreous carbon electrode in 0.5 mole fraction KCl/$ZnCl_2$ melts at 400°C, containing 0.7M Ti(III). When the potential was held at the voltammetric peak, gas evolution was observed, and after passing the argon carrier gas flowing through the cell into water, the hydrolysis products were found to contain titanium and chlorine, in the ratio 1:4, confirming that the oxidation product was indeed titanium(IV) chloride. As noted above, this result is consistant with a number of reports

Table 8.19. Voltammetric Parameters for 0.012M titanium(III) in 44/56 mole p.c. KCl/$ZnCl_2$ at 382°C

Scan rate/ mVs^{-1}	I_{pc}/I_{pa}	ΔE_p/ mV	$I_{pa}/\nu^{1/2}$/ $mA/(Vs^{-1})^{1/2}$
1000	1.05	148	1.03
500	0.99	148	0.98
200	0.89	146	0.98
100	0.82	146	0.97
50	0.71	143	0.96
20	0.58	143	0.97
	$E_{pa}-E_{pa/2}$/mV	E_{pa}/V	
1000	148	1.058	
500	141	1.058	
200	141	1.001	
100	141	1.001	
50	141	1.001	
20	141	1.001	

Table 8.20. Voltammetric Parameters for 0.012M titanium(III) in 44/56 mole p.c. KCl/$ZnCl_2$ at 236°C

Scan rate/ mVs^{-1}	I_{pc}/I_{pa}	ΔE_p/ mV	$I_{pa}/\nu^{1/2}$/ $mA/(Vs^{-1})^{1/2}$
1000	1.18	128	0.39
500	1.08	128	0.38
200	1.06	125	0.39
100	1.04	120	0.39
50	0.96	115	0.39
20	0.86	115	0.41
5	0.63	115	0.53
	$E_{pa}-E_{pa/2}$/mV	E_{pa}/V	
1000	115	0.965	
500	115	0.965	
200	113	0.960	
100	104	0.960	
50	104	0.954	
20	104	0.954	
5	104	0.950	

indicating that the latter compound is evolved during the oxidation of titanium(III) in chloride melts at relatively high temperatures (67, 123, 124).

8.4. Conclusions and Further work

The results of this study suggest that sufficiently dilute titanium(III) solutions can be reversibly oxidised to titanium(IV) in these melts, provided also that the temperature is not too high, consistant with the reversible one-electron transfers found in relatively low-temperature melts, such as the room-temperature chloroaluminates noted above (126), and also in $NaCl/AlCl_3$ melts at 260°C (127). However, at higher temperatures and with relatively high melt concentrations of titanium(III), the oxidation product appears to be physically lost from the vicinity of the electrode, and this result is consistant with reports of titanium(III) oxidation in chloride melts at relatively high temperatures, where titanium(IV) chloride is evolved (67, 123, 124). In the present work, there was no pronounced stabilisation of the IV oxidation state in the more basic melts, probably because the melt acidity was still sufficient to destabilise the presumed hexachlorotitanate(IV) complex which forms in the absence of relatively acidic cations.

It was also concluded that spontaneous evolution of $TiCl_4$ took place from the titanium(III) solutions, probably by disproportionation, with subsequent decomposition to the oxide at the cell walls.

There was also no indication of reduction of

titanium(III) to lower oxidation states within the electrochemical window of the melt. This is consistant with the reaction of titanium metal to displace zinc and form the III oxidation state, and with the strongly reducing nature of titanium(II).

Some voltammetric evidence of the presence of oxide species was obtained for the solutions of titanium(III) chloride, which are more likely to contain oxygen species through hydrolysis (of the titanium chloride) than are the solutions prepared by the reaction of titanium metal.

The titanium system in the zinc chloride melts exhibits quite complicated behaviour and a number of points remain unclear, for example, the exact nature of the black suspension formed by the reaction of titanium metal with the melts, and of the blue solutions formed by reaction of titanium(III) chloride. A study of the role of oxygen species would be desirable.

Also, a more extensive study using a wider range of concentrations and at different temperatures could be undertaken to determine the variation of the dissociation constant of the chlorotitanate(IV) melt species with melt acidity, and thus confirm the expected stabilisation in the more basic melts.

The variation of solubility of titanium(III) chloride could also be examined to assess the predictions of the Coordination Cluster theory, as discussed in chapters one and four.

REFERENCES

1) Y.Marcus, in "Advances in Molten Salt Chemistry", chapter 2, Vol. 1; J.Braunstein, G.Mamantov, G.P.Smith, Eds. Plenum Press N.Y. 1971.

2) H.Bloom, "The Chemistry of Molten Salts", W.A.Benjamin Inc. N.Y. 1967.

3) M.Blander, in "Molten Salt Chemistry: An introduction and selected applications", G.Mamantov, R.Marrassi, Eds. Nato ASI series C, D.Reidel, Dordrecht 1987.

4) B.R.Sundheim, Ed. "Fused Salts", McGraw-Hill N.Y. 1964.

5) W.J.Hamer, M.S.Malmberg, B.Rubin, J. Electrochem. Soc. 103, 8, (1956).

6) F.D.Richardson, "Physical Chemistry of Melts in Metallurgy", Vol. 1; Academic Press, London, 1974.

7) G.N.Papatheodorou, O.J.Kleppa, Z. Anorg. Allg. Chem. 401, 132, (1973).

8) M.Blander, M-L.Saboungi, P.Cerisier, Metall. Trans. 10B, 613, (1979.

9) R.Fehrmann, J.H. von Barner, N.J.Bjerrum, O.F.Nielsen, Inorg. Chem. 20, 1712, (1981).

10) M.Blander, M-L.Saboungi, Abstr. No. 431, Extended Abstr. v 81-2, Electrochem. Soc. Meeting, Denver, October 11-16, 1981, p.1048.

11) J.H.Morrey, R.H.Moore, J. Phys. Chem. 67, 748, (1963).

12) C.G.M.Dijkhuis, J.A.A.Katelaar, Electrochim. Acta, 12, 795, (1967).

13) G.Mamantov, R.A.Osteryoung, in "Characterisation of Solutes in Non-aqueous Solvents", Chapter 11, G.Mamantov, Ed. Plenum Press, N.Y. 1978.

14) N.J.Bjerrum, C.R.Boston, G.P.Smith, Inorg. Chem. 6, 1162, 1968, (1967).

15) R.K.McMullen, J.D.Corbett, J. Amer. Chem. Soc. 80, 4761, (1958).

16) J.D.Corbett, W.J.Burkhand, L.F.Dowding, ibid. 83, 76, (1961).

17) J.D.Corbett, in "Progress in Inorganic Chemistry", Vol. 21, pp. 129-158, S.J.Lippard, Ed. John Wiley and Sons, 1976.

18) Reference 13, Chapter 12.

19) R.Marrassi, G.Mamantov, J.Q.Chambers, J. Electrochem. Soc. 123, 1128, (1976).

20) H.A.Oye, D.M.Gruen, Inorg. Chem. 3(6), 836, (1964).

21) K.A.Paulsen, R.A.Osteryoung, J. Amer. Chem. Soc. 98, 6866, (1976).

22) C.A.Angell, D.M.Gruen, J. Inorg. Nucl. Chem. 29, 2243, (1967).

23) Reference 13, Chapter 11, p. 237.

24) J.A.McNeese, D.F.Bowersox, D.C.Christenson, Proc. 5th Int. Symp. Molten Salts, p. 474, M-L.Saboungi, K.E.Johnson, D.S.Newman, D.Inman, Eds. The Electrochemical Society, U.S.A. 1986.

25) S.S.Salim, A.T.Bell, Fuel 61, 745, (1982).

26) G.A.Olah, "Friedel-Crafts Chemistry", Wiley, N.Y. 1973.

27) S.Sahami, R.A.Osteryoung, Anal. Chem. 55, 1970, (1983)

28) M.Namura, K.Tereo, S.Kikkawa, Fuel 60, 699, (1981).

29) M.Namura, H.Sakashita, S.Kikkawa, Tech. Rep. Osaka Univ. 32, 439, (1982).

30) G.Picard, F.Seon, B.tremillon, J. Electroanal. Chem. 102, 65, (1979).

31) I.Yosuhiko, H.Katohala, J.Uchida, S.Yoshizawa, Nippon Kagaku Kaishi 6, 1034, (1982).

32) L.E.Gorre, R.C.Porter, Mat. Ref. Bull. 18, 1391, (1983).

33) R.Struck, C.W.Zielke, Fuel 60, 795, (1981).

34) S.Biggin, J.E.Enderby, unpublished work.

35) G.S.Perry, L.G.McDonald, S.D.Wilcox, HCTD Tech. Memo No. 3/84, AWE, Aldermaston (June 1984).

36) S.H.White, in "Ionic LIquids", chap.12, D.Inman, D.G.Lovering, Eds. Plenum Press, London 1981.

37) G.S.Perry, L.S.McDonald, J. Electroanal. Chem. 144, 251, (1983).

38) K.W.Fung, G.Mamantov, in "Advances in Molten Salt Chemistry", Vol. 2, J.Braunstein, G.Mamantov, G.P.Smith, Eds. Chap. 4, p.219. Plenum Press, London 1973.

39) J.R.Mayer, J.C.Evans, G.Y-S.Lo, J.Electrochem. Soc. 113, 158, (1966).

40) M.Itah, K.Sakai, T.Nakamura, Inorg. Chem. 21, 3552, (1982).

41) S.Biggin, J.E.Enderby, J.Phys. C, 14, 3129, (1981).

42) J.Brynestad, H.L.Yakel, Inorg. Chem. 17(5), 1376, (1978).

43) G.J.Janz, R.P.T.Tomkins, C.B.Allen, J.R.Downes, G.L.Gardner, U.Krebs, S.K.Singer, J. Phys. Chem. Ref. Data 4, 871, (1975).

44) T.Ejima, Y.Yoko, G.Saito, Y.Kato, J. Japan Inst. Metals 43(10), 929, (1979).

45) T.Yoko, R.Crescent, Y.Tsukagashi, T.Ejima, ibid. 42(12), 1179, (1979).

46) T.Ejima, Y.Yoko, K.Nakashima, ibid, 41(1), 86, (1977).

47) A.J.Easteal, C.A.Angell, J. Phys. Chem. 74, 3987, (1970).

48) C.R.Boston, L.F.Grantham, S.J.Yosim, J. Electrochem. Soc. 117, 28, (1970).

49) H.Bloom, I.A.Weeks, Trans. Far. Soc. 67, 1410, (1971).

50) G.S.Perry, L.S.McDonald, Thermochim. Acta 68, 341, (1971).

51) G.S.Perry, L.G.McDonald, S.D.Wilcox, HCTD Tech. Memo No. 3/84, AWE, Aldermaston (June 1984).

52) H.I.Moss, Ph.D Thesis, Indiana State University 1960.

53) H.Bloom, T.H.Spurling, J.Wong, Aust. J. Chem. 23, 501, (1970).

54) R.J.Robertson, A.S.Kucharski, Can. J. Chem. 51, 3114, (1973).

55) C.E.Wicks, F.E.Block, U.S. Bureau Mines Bull. 605, (1963).

56) D.Cubicciotti, M.Eding, J. Chem. Phys. 40, 978, (1965).

57) O.Kubachewskii, E.Evans, C.B.Alcock, "Metallurgical Thermochemistry", Pergamon Press, Toronto 1971.

58) S.Benhenda, J.Lesourd, J. Chim. Phys. 74, 1042, (1976).

59) J.Lesourd, Y.Rocca-serra, Y.Doucet, J. Chem. Thermodynamics 9, 333, (1977).

60) P.Dudley, D.Inman, AWRE Interim Report 17th Oct. 1982, Agreement No. 1A 84710/1110 (Imperial College, London).

61) D.R.Flinn, K.H.Stern, J.Electrochem. Soc. 123, 978, (1976).

62) M.Matsunaga, K.Hosokawa, Rep. Asahi Glass Found. Ind. Tech. 41, 255, (1982).

63) H.E.Bartlett, P.Crowther, Electrochim. Acta 15, 681, (1970).

64) P.Dudley, D.Inman, AWRE Interim Report March 1982, Agreement No. 1A 84710/1110 (Imperial College, London).

65) M.V.Susic, S.V.Mentus, Ext. Abstr. Meeting Int. Soc. Electrochem. 1979, 30th, p. 170; ibid, 1980, 30th, p. 515.

66) G.Rubel, M.Gross, Corr. Sci. 15, 251, (1975).

67) J.A.Plambeck, in "Encyclopaedia of Electrochemistry of the Elements", Vol. X, "Fused Salt Systems", A.J.Bard, Ed. Marcell Dekker Inc, N.Y. 1976.

68) L.E.Topol, W.A.McCallum Jr., S.J.Yosim, North American Rockwell Corporation, Canaga Park, Calif. Technical Report NASA-CR-72791 (1970).

69) M.Taoumi, Thesis, L'Institut National Polytechnique de Grenoble 1984.

70) M.L.Deanhardt, K.W.Hanck, J. Electrochem. Soc. 122, 1627, (1975); M.L.Deanhardt, Ph.D Thesis, North Carolina State University 1975.

71) M.M.Vetyukov, A.Francis, Elektrokhimiya 5, 362, (1969).

72) J.D. van Norman, J.S.Bookless, J.J.Egan, J. Phys. Chem. 70, 1276, (1966).

73) W.E.Smith, J.Brynestad, G.P.Smith, J. Amer. Chem. Soc. 89, 5983, (1967).

74) C.A.Angell, D.M.Gruen, J. Phys. Chem. 70, 1601, (1966).

75) Joint Committee on Powder Diffraction Standards Index.

76) "Practical Surface Analysis by Auger and XPS", D.Briggs, M.P.Seah, John Wiley and Sons, London 1983.

77) A.J.Bard, L.R.Faulkner, "Electrochemical Methods", John Wiley and Sons, New York 1980.

78) A.Weissberger, B.W.Rossiter, "Physical Methods of Chemistry", Pt. IIA, "Electrochemical Methods", Wiley-Interscience, London 1971.

79) P.Delahay, "New Instrumental Methods in Chemistry", Interscience, London 1954.

80) D.J.Schiffrin, J. Electroanal. Chem. 201, 199, (1986).

81) M.Boutillon, Private communication.

82) C.Melandres, J.P.Ackermann, R.K.Steunenberg, Proc. Int. Symp. on Molten Salts, (1976), p. 575.

83) N.Q.Minh, B.J.Welch, J. Electroanal. Chem. 92, 179, (1978).

84) R.A.Osteryoung, Molten Salt Discussion Group Lecture, Christmas 1986 Meeting, Imperial College, London.

85) G.L.Holleck, J. Electrochem. Soc. 119, 1158, (1972).

86) H.Urushibata, I.Uchida, S.Toshima, J. Electroanal. Chem. 117, 43, (1971).

87) W.E.Triaca, C.Solomons, J.O'M.Bockris, Electrochim. Acta, 13, 1949, (1968).

88) R.Tunold, H.M.Bo, K.A.Paulsen, Electrochim. Acta 16, 2101, (1971).

89) I.G.Murgelescu, S.Sternberg, L.Medintev, C.Mustetea, Electrochim. Acta 8, 65, (1963).

90) F.M.Donahue, J.A.Levisky, G.F.Reynolds, J.S.Wilkes, Proceedings of the Fifth International Symposium on Molten Salts, Vol. 86-1, p. 332, M-L.Saboungi, K.Johnson, D.S.Newman, D.Inman, Eds. The Electrochemical Society Inc. 1986.

91) A.P.Ratvik, T.Ostwald, H.A.Oye, Acta Chem. Scand. Ser. A, A39(9), 623, (1985).

92) M.Kowalski, G.W.Harrington, Inorg. Nucl. Chem. Lett. 3, 121, (1967).

93) C.Dijkhuis, R.Dijkhuis, G.J.Janz, Chem. Rev. 68(3), 253, (1968).

94) J.C.Poignet, M.J.Barbier, Electrochim. Acta 17(7), 1227, (1972).

95) J.C.L.Legey, Ph.D. Thesis, Imperial College 1973.

96) T.Vargas, Ph.D. Thesis, Imperial College, 1984.

97) R.D.Shannon, C.T.Prewitt, Acta Crystallogr. B26, 1076, (1970).

98) J.O'M.Bockris, A.K.N.Reddy, "Modern Electrochemistry", Vol. 1, p.552. MacDonald, London 1970.

99) S.C.Levy, F.W.Reinhardt, J. Electrochem. Soc. 122, 200, (1975).

100) H.A.Laitinen, Y.Yamamura, I.Uchida, ibid, 125, 1450, (1978).

101) Ref. 3, p. 372.

102) M.Abramowitz, I.A.Stegun, Eds. "Handbook of Mathematical Functions", 10th ed. NBS Applied Mathematics Series, 55, NBS, Washington 1972.

103) B.Gilbert, V.Demarteau, G.Duykaerts, J. Electroanal. Chem. 89, 123, (1978).

104) C.L.Hussey, L.A.King, J.W.Erbacher, J. Electrochem. Soc. 125(4), 561, (1978).

105) B.Gilbert, G.Mamantov, K.W.Fung, Inorg. Chem. 14(8), 1802, (1975).

106) N.V.Sidgewick, "The Chemical Elements and their Compounds", Vol. II, p. 1012. Clarendon Press, Oxford 1962.

107) B.Morosin, A.Narath, J. Chem. Phys. 40(7), 1958, (1964).

108) Ref. 69, p. 144.

109) B.Wichterlova, L.Krajcikova, Z.Tvaruzkova, S.Beran, J. Chem. Soc. Far. Trans. 1, 80, 2639, (1984).

110) B.D.Cohan, Z.Nagy, M.A.Genshaw, J. Electrochem. Soc. 119, 64, (1972); W.Meissner, Thesis, University of Erlangen-Nuremberg 1973.

111) F.A.Cotton, G.Wilkinson, "Advanced Inorganic Chemistry", 3rd. edition, Interscience, London 1972.

112) D.D.Wagman, W.H.Evans, I.Halow, V.B.Parker, S.M.Bailey, R.H.Schuum, "Selected Values of Chemical Thermodynamic Properties", NBS Tech. Note 270-2, Table 30. (1966).

113) U.Anders, J.A.Plambeck, Can. J. Chem. 47, 3055, (1969).

114) I.G.Dioum, J.Vedel, B.Tremillon, J. Electroanal. Chem. 137, 219, (1982).

115) J.H. von Barner, Inorg. Chem. 24(11), 1686, (1985).

116) H.Rossetti, "Chemical Applications of Potentiometry", Chapter 14, p. 179. D. Van Nostrand, London 1969.

117) G.N.Papatheodorou, O.J.Kleppa, J. Inorg. Nucl. Chem. 32, 889, (1970).

118) Ref. 106, Vol. 1, p. 650.

119) S.Vire, Ph.D. Thesis, Imperial College, 1981.

120) R.S.Nicholson, I.Shain, Anal. Chem. 36, 706, (1964).

121) R.L.Lister, S.N.Flengas, J. Electrochem. Soc. 111, 343, (1964).

122) R.L.Lister, S.N.Flengas, Can. J. Chem. 41, 1548, (1963); J.H.Mui, S.N.Flengas, ibid. 40, 997, (1962).

123) V.S.Maksimov, M.V.Smirnov, Trans. Inst. Electrochem. (Engl. Trans.), 6, 30, (1968).

124) D.Ferry, G.Picard, B.Tremillon, "Electrochemical reactions involving various oxidation states of titanium in LiCl/KCl eutectic at 743K", Lecture, EUCHEM conference on Molten Salts, Geiranger, Norway, 24-29th August 1986.

125) D.Ferry, G.Picard, "Electroanalysis of the Ti(III)/Ti(IV) redox couple", Lecture, EUCHEM conference on Molten Salts, St. Andrews, Scotland, 4-8th July 1988.

126) H.Linga, Z.Stojek, R.A.Osteryoung, J. Amer. Chem. Soc. 103, 3754, (1981).

127) M.Sorlie, H.A.Oye, Inorg. Chem. 20(5), 1384, (1981); K.W.Fung, G.Mamantov, J. Electroanal. Chem. 35, 27, (1972).

128) S.P.Yatsenko, V.N.Danilin, L.N.Volkova, Zh. Fiz. Khim. 42, 874, (1968).

ACKNOWLEDGEMENTS

The author would like to express thanks to the Ministry of Defence for providing financial support during the period of this research.

Thanks are also due to my supervisor, Professor Douglas Inman, for his guidance and encouragement throughout this project, and likewise to Dr. G. Perry from the Ministry of Defence.

Thanks also to my colleagues in the Nuffield "seminar" room and elsewhere, for helpful discussions and companionship, in particular, Stef Carter for help with electron microscopy and Margaret Campbell for help with X-ray diffraction.

Finally, thanks to those who provided technical support in the department, especially Mr. G. Hicks for his glass-blowing talents, and to Mr. M. Haddon for analytical expertise.